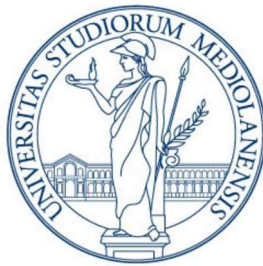


UNIVERSITÀ DEGLI STUDI DI MILANO

Doctorate School in Pharmaceutical Sciences

XXXII Cycle



Parkinson's Disease: validation of a novel target through
the development of methylphenidate analogs as
potential modulators and fluorescent probes

Supervisor: Chiar.mo Prof. Ermanno Valoti

Andrea Casiraghi

R11792

SUMMARY

Abstract	6
CHAPTER 1 – DESIGN, SYNTHESIS AND BIOLOGICAL EVALUATION OF MODULATORS OF THE INTERACTION BETWEEN α -SYNUCLEIN AND SYNAPSIN-III AS NOVEL ANTIPARKISONIAN AGENTS	1
Introduction.....	1
Pathogenesis and symptoms of PD	1
PD Therapy	4
α -synuclein: structure, function and role in PD pathogenesis	9
Therapeutic approaches targeting α -syn	13
Synapsins: structure and role in the presynaptic neurotransmission.....	15
Alpha-synuclein/Synapsin-III interaction: pathological relevance in Parkinson’s disease and modulators	19
Aim of the Work	21
Aim 1: Design of methylphenidate analogs.....	21
Aim 2: Synthesis of methylphenidate analogs	23
Aim 3: Biological evaluation of the synthesized analogs	24
Aim 4: Computational analysis of the results.....	24
Materials and Methods	25
Chemistry	25
Acceptor Photobleaching Fluorescence Resonance Energy Transfer (FRET).....	30
Fluorescence Lifetime Imaging Microscopy (FLIM)-based FRET	30
Immunocytochemistry	32
Primary Mesencephalic Neuronal Cultures and 3-(4,5-dimethylthiazol-2-yl)-2,5-diphenyltetrazolium Bromide (MTT) Assay	32
Results and Discussion	34
Acceptor Photobleaching Fluorescence Resonance Energy Transfer (FRET).....	34
Fluorescence Lifetime Imaging Microscopy (FLIM)-based FRET	35
Immunocytochemistry	36
3-(4,5-dimethylthiazol-2-yl)-2,5-diphenyltetrazolium Bromide (MTT) Assay	38
Conclusions and Future Work	39
Experimental	40
<i>N</i> -Boc pipecolic acid	42
<i>N</i> -Boc pipecolic acid morpholine amide.....	43
<i>N</i> -Boc-piperidin-2-yl(<i>p</i> -tolyl)methanone.....	44

<i>N</i> -Boc-2-(1-(<i>p</i> -tolyl)vinyl)piperidine	45
<i>N</i> -Boc-2-(piperidin-2-yl)-2-(<i>p</i> -tolyl)ethanol (<i>threo/erythro</i>)	46
<i>threo N</i> -Boc-2-(piperidin-2-yl)-2-(<i>p</i> -tolyl)acetic acid.....	47
<i>threo N</i> -Boc-methyl 2-(piperidin-2-yl)-2-(<i>p</i> -tolyl)acetate	48
<i>threo</i> 2-(piperidin-2-yl)-2-(<i>p</i> -tolyl) hydrochloride (Compound I <i>threo</i>)	49
<i>threo</i> methyl 2-(1-methylpiperidin-2-yl)-2-(<i>p</i> -tolyl)acetate hydrochloride (Compound VIII <i>threo</i>) ..	50
<i>erythro N</i> -Boc-2-(piperidin-2-yl)-2-(<i>p</i> -tolyl)acetic acid.....	52
<i>erythro N</i> -Boc-methyl 2-(piperidin-2-yl)-2-(<i>p</i> -tolyl)acetate (Compound I <i>erythro</i>)	53
<i>N</i> -Boc-[1,1'-biphenyl]-4-yl(piperidin-2-yl)methanone	54
<i>N</i> -Boc-2-(1-([1,1'-biphenyl]-4-yl)vinyl)piperidine.....	55
<i>N</i> -Boc-2-([1,1'-biphenyl]-4-yl)-2-(piperidin-2-yl)ethanol (<i>threo/erythro</i>)	56
<i>threo N</i> -Boc-2-([1,1'-biphenyl]-4-yl)-2-(piperidin-2-yl)acetic acid	57
<i>threo</i> methyl-2-([1,1'-biphenyl]-4-yl)-2-(piperidin-2-yl)acetate hydrochloride (Compound II <i>threo</i>)	58
<i>erythro N</i> -Boc-2-([1,1'-biphenyl]-4-yl)-2-(piperidin-2-yl)acetic acid	59
<i>erythro</i> methyl-2-([1,1'-biphenyl]-4-yl)-2-(piperidin-2-yl)acetate hydrochloride (Compound II <i>erythro</i>).....	60
<i>N</i> -Boc-naphthalen-2-yl(piperidin-2-yl)methanone	61
<i>N</i> -Boc-2-(1-(naphthalen-2-yl)vinyl)piperidine	62
<i>N</i> -Boc-2-(naphthalen-2-yl)-2-(piperidin-2-yl)ethanol (<i>threo/erythro</i>)	63
<i>threo N</i> -Boc-2-(naphthalen-2-yl)-2-(piperidin-2-yl)acetic acid	64
<i>threo N</i> -Boc-methyl-2-(naphthalen-2-yl)-2-(piperidin-2-yl)acetate.....	65
<i>threo</i> methyl-2-(naphthalen-2-yl)-2-(piperidin-2-yl)acetate hydrochloride (Compound III <i>threo</i>) ...	66
1-(pyridin-2-yl)-1-(<i>m</i> -tolyl)ethanol	67
2-(1-(<i>m</i> -tolyl)vinyl)pyridine	68
2-(2-(<i>m</i> -tolyl)oxiran-2-yl)pyridine	69
2-(pyridin-2-yl)-2-(<i>m</i> -tolyl)ethanol	70
2-(piperidin-2-yl)-2-(<i>m</i> -tolyl)ethanol.....	71
<i>N</i> -Boc-2-(piperidin-2-yl)-2-(<i>m</i> -tolyl)ethanol.....	72
<i>erythro N</i> -Boc-2-(piperidin-2-yl)-2-(<i>m</i> -tolyl)acetic acid	73
<i>erythro</i> methyl 2-(piperidin-2-yl)-2-(<i>m</i> -tolyl)acetate hydrochloride (Compound V <i>erythro</i>)	74
1-(naphthalen-1-yl)-1-(pyridin-2-yl)ethanol.....	75
2-(1-(naphthalen-1-yl)vinyl)pyridine	76
2-(2-(naphthalen-1-yl)oxiran-2-yl)pyridine	77
2-(naphthalen-1-yl)-2-(pyridin-2-yl)ethanol.....	78
2-(naphthalen-1-yl)-2-(piperidin-2-yl)ethanol.....	79
<i>N</i> -Boc-2-(naphthalen-1-yl)-2-(piperidin-2-yl)ethanol.....	80

<i>erythro</i> <i>N</i> -Boc-2-(naphthalen-1-yl)-2-(piperidin-2-yl)acetic acid	81
<i>erythro</i> methyl 2-(naphthalen-1-yl)-2-(piperidin-2-yl)acetate hydrochloride (Compound IV <i>erythro</i>)	82
Methyl 3-phenyl-2-(pyridin-2-yl)propanoate.....	83
Methyl 3-phenyl-2-(piperidin-2-yl)propanoate.....	84
<i>N</i> -Boc methyl 3-phenyl-2-(piperidin-2-yl)propanoate (<i>threo/erythro</i>).....	85
<i>erythro</i> methyl 3-phenyl-2-(piperidin-2-yl)propanoate hydrochloride (Compound IX <i>erythro</i>).....	86
<i>threo</i> methyl 3-phenyl-2-(piperidin-2-yl)propanoate hydrochloride (Compound IX <i>threo</i>).....	87
Methyl 2-phenyl-3-(pyridin-2-yl)propanoate.....	88
Methyl 2-phenyl-3-(piperidin-2-yl)propanoate (Compound XI <i>threo</i> + <i>erythro</i>)	89
Methyl 2-(pyridin-2-yl)-3-(<i>p</i> -tolyl)propanoate	90
Methyl 2-(piperidin-2-yl)-3-(<i>p</i> -tolyl)propanoate.....	91
<i>N</i> -Boc methyl 2-(piperidin-2-yl)-3-(<i>p</i> -tolyl)propanoate (<i>threo/erythro</i>).....	92
<i>threo</i> methyl 2-(piperidin-2-yl)-3-(<i>p</i> -tolyl)propanoate hydrochloride (Compound X <i>threo</i>)	93
<i>erythro</i> methyl 2-(piperidin-2-yl)-3-(<i>p</i> -tolyl)propanoate hydrochloride (Compound X <i>erythro</i>).....	94
<i>N</i> -methoxy- <i>N</i> -methylpicolinamide.....	95
Phenyl(pyridin-2-yl)methanone	96
Trimethyl phosphonoacetate	97
(<i>E,Z</i>)-methyl 3-phenyl-3-(pyridin-2-yl)acrylate.....	98
<i>erythro</i> methyl 3-phenyl-3-(piperidin-2-yl)propanoate hydrochloride (Compound XII <i>erythro</i>).....	99
2-(4-methoxyphenyl)-2-(pyridin-2-yl)acetonitrile.....	100
2-(4-methoxyphenyl)-2-(pyridin-2-yl)acetamide	101
2-(4-methoxyphenyl)-2-(piperidin-2-yl)acetamide	102
<i>threo</i> 2-(4-methoxyphenyl)-2-(piperidin-2-yl)acetamide.....	103
<i>threo</i> methyl 2-(4-methoxyphenyl)-2-(piperidin-2-yl)acetate	104
<i>threo</i> methyl 2-(4-methoxyphenyl)-2-(piperidin-2-yl)acetate hydrochloride (Compound VI <i>threo</i>).....	105
2-phenyl-2-(pyridin-2-yl)acetonitrile.....	106
2-phenyl-2-(pyridin-2-yl)acetamide	107
2-phenyl-2-(piperidin-2-yl)acetamide hydrochloride.....	108
2-phenyl-2-(piperidin-2-yl)acetamide	109
<i>threo</i> methylphenidate hydrochloride.....	110
<i>threo</i> 4-nitromethylphenidate (Compound VII <i>threo</i> freebase)	111
CHAPTER 2 – DESIGN, SYNTHESIS AND BINDING EVALUATION OF FLUORESCENT SMALL MOLECULE	
LIGAND-BASED PROBES FOR IMAGING THE NOREPINEPHRINE TRANSPORTER	
Introduction.....	112
Protein Labeling Techniques for Fluorescent Live-Cell Imaging.....	113

Fluorescent Small Molecule Ligand-Based Probes for Imaging Monoamine Transporters	116
Aim of the Work	119
Aim 1: Probe design.....	119
Aim 2: Radioligand binding evaluation.....	121
Aim 3: Live-cell fluorescent microscopy.....	121
Materials and Methods	123
Chemistry	123
Radioligand Binding Assays	127
Results and Discussion	129
Conclusion and Future Perspectives	130
Experimental	131
3,3-dimethyl-1,3-dihydroisobenzofuran-1-one.....	132
1-allyl-3,3-dimethyl-1-phenyl-1,3-dihydroisobenzofuran	133
3-(3,3-dimethyl-1-phenyl-1,3-dihydroisobenzofuran-1-yl)propan-1-ol.....	134
3-(3,3-dimethyl-1-phenyl-1,3-dihydroisobenzofuran-1-yl)propanal	135
<i>N</i> -(<i>N'</i> -Boc-aminoethyl)- <i>N</i> -desmethyltalopram.....	136
<i>N</i> -(2-aminoethyl)- <i>N</i> -desmethyltalopram	137
6-(Rhodamine Red-4-sulfonamido)hexanoyl-aminoethyl- <i>N</i> -desmethyltalopram (Compound XIII)	138
5-bromo-3,3-dimethyl-1,3-dihydroisobenzofuran-1-one	139
1-allyl-5-bromo-3,3-dimethyl-1-phenyl-1,3-dihydroisobenzofuran	140
1-allyl-5-cyano-3,3-dimethyl-1-phenyl-1,3-dihydroisobenzofuran.....	141
3-(5-cyano-3,3-dimethyl-1-phenyl-1,3-dihydroisobenzofuran-1-yl)-1-bromopropane	142
5-cyanotalopram	143
5-aminomethyltalopram	144
3-amino-1-phenylpropan-1-ol.....	145
<i>N</i> -Boc-3-amino-1-phenylpropan-1-ol.....	146
<i>N</i> -Boc- <i>N</i> -desmethylnisoxetine	147
<i>N</i> -desmethylnisoxetine	148
<i>N</i> -(<i>N'</i> -Boc-aminoethyl)- <i>N</i> -desmethylnisoxetine.....	149
<i>N</i> -2-aminoethyl- <i>N</i> -desmethylnisoxetine.....	150
<i>N</i> -[6-((Rhodamine Red-4-sulfonamido)hexanoyl)aminoethyl]- <i>N</i> -desmethylnisoxetine (Compound XV)	151
3-amino-1-(3-bromophenyl)propan-1-ol	152
<i>N</i> -Boc-3-amino-1-(3-bromophenyl)propan-1-ol	153
<i>N</i> -Boc- <i>m</i> -bromo- <i>N</i> -desmethylnisoxetine	154
<i>N</i> -Boc- <i>m</i> -cyano- <i>N</i> -desmethylnisoxetine	155

<i>m</i> -(aminomethyl)nisoxetine.....	156
<i>m</i> -[6-(Rhodamine Red-4-sulfonamido)hexanoyl]aminomethylnisoxetine (Compound XVI).....	157
CHAPTER 3 – DESIGN AND SYNTHESIS OF FLUORESCENT PROBES BASED ON A METHYLPHENIDATE	
SCAFFOLD	158
Introduction.....	158
Aim of the Work	158
Chemistry	159
Future Work	161
Experimental	162
<i>N</i> -Boc- <i>threo</i> -methylphenidate	163
<i>N</i> -Boc <i>threo</i> -ritalinic acid.....	164
<i>N</i> -Boc-4-aminobutanol.....	165
4-(<i>N</i> -Boc-amino)butyl- <i>N</i> -Boc- <i>threo</i> -phenidate	166
<i>threo</i> -4-aminobutylphenidate.....	167
4- <i>N</i> -[6-(Rhodamine Red-4-sulfonamido)hexanoyl]aminobutyl- <i>threo</i> -phenidate (Compound XVII).....	168
<i>N</i> -Boc-amino-PEG4-alcohol.....	169
[<i>N</i> -Boc(amino-PEG4)yl] <i>N</i> -Boc- <i>threo</i> -phenidate	170
(amino-PEG4)yl- <i>threo</i> -phenidate	171
(Rhodamine Red-4-sulfonyl)amino(PEG4)yl- <i>threo</i> -phenidate (Compound XVIII).....	172
CONCLUSIONS	173
CONTRIBUTIONS TO THE RESEARCH	174
PRODUCTS OF THE RESEARCH.....	174
Publications Related to the Thesis	174
Other Publications.....	174
Grants	175
Posters and Oral Communications.....	175
ACKNOWLEDGEMENTS	178
BIBLIOGRAPHY.....	179

Abstract

Parkinson's Disease (PD) is a neurological disorder characterized by the progressive degeneration of dopaminergic striatal neurons, which in turn leads to the onset of a typical set of motor and non-motor symptoms. α -synuclein is the most studied protein involved in the pathogenesis of PD and its accumulation, misfolding and aggregation are strongly correlated with dopaminergic neuronal derangement. Synapsin-III is a neuronal protein involved in trafficking, fusion and binding of dopaminergic presynaptic vesicles. A growing body of evidence implicates the cooperation between α -synuclein and Synapsin-III in the pathogenesis of the disease and opens up to the possibility of pharmacological modulation of their interaction as a novel therapeutic approach for the treatment of PD.

In Chapter 1 of this work, the design and synthesis of methylphenidate analogs as possible modulators of the α -synuclein/Synapsin-III interaction is presented. The parent molecule has been systematically modified in order to evaluate the effect of structural changes on biological activity. The obtained compounds have been tested for their biological activity and toxicity profile with the use of specific assays. The ability of these compounds to promote the interaction between the two target proteins, as well as their ability to slow down or prevent the aggregation of α -synuclein has been evaluated. Interestingly, one of the analogs showed a promising biological activity and, possibly, cytoprotective effects in cell models of PD. The activity data for the analogs will support the characterization of the binding modes to Synapsin-III and, hopefully, the identification of the preferential binding pocket. Moreover, very low or absent cytotoxicity corroborate our interest in these analogs as possible novel antiparkinsonian agents.

In Chapter 2, the design, synthesis and radioligand binding evaluation of a novel group of fluorescent small molecule ligand-based probes for imaging the norepinephrine transporter (NET) is presented. NET is a member of the monoamine transporters family and is implicated in PD as well as in depression, ADHD and substance abuse. The selective imaging of NET in live cells, in particular with the aid of super resolution microscopy techniques, would contribute in a better understanding of its function, localization and trafficking at a molecular level. Herein, we identified a functional design for a NET-selective high affinity probe and verified its binding capabilities at NET. The most promising candidate is at the moment under evaluation in live-cell microscopy experiments.

The work presented in Chapter 3 applies the fluorescent probes chemistry and concepts shown in Chapter 2 to the design and synthesis of novel fluorescent probes based on a methylphenidate scaffold and represents the ideal connection between the two projects previously described. The synthesized probes are now under evaluation in FRET experiments, in order to characterize the binding of methylphenidate on Synapsin-III, which would make a crucial contribution to our understanding of the interaction of the compounds presented in Chapter 1 with their target.

CHAPTER 1 – DESIGN, SYNTHESIS AND BIOLOGICAL EVALUATION OF MODULATORS OF THE INTERACTION BETWEEN α -SYNUCLEIN AND SYNAPSIN-III AS NOVEL ANTIPARKINSONIAN AGENTS

Introduction

First described as a neurological disorder in 1817 by the English physician James Parkinson, Parkinson's Disease (PD) is the second most common neurodegenerative disorder worldwide and the fastest growing one. Recent reports (Dorsey *et al.* 2018, Rossi *et al.* 2018) show a consistent increase in prevalence over the last decades in every area over the world, and projections predict that the number of patients will double in the next 20 years, exceeding 12 million by 2040. While the main risk factor is aging, other factors that fueled this unprecedented surge are longevity, decreased smoking rates and the increase of environmental toxins (e.g. organochlorine pesticides) that are associated with increased risk (Goldman 2014).

Pathogenesis and symptoms of PD

The key neuropathological alteration in the PD brain is the loss of dopaminergic neurons in the pars compacta of the substantia nigra (SNpc). The reduced release of dopamine (DA) resulting from the degeneration of the nigrostriatal pathway disrupts the homeostasis of the basal ganglia circuits and leads to the onset of the classic motor symptoms, which include rigidity, bradykinesia, tremor and postural instability. Degeneration is not limited to the SNpc and other non-dopaminergic brain regions like the locus coeruleus and nucleus basalis of Meynert are affected (Forno 1996). Neuronal loss correlates with the severity and duration of the motor dysfunction (Ma *et al.* 1997) and the appearance of motor symptoms is usually associated with a decrease of 60-80% in striatal DA levels and with over 30% nerve cell loss in the SNpc (Cheng *et al.* 2010). Non-motor symptoms, such as hyposmia, constipation, REM sleep disorders and depression usually go together with motor symptoms (Chaudhuri and Schapira 2009). Interestingly, some early non-motor symptoms can precede the onset of motor symptoms, thus suggesting that the induction site for neurodegeneration is not in the SNpc (Del Tredici *et al.* 2002). Psychiatric symptoms (anxiety, depression) and cognitive deficits are typical of later stages of the disease.

Another key histopathological hallmark of the PD brain is the presence of abnormal intraneuronal and intraneuritic insoluble protein aggregates called Lewy Bodies (LB) and Lewy Neurites (LN),

mainly containing α -synuclein (α -syn) fibrils (Spillantini *et al.* 1998, Fujiwara *et al.* 2002) dispersed in a crowded lipid enriched environment mainly composed by vesicles and organelles debris and surrounded by a ring of mitochondria (Moors *et al.* 2019, Shahmoradian *et al.* 2019). The deposition of LB in different areas of the brain follows a stereotyped caudo-rostral pattern correlated with disease progression and with the type and severity of the symptoms (Braak *et al.* 2003, Braak *et al.* 2006), suggesting a causative role in the pathogenesis of PD. More specifically, the degree of pathology can be classified in 6 progressive stages. Early stages reflect deposition in the lower brainstem and in the olfactory bulb and are associated with the onset of prodromal nonmotor symptoms (hyposmia, constipation). Clinical motor symptoms arise with the involvement of the SNpc around stage 3, while the progression to cortical regions in later stages marks the onset of late cognitive symptoms. Different mechanisms have been proposed for the transfer of α -syn pathology from cell to cell, contributing to the spreading of neurodegeneration in the PD brain (Desplats *et al.* 2009, Danzer *et al.* 2012, Lee *et al.* 2012, Illes-Toth *et al.* 2015). Moreover, healthy grafts of dopaminergic neurons previously placed in the striatum of PD patients develop α -syn pathology, in agreement with the hypothesis of prion-like transfer (Kordower *et al.* 2008, Li *et al.* 2008, Hansen *et al.* 2011, Kordower *et al.* 2011).

Remarkably, abnormal α -syn levels and/or distribution are not limited to the central nervous system, but involve peripheral areas and organs such as the vagus nerve (Beach *et al.* 2010, Del Tredici *et al.* 2010), the submucosal nerve fibers of stomach (Braak *et al.* 2006) and intestine (Shannon *et al.* 2012), cardiac sympathetic ganglia (Iwanaga *et al.* 1999, Orimo *et al.* 2008) and the superior cervical ganglion (Del Tredici *et al.* 2010). Furthermore, accumulation of α -syn can be found in the skin (Gibbons *et al.* 2016), in body fluids like cerebrospinal fluid, plasma and saliva and in red blood cells, leukocytes and platelets (Malek *et al.* 2014). This widespread diffusion supports the idea that PD could be considered as a systemic multi-organ/multi-neurotransmitter syndrome, instead of a single dopaminergic disease (Engelender and Isacson 2017, Titova *et al.* 2017). According to this hypothesis, the staged onset and severity of different symptoms is related to selective vulnerabilities of different dopaminergic and nondopaminergic neuronal populations to α -syn pathology, as well as to their functional reserve (Engelender and Isacson 2017, Surmeier *et al.* 2017).

The majority of cases are sporadic but about 5% of patients have monogenic forms of the disease (Pankratz and Foroud 2004). Mutations in the GBA gene encoding for glucocerebrosidase were

associated with an increased incidence of Parkinson's disease (PD), in both autosomal recessive Gaucher's patients as well as asymptomatic carriers (Riboldi and Di Fonzo 2019). Today we know that GBA mutations are the major genetic risk factor for PD. Impaired GCase activity has been identified also in idiopathic cases of PD patients who did not carry a mutation in the gene, suggesting a central role of this enzyme in the pathogenesis of the disease. The most frequent autosomal dominant mutation associated with familial PD is found in the SNCA gene that encodes α -syn. Other mutations are found in the Leucine rich repeat Kinase 2 (LRRK2) domain, in genes controlling mitochondrial homeostasis such as Parkin, PINK1, DJ1 and other loci encoding for proteins which are mainly involved in the control of synaptic functions or neuronal trafficking.

The exact cytotoxic pathway in PD has to be fully elucidated yet and probably derives from a combination of multiple mechanisms (toxic or oxidative metabolism of dopamine, mitochondrial dysfunction, endoplasmic reticulum stress, impaired autophagy, loss of calcium homeostasis) (Zeng *et al.* 2018). However, it is evident that α -syn aggregation correlates with loss of function and/or alterations in protein interactions, initiating a derangement in neuronal homeostasis. Interestingly, a recent model identifies synaptic degeneration, as opposed to cell death, as the initiating event in the pathogenesis of the disease. Indeed, the formation of α -syn toxic species, together with genetic and environmental factors, could trigger synaptic damage and impaired synaptic plasticity by altering the function and distribution of multiple synaptic proteins. These can in turn lead to axonal damage and retrograde cell degeneration (Bellucci *et al.* 2016, Bellucci *et al.* 2017).

Of note, PD can be classified as a member of a larger group of neurodegenerative disorders collectively named synucleinopathies, together with Dementia with Lewy Bodies (DLB) and Multiple System Atrophy (MSA) (Spillantini and Goedert 2000, Goedert *et al.* 2017). The different combinations of autonomic symptoms, cognitive impairments and parkinsonian motor symptoms for each disorder reflect specific vulnerabilities of neuroanatomical regions and cell populations (Alegre-Abarrategui *et al.* 2019).

PD Therapy

Despite the growing burden on society and the extensive research on the topic, no cure is currently available for PD. Therapeutic options are limited and mostly symptomatic, with no treatments capable of halting, let alone reversing, the progression of the neurodegeneration. An historical perspective of the main therapeutic strategies in the context of the advancement of PD research is summarized in **Figure 1**.

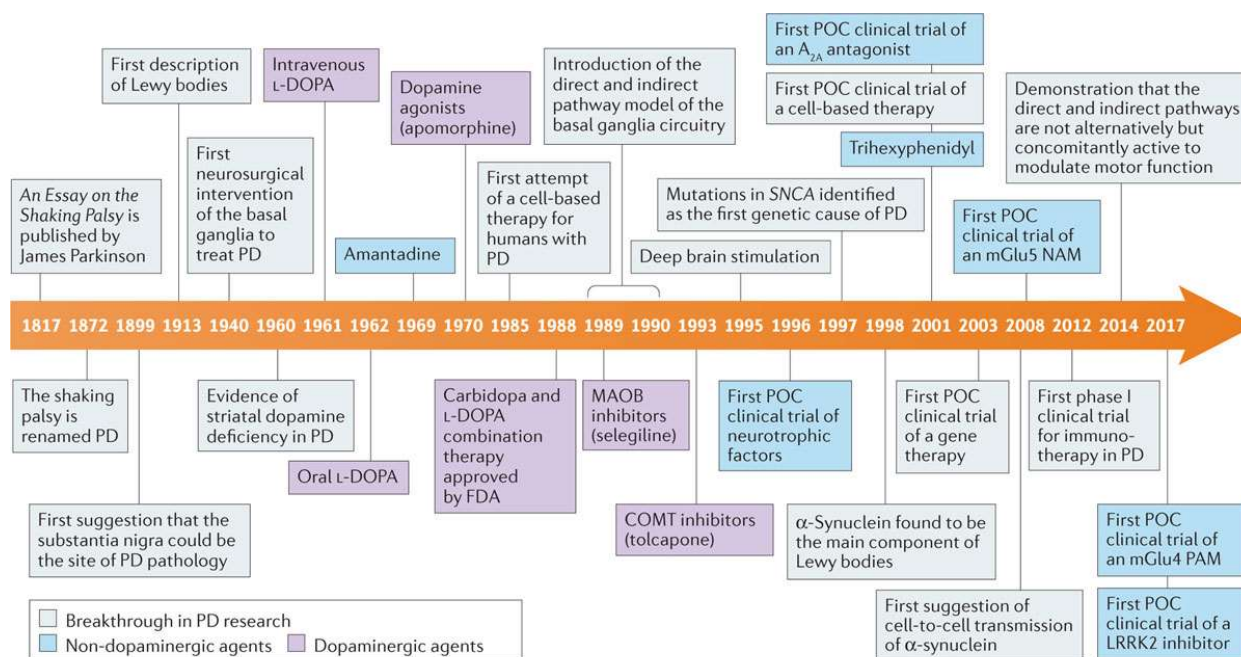


Figure 1: History of Parkinson's Disease research and therapeutic advances (from Charvin et al., 2018)

Given the central role of DA depletion and impaired transmission in the onset of the motor symptoms, the classic therapeutic approach is primarily based on DA replacement using the DA precursor levodopa (*L*-DOPA). Classic association with DOPA decarboxylase inhibitors (carbidopa, benserazide) limits the conversion of *L*-DOPA into DA outside of the CNS, increasing *L*-DOPA bioavailability and reducing peripheral side effects (Lieberman *et al.* 1975). *L*-DOPA, identified as the game changer when first introduced in the 1968, still remains the most effective treatment for the disease. This notwithstanding, its efficacy is mostly limited to early stages of PD. Indeed, 5-10 years after the beginning of therapy, the positive effects on movement control are usually accompanied by the onset of wearing on-off, dyskinesias and psychotic symptoms (Olanow and Stocchi 2018). A controversy exists about suspected cytotoxicity on nigrostriatal neurons as a result of the generation of reactive oxygen species (ROS) during DA metabolism (Fahn *et al.* 2004, Lipski *et al.* 2011, Postuma *et al.* 2015). Over time, with the progression of DA neuronal loss, striatal DA levels become more dependent on administered *L*-DOPA (Postuma *et al.* 2015)

and motor fluctuations worsen, with longer “off” times. Strategies to decrease “off” time include *L*-DOPA dose fractionation, increase in the administered dose, association with a second dopaminergic drug or with an inhibitor of dopamine metabolism (Connolly and Lang 2014). Extended release oral formulations of *L*-DOPA also proved to have a beneficial effect (Margolesky and Singer 2018). Other drugs active on dopaminergic neurotransmission can be used as a monotherapy, especially in the early phases of the disease or in case of low tolerance to *L*-DOPA, or in association with *L*-DOPA. Catechol-*O*-methyl transferase (COMT) inhibitors (e.g. entacapone and opicapone) can improve the efficacy of chronic *L*-DOPA administration and have a beneficial effect on motor complications (Müller 2015). Similarly, adjunct therapy with monoamine oxidase B (MAO-B) inhibitors (e.g. rasagiline) have shown a positive effect on the reduction of daily “off” time and in the treatment of motor complications (Fox *et al.* 2011). Recently, safinamide, a drug allowing potent, selective, and reversible inhibition of MAO-B with blockade of voltage-dependent Na⁺ and Ca²⁺ channels and inhibition of glutamate release has been also approved as add-on for PD treatment in order to reduce *L*-DOPA dosage and thus prevent long-term side effects (Caccia *et al.* 2006).

Dopaminergic agonists (e.g. pramipexole, ropinirole) are efficacious as a monotherapy for the control of motor fluctuations (Fox *et al.* 2011) but lose efficacy over time and have to be substituted with canonical *L*-DOPA therapy. Longer half-lives are associated with a reduced incidence and severity of dyskinesias compared to *L*-DOPA (Rascol *et al.* 2000). However, DA replacement is just one of the possible approaches, as PD motor symptoms are the result of functional changes in multiple neurotransmitter pathways more complex than simple DA depletion. DA neuron loss in the SNpc triggers a cascade of alterations that disrupt the balance of excitatory/inhibitory inputs and outputs along the direct and indirect pathways of the basal ganglia circuit. In particular, the output nuclei of the circuit, medial globus pallidus and substantia nigra pars reticulata, become hyperactive due to reduced direct inhibition from the striatum and to abnormally increased glutamatergic stimulation from the subthalamic nucleus (STN) (Blandini *et al.* 2000). Given the key role of glutamatergic transmission in this misbalance, agents targeting the glutamatergic system can represent a viable therapeutic option to restore basal ganglia motor function and treat parkinsonism or levodopa-induced dyskinesia (LID). In particular, amantadine, a non-selective NMDA antagonist, is currently used to treat LID in PD patients receiving *L*-DOPA-based therapy (Vijayakumar and Jankovic 2016) and allosteric modulator of

metabotropic glutamate receptors types 4 and 5 showed promising results in animal models of PD (Grégoire *et al.* 2011, Charvin *et al.* 2018) and in clinical trials (Berg *et al.* 2011). Other pharmacological nondopaminergic therapies are being extensively studied, both as symptomatic and disease-modifying treatments. These include iron chelators (Kaur *et al.* 2003, Devos *et al.* 2014), glucagon-like peptide 1 (GLP1) agonists (Athauda *et al.* 2017), leucine rich repeat kinase 2 (LRRK2) inhibitors (Di Maio *et al.* 2018), adenosine receptor type 2A antagonists (Kondo and Mizuno 2015) and serotonin receptor agonists (Paolone *et al.* 2015).

An interesting alternative to pharmacological approaches involves gene therapies that deliver key target genes directly to the basal ganglia using technologies based on viral vectors. Symptomatic treatments are based on the delivery of genes involved in dopamine metabolism or in the degradation of glutamate (Blits and Petry 2016). VY-AADC is a recently developed (AAV2)-based viral vector that delivers the aromatic l-aminoacids decarboxylase gene (AADC), in the attempt to counteract the loss of DOPA decarboxylase enzyme that occurs in nigrostriatal DA neurons in advanced PD (San Sebastian *et al.* 2014). Phase 1 trials showed improved symptomatology during “off” state (Christine *et al.* 2009, Muramatsu *et al.* 2010) and prompted interest in this approach as an adjunct therapy to control motor fluctuations induced by L-DOPA. During the endogenous synthesis of dopamine, L-tyrosine is converted into L-DOPA by tyrosine hydroxylase (TH), using tetrahydrobiopterin (BH₄) as a co-factor. ProSavin is a viral vector that aims at the complete reconstruction of the dopamine synthesis apparatus, with the delivery of the TH and AADC genes together with the gene that codifies GTP cyclohydroxylase 1, the enzyme that catalyzes the synthesis of BH₄. The three gene sequences are too long to fit the limited genome of AAV-based vectors together. To solve the problem, they can be either delivered with the simultaneous administration of a mixture of three AAV-based vectors, each containing a single transgene, or with the use of a lentiviral (LV) vector. LV-TH-GCH-AADC showed good tolerability and a dose-dependent improvement in Unified Parkinson’s Disease Rating Scale (UPDRS) motor scores in a Phase 1 trial (Palfi *et al.* 2014). A different approach is based on the subthalamic overexpression of glutamic acid decarboxylase (GAD), the enzyme that catalyzes the synthesis of γ -aminobutyric acid (GABA), to enhance GABAergic transmission in the STN. In a Phase 2 trial, AAV-GAD showed a significant reduction in UPDRS scores (LeWitt *et al.* 2011), but further follow-up data are needed. Research on disease-modifying gene therapy mainly focuses on viral vectors for the delivery of neurotrophic factors. Glial derived neurotrophic factor (GDNF)

selectively promotes the survival and morphological differentiation of midbrain DA neurons (Lin *et al.* 1993, Lei *et al.* 2011). Striatal GDNF overexpression with AAV- and LV-based viral vectors ameliorates parkinsonian behavior in murine models of PD (Chen *et al.* 2008) and improves motor behavior and cognitive performance in MPTP-treated monkeys (Eberling *et al.* 2009, Kells *et al.* 2010). At the moment, a Phase 1 trial is in progress to assess the safety and effects of the injection of an AAV2-GDNF vector in advanced PD patients (US-NIH 2012). Neurturin (NTN) is a close homologue of GDNF and another potential target for gene therapy. The administration of an AAV2 vector encoding human NTN (CERE-120) significantly improved MPTP-induced motor impairments significantly preserved nigral neurons and striatal dopaminergic innervation (Kordower *et al.* 2006). Bilateral infusion of AAV2-NTN into the putamen in a Phase 1 trial gave promising results in terms of safety and significant improvement of motor symptoms (Marks *et al.* 2008), but a subsequent Phase 2 trial failed to replicate these results, with no significant improvement in motor scores compared to sham surgery (Marks *et al.* 2010). Insufficient transfection rate and/or insufficient retrograde transport to the SN were identified as possible causes for this failure and a second Phase 1 trial was performed with higher titers of AAV2-NTN and concomitant injection in the SN, showing good tolerability and improvement in UPDRS scores (Bartus *et al.* 2013). Unfortunately, these encouraging results did not translate in a later Phase 2 study utilizing the same approach and AAV2-NTN was not found to be superior to sham surgery in improving motor scores (Warren Olanow *et al.* 2015). Some general limitations of viral vector-based gene therapy are due to the irreversibility of the procedure and to the difficult control of the amount and/or the site of injection, together with possible side effects as immunogenicity and insertional mutagenesis (Thomas *et al.* 2003). In addition, the invasive surgical procedure makes this approaches unsuitable for early PD patients.

Surgical treatments for PD grew as an area of great interest in the last 25 years, with the development of reversible and relatively non-invasive procedures. Deep brain stimulation (DBS) is based on the focal stimulation of specific subthalamic brain regions, usually the STN or globus pallidus pars interna, with a semi-permanent electrode connected to a power source implanted under the skin, usually in the subclavicular area. Recent improvements in power sources and directional electrodes, that allow for a more precise stimulation (Wagle Shukla *et al.* 2017), are increasing the practicability of the technique. High-frequency trains of electrical pulses induce action potentials that can override the intrinsic activity in the stimulated pathways, interrupting

and resetting any abnormal feedback loops in the basal ganglia circuits (Lozano *et al.* 2019). The treatment is symptomatic and proved to perform better than other medical treatments in the control of motor disturbances in both early and advanced PD patients (Follett *et al.* 2010, Schuepbach *et al.* 2013). However, current modalities of DBS are not effective in the treatment of other PD symptoms (e.g. gait disorders) and have no positive influence on cognitive impairment (Merola *et al.* 2017). Possible side effects include hemorrhage, ischemic stroke, infections in the implantation site and seizures, but the continuous parallel improvement of imaging and microelectrode recording techniques is increasing the specificity and safety of the treatment.

Cell-based therapies are currently being studied for the treatment of PD motor symptoms through the implant of undifferentiated stem cell in the striatum of patients, in the attempt to promote neuronal growth and innervation and counteract the progression of cell loss. Some success has been obtained with the use of fetal ventral mesencephalic cells in the late 1990s, but the research came to a halt shortly after that due to some conflicting results, together with ethical and safety concerns (Sonntag *et al.* 2018). Interestingly, despite the evidence of prion-like transfer of α -syn pathology, graft-derived neurons and innervation have shown survival for over 20 years after the implant, with presence of LBs in only 1-12% of cells (Kurowska *et al.* 2011, Li *et al.* 2016). In recent years, the development of protocols based on induced pluripotent stem cells of autologous origin fostered a renewed interest in this type of research, with the prospect of reduced immunogenicity and improved safety.

Since its key role in PD pathogenesis, therapies targeting α -syn are under extensive study. See the *Therapeutic approaches targeting α -syn* section for a review of the most relevant approaches.

α -synuclein: structure, function and role in PD pathogenesis

Full length α -syn (14 kDa, 140 aminoacids) is the most widely expressed of the three isoforms of human α -syn. It is abundant in neurons and specifically localizes in presynaptic terminals (Maroteaux *et al.* 1988, Kahle *et al.* 2000, Yang *et al.* 2010), where it is associated with the distal reserve pool of synaptic vesicles. Its sequence can be divided into three main regions:

1) the *N*-terminal region (residues 1-60) is a positively charged lysine-rich region containing four 11-aminoacid imperfect repeats. Each repeat comprises a highly conserved hexameric motif (KTKEGV) that promotes the formation of amphipathic α -helical secondary structures upon the binding with lipid membranes, in a similar fashion to the lipid-binding domain of apolipoprotein-like class A₂ (Clayton and George 1998, Vamvaca *et al.* 2009). Three mutations involved in familial forms of PD occur in this region: A30P, E46K and A53T. Interestingly, A30P and E46K influence the ability to bind biological membranes (Jensen *et al.* 1998, Bodner *et al.* 2010, Gaugler *et al.* 2012), supporting the idea that this region is crucial for the interaction of α -syn with lipid membranes and that alterations in this process may play a role in the pathogenesis of PD. The presence in the *N*-terminal domain of one of the two conserved characteristic sequences of fatty acid binding proteins (FABPs) (Sharon *et al.* 2001), that mediates the interaction with lipid membranes and micelles (Zhu *et al.* 2003), further reinforces this hypothesis. In particular, α -syn preferentially associates with high curvature membranes enriched in phospholipids similar to synaptic vesicles (Davidson *et al.* 1998). Post-translational modifications may have a critical role in determining the structure and function of both native and pathogenetic forms of protein. More specifically, *N*-terminal acetylation may be involved in the conversion of aggregation-stable alpha-helical tetramers into more aggregation-prone alpha-helical oligomers (Trexler and Rhoades 2012) and nitration of tyrosine Y39, which can occur under oxidative stress conditions, can disrupt the binding to lipid membranes (Sevcsik *et al.* 2011) and is also crucial for the formation of high-ordered oligomers through 3-nitrotyrosine cross-linking (Souza *et al.* 2000).

2) the central region (residues 61-95) contains a highly aggregation-prone (Uéda *et al.* 1993) non-amyloid-beta-component (NAC) sequence. In particular, the central, highly hydrophobic domain corresponding to residues 71-82 is implicated in the misfolding and aggregation of α -syn into fibrils, as supported by its ability to aggregate in isolation (Giasson *et al.* 2001) and by absence of polymerization and increased tendency to form oligomers observed after its total or partial deletion (Du *et al.* 2003, Waxman *et al.* 2009). Interestingly, deletions in other sections of

the NAC sequence have the effect of slowing down the rate of fibril formation without completely inhibiting it. Moreover, the comparison between the aggregation behavior of α -syn, β -synuclein and some chimeric variants in presence of a lipid mimetic suggests that a very specific distribution of charged and hydrophobic residues is necessary for polymerization, rather than the commonly assumed presence or absence of the whole NAC region (Waxman *et al.* 2009). This part of α -syn can adopt different conformations from random coil to β -sheet structures (el-Agnaf and Irvine 2002), cylindrical β -sheets (Perutz *et al.* 2002) and amyloid- β -like fibrils and protofibrils (Dev *et al.* 2003). When the protein is in a disordered state, transient intramolecular interactions shield this region from the cytoplasm to prevent aggregation (Theillet *et al.* 2016). After β -sheet formation and/or ordered aggregation, the structure exposes a chaperone-binding site for target protein binding (Rekas *et al.* 2012). The central region takes part in the specific interaction with dopamine (residue E83), which is able to inhibit α -syn polymerization (Herrera *et al.* 2008).

3) The C-terminal region (residues 96-140), highly enriched in acidic aminoacids and proline residues, is involved in the conformation and aggregation kinetics of α -syn (Meuvis *et al.* 2010). Mutations in these domains inhibit fibril formation (Ulrih *et al.* 2008), while C-terminally truncated forms aggregate faster than full length ones (Crowther *et al.* 1998, Li *et al.* 2005). Post translational modifications (PTMs) of this region can influence α -syn aggregation properties and molecular interaction dynamics. Nitration of tyrosine residues Tyr125, Tyr133 and Tyr136 has been reported to alter the conformational state of the protein, reduce its membrane-binding affinity and to promote the formation of fibrils or oligomers (Giasson *et al.* 2000). Phosphorylation at Ser139 is likely to play a key role in α -syn oligomerization, and ultimately in PD pathology, being the most prevalent PTM of α -syn detected in PD brains with LBs (Fujiwara *et al.* 2002). Moreover, phosphorylation can promote the accumulation of oligomeric α -syn *in vitro* (Anderson *et al.* 2006) and can accelerate the formation of α -syn inclusions *in vivo* (Smith *et al.* 2005, Sugeno *et al.* 2008) and neuronal loss in transgenic mice overexpressing α -syn (Wakamatsu *et al.* 2007, Schell *et al.* 2009, Rieker *et al.* 2011). However, other results conflict with this hypothesis (Paleologou *et al.* 2008) and the specific role of serine phosphorylation in α -syn toxicity remains unclear. This part of the protein interacts non-specifically with DA (Herrera *et al.* 2008) and may be involved in DA homeostasis, as supported by the formation of C-terminally truncated forms of α -syn in PD brains (Prasad *et al.* 2012).

A current opinion is that α -syn plays a crucial role in synaptic plasticity and vesicular trafficking promoting membrane curvature, vesicle budding and packaging (Varkey *et al.* 2010). Moreover, it is believed to regulate the amount of synaptic vesicles docked at the synapse and their exocytosis during neurotransmitter release (Wislet-Gendebien *et al.* 2006), as supported by its association with SNARE complexes (Burré *et al.* 2010).

The conformation and aggregation properties of α -syn are highly dynamic and highly modifiable by post-translational modifications and/or by the cellular environment. Both the physiologic function and the pathological manifestations of α -syn appear to be largely influenced by the protein's conformation and its organization in higher-order aggregates (Figure 2).

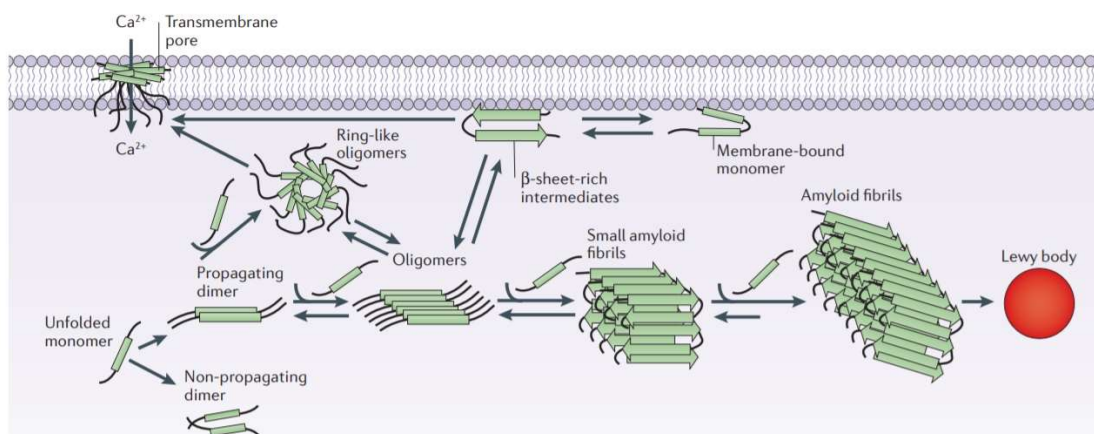


Figure 2: α -synuclein aggregation and oligomeric intermediates (adapted from Lashuel *et al.*, 2013): both cytosolic and membrane-bound α -syn can form oligomeric species. Further aggregation leads to the formation of fibrils and ultimately to the deposition of Lewy Bodies. Different oligomeric structures can also form transmembrane pores, altering calcium ion homeostasis and contributing to cytotoxicity.

In physiological conditions, it is thought to be natively unfolded and its conformation is slightly more compact than a random coil (Eliezer *et al.* 2001). Native α -syn stable tetrameric forms have been observed with nuclear magnetic resonance (NMR), analytical centrifugation and transmission electron microscopy (TEM). Tetramers display α -helix conformations and are resistant to aggregation (Bartels *et al.* 2011, Gurry *et al.* 2013). Different dimeric, trimeric and multimeric forms, as well as partially folded intermediates and kinetically trapped transition states have been reported (Pivato *et al.* 2012, Gould *et al.* 2014, Mor *et al.* 2016, Peelaerts and Baekelandt 2016, Salveson *et al.* 2016). *In vitro*, different oligomeric species with different morphologies, including spherical, chain-like, annular have been observed prior to α -syn fibril formation have been observed. Also, oligomers can be classified by their size into small (2-5

mers), medium (5-15 mers) and large (15-150 mers) oligomers (Cremades *et al.* 2012). The relationship between the various oligomeric forms and the mechanisms of their reciprocal interconversion has yet to be fully clarified. The current paradigm is that α -syn is likely to exist as an equilibrium mixture of unstructured monomer and statistically disfavored helical oligomers, perhaps partially folded at membranes through phospholipid interaction (Meade *et al.* 2019). In live neurons, α -syn conformation is dependent on the protein's localization and/or synaptic activity and it is likely that different multimers are involved in specific functions (Wang *et al.* 2014, Nam *et al.* 2015, Longhena *et al.* 2019). Interestingly, dopamine can stabilize oligomeric intermediates of α -syn and influence their aggregation dynamics by altering α -syn conformation (Conway *et al.* 2001, Outeiro *et al.* 2009). The exact conformational nature of the α -syn toxic form has not yet identified and it is likely that various oligomeric prefibrillary species play a role in toxicity. Interestingly, the presence of LBs and LNs is not considered to be a cause for toxicity on its own, as it may reflect an attempt by the neurons to isolate and/or convert toxic α -syn oligomers into more stable and less toxic fibrillary structures (Lashuel *et al.* 2013). Abnormal levels of α -syn, as a result of increased biosynthesis or impaired degradation, may promote the formation and/or accumulation of oligomers and may play a role in toxicity. Multiplications in the SNCA gene lead to increased α -syn accumulation because of increased protein expression (Chartier-Harlin *et al.* 2004). Various proteolytic systems, including the ubiquitin-proteasome system (UPS) and the autophagy-lysosomal pathway (ALP) take part in the clearance of α -syn from neurons (Tofaris *et al.* 2011). Failure in this systems can lead to higher levels of α -syn and to the generation of aberrant toxic species. These, in turn, can further impair UPS and ALP functionality, generating a positive feedback loop that results in neuronal death (Xilouri *et al.* 2013). Cytotoxicity may arise as a combination of the sequestration of functional α -syn oligomers into non-functional oligomeric forms, with partial loss of α -syn function, and disruption of specific cellular pathways due to the interaction of aberrant α -syn species with membranes, proteins and small molecules inside the cell. Annular protofibrils can form pore-like structures and cause alterations in membrane permeability *in vitro*, resulting in increased calcium influx from the extracellular space and in cell death (Danzer *et al.* 2007, Tsigelny *et al.* 2012). Functional α -syn interacts with tubulin and can regulate microtubule dynamics (Zhou *et al.* 2010, Carnwath *et al.* 2018). It also interacts with a variety of cytoskeletal proteins involved in the maintenance of cell structure and in neuronal protein trafficking (Jensen *et al.* 1999, Alim *et al.* 2002, Thayanidhi *et al.* 2010), including kinesin, dynein, Kinesin Family Member 5A (KIF5A), microtubule-associated

protein 2 (MAP2), tau and actin (Longhena *et al.* 2019). Aberrant accumulation and aggregation of α -syn result in the perturbation of these cellular mechanisms and, in turn, to impaired axonal retrograde and anterograde transport, with disastrous consequences for neuronal function and survival (Volpicelli-Daley 2017). At the synapse level, α -syn aggregation has been showed to alter the size of the reserve pool and to block vesicle docking, with inhibitory effect on neurotransmitter release (Choi *et al.* 2013, Lai *et al.* 2014). It interacts and cooperates with a variety of proteins involved in synaptic vesicle (SV) trafficking, including complexins (Chandra *et al.* 2004), cysteine-string protein- α (CSP- α) (Chandra *et al.* 2005), synphilin (Alvarez-Castelao and Castaño 2011) and Rab proteins (Shi *et al.* 2017). The pathological aggregation of α -syn can alter the intracellular distribution of its presynaptic binding partners and perturbate their function. More specifically, the overexpression of C-terminally truncated (1-120) α -syn resulted in the redistribution of SNAREs, with consequent inhibition of vesicle release *in vitro* and reduced dopamine release *in vivo* (Garcia-Reitböck *et al.* 2010). α -syn overexpression can also affect multiple members of the Rab protein (Rabs) family and impair SV tethering to membranes and ER-Golgi trafficking (Gitler *et al.* 2008). Moreover, overexpression has been showed to alter the levels and distribution of vesicular monoamine transporter 2 (VMAT2), that is responsible for SV DA uptake (Phan *et al.* 2017). Aggregation of α -syn induces redistribution of the dopamine transporter (DAT) in transgenic mice disease (Bellucci *et al.* 2011), suggesting that DAT loss of function may be one of the mechanisms underlying nigrostriatal neuronal loss. The interaction of toxic α -syn species with mitochondrial components results in alterations in mitochondrial dynamics (fission, fusion, transport and autophagy), bioenergetic defects and increased production of ROS implicated in neuron cell death (Faustini *et al.* 2017). Misfolded α -syn can trigger microglial activation (Reynolds *et al.* 2009, Béraud *et al.* 2013) and neuroinflammation can promote PTMs of α -syn, which in turn increase its tendency to aggregation (Gao *et al.* 2008).

Therapeutic approaches targeting α -syn

α -syn is by far the most studied protein in the pathogenesis of PD. It plays a key role in PD pathogenesis and therapies targeting it are under extensive study (Brundin *et al.* 2017). Intracellular accumulation of α -syn is a major risk factor for PD and the various therapeutic strategies aim at the reduction of α -syn levels in neurons. The main approaches are:

1. Reducing α -syn production: RNA interference (RNAi) has shown interesting results, being able to induce a 35-50% reduction of α -syn levels in animal models (McCormack *et al.* 2010,

Zharikov *et al.* 2015). Major challenges in this approach are dosing and specific delivery to target areas to avoid neurotoxicity and peripheral side effects. Another approach to reduce α -syn expression could be to modify the transcription of the SNCA gene. A high-throughput screening identified β_2 -adrenergic agonism as a possible mechanism and β_2 -adrenergic agonist clenbuterol is able to lower α -syn expression in a dose-dependent manner *in vitro* and in wild type mice. In mice, it was also able to protect TH-neurons from MPTP-induced toxicity (Mittal *et al.* 2017).

2. Inhibiting α -syn aggregation: interesting results have been obtained with intrabodies, small antibody fragments (140-250 aa) obtained from the expression of the variable region responsible for antibody specificity as separated from the full length immunoglobulin. They retain the specificity and affinity of conventional antibodies and are able to target intracellular antigens. Various intrabodies showed different specificity for different α -syn species (Bhatt *et al.* 2013) and can bind to monomeric species to prevent them from oligomerizing. Viral vector-mediated delivery of two intrabodies (VH14*PEST and NbSyn87) was able to counteract nigrostriatal degeneration and protect motor function in rats overexpressing α -syn (Chatterjee *et al.* 2018). Other promising approaches rely on the use of small molecules (Price *et al.* 2018) or fusion proteins (Krishnan *et al.* 2014).
3. Promoting the degradation of intracellular α -syn aggregates: targeting enhancement of autophagy is expected to promote the clearance of α -syn pathology. mTOR agonists (rapamycin and its analogs) have shown reduced α -syn aggregation and neurotoxicity in various cell and animal models of PD (Moors *et al.* 2017) but their clinical use is limited by lack of specificity and side effects (immunosuppression). Another strategy to enhance of the autophagy-lysosomal pathway is to increase the expression, stability or delivery of glucocerebrosidase (GCase). Mutated forms of GCase have a reduced ability to degrade α -syn aggregates and are associated with synucleinopathies (Sardi *et al.* 2015). FDA-approved mucolytic Ambroxol is thought to act as a chaperone able to rescue mutated GCase function and is currently being evaluated in two Phase 2 trials.
4. Increasing extracellular α -syn degradation: non cell-permeant antibodies can target extracellular α -syn, reduce its aggregation and improve motor impairment in animal PD models (George and Brundin 2015). This approach poses significant challenges, including prevention of off-target inflammatory reactions, definition of administration protocols and efficacious delivery to the CNS. PRX002, an antibody targeting α -syn, gave promising results

in Phase 1 studies being able to reduce up 96.5% of free serum α -syn (Schenk *et al.* 2017) in front of limited toxicity and acceptable pharmacokinetics (Jankovic *et al.* 2018).

5. Reducing extracellular α -syn uptake: at the present, a limited amount of information is available on the mechanisms of α -syn endocytosis in neurons and glial cells. The main strategies in this direction rely on the interference with α -syn binding to heparin sulfate proteoglycans, which appears to be fundamental for endocytosis (Holmes *et al.* 2013), and on the blockage of LAG3 receptor, involved in the endocytosis of α -syn preformed fibrils (Mao *et al.* 2016).

Synapsins: structure and role in the presynaptic neurotransmission

In chemical synapses, the presynaptic terminal is a highly organized dynamic environment dedicated to the integration of action potentials and their transduction into a chemical signal in the form of neurotransmitter release. Synaptic transmission is triggered when an action potential opens voltage-gated Ca^{2+} channels and the transient Ca^{2+} influx stimulates the exocytosis of presynaptic vesicles (Augustine *et al.* 1985). This group of events relies on vesicle trafficking, which can be divided into sequential steps (Sudhof 2004): first, the vesicles are loaded with neurotransmitter, in a process mediated by substrate-specific active transporters (e.g. VMAT2 for monoamines) and tethered in clusters in the “active zone”, the portion of the membrane that faces postsynaptic density across the synaptic cleft. The vesicles are primed for Ca^{2+} -induced fusion pore opening and for neurotransmitter release. After exocytosis, vesicles are recycled via endocytosis in specific areas adjacent to the active zone (endocytic zone) (Roos and Kelly 1999), and become available to be filled with neurotransmitter and restart the cycle. Vesicle recycling allows for sustained activity and is based on the presence and function of different vesicle pools with different ability to be released (Rizzoli and Betz 2005). The readily releasable pool (RRP) is composed by the vesicles that are docked in the active zone, primed for release and immediately available on stimulation (Rosenmund and Stevens 1996, Schikorski and Stevens 2001). All the vesicles that maintain the physiological level of transduction are classified in the recycling pool, which contains 5-20% of all vesicles and includes the RRP. At physiological levels of stimulation, it is continuously recycled and refills with newly recycled vesicles. The reserve pool (RP) includes vesicles that are not usually involved in neurotransmission but become available when the RRP is depleted after intense stimulation. The type of synapse determines both the total number of vesicles and their distribution in the different pools (Murthy and Stevens 1999, Bollmann *et al.*

2000, Richards *et al.* 2003). Together with synaptic vesicles, other cell structures and presynaptic proteins take part in this highly dynamic process. SNARE proteins (SNAREs) are involved in different stages of vesicle targeting and fusion (Chen and Scheller 2001, Jahn *et al.* 2003). They are characterized by a conserved 70-residue motif (SNARE motif) able to assemble into a quadruple helical bundle called core complex, associating 3 or 4 different SNARE proteins together. The formation of the synaptic core complex between the SNARE motifs of vesicle-associated syntaxin and synaptobrevin and membrane-associated SNAP-25 (Söllner *et al.* 1993) pulls the vesicle and the membrane close together. The assembly of the SNARE complex creates an unstable intermediate which is susceptible of pore formation but is not sufficient for exocytosis on its own. Interaction of the complex with synaptotagmin, a calcium binding protein acting as a Ca^{2+} sensor, promotes pore formation and initiates exocytosis. Other proteins, such as complexins (McMahon *et al.* 1995) and munc-18 (Jahn *et al.* 2003), regulate and promote the complex dynamics. Various Rab proteins, a group of small GTP-binding proteins, mediate different steps of the process by interacting with plasma membranes and several effector proteins (Novick and Zerial 1997, Schimmöller *et al.* 1998). Actin filaments and microtubules are involved in synapse regulation and dynamics (Dent and Kalil 2001, Cingolani and Goda 2008) and are thought to participate in vesicle trafficking and targeting towards the active zone (Hirokawa *et al.* 1989, Cole *et al.* 2000, Shupliakov *et al.* 2002, Sankaranarayanan *et al.* 2003).

Synapsins are a family of three distinct neuron-specific genes (synapsin I, II and III) that encode a group of ten phosphoproteins that regulate synaptic transmission and neurodevelopment (Greengard *et al.* 1993). They are key regulators of multiple steps in SVs dynamics, including the storage and mobilization in the RP, trafficking, fusion with plasma membranes and endocytosis (Hilfiker *et al.* 1999, Gitler *et al.* 2004). They have been proposed to tether SV vesicles to each other to maintain the RP close to the active zone, through the interaction with a matrix of actin filaments (Dresbach *et al.* 2001). Alternative splicing of the synapsins genes transcripts generates different isoforms with two isoforms described for synapsin I and II (Ia, Ib and IIa, IIb, respectively) and six for synapsin III (IIIa-IIIg), with the major one being IIIa (63 kDa) (Porton *et al.* 1999, Porton *et al.* 1999). The structure of the various isoforms consists of a combination of multiple domains: specifically, N-terminal domains A-C are conserved among isoforms, while C-terminal domains D-J are variable. Different isoforms perform different functions, presumably mediated by the isoform-specific combination of C-terminal domains (Song and Augustine 2015) (**Figure 3**).

Domain A contains the phosphorylation site for cAMP-dependent protein kinase (PKA) and Ca²⁺/calmodulin-dependent kinase I (CaMKI) (Hosaka and Südhof 1999). Phosphorylation at this site inhibits the reversible association with vesicle membrane phospholipids and may be central for the regulation of neurotransmitter release (Hosaka *et al.* 1999, Chi *et al.* 2003, Bonanomi *et al.* 2005, Menegon *et al.* 2006). Domain B is only partially conserved among isoforms and is considered to be a linker region between Domains A and C. It hosts the phosphorylation site for the mitogen-activated protein kinase (MAPK), presumably involved in the regulation of synapsins activity (Jovanovic *et al.* 1996). Domain C is the largest domain (300 aa) and the most conserved among isoforms. This region has a central role in synapsins function and mediates the interaction with SV phospholipids and actin (Bähler and Greengard 1987, Bähler *et al.* 1989, Cheetham *et al.* 2003) and homo- and heterodimerization (Font and Aubert-Foucher 1989, Hosaka and Südhof 1999). A portion of the C domain inserts into the hydrophobic phase of phospholipid layers and is thought to mediate the interaction with SV (Benfenati *et al.* 1989, Südhof *et al.* 1989, Stefani *et al.* 1997). The region that penetrates into membranes does not overlap with the regions mediating dimerization, suggesting that dimerization may promote SV clustering (Benfenati *et al.* 1993, Cheetham *et al.* 2001). Domain D is found exclusively in synapsin I isoforms and it may be implicated in the regulation of their interaction with SVs (Gitler *et al.* 2004). Domain E is common to all “a” forms and participates in the formation of dimers and SVs clustering (Monaldi *et al.* 2010), while the exact functions of domains F-I are not completely clear. Domain J is found exclusively in Synapsin-IIIa. It contains multiple sites for MAPK-mediated phosphorylation but its function is largely unknown (Kao *et al.* 1998).

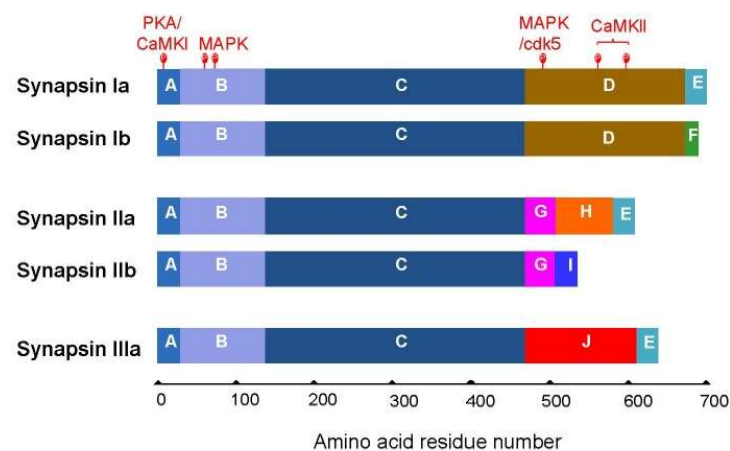


Figure 3: Domain model of the vertebrate synapsin family (from Song *et al.*, 2015)

Synapsin III (Syn-III) was discovered in 1998 and it is the most recently reported member of the synapsins class (Hosaka and Südhof 1998, Kao *et al.* 1998). Its gene is located on chromosome 22 and spans a much larger region of the genome compared to synapsins I and II. Syn-III has a very complex and highly regulated expression: six different mRNAs can be transcribed from the Syn-III gene, corresponding to six different isoforms (IIIa-IIIf). Contrarily to other synapsins, which are found only in the adult brain, the synapsin III mRNAs show differential tissue- and developmental stage-specific expression. More specifically, transcripts IIIa-IIIc are detected in the fetal brain and to a lesser extent in adult brain, III d is detected only in the fetal brain and IIIe-III f are detected only in non-neuronal tissues (Porton *et al.* 1999). In the adult brain, Syn-III expression is much lower than that of synapsin I and II (Kao *et al.* 1998). Syn-III is found in cell bodies and growth cones and shows a wider subcellular distribution compared to synapsin I and II, which almost exclusively localize at the synaptic level (Ferreira *et al.* 2000). Differences in structure, expression and subcellular localization of Syn-III suggest a function distinct from the other two synapsins, even though the interaction with synapsins I and II is required for its proper function (Hosaka and Südhof 1998). According to the current opinion, Syn-III is implicated in the regulation of synaptic neurotransmission and neural development. All three synapsins play a role in neurotransmitter release with different effects on neurotransmission. In both synapsin I and II knockout mice there is depletion of in the RP of SVs, which results in decreased neurotransmission after repeated stimulation (Li *et al.* 1995, Rosahl *et al.* 1995, Ryan *et al.* 1996). Conversely, in Syn-III knockout mice the size of the SV recycling pool is increased but the kinetics of release are slower. In these mice, the density and distribution of the SV pools are unchanged compared to wild-type controls, while neurons lacking Syn-III show a significant reduction of postsynaptic inhibitory currents (Feng *et al.* 2002). In the light of this, synapsins I and II are likely to act as positive modulators of neurotransmission while Syn-III appears to have a negative modulatory action. Interestingly, synapsins I and II are mainly involved in GABAergic and glutamatergic transmission respectively (Gitler *et al.* 2004, Baldelli *et al.* 2007, Gitler *et al.* 2008), while Syn-III is specifically involved in the regulation of DA release in the striatum. In triple knockout mice (TKO, mice lacking all the three synapsins) the release of DA is approximately doubled in response to electrical stimulation and a similar increase is observed in brain slices derived from Syn-III knockout mice (Kile *et al.* 2010). Syn-III is also thought to take part in axonogenesis (Ferreira *et al.* 1994, Chin *et al.* 1995, Ferreira *et al.* 1998) and in neuronal cell development. Neurogenesis is substantially altered in Syn-III knockout mice with a marked reduction in the proliferation and differentiation rate

compared to wild-type controls (Kao *et al.* 2008). Syn-III knockout animals also showed deficits in cognition and emotional processing (Porton *et al.* 2010). Neurodevelopmental disorders are central to psychiatric disorders such as schizophrenia, bipolar disorders and depression. Notably, Syn-III levels are decreased in the prefrontal cortex of patients with schizophrenia (Porton and Wetsel 2007) and a rare polymorphism in the Syn-III gene has been correlated with schizophrenia (Porton *et al.* 2004). These evidences support the idea that alterations in the structure, expression and/or function of Syn-III may be implicated in psychiatric disorders.

Alpha-synuclein/Synapsin-III interaction: pathological relevance in Parkinson's disease and modulators

In recent years, a growing body of evidence supports the role of the interaction between α -syn and Syn-III in the pathogenesis of PD. The co-aggregation of the two proteins inside LBs and LNs has been demonstrated with a variety of experimental techniques and in post mortem PD brain examinations (Longhena *et al.* 2018). Interestingly, synapsin I and synapsin II do not co-localize with α -syn-positive fibrils extracted from the brain of PD patients. Even though α -syn fibrils can incorporate several proteins during their formation, Syn-III appears to be involved in the aggregation mechanisms. Levels of α -syn and Syn-III are correlated in the caudate-putamen, suggesting that these proteins co-dysregulated in the striatum of PD patients and that a pathological interplay exists between the two proteins. Further studies on Syn-III knock out mice overexpressing human α -syn after injection with a viral vector (AAV- α -syn) support the hypothesis that Syn-III is instrumental in α -syn aggregation. In these mice, Syn-III deficiency prevented α -syn aggregation, nigral neuron degeneration and alterations in the expression and/or distribution of α -syn protein interactants after 8 weeks from the injection (Faustini *et al.* 2018). Moreover, α -syn and Syn-III cooperate in the functional regulation of the dopaminergic synapse (Zaltieri *et al.* 2015). Both the absence and the aggregation of α -syn induces alterations in Syn-III expression and distribution at synapses, which is associated with a decrease of DA overflow. The lack of α -syn in α -syn-null transgenic mice is correlated with increased Syn-III levels and reduced DA release, in line with previous studies demonstrating a negative regulatory effect of Syn-III on striatal DA release (Kile *et al.* 2010). Cocaine is able to mobilize a synapsin-dependent pool of synaptic vesicles (Venton *et al.* 2006) and α -syn-null mice show an increased motor response to the administration of cocaine, attributable to the increase of striatal Syn-III. Methylphenidate, like cocaine, is able to modulate DA release (Volz *et al.* 2008) and to modify

overflow and presynaptic compartmentalization of DA through an α -syn-dependent mechanism (Chadchankar *et al.* 2012). Taken together, these results support the idea that drugs which mobilize DA vesicle pools act by regulating the function of α -syn-Syn-III complexes. The loss of α -syn function derived from its aggregation may contribute to the pathological dysregulation of DA release as a consequence of the lack of α -syn-Syn-III-mediated control of synaptic vesicles (Zaltieri *et al.* 2015). In a recent work, Bellucci and coworkers investigated whether the interplay between α -syn and Syn-III could be modulated pharmacologically (Faustini *et al.* 2019). The locomotor response to cocaine and methylphenidate in transgenic mice overexpressing C-terminally truncated (1-120) α -syn (SYN120), wild type mice and α -syn-null mice was evaluated along aging. Interestingly, Syn-III-dependent locomotor response stimulated by methylphenidate is enhanced in the presence of α -syn-Syn-III co-aggregates and elevated levels of α -syn, and this effect looks to be influenced by the conformations of the two proteins and their spatial proximity. *In silico* conformational studies of α -syn bound to methylphenidate highlighted the drug's ability to stabilize a partially folded α -helical conformation with low propensity to aggregation, improved binding to lipids (Rao *et al.* 2010) and improved capacity to form functional complexes with Syn-III. Taken together, this evidence supports the relevance of the interaction between α -syn and Syn-III in the pathogenesis of PD and opens up interesting possibilities for its pharmacological modulation with methylphenidate and analog molecules with improved biological activity.

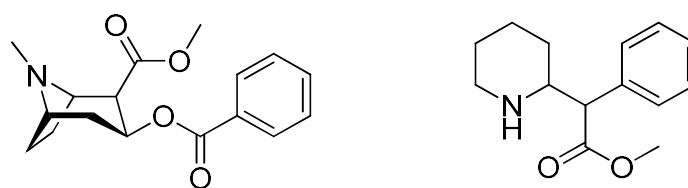


Figure 4: Structure of cocaine (left) and methylphenidate (right)

In literature, several studies on methylphenidate have been carried out in the late 90s and early 00s, trying to deepen the knowledge of its SAR as a CNS stimulant, synthesizing a variety of derivatives and evaluating their biological activity on the dopamine, serotonin and norepinephrine transporters (Gatley *et al.* 1996, Thai *et al.* 1998, Wayment *et al.* 1999, Deutsch *et al.* 2001, Schweri *et al.* 2002, Davies *et al.* 2004, Froimowitz *et al.* 2005, Froimowitz *et al.* 2007, Misra *et al.* 2010).

Aim of the Work

Given the relevance of the α -syn/Syn-III cooperation in the pathogenesis of PD and the modulatory action of methylphenidate on the interaction, methylphenidate analogs could represent a novel therapeutic approach for the treatment of PD. The proposed mechanism of action for these compounds involves the positive modulation of the α -syn/Syn-III interaction through the binding to Syn-III, which in turn could promote α -syn folding into conformations with reduced aggregation propensity.

Aim 1: Design of methylphenidate analogs

Preliminary computational studies were performed in order to identify possible binding sites for methylphenidate on the surface of Syn-III. Firstly, the structural determinants for the binding of cocaine on the dopamine transporter DAT were identified, given the existence of a well-characterized model for the interaction (Uhl and Lin 2003, Volz and Schenk 2005, Vaughan *et al.* 2007, Beuming *et al.* 2008) and the structural similarities between cocaine and methylphenidate. In particular, a negatively charged aspartic acid residue can form an ionic interaction with the tertiary nitrogen, protonated at physiologic pH, while a lipophilic pocket is required to accommodate the aromatic benzoate moiety. In previous crystallographic studies on human Syn-III (Turnbull *et al.* 2007) several negatively charged residues (Asp or Glu) capable of forming similar salt-bridges with the secondary nitrogen of methylphenidate were identified. Computational simulations were performed to identify the Asp and Glu residues at a compatible distance from a lipophilic pocket able to accommodate the aromatic moiety and the sterically not accessible sites were discarded. The number of putative binding sites was restricted to five, in correspondence of Asp98, Glu175, Asp358, Glu361 and Asp379 residues (**Figure 5**).

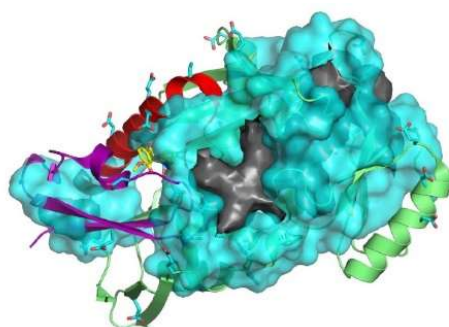
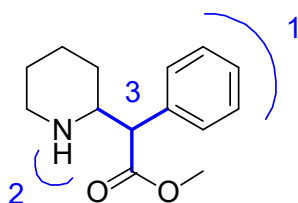


Figure 5: Putative binding sites on the surface of Synapsin-III

Mutagenesis studies were performed in order to define the preferential binding pocket, but the obtainment of suitable primers proved to be especially complex due to the chemical composition of the sequences of interest.

In the design of the analogs, the structure of methylphenidate has been systematically modified and modifications can be organized into three main groups:



1. Group I: Modifications of the phenyl ring:

The phenyl group has been replaced by differently hindered aryl groups, in order to assess the size of the target's lipophilic pocket (I-V, Figure 6). Also, a series of para-substituted derivatives was designed and two have been synthesized so far (VI-VII, Figure 6).

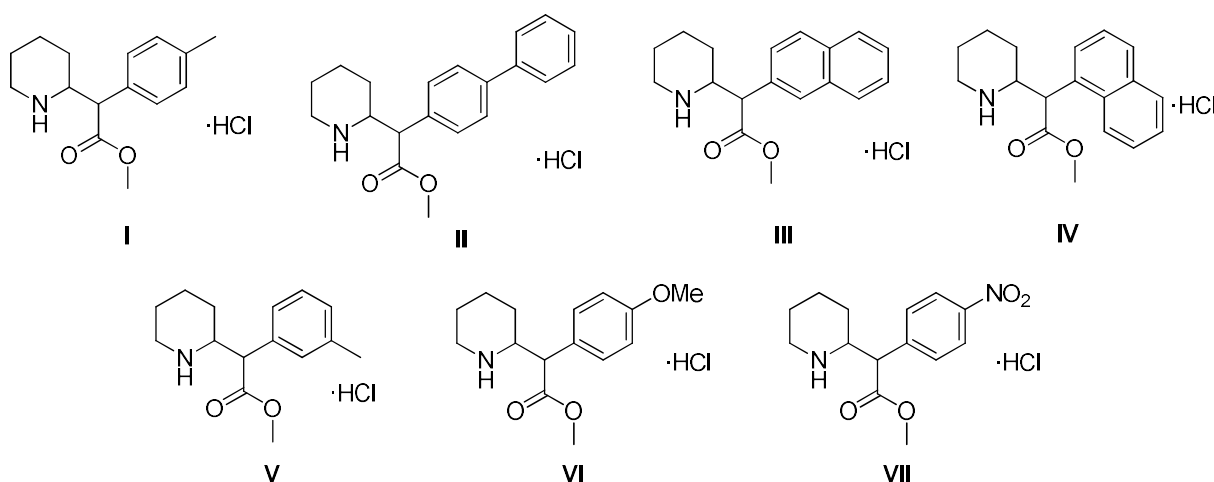


Figure 6: Phenyl ring-modified methylphenidate analogs

Compounds I and II were synthesized as both *threo* and *erythro* racemates, in order to determine the most active configuration.

2. Modification of the secondary amine:

In analogy with cocaine, which shows a tertiary amine, the secondary amine has been methylated, in order to evaluate the effect of different basic properties on the interaction with the target (Figure 7).

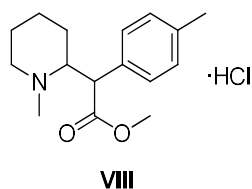


Figure 7

3. Superior homologues:

The distance between the main functional groups of the parent molecule has been modified, in order to evaluate positive structural variations and to attain higher discrimination in the determination of the preferential binding pocket (**Figure 8**).

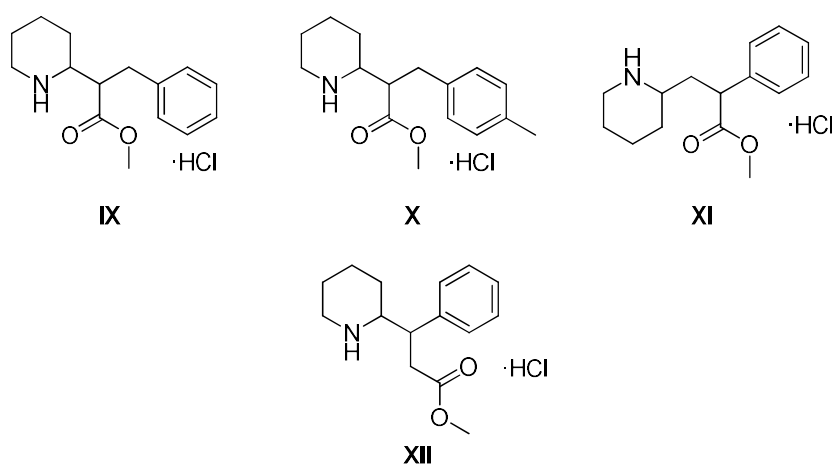


Figure 8: Superior homologues of methylphenidate

Notably, some of the presented analogs had been already synthesized in previous works by various research groups and their SAR as psychostimulants had been studied. Their activities in terms of binding at DAT and inhibition of DA uptake (Compound I, VI, VII (Deutsch *et al.* 1996), Compounds VIII (Wayment *et al.* 1999), Compounds III, IV, IX (Axten *et al.* 1998)) and binding at DAT, SERT and NET (Compounds VI and VII (Gatley *et al.* 1996)) have been evaluated.

Aim 2: Synthesis of methylphenidate analogs

The development or adaptation of synthetic schemes will allow the synthesis of a first series of analogs. All the compounds proposed can exist as two racemates (*threo* and *erythro*) and particular attention will be dedicated to the identification of the active racemate and to its selective or preferential obtainment.

Aim 3: Biological evaluation of the synthesized analogs

A group of biological assays will be developed and employed to evaluate the effect of the analogs on the α -syn/Syn-III interaction and on the formation of α -syn aggregates. In addition, the neurotoxicity of the analogs will be assessed using specific assays.

Aim 4: Computational analysis of the results

The obtainment of SAR data for this class and their integration with computational simulations will support the identification of the preferential binding pocket or the development of a pharmacophore model.

In this context, methylphenidate analogs are designed and synthesized both as possible novel therapeutic agents and as tools to elucidate the binding to Syn-III.

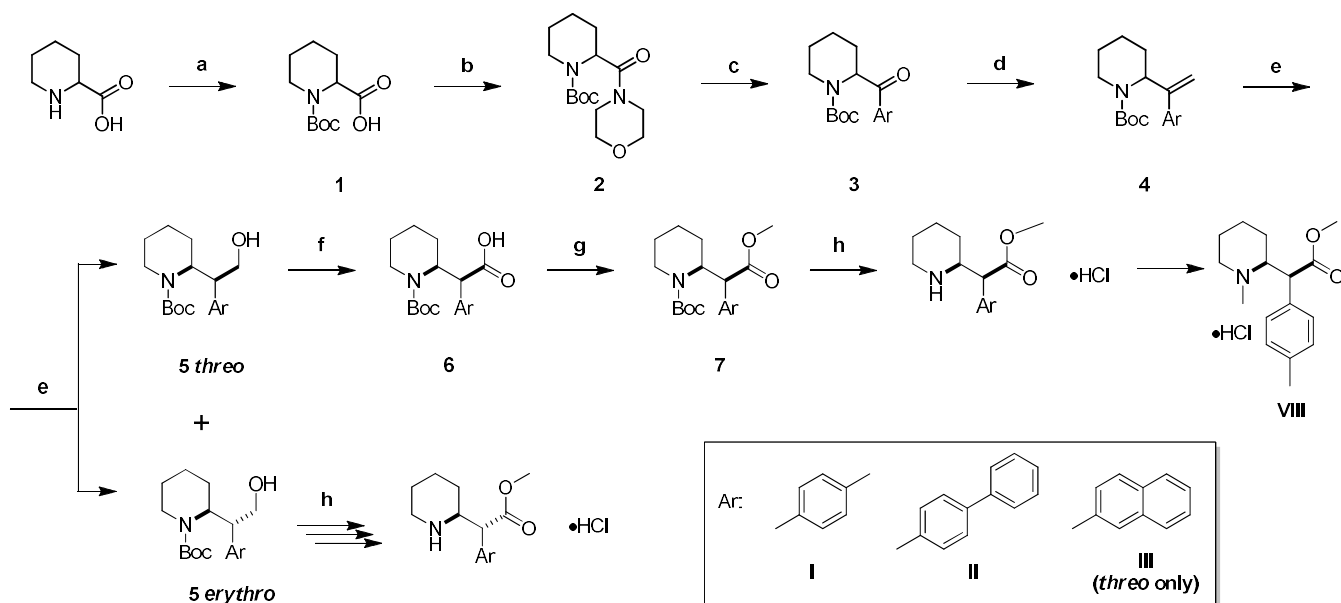
Materials and Methods

Chemistry

The attempt to develop or adapt a single modular and flexible synthetic scheme for a large number of analogs was hampered by substantial substrate-dependent differences in reactivity, regiochemistry and stereochemistry and different synthetic schemes had to be followed for the different compounds.

The synthetic Scheme initially adopted, based on the one proposed by Thai and coworkers (Thai *et al.* 1998) (**Scheme 1**). The synthesis started from commercially available racemic pipecolic acid, whose amine function was protected with Boc carbonate (**1**), prior to conversion into the corresponding morpholine amide **2**, using TBTU as coupling agent. The consecutive reaction with the suitably substituted aryl lithium salt, generated *in situ* by the treatment of the corresponding aryl bromides with *n*-BuLi, afforded aryl ketones **3a-c**. The carbonyl function then underwent Wittig reaction with methyltriphenylphosphonium bromide, accomplishing vinyl aryl derivatives **4a-c**, which were then converted into the respective primary alcohols **5a-c** *via* hydroboration.

At this stage, the *threo* and *erythro* racemates, resulting from the generation of the second stereocenter, were readily isolated through separation on column chromatography in silica gel, and then oxidized to the corresponding carboxylic acids **6a-c**. Subsequent reaction with trimethylsilyldiazomethane led to accomplish methyl esters **7a-c**, whose amine function underwent deprotection in acidic conditions, affording compounds **I**, **II** and **III**. The treatment of **I** with formic acid and formaldehyde in reductive amination conditions yielded compound **VIII**.



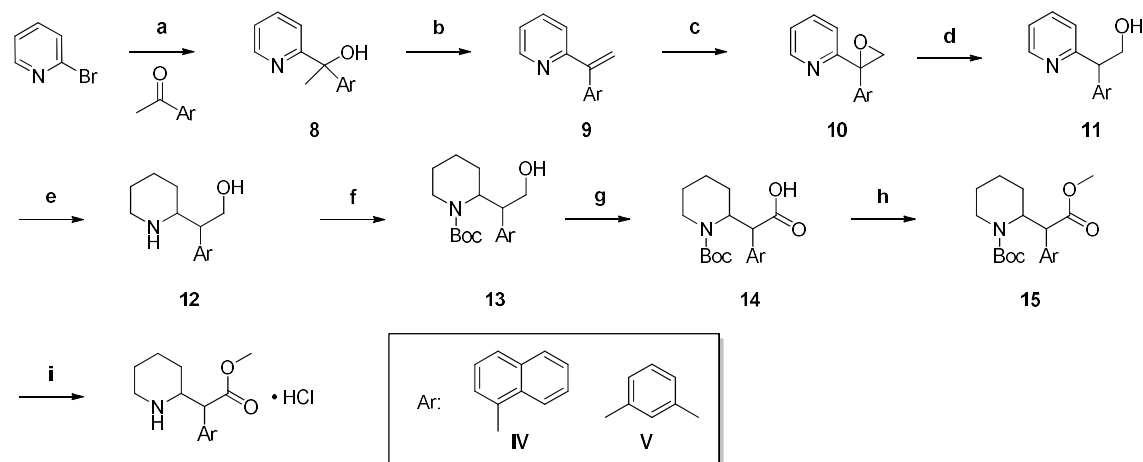
Scheme 1

Reagents and conditions: (a) Boc_2O , TEA, MeOH, 50°C /RT; (b) TBTU, TEA, morfoline, RT; (c) ArBr, $n\text{-BuLi}$, THF, -78°C ; (d) $\text{PPh}_3\text{CH}_3\text{Br}$, $t\text{BuOK}$, THF, RT; (e) $\text{BH}_3\text{-THF}$, H_2O , NaOH, H_2O_2 , THF, RT, (f) PDC, DMF, RT; (g) TMSCHN_2 , toluene, MeOH; (h) HCl/MeOH, RT to 60°C ; (i) HCOOH , formaldehyde, 18 h, 50°C .

This scheme relies on the formation of a C-C bond *via* extremely sensitive Weinreb ketone synthesis. The reaction gave very unpredictable outcomes depending on the arylbromide used and was not suitable for the synthesis of some of the bulkier derivatives we were most interested in (e.g. **Compound IV**).

The attempt to circumvent the most troublesome steps of the initial Scheme led to a series of downstream modifications, with the definition a new synthetic scheme (Scheme 2) that solved some of the issues of the initial approach. In this alternative Scheme, the formation of the C-C bond is obtained in the first step with the reaction of a suitable acetophenone with the 2-pyridil lithium salt, obtained *in situ* from 2-bromopyridine, to give the biaryl tertiary alcohols **8** with consistently good yields. In the following steps, **8** get easily dehydrated to afford the corresponding diarylalkenes **9** and then converted into epoxides **10** in a 2-step hydroxybromination/substitution reaction. Regioselective reduction in Hydrogen Transfer conditions gives the primary alcohols **11**, which in turn undergo Pt-catalyzed hydrogenation of the pyridyl ring to yield piperidyl derivatives **12**. Oxidation to carboxylic acids **14** in a TEMPO-mediated oxidation protocol and subsequent esterification and deprotection afford the final products. In the evaluated reaction conditions for hydrogenation step **e** we observed the predominant formation of the *erythro* isomers (approx. 80:20 ratio). Our limited interest in

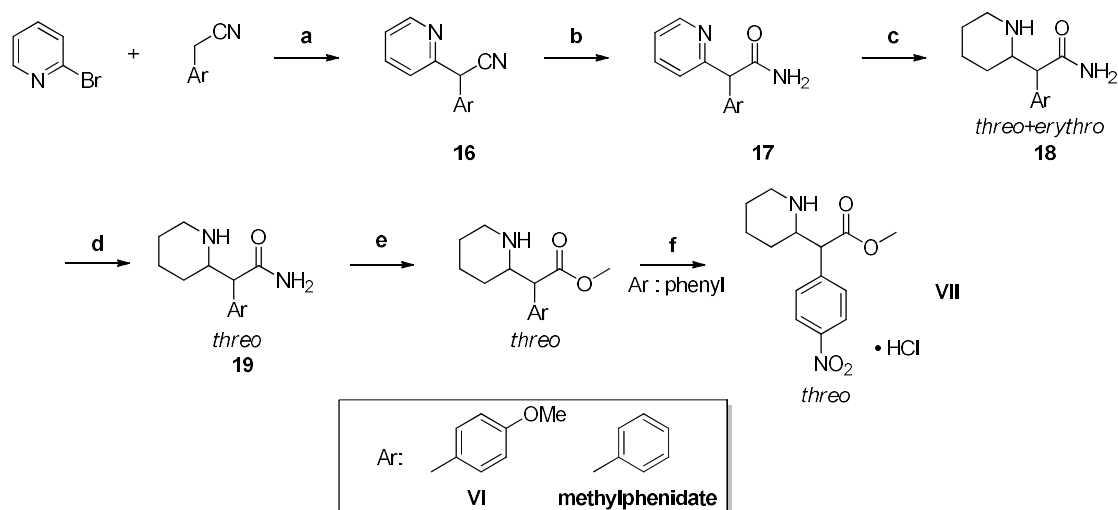
erythro racemates (see *Results and Discussion*) and the lengthiness of the scheme prompted us to the evaluation of other alternative schemes.



Scheme 2

Reagents and conditions: (a) *n*-BuLi, THF, -78°C to -20°C; (b) H₂SO₄; (c) 1- NBS, dioxane, H₂O, 2 – NaOH, IPA; (d) NH₄COOH, Pd/C; (e) H₂ (5 atm), Pd/C, 70° C, AcOH, HCl/Et₂O; (f) Boc₂O, TEA, DCM; (g) TEMPO, NaClO₂, NaClO, DCM/phosphate buffer; (h) TMSCHN₂, toluene, MeOH; (i) HCl/MeOH.

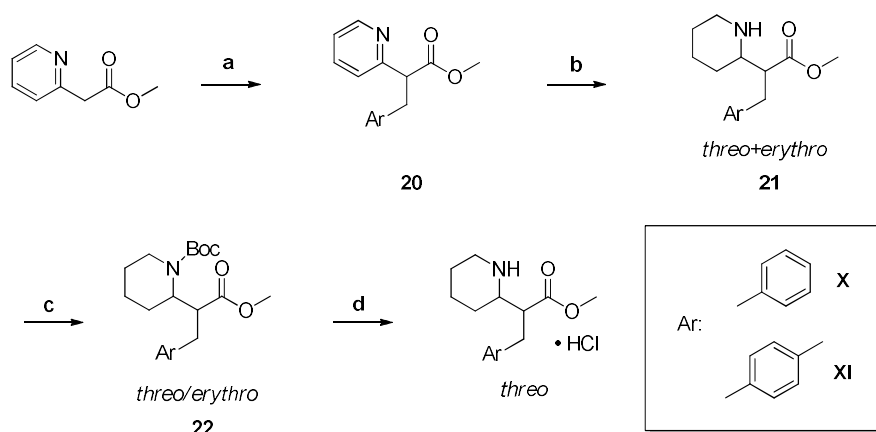
In **Scheme 3**, adapted from the one proposed by Xing and coworkers (Xing *et al.* 2017), a suitable phenylacetonitrile is alkylated at the benzylic position with 2-bromopyridine, to give pyridylarylacetonitriles **16**. Hydrolysis of the cyano group affords the corresponding amides **17** and subsequent catalytic hydrogenation leads to piperidyl- derivatives **18** as a mixture of *threo* and *erythro* racemates. Epimerization of amides **19** with *t*BuOK completely converts the mixture in the single *threo* racemate. Conversion of the amide into methyl ester affords either **Compound VI** or methylphenidate. Methylphenidate undergoes classic nitration reaction to give **Compound VII**.



Scheme 3

Reagents and conditions: (a) NaNH_2 , toluene, RT; (b) H_2SO_4 , RT; (c) H_2 , Pd/C, AcOH, 70°C ; (d) $t\text{BuOK}$, toluene, 70°C ; (e) HCl/MeOH; (f) H_2SO_4 , HNO_3 , 0°C .

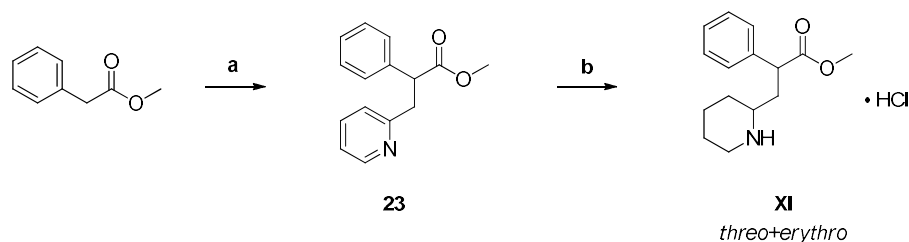
For the synthesis of **Compound X-XI (Scheme 4)** commercially available methyl 2-pyridylacetate is alkylated with either benzyl bromide or 4-methylbenzyl bromide to afford methyl 2-(2-pyridyl)-3-arylpropanoate derivatives **20**. Catalytic hydrogenation gives 2-piperidyl derivatives **21** as a mixture of *threo* and *erythro* racemates. Protection of the piperidine nitrogen with Boc allows for the separation of racemates by column chromatography on silica gel and subsequent deprotection of the isolated *threo* racemate with excess 2N HCl/MeOH yields the final compounds as hydrochloride salts.



Scheme 4

Reagents and conditions: (a) 1) $t\text{BuOK}$, THF, 2) ArCH_2Br (b) H_2 (1.5 atm), Pt_2O (cat.), HCl conc., MeOH; (c) Boc_2O , TEA, DCM; (d) HCl/MeOH.

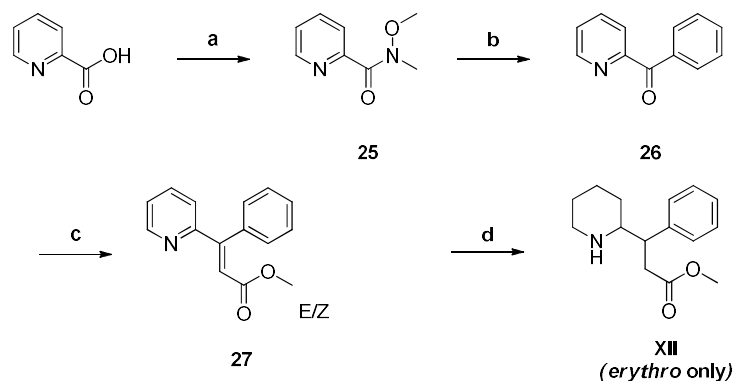
In a similar fashion (**Scheme 5**), **Compound XII** is synthesized starting with the alkylation of commercially available methyl phenylacetate with 2-(bromomethyl)pyridine to give methyl 3-(2-pyridyl)-2-phenylpropionate **23**. Reduction via catalytic hydrogenation gives 3-piperidyl derivative **24** as a mixture of *threo* and *erythro* racemates. Unfortunately, neither the *N*-Boc or bulkier *N*-Cbz compounds are separable into single racemates and strategies for purification are now under evaluation.



Scheme 5

Reagents and conditions: (a) 2-(bromomethyl)pyridine hydrobromide, *t*BuOK, THF (b) H₂ (1.5 atm), Pt₂O (cat.), HCl conc., MeOH.

In the synthesis of **Compound XIII** (**Scheme 6**), commercially available 2-picolinic acid is converted into the corresponding Weinreb amide **25** and treated with phenyllithium to give biarylketone **26**. Wittig-Horner reaction with diethylmethylphosphonacetate affords **27** as a mixture of *E* and *Z* isomers, that are not separated and undergo catalytic hydrogenation to reduce both the olefin and the pyridyl ring. The stereoselectivity of the hydrogenation step is heavily biased with nearly total selectivity for the *erythro* form and strategies to obtain the *threo* racemate in reasonable yields are now under evaluation.



Scheme 6

Reagents and conditions: (a) *N,O*-dimethylhydroxylamine hydrochloride, CDI, DCM; (b) phenyllithium, THF, -20° C; (c) diethylmethylphosphonacetate, NaH; (d) H₂ (1.5 atm), Pt₂O (cat.), HCl conc., MeOH.

Acceptor Photobleaching Fluorescence Resonance Energy Transfer (FRET)

Human neuroblastoma SK-N-SH cells were grown in complete medium comprising Dulbecco's modified Eagle's medium with 1000 mg glucose/l supplemented with 10% heat-inactivated fetal bovine serum, 100 µg/mL penicillin and 100 µg/mL streptomycin. Cells were maintained at 37°C under a humidified atmosphere of 5% CO₂ and 95% O₂. For FRET studies, SK-N-SH cells were seeded onto poly-D-lysine-coated 13 mm glass coverslips in 24-well plates (15000 cells per coverslip) and were maintained in differentiation medium for ten days by daily adding 10 µM retinoic acid to the medium. At day 7, cells were transiently transfected with pGFP-human Syn-III (transducing human green fluorescent protein (GFP)-tagged Syn-III and pCMV6-RFP- α -syn (transducing red fluorescent protein (RFP)-tagged α -syn) constructs, by using Lipofectamine 3000, according to the manufacturer's instructions. pCMV6-RFP- α -syn single-transfected cells were used as negative controls during the FRET experiments. Three days after transfection, cells were treated for 15 min with vehicle (normal saline 0.9% - control), 10 µM MPH (*d-threo*), 10 µM PK1, 10 µM PK2, 10 µM PK3, 10 µM PK4 or 10 µM PK6, then immediately fixed with Immunofix for 15 min and subsequently mounted on glass slides. Fixed cells were analyzed by means of a Zeiss confocal laser microscope LSM 880 (Carl Zeiss) with the laser set on $\lambda=488-543$. After identifying double positive cells three-to-six regions of interest (ROI) were analyzed for 4 series. Two images of basal condition (Pre-bleaching) were acquired before bleaching the RFP acceptor fluorophore with laser 543 set at 65% power. Then, other two images were acquired after the bleaching (Post-bleaching). The FRET efficiency (intended as the GFP recovery after RFP photobleaching) was measured by using Zen black software (Carl Zeiss). The average intensity of the background (outside the cell) was subtracted from the average intensity of the ROI and all the FRET values resulting from the different ROI were used for statistical analysis.

Fluorescence Lifetime Imaging Microscopy (FLIM)-based FRET

Human neuroblastoma SK-N-SH cells were grown in complete medium comprising Dulbecco's modified Eagle's medium with 1000 mg glucose/l supplemented with 10% heat-inactivated fetal bovine serum, 100 µg/mL penicillin and 100 µg/mL streptomycin. Cells were maintained at 37°C under a humidified atmosphere of 5% CO₂ and 95% O₂. For FRET/FLIM studies, SK-N-SH cells were seeded onto poly-D-lysine-coat 1.7 cm² glass chamber (15000 cells per well) and were maintained in differentiation medium for ten days by daily adding 10 µM retinoic acid to the medium. At day 7, cells were transiently transfected with pGFP-human Syn-III (transducing human green

fluorescent protein (GFP)-tagged Syn-III and pCMV6-RFP- α -syn (transducing RFP-tagged α -syn) constructs, by using Lipofectamine 3000, according to the manufacturer's instructions. pCMV6-RFP- α -syn single-transfected cells were used as negative controls during the FRET experiments. Three days after transfection, cells were placed under a confocal Zeiss LSM 880 microscope, operated with ZEN software (Zeiss), equipped with an environmental chamber that maintains the temperature at 37 °C and with a supply of humidified 5% CO₂ to the cells. Cells were imaged with 488 and 594 nm confocal lasers for GFP and RFP, respectively, with a 63 \times oil immersion objective, immediately prior to FLIM) of the same field of view. Cells were treated with vehicle (normal saline 0.9% - control), 10 μ M MPH (*d-threo*), 10 μ M PK1, 10 μ M PK3 or 10 μ M PK6 and the image were recorded 15 min after the treatment. The time-domain FLIM was measured using a Time-Correlated Single Photon Counting (TCSPC) (PicoQuant) operated with SymPhoTime 64 software (PicoQuant). The two-photon laser (Chameleon) integrated with a Zeiss 880 microscope and operated with ZEN software generated the required pulsed illumination with a repetition rate of 80 MHz and pulse width of 500 fs. For GFP excitation, the wavelength was set to 860 nm. The images of GFP fluorescence generated in ZEN software were stored and processed with SymPhoTime 64. The mean fluorescence intensities within cell body were determined using the ROI tool in SymPhoTime 64. The mean intensity of the background measured in several regions that did not contain cells was further subtracted from the fluorescence intensity data. The fluorescence lifetime analysis was performed in the SymPhoTime 64 software within the cell body, automatically recognized by the software as ROI 0. Individual photon arrivals were detected using a SPAD detector and events were recorded by a PicoHarp 300 TCSPC module. Mono and bi exponential fittings were obtained for GFP alone and in the presence of RFP, respectively. The samples of GFP alone were performed under identical conditions in the absence of RFP. The percentage FLIM-FRET efficiency was calculated as: $100 \times [1 - (\text{lifetime of donor with FRET}/\text{lifetime of donor without FRET})]$. For lifetime analysis, fifteen cells were recorded for each condition, included GFP alone.

Immunocytochemistry

Human neuroblastoma SK-N-SH full length (fl) α -synuclein stable clones were seeded onto poly-D-lysine-coated glass coverslides in 24-well plates and were grown in complete medium comprising Dulbecco's modified Eagle's medium with 1000 mg glucose/l supplemented with 10% heat-inactivated fetal bovine serum, 100 μ g/mL penicillin and 100 μ g/mL streptomycin. Cells were maintained at 37°C under a humidified atmosphere of 5% CO₂ and 95% O₂. At 80% confluence, cells underwent glucose deprivation (GD) in order to induce α -syn aggregation (Bellucci *et al.* 2008). Briefly, GD was performed through an incubation of the cells with Hank's balanced salt solution supplemented with 2 mM glutamine and 10% heat-inactivated fetal bovine serum, for 1 h at 37 °C. Then this medium was removed and replaced either with complete medium or with complete medium plus 10 μ M methylphenidate (*d-threo*), 10 μ M PK1 or 10 μ M PK6. After 24 h of treatment, cells were fixed by incubating for 15 min in 4% paraformaldehyde with 4% sucrose in 1 M PBS, pH 7.4; the fixed cells were then stored in PBS-containing 0.05% sodium azide. Slides were incubated for 1 h at room temperature in blocking solution [2% w/v bovine serum albumin (BSA) plus 3% v/v normal goat serum in PBS], then overnight at 4°C with the primary antibody (Syn211 antibody against α -syn) at the optimal working dilution. On the following day, cells were incubated for 1 h at room temperature with the Cy3-conjugated secondary antibody diluted in 0.1% Triton X-100 PBS plus BSA 1 mg/mL. Finally, cell nuclei were counterstained with Hoechst 33258 dye, and the coverslips were mounted onto glass slides using Vectashield.

Primary Mesencephalic Neuronal Cultures and 3-(4,5-dimethylthiazol-2-yl)-2,5-diphenyltetrazolium Bromide (MTT) Assay

The cytotoxic effect of compounds treatment was measured by evaluating mitochondrial dehydrogenase activity using the MTT salt assay. Primary neuronal cultures from mesencephalic tissues were dissected from C57BL/6J 13-days embryos. Briefly, after mechanical dissociation the single cells were re-suspended in Neurobasal medium containing 100 μ g/mL penicillin, 100 μ g/mL streptomycin, 0.5 mM glutamine and 1% B27 supplement. Cells were then centrifuged and cell count and viability assays were performed using the Trypan Blue exclusion test. Cells were seeded onto poly-D-lysine-coated glass coverslides in 24-well plates (14 μ g/mL) for immunocytochemistry (100000 cells/well). Cells were maintained at 37°C under a humidified atmosphere of 5% CO₂ and 95% O₂ for at least 10 days in vitro (DIV 10) prior to their use to allow

their maturation. At DIV 10, cells were treated with 10 μM methylphenidate or increasing concentrations (0.01 μM – 0.1 μM – 1 μM – 10 μM – 100 μM) or the different compounds (PK1, PK2, PK3, PK4, PK6). Twenty-four h after the treatments, culture medium was removed and 300 μL of MTT 0,5 mg/mL diluted in culture medium was added to each well. After 90' incubation at 37°C, the medium was removed and 250 μL aliquots of DMSO were added to each well to solubilize the formazan crystals. Absorbance was measured at 570 nm using a microplate reader. Cell viability was expressed as absorbance value.

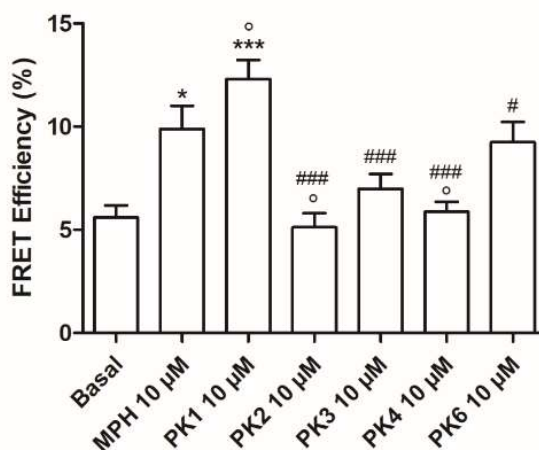
Results and Discussion

Note: some of the compounds shown are currently undergoing a patenting process and the relationships between their structures and their activities are considered confidential. Therefore, the use of two different numbering systems in the *Aim of the Work* section and in the *Results and Discussion* section is intentional.

Acceptor Photobleaching Fluorescence Resonance Energy Transfer (FRET)

In order to understand how the compounds could affect the interaction between α -syn and Syn-III, an acute 15 min treatment was performed on SK-N-SH cell culture overexpressing Syn-III-GFP together with α -syn-RFP. In FRET, an increase with energy transfer between the donor-acceptor fluorophore pair (GFP-Syn-III/RFP- α -syn) is directly correlated with increased spatial proximity and, presumably, with an increased interaction between the two proteins.

In Acceptor Photobleaching FRET, after the identification of double positive cells, three-to-six ROI were analysed for 4 series. Two images of basal condition (Pre-bleaching) were acquired before bleaching the RFP acceptor fluorophore with laser 543 set at 65% power. Then, other two images were acquired after the bleaching (Post-bleaching). The FRET efficiency, intended as the GFP recovery after RFP photobleaching, was measured in the selected ROI. Negative controls were also performed to confirm the specificity of FRET signal. Briefly, in order to assess that GFP signal recovery was directly dependent on RFP bleaching, FRET efficiency was measured on pCMV6-RFP- α -syn single-transfected cells. Results (not shown) supported the absence of photobleaching recovery in single pCMV-RFP- α -syn-transfected cells.



* P < 0.05 vs Basal; *** P < 0.001 vs Basal; ° P < 0.05 vs MPH; # P < 0.05 vs. PK1; ### P < 0.001 vs. PK1.
One-way ANOVA + Newman Keuls Comparison test

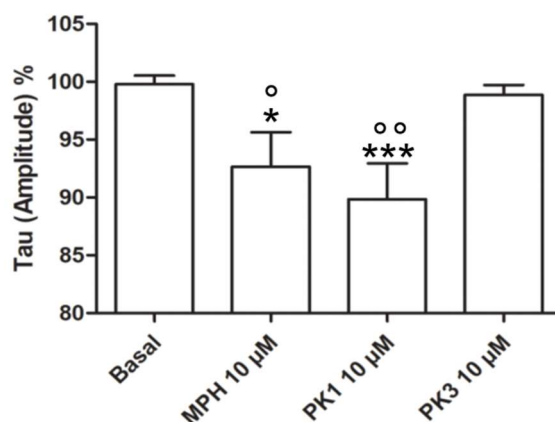
Figure 9

The evaluation (**Figure 9**) of PK1 (*threo*) showed a significant increase in the FRET efficiency both compared to basal level and MPH. No significant increase was observed for the PK3 (same compound, *erythro*), indicating that *threo* is the active configuration. Of note, the more sterically hindered derivatives PK2 (*threo*) and PK4 (*threo*) did not show any increase in FRET efficiency compared to baseline, suggesting a limited size for the hydrophobic domain of the binding pocket. Interestingly, *N*-methylation had a detrimental effect on activity, as shown by the significant decrease in FRET efficiency between PK1 and its *N*-methyl analog PK6.

Fluorescence Lifetime Imaging Microscopy (FLIM)-based FRET

Fluorescence lifetime is defined as the average time that a fluorophore spends in the excited state after the absorption of light, prior to returning to the ground state by emitting a photon. Donor fluorescence lifetime is decreased when FRET occurs between the fluorophore pair. The comparison of the lifetimes of the donor alone and in presence of the acceptor allows for precise and concentration-independent measurements of FRET efficiency. In order to evaluate the effect of MPH analogs on the α -syn/Syn-III interaction, SK-N-SH cells were transfected with pGFP-human Syn-III (transducing human green fluorescent protein (GFP)-tagged Syn-III) and pCMV6-RFP- α -syn (transducing RFP-tagged α -syn) constructs. Cells were treated with vehicle (normal saline 0.9% - control), 10 μ M MPH, 10 μ M PK1, 10 μ M PK3 or 10 μ M PK6 for 15 min. GFP excitation was obtained at 860 nm and fluorescence lifetime was recorded in presence and in absence of

RFP, in the same conditions. For lifetime analysis, fifteen cells were recorded for each condition, included GFP alone.



* P < 0.05 vs Basal; *** P < 0.001 vs Basal; ° P < 0.05 vs PK3; ° ° P < 0.01 vs PK3
One-way ANOVA + Newman Keuls Comparison test

Figure 10

FLIM-FRET assays on PK1 and PK3 (**Figure 10**) confirm that the *threo* isomer promotes the α -syn/Syn-III spatial proximity and, presumably, their interaction. This assay also shows no significant effect for the *erythro* isomer and confirms the results of FRET in the determination of the active configuration.

Immunocytochemistry

Immunocytochemistry relies on the visualization of specific cellular components with the aid of fluorescent antibodies on fixated cell samples. Indirect techniques involve a primary antibody with high selectivity for the imaging target and a secondary fluorescent antibody with affinity for the primary one.

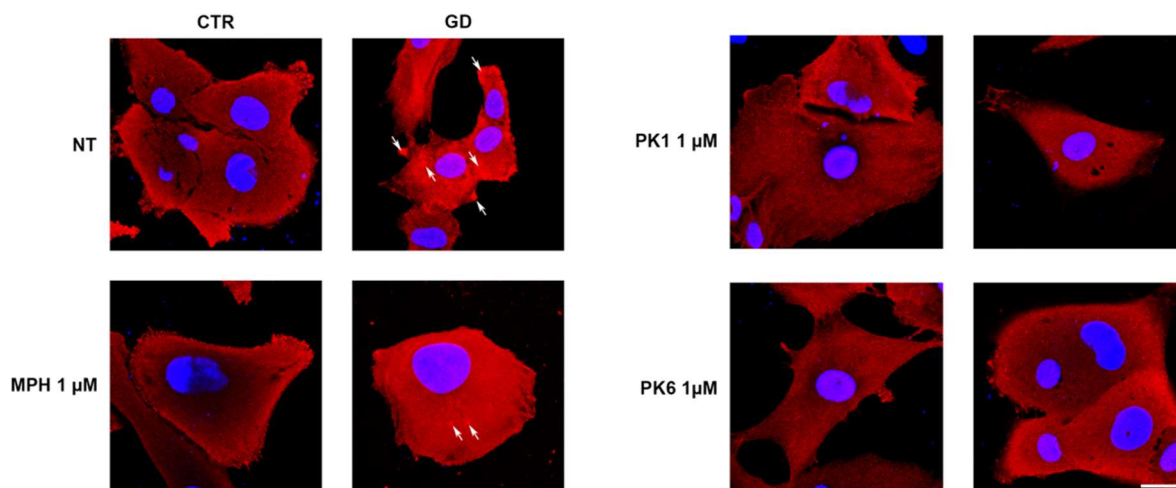


Figure 11

Human neuroblastoma SK-N-SH cells overexpressing α -syn underwent glucose deprivation (GD) for 1 h to induce α -syn aggregation. Their culture medium was removed and replaced either with complete medium or with complete medium plus 1 μ M MPH (*d-threo*), 1 μ M PK1 or 1 μ M PK6. Cells were then fixated and incubated at first with the primary antibody (Syn211 antibody against α -syn) and subsequently with the Cy3-conjugated antibody.

This set of preliminary results shows (**Figure 11**) a reduction in the formation of α -syn aggregates (white arrows) induced by GD in neuroblastoma cells treated with MPH compared to non-treated (NT) cells. Interestingly, after treatment with PK1 and PK6 no aggregates were observed, suggesting a positive effect of these compounds on α -syn misfolding and supporting a neuroprotective effect. Further evaluations, including the quantitative analysis of the results, are ongoing.

3-(4,5-dimethylthiazol-2-yl)-2,5-diphenyltetrazolium Bromide (MTT) Assay

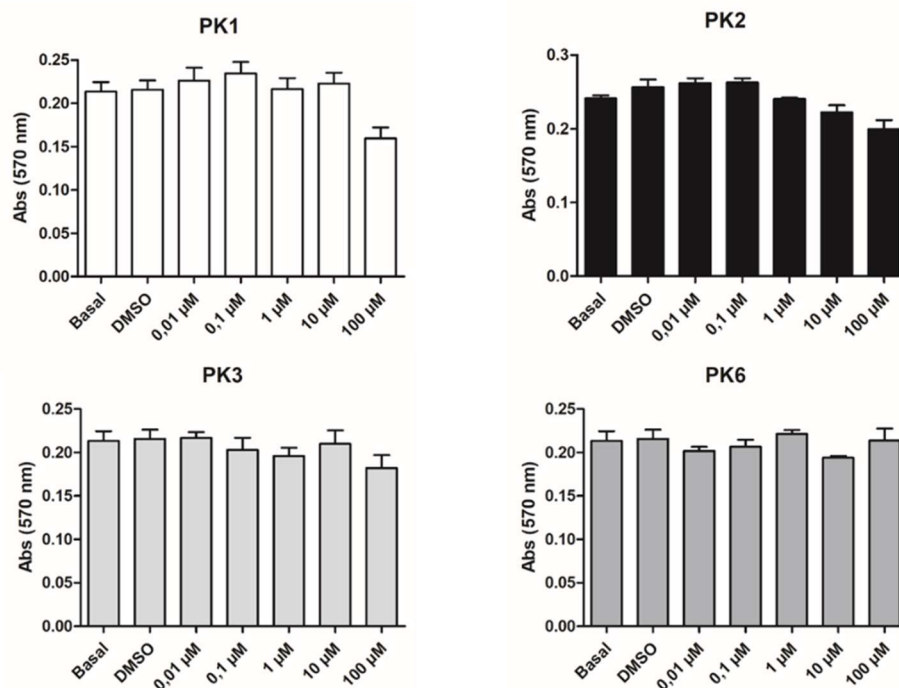


Figure 12

The MTT assay is a colorimetric assay for the evaluation of cell metabolic activity. The water soluble tetrazolium dye (MTT) is reduced by mitochondrial dehydrogenases to the water insoluble formazan salts, which has a purple color. Quantification of absorbance at a specific wavelength gives a measurement of cell viability in terms of variations in metabolic activity. Primary mesencephalic cells were treated with increasing concentrations (0.01 μM – 0.1 μM – 1 μM – 10 μM – 100 μM) of the different compounds (PK1, PK2, PK3, PK6) and incubated with MTT 24 h post treatment. Absorbance was measured at 570 nm and cell viability is expressed as an absorbance value.

MTT assays (**Figure 12**) showed significant decrease in cell viability after exposure only at high or very high concentrations (10-100 μM). In the light of that, the compounds assayed are considered to have low to very low cytotoxicity.

As mentioned earlier in the text, some of the compounds shown have been evaluated for their effects on monoaminergic transmission. These effects are certainly to be taken into account for a complete description of the analogs pharmacology. However, at the present moment, the limited availability of activity data on the α -syn/Syn-III interaction prevents the definition of a detailed SAR and the comparison with the structural determinants of monoaminergic activity.

Specifically, the acquisition of binding data through cell-free assays (e.g. ITC: Isothermal Titration Calorimetry, CD: circular dichroism) could provide valuable insight in the elucidation of this subject.

Conclusions and Future Work

Taken together this evidence suggest the ability of some of the analogs to promote α -syn/Syn-III interaction. Specifically, for PK1 the effect was more marked than the one observed for MPH. Presumably, this effect also translates in increased neuroprotective activity and corroborates the idea that the interaction between the target proteins is involved in α -syn aggregation and, ultimately, in the pathogenesis of PD. These results, together with the very limited cytotoxicity observed, support our interest in the development of this class of analogs as novel antiparkinsonian agents.

In this work, we identified methylphenidate analogs with promising neuroprotective activity and low cytotoxicity. The synthetic schemes for the synthesis of a larger group of compounds were developed, as well as specific biological assays to evaluate their modulatory activity on the α -syn/Syn-III interaction and their ability to reduce α -syn aggregation.

Future directions for this project will include:

- The synthesis of a larger number of compounds and their biological evaluation in order to expand the SAR of the class. The very first goals will be the completion of the sterically hindered and para-substituted series and the biological evaluation of the superior homologues;
- The acquisition of further *in vitro* binding data and the completion of the ongoing computational studies, with the goal to restrict the number of possible binding pockets and, possibly, to identify the preferential one;
- The employment of fluorescence microscopy techniques to quantify the effect of the analogs on dopaminergic vesicle trafficking, in order to better characterize their mechanism of action;
- The evaluation of the pharmacokinetics of the most promising compounds with the aid of mass spectrometry techniques.

Experimental

Starting materials and solvents were purchased from commercial suppliers and were used without further purification. Reaction conditions and yields were not optimized;

^1H and ^{13}C NMR spectra were acquired on a Varian 300 Mercury NMR spectrometer operating at 300 MHz for ^1H NMR, and 75 MHz for ^{13}C NMR; the chemical shifts are reported in ppm. Signal multiplicity is used according to the following abbreviations: s= singlet, d= doublet, dd= doublet of doublets, t = triplet, td= triplet of doublets, q = quadruplet, m = multiplet, sept= septuplet, and bs= broad singlet;

Melting points were measured either on a Büchi Melting Point B-540 apparatus or a TA Instruments Q20 DSC system;

TLC were performed on standard analytical silica gel layers (thickness 0.20 mm; Macherey-Nagel ALUGRAM SIL G/UV254);

Chromatographic purifications were performed, in normal phase, using Biotage instruments (Isolera or SP1) over different Biotage SNAP Ultra flash chromatography cartridges, filled of Merck Silica Gel 60 (0.040-0.063 μm).

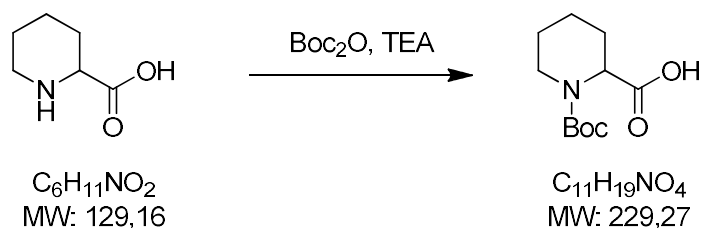
The final Compounds purity was assessed on **HPLC** by using Elite LaChrom HPLC system with diode array detector (190–400 nm) and a Water XBridgeTM C-18 column (5 μm , 4.6x150mm). The specific method is here reported and proved to be effective in separating threo and erythro isomers.

Time (minutes)	Solvents %		Flow rate (mL/min)
	Water +TFA 1‰	ACN + TFA‰	
0	90%	10%	1
20	10%	90%	1
25	10%	90%	1
30	90%	10%	1
35	90%	10%	1

The HPLC method was set up using a Water XBridgeTM C-18 column flushed with freshly prepared 90% Water/10% ACN + TFA 1‰ until column pressure was stable. All the investigated samples were prepared through dissolution of the purified products in the selected mobile

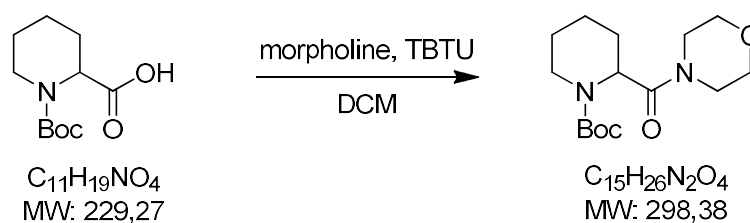
phase, at the approximate concentrations of 1 mg/mL, filtered through a 0.45 μm filter and analyzed. The injection volume was 20 μL . Owing to the presence of the substituted phenyl ring in each compound, purity was evaluated on chromatograms recorded at 217 nm.

Abbreviations used: ACN: acetonitrile; DCM: dichloromethane; DMF: dimethylformamide; DMSO: dimethylsulfoxide; EDAC: 1-Ethyl-3-(3-dimethylaminopropyl)carbodiimide; EDTA: ethylenediaminetetraacetic acid; HOBt: hydroxybenzotriazole; IPA: isopropyl alcohol; IPE: diisopropylether; mp: melting point; MW: molecular weight; NBS: *N*-bromosuccinimide; RT: room temperature; TBTU: *O*-(benzotriazol-1-yl)-*N,N,N',N'*-tetramethyluronium tetrafluoroborate; TEA: triethylamine; TFA: trifluoroacetic acid; THF: tetrahydrofuran.

N-Boc pipercolic acid

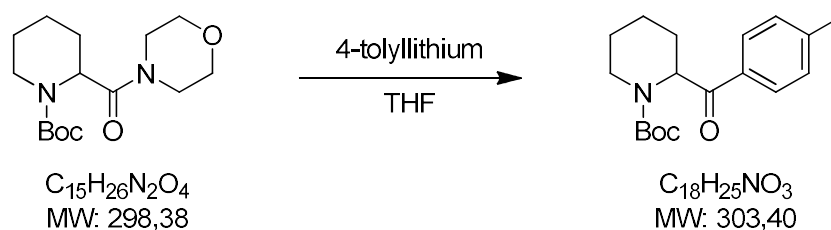
Pipercolic acid (10.0 g, 77.4 mmol) was dissolved in MeOH (50 mL) and TEA (11.9 mL, 85.2 mmol) was added. The mixture was heated up to 50° C and a solution of Boc₂O (33.8 g, 155 mmol) in MeOH (50 mL) was added. After stirring at RT for 20 hours, MeOH was evaporated under reduced pressure, the residue was taken up in ethyl acetate (90 mL) and extracted with 10% NaHCO₃ (3x30 mL). The aqueous phase was acidified to pH=1 with 37% HCl and the white precipitate was filtered and washed with water to afford 16.2 g (92%) of *N*-Boc pipercolic acid as a white solid (mp: 130-133° C).

¹H NMR (300 MHz, CDCl₃) δ 4.83 (bs, 1H), 4.14 – 3.81 (m, 1H), 3.06 – 2.79 (m, 1H), 2.29 – 2.10 (m, 1H), 1.75 – 1.11 (m, 15H).

N-Boc pipercolic acid morpholine amide

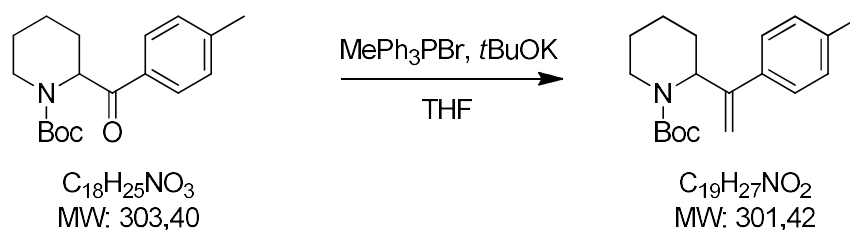
N-Boc pipercolic acid (7.80 g, 34.0 mmol), TBTU (14.20 g, 44.2 mmol) and TEA (6.64 mL, 47.6 mmol) were suspended in DCM (80 mL) and stirred at RT for 30 minutes. Morpholine (4.16 mL, 47.63 mmol) was added and the mixture was stirred at RT for 24 hours. The organic phase was washed with 10% HCl (25 mL), 10% NaHCO₃ (25 mL) and saturated NaCl (25 mL) and the organic phase was dried over MgSO₄ and evaporated under reduced pressure. Rotary evaporation was protracted to remove leftover tetramethylurea and gave 8.58 g (85%) of *N*-Boc pipercolic acid morpholine amide as a light orange waxy solid.

¹H NMR (300 MHz, CDCl₃) δ 5.00 – 4.56 (m, 1H), 3.84 (d, *J* = 12.3 Hz, 1H), 3.71 – 3.29 (m, 8H), 3.18 (t, *J* = 12.4 Hz, 1H), 1.90 – 1.49 (m, 5H), 1.38 (s, 10H).

N-Boc-piperidin-2-yl(*p*-tolyl)methanone

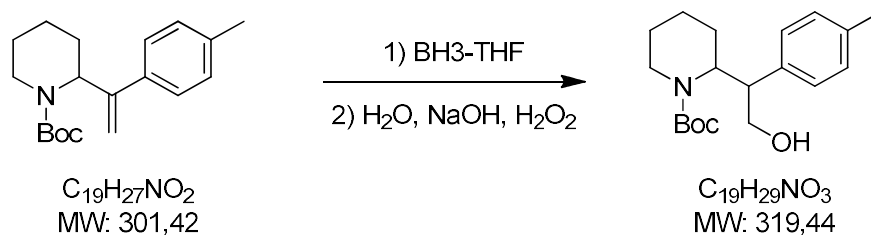
2.7M *n*-BuLi (10.4 mL, 28.2 mmol) was added dropwise to a solution of 4-bromotoluene (4.82 g, 28.2 mmol) in anhydrous THF (50 mL) at -78°C under nitrogen atmosphere. The mixture was stirred at the same temperature for 30 minutes and a solution of *N*-Boc pipercolic acid morpholine amide (2.80 g, 9.39 mmol) in anhydrous THF (30 mL) was added. After stirring for 4.5 hours, the reaction was quenched at -78°C with a solution of 10% HCl (9 mL) in MeOH (20 mL). The mixture was brought to RT and ethyl acetate (50 mL) and phosphate buffer (50 mL) were added. THF was evaporated under reduced pressure, phases were separated and the aqueous phase was extracted with ethyl acetate (2x25 mL). The collected organic phases were dried over MgSO_4 and evaporated under reduced pressure. The obtained crude was purified by column chromatography on silica gel. Elution with cyclohexane/ethyl acetate 95:5 gave 1.99 g (70%) of *N*-Boc-piperidin-2-yl(*p*-tolyl)methanone as a white solid (mp: $95\text{--}97^\circ\text{C}$).

$^1\text{H NMR}$ (300 MHz, CDCl_3) δ 7.81 (d, $J = 7.7$ Hz, 2H), 7.23 (d, $J = 7.7$ Hz, 2H), 5.70 – 5.41 (m, 1H), 4.05 – 3.84 (m, 1H), 3.28 – 3.06 (m, 1H), 2.40 (s, 3H), 2.20 – 1.95 (m, 1H), 1.91 – 1.71 (m, 1H), 1.72 – 1.23 (m, 13H).

N-Boc-2-(1-(*p*-tolyl)vinyl)piperidine

Potassium *tert*-butylate (0.69 g, 6.18 mmol) was added to a solution of methyltriphenylphosphonium bromide (2.21 g, 6.18 mmol) in anhydrous THF (10 mL) under nitrogen atmosphere. After stirring at RT for 4 hours, the reaction was quenched with water (50 mL) and extracted with ethyl acetate (3x20 mL). The organic phase was dried over MgSO_4 , evaporated under reduced pressure and the obtained crude was purified by filtration on silica gel plug (eluent cyclohexane/ethyl acetate 7:3) to give 0.97 g (90%) of *N*-Boc-2-(1-(*p*-tolyl)vinyl)piperidine as colorless oil.

$^1\text{H NMR}$ (300 MHz, CDCl_3) δ 7.14 (d, $J = 8.0$ Hz, 2H), 7.04 (d, $J = 8.2$ Hz, 2H), 5.16 (s, 1H), 5.25 - 5.11 (m, 1H), 4.92 (s, 1H), 3.97 - 3.81 (m, 1H), 2.89 - 2.75 (m, 1H), 2.26 (s, 3H), 1.80 - 1.67 (m, 1H), 1.62 - 1.44 (m, 2H), 1.45 - 1.26 (m, 12H).

N-Boc-2-(piperidin-2-yl)-2-(p-tolyl)ethanol (*threo/erythro*)

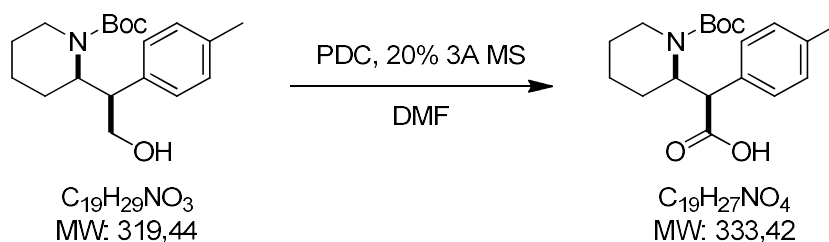
1M borane THF complex (22.9 mL, 22.9 mmol) was added dropwise to a solution of *N*-Boc-2-(1-(p-tolyl)vinyl)piperidine (3.45 g, 11.4 mmol) in anhydrous THF (50 mL) under nitrogen atmosphere. The mixture was stirred at RT overnight and water (20 mL), 2.5N NaOH (20 mL) and 35% H₂O₂ (40 mL) were added in succession and stirring was continued for additional 4 hours. Water (40 mL) was added and the mixture was extracted with ethyl acetate (3x50 mL). The organic phase was washed with 5% sodium bisulfite (50 mL), dried over MgSO₄ and evaporated under reduced pressure. The obtained crude was purified by column chromatography on silica gel. Elution with cyclohexane/ethyl acetate 90:10 gave 1.54 g (42%) of *threo* *N*-Boc-2-(piperidin-2-yl)-2-(p-tolyl)ethanol as a white solid (mp: 138-141° C) and 0.12 g (22%) of *erythro* *N*-Boc-2-(piperidin-2-yl)-2-(p-tolyl)ethanol as a colorless oil.

¹H NMR (300 MHz, CDCl₃)

threo δ 7.23 (d, *J* = 6.4 Hz, 2H), 7.13 (d, *J* = 7.9 Hz, 2H), 4.63 – 4.21 (m, 1H), 4.10 – 3.83 (m, 1H), 3.75 – 3.61 (m, 1H), 3.62 – 3.39 (m, 1H), 3.11 – 2.89 (m, 1H), 2.77 (dt, *J* = 13.2, 2.9 Hz, 1H), 2.26 (s, 3H), 1.65 – 1.17 (m, 15H).

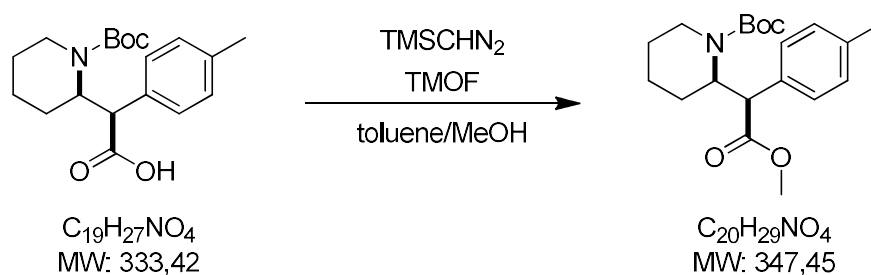
erythro: δ 7.13 (d, *J* = 8.2 Hz, 2H), 7.09 (d, *J* = 8.2 Hz, 2H), 4.53 - 4.42 (m, 1H), 3.83 (dd, *J* = 12.1, 5.9 Hz, 1H), 3.78 - 3.67 (m, 2H), 3.28 - 3.16 (m, 1H), 2.67 - 2.52 (m, 1H), 2.28 (s, 3H), 1.80 - 1.40 (m, 6H), 1.29 (s, 9H).

threo N-Boc-2-(piperidin-2-yl)-2-(p-tolyl)acetic acid



Pyridinium dichromate (0.62 g, 1.64 mmol) and 3Å molecular sieves (0.03 g) were added to a solution of *threo* N-Boc-2-(piperidin-2-yl)-2-(p-tolyl)ethanol (0.15 g, 0.47 mmol) in DMF (2 mL) and the mixture was stirred at RT overnight. Ethyl ether (5 mL) was added and the reaction was quenched by adding 10% HCl (5 mL) dropwise at 0° C. The aqueous phase was extracted with ethyl ether (3x5 mL) and the collected organic phases were extracted with 10% NaOH (3x10 mL). The collected aqueous phases were brought to pH=1 with conc. HCl and extracted with DCM (3x15 mL). The collected organic phases were dried over MgSO₄ and evaporated under reduced pressure to give 0.11 g (70%) of *threo* N-Boc-2-(piperidin-2-yl)-2-(p-tolyl)acetic acid as a white waxy solid.

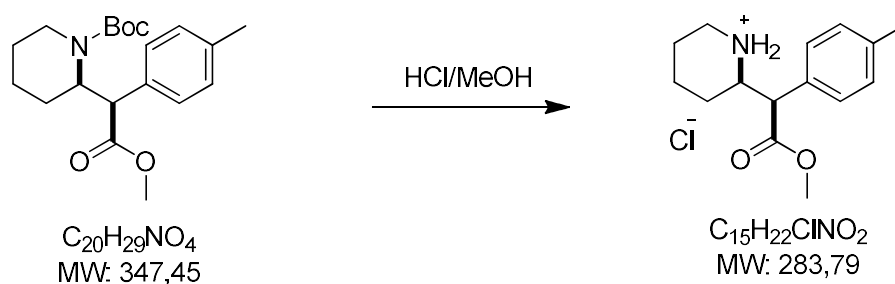
¹H NMR (300 MHz, CDCl₃) δ 7.37 (d, J = 11.0 Hz, 2H), 7.07 (d, J = 11.0 Hz, 2H), 4.85 - 4.80 (m, 1H), 4.02 (d, J = 16.2 Hz, 1H), 4.05 - 3.90 (m, 1H), 3.29 - 3.13 (m, 1H), 2.28 (s, 3H), 1.75 - 1.17 (m, 6H), 1.48 (s, 9H).

threo N-Boc-methyl 2-(piperidin-2-yl)-2-(p-tolyl)acetate

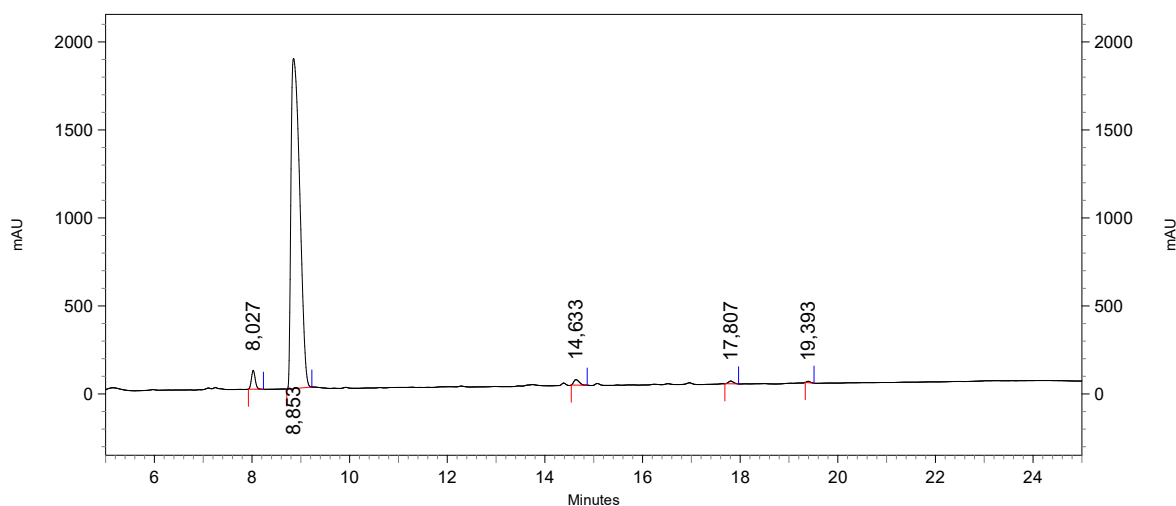
2M trimethylsilyldiazomethane (1.27 mL, 2.53 mmol) was added to a solution of *threo* N-Boc-2-(piperidin-2-yl)-2-(p-tolyl)acetic acid (0.65 g, 1.95 mmol) and trimethylorthoformate (2 mL) in toluene/MeOH (15 mL + 15 mL) under nitrogen atmosphere. The mixture was stirred at RT overnight and solvents were evaporated under reduced pressure to give 0.60 g (88%) of *threo* N-Boc-methyl 2-(piperidin-2-yl)-2-(p-tolyl)acetate as a green/brown oil.

$^1\text{H NMR}$ (300 MHz, CDCl_3) δ 7.40 – 7.28 (m, 2H), 7.14 (d, $J = 7.9$ Hz, 2H), 5.06 – 4.74 (m, 1H), 4.11 (d, $J = 11.7$ Hz, 1H), 4.25 – 3.90 (m, 1H), 3.61 (s, 3H), 3.13 – 2.88 (m, 1H), 2.33 (s, 3H), 1.76 – 1.18 (m, 15H).

threo 2-(piperidin-2-yl)-2-(*p*-tolyl) hydrochloride (Compound I *threo*)



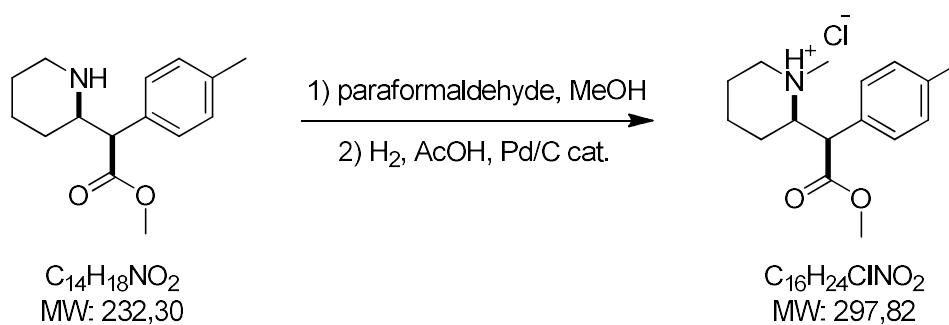
threo *N*-Boc-methyl 2-(piperidin-2-yl)-2-(*p*-tolyl)acetate (0.60 g, 1.72 mmol) was dissolved in excess 2N HCl/MeOH and stirred at RT for 1 hour. Solvents were evaporated under reduced pressure and the resulting crude was crystallized from toluene/MeOH 85:15 to give 0.22 g (44%) of *threo* 2-(piperidin-2-yl)-2-(*p*-tolyl) hydrochloride (Compound I *threo*) as a white solid (mp: 205° C with decomposition). Retention Time (HPLC) = 8.85'; A% (HPLC) = 96%.



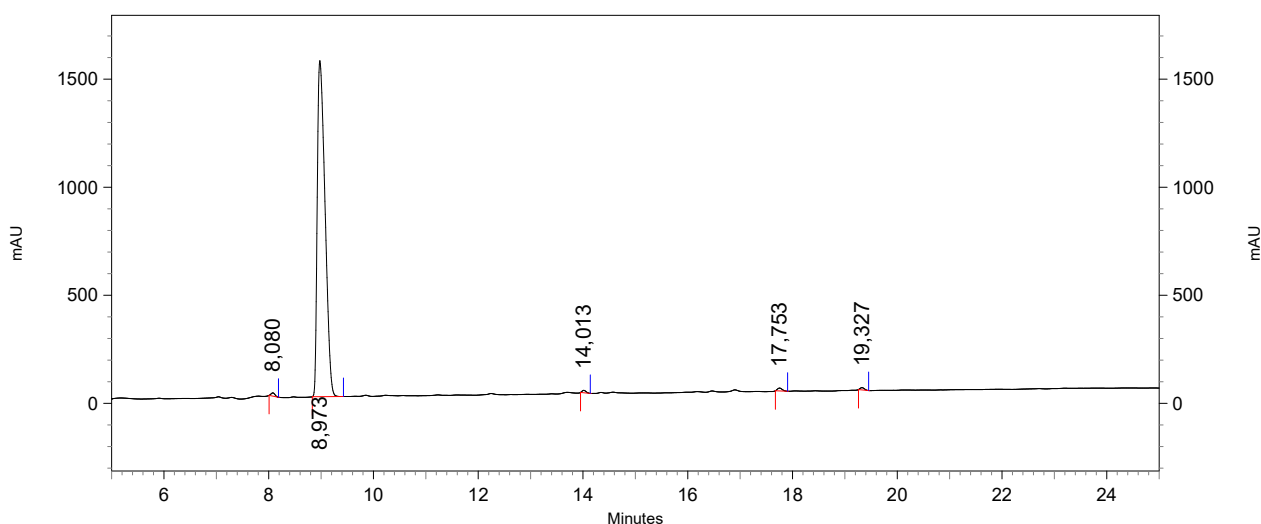
1H NMR (300 MHz, CD_3OD) δ 7.22 (d, $J = 8.0$ Hz, 1H), 7.15 (d, $J = 8.1$ Hz, 1H), 3.81 – 3.75 (m, 1H), 3.71 (s, 1H), 3.47 – 3.38 (m, 1H), 3.09 (dt, $J = 12.8, 9.5$ Hz, 1H), 2.33 (s, 2H), 1.94 – 1.24 (m, 3H).

^{13}C NMR (75 MHz, CD_3OD) δ 171.98, 138.46, 130.59, 129.60, 127.94, 57.85, 53.59, 51.94, 45.21, 26.34, 22.00, 21.34, 19.66.

threo methyl 2-(1-methylpiperidin-2-yl)-2-(p-tolyl)acetate hydrochloride (Compound VIII *threo*)

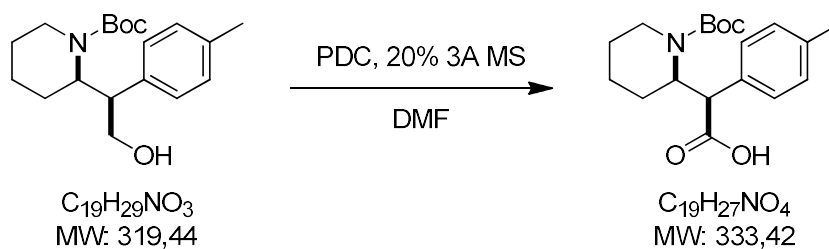


threo methyl 2-(piperidin-2-yl)-2-(p-tolyl)acetate (260 g, 0.91 mmol) was dissolved in MeOH (20 mL), 37% paraformaldehyde (0.09 mL, 1.18) was added and the mixture was stirred at RT for 20 minutes. Acetic acid (0.03 mL) and Pd/C (KF=50%) (90 mg) were added and the mixture was vigorously shaken under 2.5 atm hydrogen at RT for 2.5 hours. After filtering on a celite pad, solvents were evaporated under reduced pressure and the residue was taken up in ethyl acetate (20 mL) and washed with 10% NaHCO₃ (10 mL) The aqueous phase was extracted with ethyl acetate (2x5mL) and the solvent was evaporated under reduced pressure. The residue was treated with excess HCl/MeOH, solvents were evaporated under reduced pressure. The resulting crude was treated with acetone (1 mL) to precipitate 47 mg (17%) *threo* methyl 2-(1-methylpiperidin-2-yl)-2-(p-tolyl)acetate hydrochloride (Compound VIII *threo*) as a white solid (mp: 187° C with decomposition). Retention Time (HPLC) = 8.97'; A% (HPLC) = 98%.



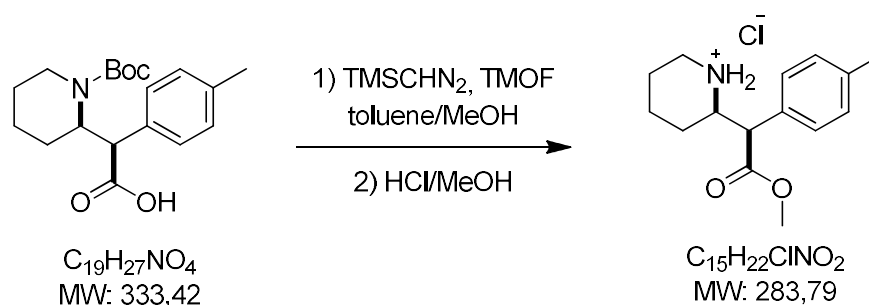
^1H NMR (freebase) (300 MHz, CD_3OD) δ 7.17 (d, $J = 8.3$ Hz, 2H), 7.12 (d, $J = 8.3$ Hz, 2H), 3.74 (d, $J = 9.9$ Hz, 1H), 3.63 (s, 3H), 3.21 – 3.07 (m, 1H), 2.93 (dt, $J = 9.1, 4.2$ Hz, 1H), 2.59 – 2.43 (m, 1H), 2.38 (s, 3H), 2.30 (s, 3H), 1.66 – 1.46 (m, 3H), 1.37 – 1.13 (m, 2H), 1.12 – 0.86 (m, 1H).

^{13}C NMR (freebase) (75 MHz, CDCl_3) δ 174.50, 137.03, 129.26, 128.68, 63.35, 54.08, 54.02, 52.04, 40.83, 24.70, 22.97, 22.31, 21.03.

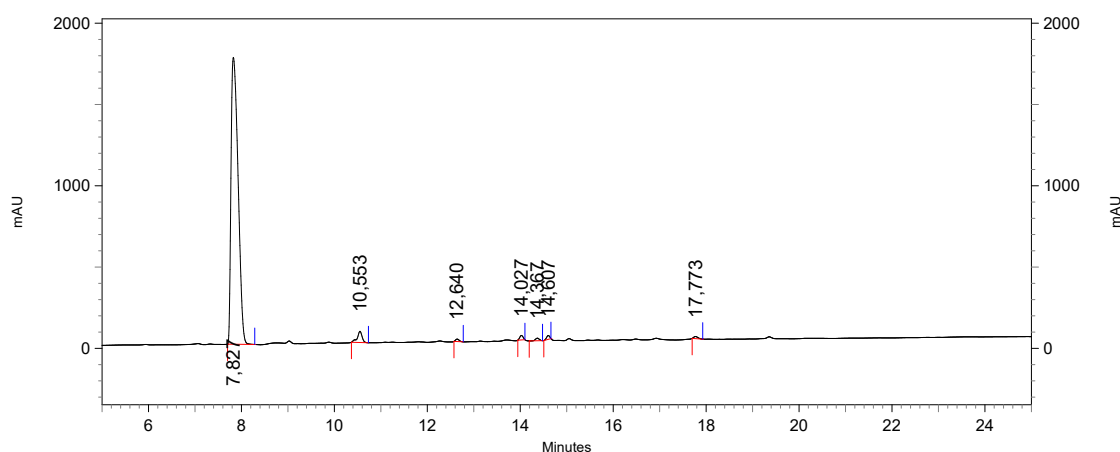
erythro N-Boc-2-(piperidin-2-yl)-2-(p-tolyl)acetic acid

Pyridinium dichromate (3.38 g, 8.98 mmol) and 3Å molecular sieves (0.67 g) were added to a solution of *erythro* N-Boc-2-(piperidin-2-yl)-2-(p-tolyl)ethanol (0.82 g, 2.56 mmol) in DMF (10 mL) and the mixture was stirred at RT overnight. Ethyl ether (25 mL) was added and the reaction was quenched by adding 10% HCl (25 mL) dropwise at 0° C. The aqueous phase was extracted with ethyl ether (3x25 mL) and the collected organic phases were extracted with 10% NaOH (3x50 mL). The collected aqueous phases were brought to pH=1 with conc. HCl and extracted with DCM (3x50 mL). The collected organic phases were dried over MgSO₄ and evaporated under reduced pressure to give 0.54 g (63%) of *erythro* N-Boc-2-(piperidin-2-yl)-2-(p-tolyl)acetic acid as a white waxy solid.

¹H NMR (300 MHz, CDCl₃) δ 7.26 (d, J = 9.3 Hz, 2H), 7.07 (d, J = 9.3 Hz, 2H), 5.04 - 4.79 (m, 1H), 4.07 (d, J = 10.5 Hz, 1H), 4.12 - 3.78 (m, 1H), 2.64 (t, J = 13.2 Hz, 1H), 2.27 (s, 3H), 1.78 - 1.13 (m, 6H), 1.22 (s, 9H).

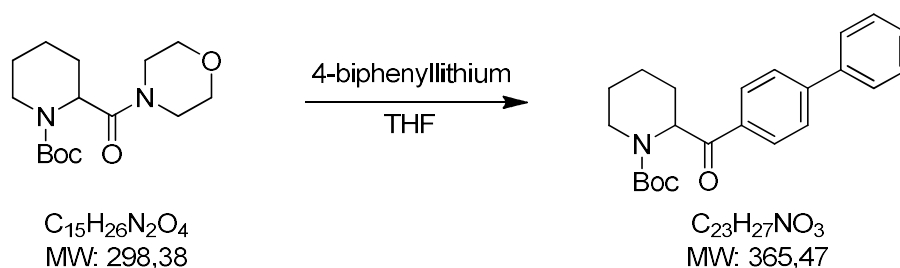
erythro N-Boc-methyl 2-(piperidin-2-yl)-2-(p-tolyl)acetate (Compound I *erythro*)

2M trimethylsilyldiazomethane (1.08 mL, 2.16 mmol) was added to a solution of *erythro* N-Boc-2-(piperidin-2-yl)-2-(p-tolyl)acetic acid (0.48 g, 1.44 mmol) and trimethylorthoformate (2 mL) in toluene/MeOH (9 mL + 9 mL) under nitrogen atmosphere. The mixture was stirred at RT overnight and solvents were evaporated under reduced pressure to give 0.47 g (94%) of *erythro* N-Boc-methyl 2-(piperidin-2-yl)-2-(p-tolyl)acetate as a green oil. The product was dissolved in excess 2N HCl/MeOH and stirred at RT for 1 hour. Solvents were evaporated under reduced pressure and the resulting crude was crystallized from toluene to give 0.26 g (68%) of *erythro* 2-(piperidin-2-yl)-2-(p-tolyl) hydrochloride (Compound I *erythro*) as a white solid (mp: 190.64° C). Retention Time (HPLC) = 7.83'; A% (HPLC) = 95%.



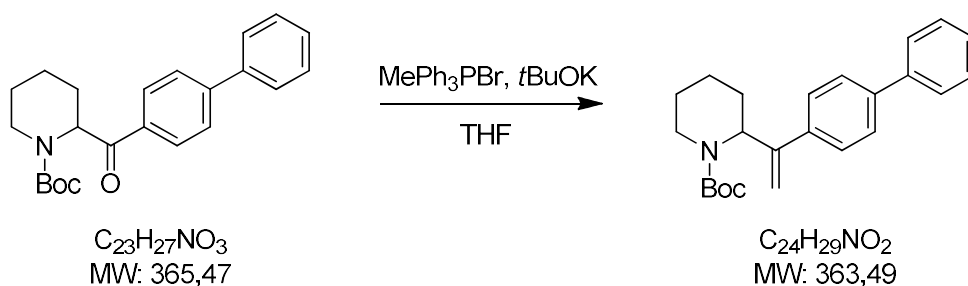
1H NMR (300 MHz, DMSO- d_6) δ 9.65 (bs, 1H), 7.64 (bs, 1H), 7.28 (d, J = 7.9 Hz, 2H), 7.20 (d, J = 7.9 Hz, 2H), 4.05 (d, J = 9.8 Hz, 1H), 3.67-3.54 (m, 1H), 3.59 (s, 3H), 3.12 – 3.03 (m, 1H), 2.84 – 2.71(m, 1H), 2.29 (s, 3H), 1.90 – 1.35 (m, 6H).

^{13}C NMR (75 MHz, DMSO- d_6) δ 171.53, 138.27, 130.68, 130.21, 129.19, 57.55, 53.90, 52.79, 45.33, 27.27, 21.99, 21.16.

N-Boc-[1,1'-biphenyl]-4-yl(piperidin-2-yl)methanone

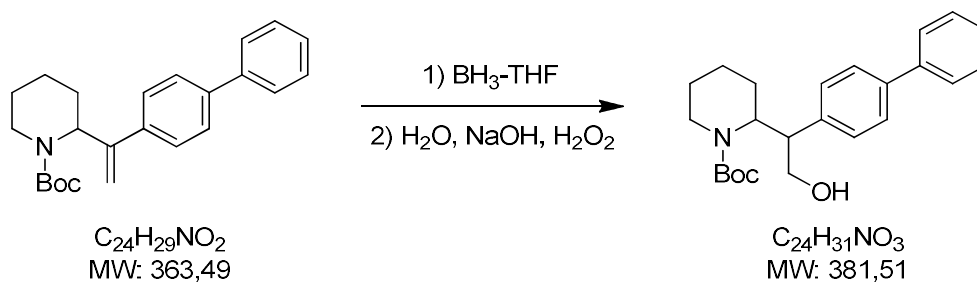
2.7M *n*-BuLi (3.72 mL, 10.06 mmol) was added dropwise to a solution of 4-bromobiphenyl (2.34 g, 10.06 mmol) in anhydrous THF (25 mL) at -78° C under nitrogen atmosphere. The mixture was stirred at the same temperature for 1 hour and a solution of *N*-Boc pipercolic acid morpholine amide (1.00 g, 3.35 mmol) in anhydrous THF (10 mL) was added. After stirring for 4 hours, the reaction was quenched with a solution of MeOH (1 mL) in THF (5 mL). Solvents were evaporated under reduced pressure and the residue was taken up in ethyl acetate (30 mL) and washed with phosphate buffer (2x15 mL). The organic phase was dried over MgSO₄ and evaporated under reduced pressure. The obtained crude was purified by column chromatography on silica gel. Elution with cyclohexane/ethyl acetate 95:5 gave 0.53 g (48%) of *N*-Boc-[1,1'-biphenyl]-4-yl(piperidin-2-yl)methanone as a colorless oil.

¹H NMR (300 MHz, CDCl₃) δ 7.93 (d, *J* = 6.5 Hz, 2H), 7.68 – 7.52 (m, 4H), 7.46 – 7.29 (m, 3H), 5.73 – 5.46 (m, 1H), 4.17 – 3.71 (m, 1H), 3.28 – 3.05 (m, 1H), 2.26 – 2.03 (m, 1H), 1.94 – 1.28 (m, 14H).

N-Boc-2-(1-([1,1'-biphenyl]-4-yl)vinyl)piperidine

Potassium *tert*-butylate (0.27 g, 2.38 mmol) was added to a solution of methyltriphenylphosphonium bromide (0.85 g, 2.38 mmol) in anhydrous THF (3 mL) under nitrogen atmosphere. The mixture was stirred at RT for 10 minutes and a solution of *N*-Boc-[1,1'-biphenyl]-4-yl(piperidin-2-yl)methanone (0.58 g, 1.59 mmol) in anhydrous THF (7 mL) was added. After stirring at RT overnight, the reaction was quenched with water (25 mL) and extracted with ethyl acetate (3x10 mL). The organic phase was dried over MgSO_4 , evaporated under reduced pressure and the obtained crude was purified by filtration on silica gel plug (eluent cyclohexane/ethyl acetate 7:3) to give 0.56 g (96%) of *N*-Boc-2-(1-([1,1'-biphenyl]-4-yl)vinyl)piperidine as a white solid (mp: 119-124° C).

$^1\text{H NMR}$ (300 MHz, CDCl_3) δ 7.61 – 7.52 (m, 4H), 7.47 – 7.33 (m, 5H), 5.33 (s, 1H), 5.36 – 5.27 (m, 1H), 5.07 (s, 1H), 4.01 – 3.91 (m, 1H), 2.97 – 2.84 (m, 1H), 1.90 – 1.81 (m, 1H), 1.69 – 1.41 (m, 14H).

N-Boc-2-([1,1'-biphenyl]-4-yl)-2-(piperidin-2-yl)ethanol (*threo/erythro*)

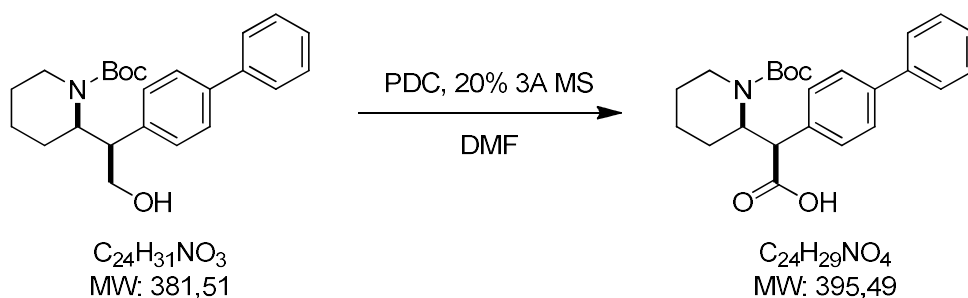
1M borane THF complex (6.44 mL, 6.44 mmol) was added dropwise to a solution of *N*-Boc-2-([1,1'-biphenyl]-4-yl)vinylpiperidine (1.17 g, 3.22 mmol) in anhydrous THF (20 mL) under nitrogen atmosphere. The mixture was stirred at RT overnight and water (12 mL), 2.5N NaOH (12 mL) and 35% H₂O₂ (24 mL) were added in succession and stirring was continued for additional 2.5 hours. Water (25 mL) was added and the mixture was extracted with ethyl acetate (3x30 mL). The organic phase was dried over MgSO₄ and evaporated under reduced pressure. The obtained crude was purified by column chromatography on silica gel. Elution with cyclohexane/ethyl acetate 75:25 gave 0.38 g (31%) of *threo* *N*-Boc-2-([1,1'-biphenyl]-4-yl)-2-(piperidin-2-yl)ethanol as a white solid (mp: 150-152.5° C) and 0.12 g (10%) of *erythro* *N*-Boc-2-([1,1'-biphenyl]-4-yl)-2-(piperidin-2-yl)ethanol as a colorless oil.

¹H NMR (300 MHz, CDCl₃)

threo: δ 7.63 – 7.51 (m, 4H), 7.68 – 7.28 (m, 5H), 4.79 – 4.59 (m, 1H), 4.13 – 3.99 (m, 1H), 3.81 – 3.71 (m, 1H), 3.63 – 3.57 (m, 1H), 3.22 – 3.06 (m, 1H), 2.87 (dt, *J* = 13.2, 2.4 Hz, 1H), 1.71 – 1.37 (m, 15H).

erythro: δ 7.58 – 7.48 (m, 4H), 7.46 – 7.38 (m, 2H), 7.37 – 7.31 (m, 3H), 4.54 – 4.44 (m, 1H), 3.86 – 3.70 (m, 3H), 3.32 – 3.18 (m, 1H), 2.68 – 2.50 (m, 1H), 1.89 – 1.37 (m, 6H), 1.28 (s, 9H).

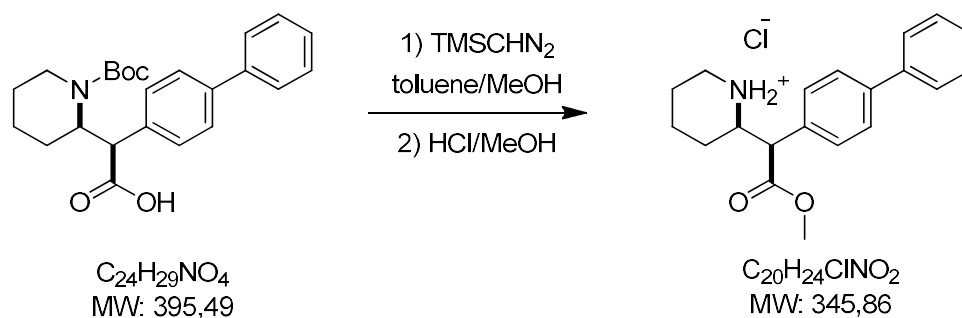
threo N-Boc-2-([1,1'-biphenyl]-4-yl)-2-(piperidin-2-yl)acetic acid



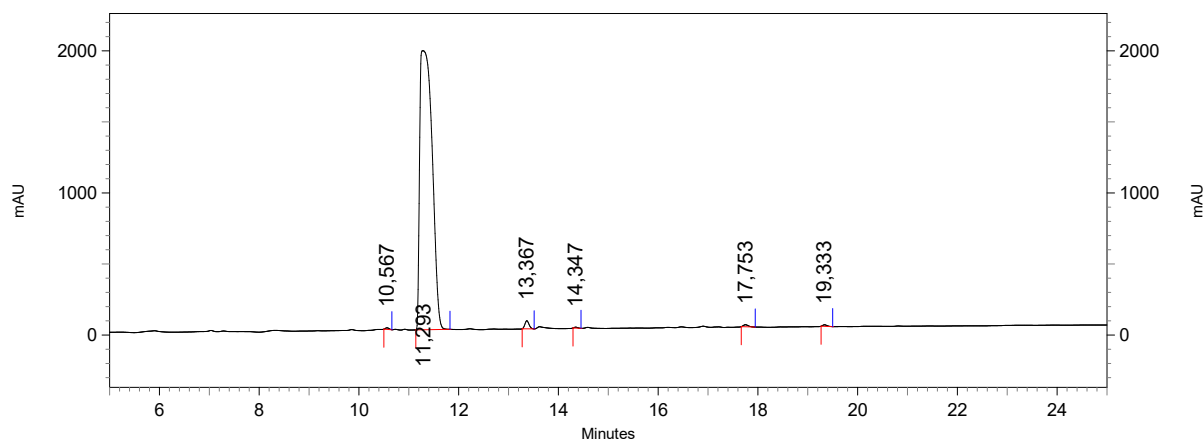
Pyridinium dichromate (1.31 g, 3.48 mmol) and 3Å molecular sieves (0.08 g) were added to a solution of *threo* N-Boc-2-([1,1'-biphenyl]-4-yl)-2-(piperidin-2-yl)ethanol (0.38 g, 0.99 mmol) in DMF (5 mL) and the mixture was stirred at RT overnight. Ethyl ether (5 mL) was added and the reaction was quenched by adding 10% HCl (5 mL) dropwise at 0° C. The aqueous phase was extracted with ethyl ether (3x5 mL) and the collected organic phases were extracted with 10% NaHCO₃ (3x10 mL). The collected aqueous phases were brought to pH=1 with conc. HCl and extracted with DCM (3x15 mL). The collected organic phases were dried over MgSO₄ and evaporated under reduced pressure to give 0.33 g (84%) of *threo* N-Boc-2-([1,1'-biphenyl]-4-yl)-2-(piperidin-2-yl)acetic acid as a brown oil.

¹H NMR (300 MHz, CDCl₃) δ 7.62 – 7.28 (m, 9H), 5.11 – 4.77 (m, 1H), 4.17 (d, *J* = 11.7 Hz, 1H), 4.07 – 3.86 (m, 1H), 3.12 – 2.93 (m, 1H), 1.76 – 1.01 (m, 15H).

threo methyl-2-([1,1'-biphenyl]-4-yl)-2-(piperidin-2-yl)acetate hydrochloride (Compound II *threo*)



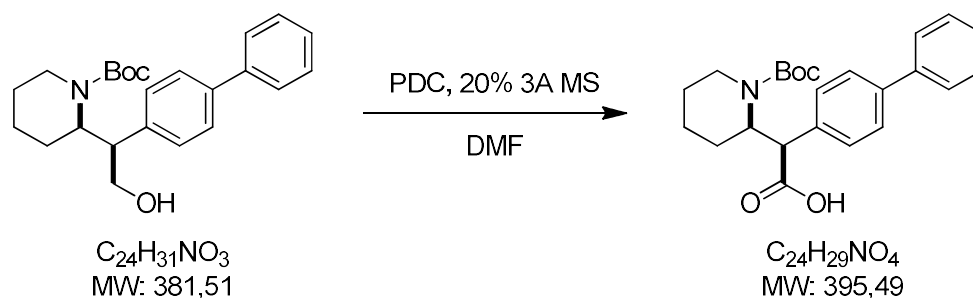
2M trimethylsilyldiazomethane (0.54 mL, 1.08 mmol) was added to a solution of *threo* *N*-Boc-2-([1,1'-biphenyl]-4-yl)-2-(piperidin-2-yl)acetic acid (0.33 g, 0.83 mmol) in toluene/MeOH (7 mL + 7 mL) under nitrogen atmosphere. The mixture was stirred at RT overnight and solvents were evaporated under reduced pressure. The crude was purified by column chromatography on silica gel. Elution with cyclohexane/ethyl acetate 90:10 gave 0.18 g (53%) of *threo* *N*-Boc-methyl-2-([1,1'-biphenyl]-4-yl)-2-(piperidin-2-yl)acetate as a colorless oil. The obtained product was dissolved in excess 2N HCl/MeOH and stirred at RT for 30 minutes. Solvents were evaporated under reduced pressure and the resulting crude was slurried in hot toluene to give 0.08 g (53%) of *threo* methyl-2-([1,1'-biphenyl]-4-yl)-2-(piperidin-2-yl)acetate hydrochloride (Compound II *threo*) as a white solid (mp: 211-213° C). Retention Time (HPLC) = 11.30'; A% (HPLC) = 98%.



$^1\text{H NMR}$ (300 MHz, CD_3OD) δ 7.68 – 7.58 (m, 4H), 7.47 – 7.31 (m, 5H), 3.97 – 3.80 (m, 2H), 3.75 (s, 3H), 3.51 – 3.40 (m, 1H), 3.12 (dt, $J = 12.7, 3.1$ Hz, 1H), 1.96 – 1.77 (m, 2H), 1.77 – 1.35 (m, 4H).

$^{13}\text{C NMR}$ (75 MHz, CD_3OD) δ 171.80, 141.53, 139.98, 132.61, 128.65, 128.56, 127.51, 127.35, 126.54, 57.80, 53.58, 52.04, 45.26, 26.39, 22.00, 21.37.

erythro N-Boc-2-([1,1'-biphenyl]-4-yl)-2-(piperidin-2-yl)acetic acid



Pyridinium dichromate (0.76 g, 2.02 mmol) and 3Å molecular sieves (0.05 g) were added to a solution of *erythro* N-Boc-2-([1,1'-biphenyl]-4-yl)-2-(piperidin-2-yl)ethanol (0.22 g, 0.57 mmol) in DMF (3 mL) and the mixture was stirred at RT overnight. Ethyl ether (5 mL) was added and the reaction was quenched by adding 10% HCl (5 mL) dropwise at 0° C. The aqueous phase was extracted with ethyl ether (3x5 mL) and the collected organic phases were extracted with 10% NaHCO₃ (3x10 mL). The collected aqueous phases were brought to pH=1 with conc. HCl and extracted with DCM (3x15 mL). The collected organic phases were dried over MgSO₄ and evaporated under reduced pressure to give 0.14 g (64%) of *erythro* N-Boc-2-([1,1'-biphenyl]-4-yl)-2-(piperidin-2-yl)acetic acid as a brown oil.

¹H NMR (300 MHz, CDCl₃) δ 7.55 – 7.45 (m, 6H), 7.45 – 7.36 (m, 2H), 7.36 – 7.28 (m, 1H), 5.28 – 4.82 (m, 1H), 4.17 (d, *J* = 11.6 Hz, 1H), 4.11 – 3.73 (m, 1H), 2.70 (dd, *J* = 27.9, 15.1 Hz, 1H), 1.86 – 1.55 (m, 1H), 1.55 – 1.31 (m, 4H), 1.31 – 1.05 (m, 2H), 1.21 (s, 9H).

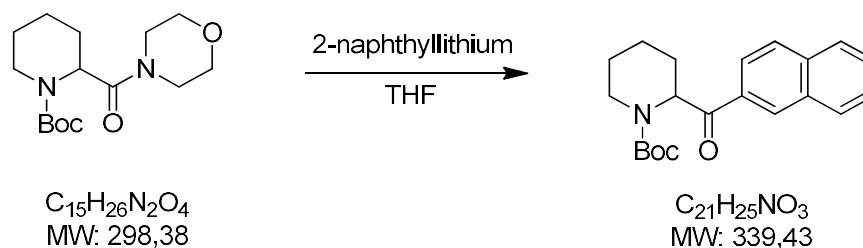
erythro methyl-2-([1,1'-biphenyl]-4-yl)-2-(piperidin-2-yl)acetate hydrochloride (Compound II *erythro*)



2M trimethylsilyldiazomethane (0.23 mL, 0.46 mmol) was added to a solution of *erythro*-N-Boc-2-([1,1'-biphenyl]-4-yl)-2-(piperidin-2-yl)acetic acid (0.14 g, 0.35 mmol) in toluene/MeOH (3 mL + 3 mL) under nitrogen atmosphere. The mixture was stirred at RT overnight and solvents were evaporated under reduced pressure. The resulting crude was purified by column chromatography on silica gel. Elution with cyclohexane/ethyl acetate 90:10 gave 0.12 g (86%) of *erythro*-N-Boc-methyl-2-([1,1'-biphenyl]-4-yl)-2-(piperidin-2-yl)acetate as a colorless oil. The obtained product was dissolved in excess 2N HCl/MeOH and stirred at RT for 30 minutes. Solvents were evaporated under reduced pressure and the resulting crude was slurried in hot toluene to give 30.4 mg (30%) of *erythro* methyl-2-([1,1'-biphenyl]-4-yl)-2-(piperidin-2-yl)acetate hydrochloride (Compound II *erythro*) as a white solid (mp: 207-209° C).

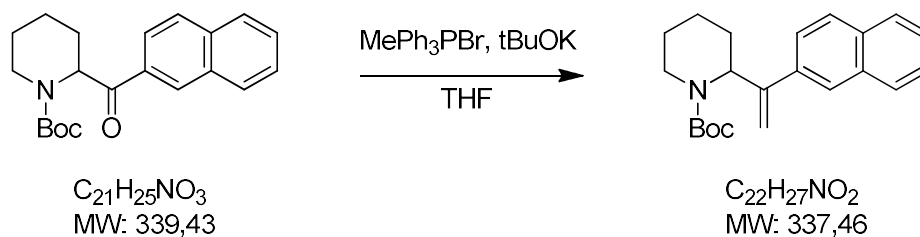
$^1\text{H NMR}$ (300 MHz, CD_3OD) δ 7.74 – 7.69 (m, 2H), 7.65 – 7.61 (m, 2H), 7.51 – 7.42 (m, 4H), 7.39 – 7.32 (m, 1H), 3.95 (d, $J = 9.1$ Hz, 1H), 3.88 – 3.77 (m, 1H), 3.72 (s, 3H), 3.34 – 3.26 (m, 1H), 3.06 – 2.92 (m, 1H), 2.16 – 2.07 (m, 1H), 1.97 – 1.84 (m, 2H), 1.77 – 1.53 (m, 3H).

$^{13}\text{C NMR}$ (75 MHz, CD_3OD) δ 171.15, 141.98, 140.00, 131.42, 129.08, 128.59, 127.85, 127.42, 126.57, 58.09, 54.18, 51.80, 45.60.

N-Boc-naphthalen-2-yl(piperidin-2-yl)methanone

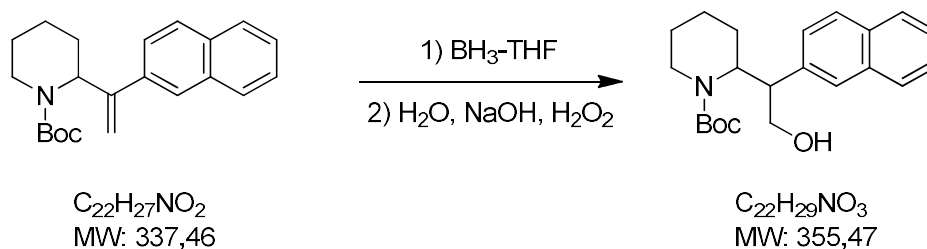
2.7M *n*-BuLi (0.89 mL, 2.41 mmol) was added dropwise to a solution of 2-bromonaphthyl (0.5 g, 2.41 mmol) in anhydrous THF (5 mL) at -78° C under nitrogen atmosphere. The mixture was stirred at the same temperature for 45 minutes and a solution of *N*-Boc pipercolic acid morpholine amide (0.24 g, 0.79 mmol) in anhydrous THF (2.5 mL) was added. After stirring for 5 hours, the reaction was quenched with a solution of MeOH (1 mL) in THF (5 mL). Solvents were evaporated under reduced pressure and the residue was taken up in ethyl acetate (20 mL) and washed with 10% NaCl (3x10 mL) to a neutral pH. The organic phase was dried over MgSO₄ and evaporated under reduced pressure. The obtained crude was purified by column chromatography on silica gel. Elution with cyclohexane/ethyl acetate 90:10 gave 0.19 g (70%) of *N*-Boc-naphthalen-2-yl(piperidin-2-yl)methanone as a colorless oil.

¹H NMR (300 MHz, CDCl₃) δ 8.53 – 8.38 (m, 1H), 8.00 – 7.82 (m, 4H), 7.65 – 7.50 (m, 2H), 5.87 – 5.58 (m, 1H), 4.09 – 3.81 (m, 1H), 3.34 – 3.05 (m, 1H), 2.27 – 2.07 (m, 1H), 1.94 – 1.77 (m, 1H), 1.69 – 1.39 (m, 4H), 1.42 (s, 9H).

N-Boc-2-(1-(naphthalen-2-yl)vinyl)piperidine

Potassium *tert*-butylate (0.29 g, 2.56 mmol) was added to a solution of methyltriphenylphosphonium bromide (0.92 g, 2.56 mmol) in anhydrous THF (5 mL) under nitrogen atmosphere. The mixture was stirred at RT for 10 minutes and a solution of *N*-Boc-naphthalen-2-yl(piperidin-2-yl)methanone (0.29 g, 0.85 mmol) in anhydrous THF (5 mL) was added. After stirring at RT for 7 hours, the reaction was quenched with water (25 mL) and extracted with ethyl acetate (3x10 mL). The organic phase was dried over MgSO_4 and evaporated under reduced pressure. Triphenylphosphine oxide was precipitated from diisopropylether and the solvent was evaporated under reduced pressure to yield 0.21 g (73%) of *N*-Boc-2-(1-(naphthalen-2-yl)vinyl)piperidine as a light yellow oil.

^1H NMR (300 MHz, CDCl_3) δ 7.85– 7.37 (m, 7H), 5.47 – 5.36 (m, 1H), 5.39 (s, 1H), 5.13 (s, 1H), 4.00 – 3.90 (m, 1H), 2.97 – 2.84 (m, 1H), 1.88 – 1.76 (m, 2H), 1.68 – 1.35 (m, 4H), 1.45 (s, 9H).

N-Boc-2-(naphthalen-2-yl)-2-(piperidin-2-yl)ethanol (*threo/erythro*)

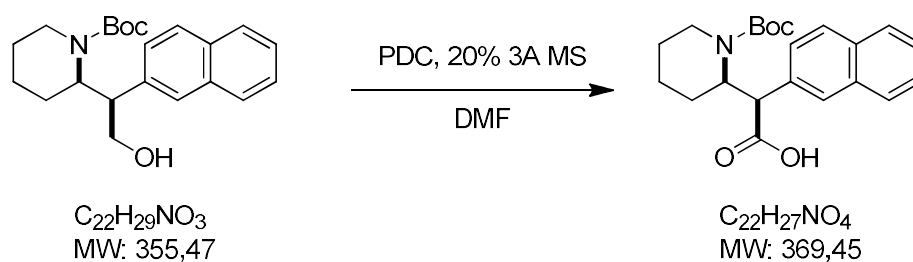
1M borane THF complex (0.99 mL, 0.99 mmol) was added dropwise to a solution of *N*-Boc-2-(1-(naphthalen-2-yl)vinyl)piperidine (0.15 g, 0.50 mmol) in anhydrous THF (2.5 mL) under nitrogen atmosphere. The mixture was stirred at RT for 6 hours and water (1 mL), 2.5N NaOH (1 mL) and 35% H₂O₂ (2 mL) were added in succession and stirring was continued over a weekend. Water (10 mL) was added and the mixture was extracted with ethyl acetate (3x10 mL). The organic phase was dried over MgSO₄ and evaporated under reduced pressure. The obtained crude was purified by column chromatography on silica gel. Elution with cyclohexane/ethyl acetate 80:20 gave 0.06 g (34%) of *threo* *N*-Boc-2-(naphthalen-2-yl)-2-(piperidin-2-yl)ethanol and 0.03 g (17%) of *erythro* *N*-Boc-2-(naphthalen-2-yl)-2-(piperidin-2-yl)ethanol as colorless oils.

¹H NMR (300 MHz, CDCl₃)

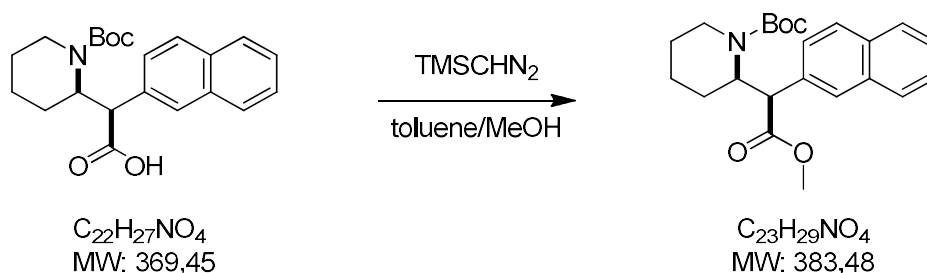
threo: δ 7.89 - 7.68 (m, 4H), 7.57 - 7.37 (m, 3H), 4.84 - 4.71 (m, 1H), 4.13 - 4.00 (m, 1H), 3.90 - 3.78 (m, 1H), 3.70 - 3.61 (m, 1H), 3.31 - 3.20 (m, 1H), 2.93 - 2.79 (m, 1H), 1.73 - 1.24 (m, 6H), 1.50 (s, 9H).

erythro: δ 7.85 - 7.75 (m, 4H), 7.69 (s, 1H), 7.49 - 7.39 (m, 3H), 4.69 - 4.57 (m, 1H), 3.95 - 3.6 (m, 3H), 3.49 - 3.38 (m, 1H), 1.85 - 1.13 (m, 6H), 1.22 (s, 9H).

threo N-Boc-2-(naphthalen-2-yl)-2-(piperidin-2-yl)acetic acid



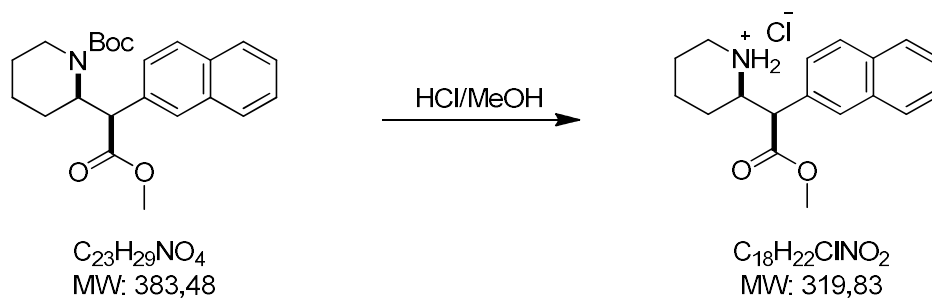
Pyridinium dichromate (0.48 g, 1.28 mmol) and 3Å molecular sieves (0.03 g) were added to a solution of *threo* N-Boc-2-(naphthalen-2-yl)-2-(piperidin-2-yl)ethanol (0.13 g, 0.36 mmol) in DMF (3 mL) and the mixture was stirred at RT overnight. Ethyl ether (5 mL) was added and the reaction was quenched by adding 10% HCl (2.5 mL) dropwise at 0° C. The aqueous phase was extracted with ethyl ether (3x5 mL) and the collected organic phases were extracted with 10% NaOH (3x10 mL). The collected aqueous phases were brought to pH=1 with conc. HCl and extracted with DCM (3x15 mL). The collected organic phases were dried over MgSO₄ and evaporated under reduced pressure to give 0.10 g (75%) of *threo* N-Boc-2-(naphthalen-2-yl)-2-(piperidin-2-yl)acetic acid as a viscous green oil. The obtained crude was used in the next step without further purification.

threo N-Boc-methyl-2-(naphthalen-2-yl)-2-(piperidin-2-yl)acetate

2M trimethylsilyldiazomethane (0.16 mL, 0.32 mmol) was added to a solution of *threo* N-Boc-2-(naphthalen-2-yl)-2-(piperidin-2-yl)acetic acid (90 mg, 0.24 mmol) in toluene/MeOH (2 mL + 2 mL) under nitrogen atmosphere. The mixture was stirred at RT overnight and solvents were evaporated under reduced pressure. The resulting crude was taken up in ethyl acetate (2.5 mL) and washed with 10% EDTA (2 mL). The organic phase was dried over MgSO_4 and evaporated under reduced pressure to give 90 mg (98%) of *threo* N-Boc- methyl 2-(naphthalen-2-yl)-2-(piperidin-2-yl)acetate as a green oil.

$^1\text{H NMR}$ (300 MHz, CDCl_3) δ 8.02 – 7.75 (m, 4H), 7.72 – 7.56 (m, 1H), 7.53 – 7.43 (m, 2H), 5.22 – 4.90 (m, 1H), 4.33 (d, $J = 11.6$ Hz, 1H), 4.27 – 3.94 (m, 1H), 3.64 (s, 3H), 3.20 – 2.96 (m, 1H), 1.78 – 1.26 (m, 15H).

threo methyl-2-(naphthalen-2-yl)-2-(piperidin-2-yl)acetate hydrochloride (Compound III *threo*)

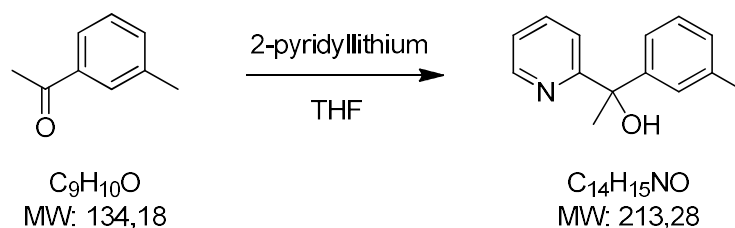


threo *N*-Boc methyl 2-(naphthalen-2-yl)-2-(piperidin-2-yl)acetate (51 mg, 0.13 mmol) was dissolved in excess 2N HCl/MeOH and stirred at RT for 1 hour. Solvents were evaporated under reduced pressure and the resulting crude was decanted in diisopropylether to give 10 mg (24%) of *threo* methyl-2-(naphthalen-2-yl)-2-(piperidin-2-yl)acetate hydrochloride (Compound III *threo*) as a beige solid (mp: 205° C with decomposition).

^1H NMR (300 MHz, CDCl_3) δ 7.92 – 7.83 (m, 3H), 7.80 (s, 1H), 7.57 – 7.49 (m, 2H), 7.39 (dd, J = 8.5, 1.7 Hz, 1H), 4.03 (d, J = 9.7 Hz, 1H), 3.95 (dt, J = 10.5, 2.4 Hz, 1H), 3.74 (s, 3H), 3.50 – 3.41 (m, 1H), 3.13 (td, J = 12.7, 3.3 Hz, 1H), 1.97 – 1.27 (m, 6H).

^{13}C NMR (75 MHz, CD_3OD) δ 171.83, 133.48, 133.16, 130.91, 128.91, 127.77, 127.46, 127.34, 126.47, 126.41, 124.93, 57.78, 54.03, 52.04, 45.28, 26.51, 22.02, 21.33.

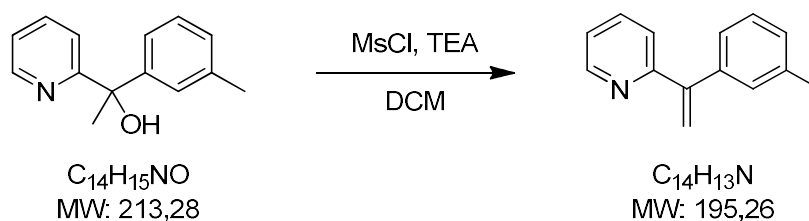
1-(pyridin-2-yl)-1-(m-tolyl)ethanol



2.7M *n*-BuLi (8.67 mL, 23.4 mmol) was added dropwise to a solution of 2-bromopyridine (2.03 mL, 21.3 mmol) in anhydrous THF (15 mL) at -78° C under nitrogen atmosphere. The mixture was stirred at the same temperature for 45 minutes and a solution of 3-methylacetophenone (3.10 g, 22.4 mmol) in anhydrous THF (15 mL) was added. Stirring was continued at -78° C for 15 minutes and then the mixture was left stirring overnight at RT. The reaction was quenched with the addition of saturated NH₄Cl (50 mL), the separated organic phase was dried over MgSO₄ and evaporated under reduced pressure. The resulting crude was purified by flash chromatography on silica gel. Elution with cyclohexane/ethyl acetate 80/20 gave 1.94 g (45%) of 1-(pyridin-2-yl)-1-(m-tolyl)ethanol as a brown oil.

¹H NMR (300 MHz, CDCl₃) δ 8.54 – 8.51 (m, 1H), 7.65 (dt, *J* = 7.7, 1.7 Hz, 1H), 7.34 – 7.15 (m, 5H), 7.04 (d, *J* = 7.2 Hz, 1H), 5.84 (s, 1H), 2.33 (s, 3H), 1.92 (s, 3H).

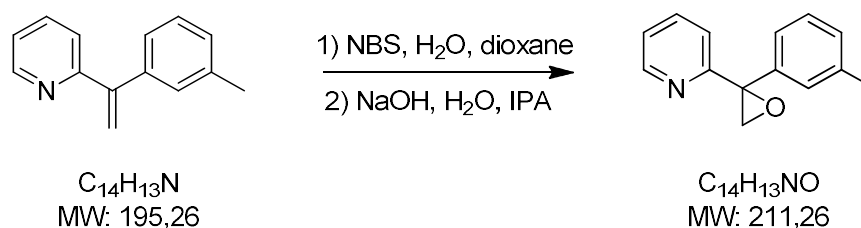
2-(1-(m-tolyl)vinyl)pyridine



TEA (5.07 mL, 36.4 mmol) and methanesulfonyl chloride (2.11 mL, 27.3 mmol) are added to a solution of 1-(pyridin-2-yl)-1-(m-tolyl)ethanol (1.94 g, 9.10 mmol) in DCM (45 mL) at 0° C. After stirring at RT overnight, the mixture was diluted with DCM (30 mL) and washed with 10% NaHCO₃ (25 mL) and 10% NaCl (3x25 mL). The organic phase was dried over MgSO₄, evaporated under reduced pressure and the resulting crude was purified by flash chromatography on silica gel. Elution with cyclohexane/ethyl acetate 90/10 gave 1.15 g (65%) of 2-(1-(m-tolyl)vinyl)pyridine as a brown oil.

¹H NMR (300 MHz, CDCl₃) δ (ddd, *J* = 4.9, 1.8, 0.9 Hz, 1H), 7.64 (dt, *J* = 7.7, 1.9 Hz, 1H), 7.30 – 7.11 (m, 6H), 5.97 (d, *J* = 1.5 Hz, 1H), 5.59 (d, *J* = 1.6 Hz, 1H), 2.36 (s, 3H).

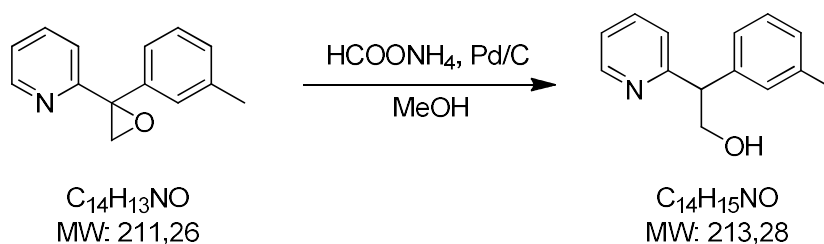
2-(2-(m-tolyl)oxiran-2-yl)pyridine



2-(1-(m-tolyl)vinyl)pyridine (1.15 g, 5.89 mmol) was dissolved in a 3:1 mixture of dioxane (36 mL) and water (12 mL). NBS (1.57 g, 8.83 mmol) was added and the mixture was stirred for 5 hours at RT. Ethyl acetate (50 mL) was added and the organic phase was washed with 10% $\text{Na}_2\text{S}_2\text{O}_5$ (30 mL) and 10% NaCl (20 mL) and evaporated under reduced pressure. The obtained residue was dissolved in IPA (40 mL), 10% NaOH (9 mL) was added and the mixture was stirred at RT for 4 hours. IPA was evaporated under reduced pressure, ethyl acetate (60 mL) was added and the organic phase was washed with 10% NaCl (20 mL), dried over MgSO_4 and evaporated under reduced pressure to give 1.01 g (81%) of 2-(2-(m-tolyl)oxiran-2-yl)pyridine as a dark orange oil.

$^1\text{H NMR}$ (300 MHz, CDCl_3) δ 8.62 (ddd, $J = 4.8, 1.8, 0.9$ Hz, 1H), 7.66 (dt, $J = 7.8, 1.8$ Hz, 1H), 7.39 (dt, $J = 7.9, 1.1$ Hz, 1H), 7.31 – 7.19 (m, 4H), 7.18 – 7.11 (m, 1H), 3.54 (d, $J = 5.9$ Hz, 1H), 3.26 (d, $J = 5.9$ Hz, 1H), 2.35 (s, 3H).

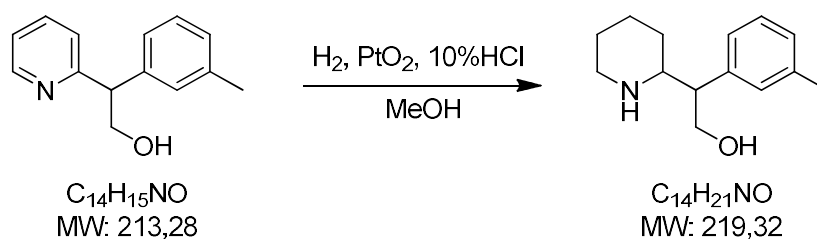
2-(pyridin-2-yl)-2-(m-tolyl)ethanol



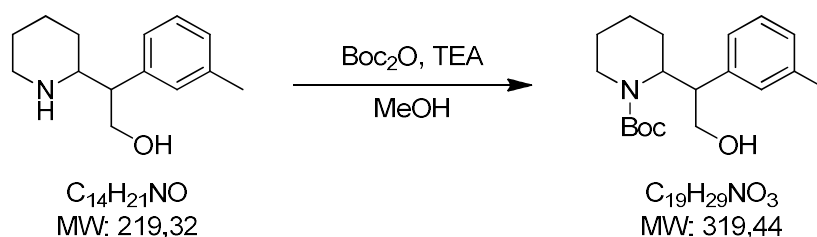
Ammonium formate (2.98 g, 47.3 mmol) and Pd/C (KF=50%, 0.10 g) were added to a solution of 2-(2-(m-tolyl)oxiran-2-yl)pyridine (1.00 g, 4.73 mmol) in anhydrous MeOH (25 mL) under nitrogen atmosphere. The mixture was refluxed for 4 hours and the solvent was evaporated under reduced pressure. The obtained residue was taken up in DCM (30 mL) and washed with 10% NaCl (10 mL). The organic phase was dried over MgSO_4 , evaporated under reduced pressure and the resulting crude was purified by flash chromatography on silica gel. Elution with cyclohexane/ethyl acetate 70/30 gave 0.50 g (62%) of 2-(pyridin-2-yl)-2-(m-tolyl)ethanol as a brown oil.

$^1\text{H NMR}$ (300 MHz, CDCl_3) δ 8.56 (ddd, $J = 5.0, 1.8, 0.9$ Hz, 1H), 7.58 (dt, $J = 7.7, 1.9$ Hz, 1H), 7.24 – 7.14 (m, 2H), 7.09 – 6.97 (m, 4H), 4.41 – 4.22 (m, 2H), 4.05 (dd, $J = 10.3, 3.7$ Hz, 1H), 2.32 (s, 3H).

2-(piperidin-2-yl)-2-(m-tolyl)ethanol



2-(pyridin-2-yl)-2-(m-tolyl)ethanol (0.62 g, 2.34 mmol) were dissolved in MeOH (50 mL) and 10% HCl (0.5 mL) and PtO₂ (0.10 g) were added. The mixture was vigorously stirred under 5 atm H₂ at RT for 4 hours and filtered on a celite/Florisil pad. The solvent was evaporated under reduced pressure to yield 0.64 g of 2-(piperidin-2-yl)-2-(m-tolyl)ethanol as a brown oil. The crude was used in the next step with no further purification.

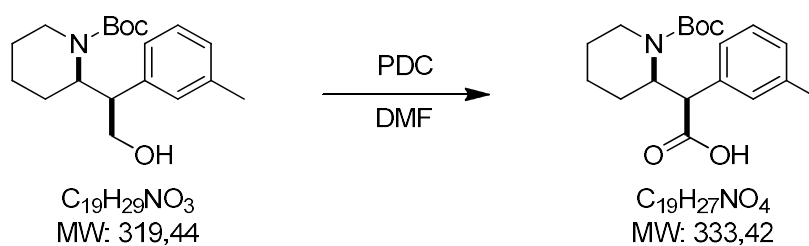
N-Boc-2-(piperidin-2-yl)-2-(*m*-tolyl)ethanol

A solution of Boc_2O (1.31 g, 6.02 mmol) in MeOH (10 mL) was added dropwise to a solution of 2-(piperidin-2-yl)-2-(*m*-tolyl)ethanol (0.66 g, 3.01 mmol) and TEA (0.88 mL, 6.32 mmol) in MeOH (10 mL). The mixture was refluxed for 4 hours, brought to RT and diluted with ethyl acetate (100 mL). The organic phase was washed with brine (3x30 mL), dried over MgSO_4 , evaporated under reduced pressure and the resulting crude was purified by flash chromatography on silica gel. Elution with cyclohexane/ethyl acetate 80/20 gave 0.05 g (5%) of *threo* *N*-Boc-2-(piperidin-2-yl)-2-(*m*-tolyl)ethanol and 0.31 g (32%) of *erythro* *N*-Boc-2-(piperidin-2-yl)-2-(*m*-tolyl)ethanol as yellow oils.

 ^1H NMR (300 MHz, CDCl_3)

threo: δ 7.23 – 7.02 (m, 4H), 4.70 – 4.58 (m, 1H), 4.10 – 3.96 (m, 1H), 3.65 – 3.48 (m, 1H), 3.40 (dd, $J = 10.9, 3.1$ Hz, 1H), 3.11 – 3.00 (m, 1H), 2.90 – 2.74 (m, 1H), 2.34 (s, 3H), 1.50 (s, 9H), 1.64 – 1.28 (m, 6H).

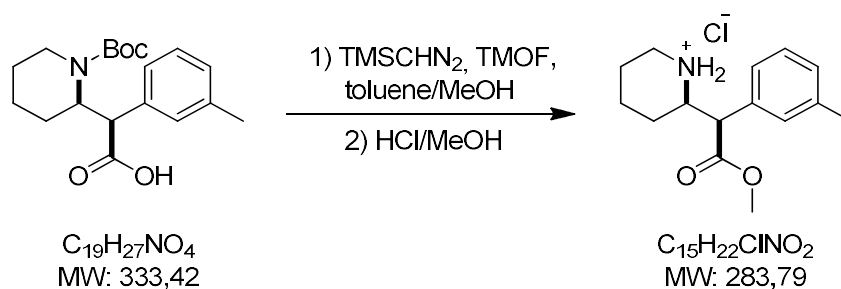
erythro: δ 7.21 – 7.15 (m, 1H), 7.08 – 7.01 (m, 3H), 4.59 – 4.41 (m, 1H), 3.88 – 3.61 (m, 3H), 3.35 – 3.14 (m, 1H), 2.72 – 2.49 (m, 1H), 2.31 (s, 3H), 1.84 – 1.19 (m, 6H), 1.29 (s, 9H).

erythro N-Boc-2-(piperidin-2-yl)-2-(*m*-tolyl)acetic acid

Pyridinium dichromate (1.41 g, 3.76 mmol) was added to a solution of *erythro N*-Boc-2-(piperidin-2-yl)-2-(*m*-tolyl)ethanol (0.30 g, 0.94 mmol) in DMF (5 mL) and the mixture was stirred at RT for 6 hours. Ethyl ether (5 mL) was added and the reaction was quenched by adding 10% HCl (2.5 mL) dropwise at 0° C. The aqueous phase was extracted with ethyl ether (3x5 mL) and the collected organic phases were extracted with 10% NaOH (3x10 mL). The collected aqueous phases were brought to pH=1 with conc. HCl and extracted with DCM (3x15 mL). The collected organic phases were dried over MgSO₄ and evaporated under reduced pressure to give 0.23 g (73%) of *erythro N*-Boc-2-(piperidin-2-yl)-2-(*m*-tolyl)acetic acid as a greenish brown oil.

¹H NMR (300 MHz, CDCl₃) δ 7.37 – 7.01 (m, 4H), 5.27 – 4.75 (m, 1H), 4.10 (d, *J* = 9.7 Hz, 1H), 4.22 – 3.62 (m, 1H), 2.81 – 2.59 (m, 1H), 2.34 (s, 3H), 1.90 – 1.53 (m, 3H), 1.55 – 1.05 (m, 3H), 1.27 (s, 9H).

erythro methyl 2-(piperidin-2-yl)-2-(*m*-tolyl)acetate hydrochloride (Compound V *erythro*)

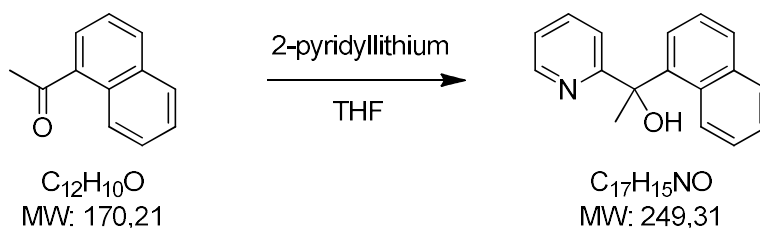


Trimethylorthoformate (0.10 mL, 0.90 mmol) and 2M trimethylsilyldiazomethane (0.45 mL, 0.90 mmol) were added to a solution of *erythro* *N*-Boc-2-(piperidin-2-yl)-2-(*m*-tolyl)acetic acid (0.23 g, 0.69 mmol) in toluene/MeOH (4.5 mL + 4.5 mL) and the mixture was stirred at RT for 5 hours. MeOH (5 mL) and 10% HCl (5 mL) were added and stirring was continued for additional 45 minutes. Solvents were evaporated under reduced pressure and the obtained crude was crystallized from IPE/IPA 90:10 to yield 0.10 g (51%) of *erythro* methyl 2-(piperidin-2-yl)-2-(*m*-tolyl)acetate hydrochloride (Compound V *erythro*) as a white solid (mp: 193° C with decomposition).

^1H NMR (300 MHz, CD_3OD) δ 7.33 (t, J = 7.7 Hz, 1H), 7.27 – 7.15 (m, 3H), 3.85 (d, J = 9.2 Hz, 1H), 3.81 – 3.72 (m, 1H), 3.69 (s, 3H), 3.30 – 3.24 (m, 1H), 3.05 – 2.90 (m, 1H), 2.38 (s, 3H), 2.18 – 2.03 (m, 1H), 1.98 – 1.81 (m, 2H), 1.77 – 1.49 (m, 3H).

^{13}C NMR (75 MHz, CD_3OD) δ 171.23, 139.39, 132.36, 129.56, 129.23, 129.08, 125.59, 58.03, 54.46, 51.72, 45.57, 27.48, 21.92, 21.59, 20.05.

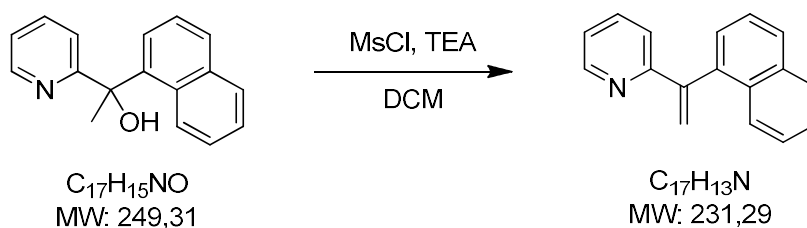
1-(naphthalen-1-yl)-1-(pyridin-2-yl)ethanol



2.7M *n*-BuLi (22.8 mL, 61.3 mmol) was added dropwise to a solution of 2-bromopyridine (5.33 mL, 55.9 mmol) in anhydrous THF (40 mL) at -78° C under nitrogen atmosphere. The mixture was stirred at the same temperature for 45 minutes and a solution of 3-methylacetophenone (8.93 mL, 58.7 mmol) in anhydrous THF (40 mL) was added. Stirring was continued at -78° C for 15 minutes and then the mixture was left stirring overnight at RT. The reaction was quenched with the addition of saturated NH₄Cl (50 mL), the separated organic phase was dried over MgSO₄ and evaporated under reduced pressure. The resulting crude was purified by flash chromatography on silica gel. Elution with cyclohexane/ethyl acetate 80/20 gave 4.60 g (34%) of 1-(naphthalen-1-yl)-1-(pyridin-2-yl)ethanol as a brown oil.

¹H NMR (300 MHz, CDCl₃) δ 8.67 – 8.63 (m, 1H), 7.88 – 7.78 (m, 4H), 7.53 – 7.44 (m, 2H), 7.37 – 7.31 (m, 1H), 7.23 – 7.15 (m, 2H), 6.87 – 6.83 (m, 1H), 5.83 (s, 1H), 2.02 (s, 3H).

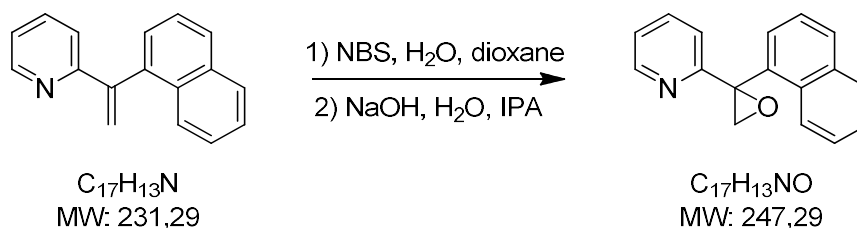
2-(1-(naphthalen-1-yl)vinyl)pyridine



TEA (0.76 mL, 5.46 mmol) and methanesulfonyl chloride (0.32 mL, 4.09 mmol) are added to a solution of 1-(1-(naphthalen-1-yl)-1-(pyridin-2-yl)ethanol) (0.34 g, 1.36 mmol) in DCM (4 mL) at 0° C. After stirring at RT overnight, the mixture was diluted with DCM (20 mL) and washed with 10% NaHCO₃ (10 mL) and 10% NaCl (3x10 mL). The organic phase was dried over MgSO₄, evaporated under reduced pressure and the resulting crude was purified by flash chromatography on silica gel. Elution with cyclohexane/ethyl acetate 80/20 gave 0.26 g (83%) of 2-(1-(naphthalen-1-yl)vinyl)pyridine as a brown oil.

¹H NMR (300 MHz, CDCl₃) δ 8.67 (ddd, *J* = 4.8, 1.8, 0.9 Hz, 1H), 7.88 (d, *J* = 7.8 Hz, 2H), 7.72 (d, *J* = 8.3 Hz, 1H), 7.58 – 7.42 (m, 4H), 7.41 – 7.30 (m, 1H), 7.15 (ddd, *J* = 7.5, 4.8, 1.1 Hz, 1H), 6.85 (d, *J* = 7.9 Hz, 1H), 6.67 (d, *J* = 2.1 Hz, 1H), 5.58 (d, *J* = 2.1 Hz, 1H).

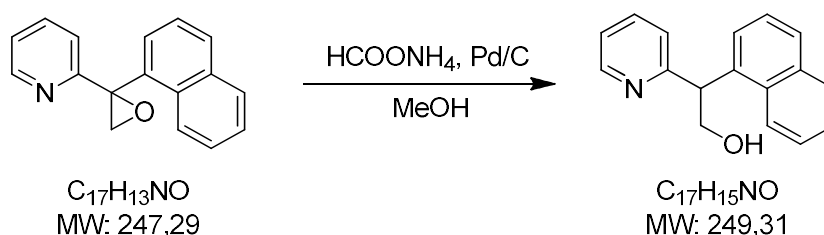
2-(2-(naphthalen-1-yl)oxiran-2-yl)pyridine



2-(1-(naphthalen-1-yl)vinyl)pyridine (2.26 g, 9.77 mmol) was dissolved in a 3:1 mixture of dioxane (70 mL) and water (25 mL). NBS (2.61 g, 14.6 mmol) was added and the mixture was stirred for 3 hours at RT. Ethyl acetate (50 mL) was added and the organic phase was washed with 10% $\text{Na}_2\text{S}_2\text{O}_5$ (30 mL) and 10% NaCl (20 mL) and evaporated under reduced pressure. The obtained residue was dissolved in IPA (80 mL), 10% NaOH (10 mL) was added and the mixture was stirred at RT for 2 hours. IPA was evaporated under reduced pressure, ethyl acetate (50 mL) was added and the organic phase was washed with 10% NaCl (20 mL), dried over MgSO_4 and evaporated under reduced pressure to give 2.81 g (90%) of 2-(2-(naphthalen-1-yl)oxiran-2-yl)pyridine as a dark orange oil.

$^1\text{H NMR}$ (300 MHz, CDCl_3) δ 8.62 (ddd, $J = 4.7, 1.6, 0.8$ Hz, 1H), 7.98 – 7.86 (m, 3H), 7.79 (d, $J = 7.0$ Hz, 1H), 7.59 – 7.38 (m, 4H), 7.22 – 7.15 (m, 1H), 7.12 (d, $J = 7.9$ Hz, 1H), 3.94 (d, $J = 6.3$ Hz, 1H), 3.38 (d, $J = 6.3$ Hz, 1H).

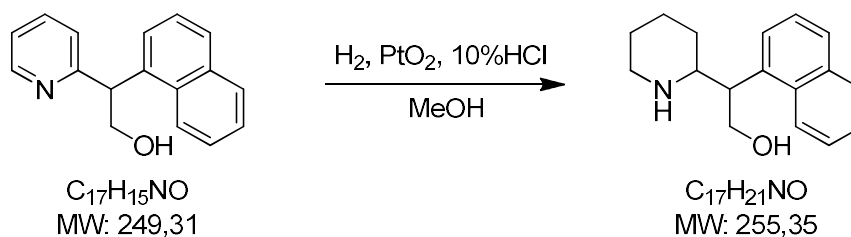
2-(naphthalen-1-yl)-2-(pyridin-2-yl)ethanol



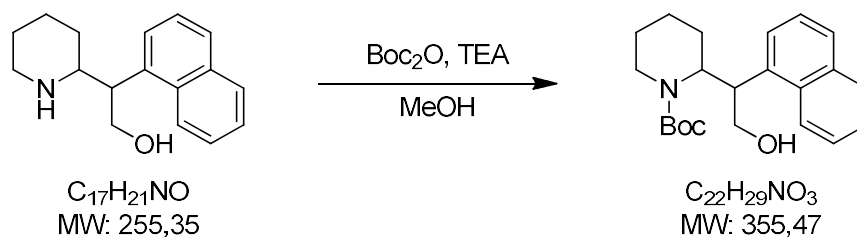
Ammonium formate (8.34 g, 132 mmol) and Pd/C (KF=50%, 0.22 g) were added to a solution of 2-(2-(naphthalen-1-yl)oxiran-2-yl)pyridine (2.18 g, 8.81 mmol) in anhydrous MeOH (50 mL) under nitrogen atmosphere. The mixture was refluxed for 4 hours, filtered on a celite pad and evaporated under reduced pressure. The obtained residue was taken up in ethyl acetate (50 mL) and washed with 10% NaCl (20 mL). The organic phase was dried over MgSO_4 , evaporated under reduced pressure and the resulting crude was purified by flash chromatography on silica gel. Elution with cyclohexane/ethyl acetate 80/20 gave 0.64 g (29%) of 2-(naphthalen-1-yl)-2-(pyridin-2-yl)ethanol as a brown oil.

$^1\text{H NMR}$ (300 MHz, CDCl_3) δ 8.63 (ddd, $J = 5.0, 1.8, 0.9$ Hz, 1H), 8.14 – 8.06 (m, 1H), 7.92 – 7.86 (m, 1H), 7.79 (d, $J = 8.2$ Hz, 1H), 7.58 (dt, $J = 7.8, 1.9$ Hz, 1H), 7.53 – 7.46 (m, 2H), 7.46 – 7.38 (m, 1H), 7.26 – 7.20 (m, 2H), 6.97 (d, $J = 8.2$ Hz, 1H), 5.24 (dd, $J = 8.7, 4.2$ Hz, 1H), 4.55 (dd, $J = 11.1, 8.7$ Hz, 1H), 4.20 (dd, $J = 11.1, 4.2$ Hz, 1H).

2-(naphthalen-1-yl)-2-(piperidin-2-yl)ethanol



2-(naphthalen-1-yl)-2-(pyridin-2-yl)ethanol (0.64 g, 2.57 mmol) were dissolved in MeOH (70 mL) and 10% HCl (0.5 mL) and PtO₂ (0.10 g) were added. The mixture was vigorously stirred under 5 atm H₂ at RT for 4 hours and filtered on a celite/Florisil pad. The solvent was evaporated under reduced pressure to yield 0.58 g (89%) of 2-(naphthalen-1-yl)-2-(piperidin-2-yl)ethanol as a brown oil. The obtained crude was used in the next step without further purification.

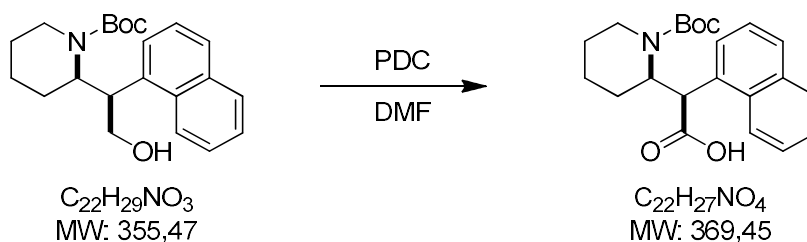
N-Boc-2-(naphthalen-1-yl)-2-(piperidin-2-yl)ethanol

A solution of Boc_2O (0.99 g, 4.54 mmol) in MeOH (10 mL) was added dropwise to a solution of 2-(naphthalen-1-yl)-2-(piperidin-2-yl)ethanol (0.58 g, 2.27 mmol) and TEA (0.66 mL, 4.77 mmol) in MeOH (10 mL). The mixture was refluxed for 1.5 hours, brought to RT and diluted with ethyl acetate (75 mL). The organic phase was washed with brine (3x20 mL), dried over MgSO_4 , evaporated under reduced pressure and the resulting crude was purified by flash chromatography on silica gel. Elution with cyclohexane/ethyl acetate 80/20 gave 0.08 g (10%) of *threo* *N*-Boc-2-(naphthalen-1-yl)-2-(piperidin-2-yl)ethanol and 0.15 g (18%) of *erythro* *N*-Boc-2-(naphthalen-1-yl)-2-(piperidin-2-yl)ethanol as yellow oils.

 ^1H NMR (300 MHz, CDCl_3)

threo: δ 8.0 (d, $J = 6.8$ Hz, 1H), 7.87 (d, $J = 9.3$ Hz, 1H), 7.75 (d, $J = 8.7$ Hz, 1H), 7.54 - 7.44 (m, 4H), 4.61 (d, $J = 6.3$ Hz, 1H), 4.13 - 4.01 (m, 2H), 3.77 - 3.69 (m, 1H), 3.64 - 3.59 (m, 1H), 2.68 - 2.55 (m, 1H), 1.9 - 1.23 (m, 6H), 1.45 (s, 9H).

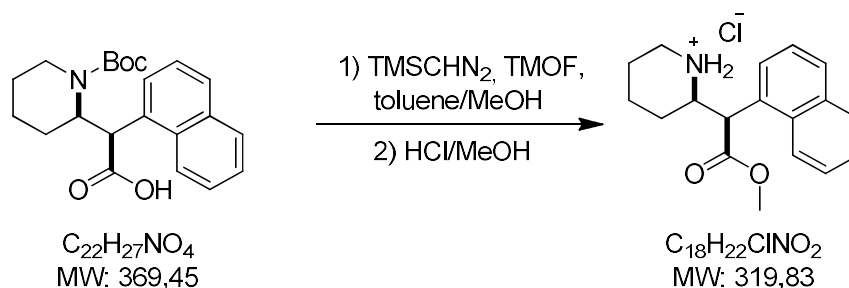
erythro: δ 9.2 (d, $J = 12.0$ Hz, 1H), 7.88 (d, $J = 6.7$ Hz, 1H), 7.76 (d, $J = 10.6$ Hz, 1H), 7.6 - 7.39 (m, 4H), 4.88 - 4.76 (m, 1H), 4.33 - 4.19 (m, 1H), 4.0 - 3.91 (m, 1H), 3.9 - 3.75 (m, 1H), 3.67 - 3.51 (m, 1H), 2.49 - 2.35 (m, 1H), 1.89 - 1.25 (m, 6H), 1.45 (s, 9H).

erythro N-Boc-2-(naphthalen-1-yl)-2-(piperidin-2-yl)acetic acid

PDC (670 mg, 1.79 mmol) was added to a solution of *erythro* 2-(naphthalen-1-yl)-2-(piperidin-2-yl)ethanol (150 mg, 0.45 mmol) in DMF (5 mL) and the mixture was stirred at RT for 4 hours. Ethyl ether (5 mL) was added and the reaction was quenched by adding 10% HCl (2.5 mL) dropwise at 0° C. The aqueous phase was extracted with ethyl ether (3x5 mL) and the collected organic phases were extracted with 10% NaOH (3x10 mL). The collected aqueous phases were brought to pH=1 with conc. HCl and extracted with DCM (3x15 mL). The collected organic phases were dried over MgSO₄ and evaporated under reduced pressure to give 60 mg (36%) of *erythro* N-Boc-2-(naphthalen-1-yl)-2-(piperidin-2-yl)acetic acid as a greenish brown oil.

¹H NMR (300 MHz, CDCl₃) δ 8.27 (d, *J* = 8.5 Hz, 1H), 7.89 – 7.71 (m, 3H), 7.56 (t, *J* = 7.1 Hz, 1H), 7.51 – 7.38 (m, 2H), 5.36 – 5.21 (m, 1H), 5.09 (d, *J* = 11.8 Hz, 1H), 3.80 – 3.59 (m, 1H), 2.47 (t, *J* = 13.0 Hz, 1H), 2.04 – 1.68 (m, 4H), 1.68 – 1.50 (m, *J* = 12.5 Hz, 1H), 1.50 – 1.12 (m, 10H).

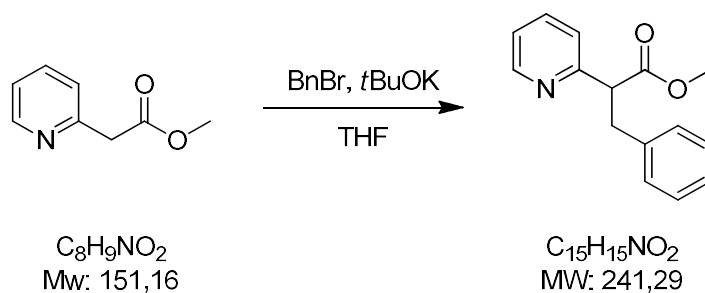
erythro methyl 2-(naphthalen-1-yl)-2-(piperidin-2-yl)acetate hydrochloride (Compound IV *erythro*)



Trimethylorthoformate (20 μl , 0.18 mmol) and 2M trimethylsilyldiazomethane (90 μl , 0.18 mmol) were added to a solution of *erythro* N-Boc-2-(naphthalen-1-yl)-2-(piperidin-2-yl)acetic acid (50 mg, 0.13 mmol) in toluene/MeOH (1 mL + 1 mL) and the mixture was stirred at RT for 2 hours. MeOH (5 mL) and 10% HCl (5 mL) were added and stirring was continued for additional 45 minutes. Solvents were evaporated under reduced pressure and the obtained crude was slurried in hot IPE to yield 18 mg (44%) of a mixture of *threo* and *erythro* methyl 2-(naphthalen-1-yl)-2-(piperidin-2-yl)acetate hydrochloride (Compound IV *erythro*) as a light brown solid.

$^1\text{H NMR}$ (300 MHz, CD_3OD) δ 8.28 – 8.23 (m, 1H), 8.00 – 7.95 (m, 2H), 7.69 – 7.54 (m, 4H), 4.09 – 3.98 (m, 1H), 3.66 (s, 3H), 3.28 – 3.19 (m, 1H), 3.09 – 2.94 (m, 1H), 2.29 – 2.18 (m, 1H), 1.98 – 1.82 (m, 3H), 1.76 – 1.61 (m, 3H).

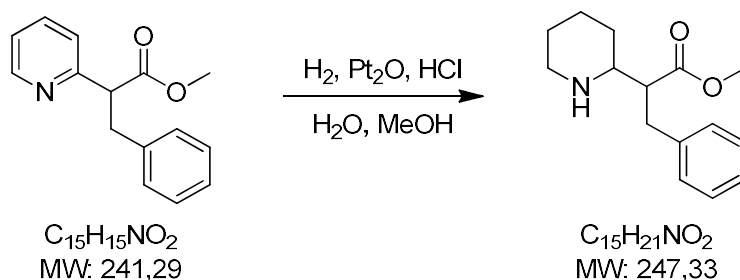
Methyl 3-phenyl-2-(pyridin-2-yl)propanoate



Potassium *tert*-butylate (3.89 g, 34.7 mmol) was added to a solution of methyl 2-(pyridin-2-yl)acetate (4.42 mL, 33.1 mmol) in anhydrous THF (165 mL) at 0° C under nitrogen atmosphere and the mixture was stirred at the same temperature for 30 minutes. Benzyl bromide (0.79 mL, 6.62 mmol) was added and stirring was continued at RT overnight. The solvent was evaporated under reduced pressure, the residue was taken up in ethyl ether (100 mL) and washed with 10% NaCl (30 mL). The organic phase was dried over MgSO₄, evaporated under reduced pressure and the resulting crude was purified by flash chromatography on silica gel. Elution with cyclohexane/ethyl acetate 80/20 gave 4.56 g (57%) of methyl 3-phenyl-2-(pyridin-2-yl)propanoate as a light yellow oil.

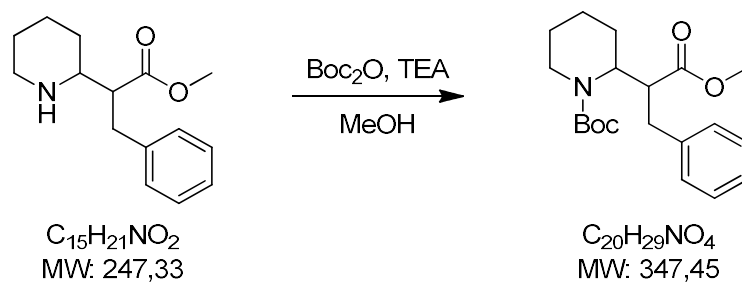
¹H NMR (300 MHz, CDCl₃) δ 8.59 (ddd, *J* = 4.9, 1.8, 0.9 Hz, 1H), 7.59 (dt, *J* = 7.7, 1.8 Hz, 1H), 7.24 – 7.10 (m, 7H), 4.14 – 4.08 (m, 1H), 3.64 (s, 3H), 3.46 (dd, *J* = 13.8, 8.2 Hz, 1H), 3.24 (dd, *J* = 13.8, 7.4 Hz, 1H).

Methyl 3-phenyl-2-(piperidin-2-yl)propanoate



Methyl 3-phenyl-2-(pyridin-2-yl)propanoate (0.70 g, 2.90 mmol) was dissolved in MeOH (30 mL) and Pt₂O (0.07 g) and conc. HCl (0.2 mL) were added. The mixture was vigorously stirred under H₂ (1.5 atm) at RT for 5 hours and filtered on a celite/Florisil pad. The solvents were evaporated under reduced pressure and the obtained residue was taken up in ethyl acetate (30 mL) and washed with 10% NaOH (10 mL) and 10% EDTA (10 mL). The organic phase was dried over MgSO₄, evaporated under reduced pressure to yield 0.60 g (73%) of methyl 3-phenyl-2-(piperidin-2-yl)propanoate as a yellow oil.

¹H NMR (300 MHz, CDCl₃) δ 7.30 – 7.15 (m, 5H), 3.56 (s, 3H), 3.23 (t, *J* = 12.8 Hz, 1H), 3.13 – 2.92 (m, 2H), 2.92 – 2.77 (m, 1H), 2.73 – 2.61 (m, 1H), 1.92 – 1.78 (m, 1H), 1.75 – 1.31 (m, 5H).

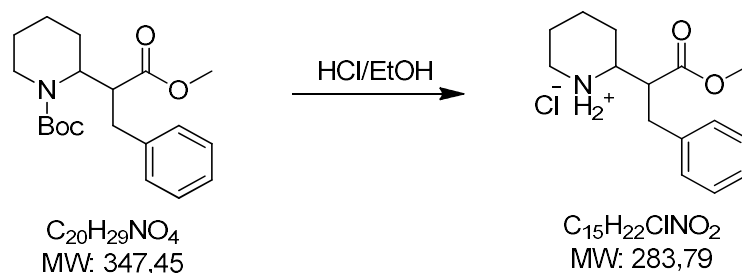
N-Boc methyl 3-phenyl-2-(piperidin-2-yl)propanoate (*threo/erythro*)

Methyl 3-phenyl-2-(piperidin-2-yl)propanoate (1.08 g, 4.37 mmol) and TEA (1.28 mL, 9.17 mmol) were dissolved in MeOH (20 mL) and a solution of Boc_2O (1.90 g, 8.73 mmol) in MeOH (10 mL) was added dropwise. The mixture was refluxed for 2 hours and the solvent was evaporated under reduced pressure. The obtained residue was taken up in ethyl acetate (20 mL) and washed with 10% NaCl (2x10 mL). The organic phase was dried over MgSO_4 , evaporated under reduced pressure and the resulting crude was purified by flash chromatography on silica gel. Elution with cyclohexane/ethyl acetate 100/0 to 85/15 gave 0.10 g (6%) of *threo* *N*-Boc methyl 3-phenyl-2-(piperidin-2-yl)propanoate and 0.10 g (6%) of *erythro* *N*-Boc methyl 3-phenyl-2-(piperidin-2-yl)propanoate as colorless oils.

***threo*:** $^1\text{H NMR}$ (300 MHz, CDCl_3) δ 7.31 – 7.23 (m, 2H), 7.23 – 7.13 (m, 3H), 4.56 – 4.46 (m, 1H), 4.06 – 3.92 (m, 1H), 3.49 (s, 3H), 3.24 (dt, $J = 11.1, 4.2$ Hz, 1H), 3.01 – 2.85 (m, 2H), 2.83 – 2.72 (m, 1H), 1.92 – 1.79 (m, 1H), 1.69 – 1.53 (m, 5H), 1.45 (s, 9H).

***erythro*:** $^1\text{H NMR}$ (300 MHz, CD_3OD) δ 7.28 – 7.21 (m, 2H), 7.21 – 7.16 (m, 1H), 7.14 – 7.09 (m, 2H), 4.56-4.41 (m, 1H), 4.14 – 3.97 (m, 1H), 3.49 (s, 3H), 3.24 (dd, $J = 11.2, 4.4$ Hz, 1H), 2.94 – 2.73 (m, 1H), 2.79 (dd, $J = 13.5, 11.1$ Hz, 1H), 2.67 (dd, $J = 13.5, 4.3$ Hz, 1H), 1.76 – 1.41 (m, 6H), 1.50 (s, 9H).

erythro methyl 3-phenyl-2-(piperidin-2-yl)propanoate hydrochloride (Compound IX *erythro*)

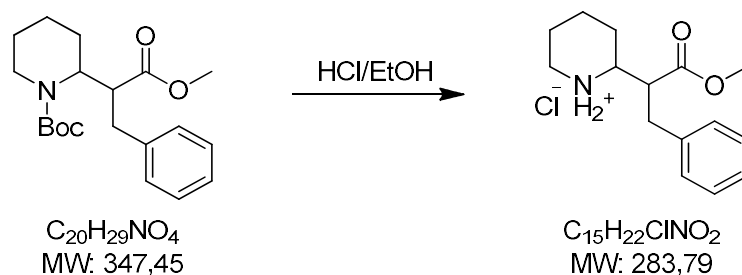


erythro *N*-Boc methyl 3-phenyl-2-(piperidin-2-yl)propanoate (100 mg, 0.29 mmol) was dissolved in excess 3N HCl/EtOH and stirred at RT overnight. The solvent was evaporated under reduced pressure to give 80 mg (100%) of *erythro* methyl 3-phenyl-2-(piperidin-2-yl)propanoate hydrochloride (Compound IX *erythro*) as a white solid (mp: 153.64° C).

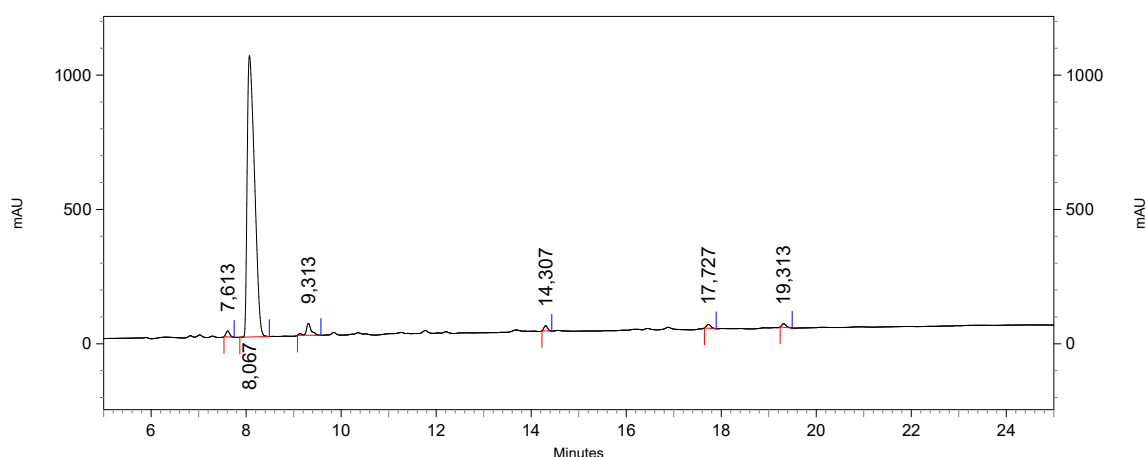
^1H NMR (300 MHz, CDCl_3) δ 9.71 – 9.39 (m, 2H), 7.29 – 7.14 (m, 5H), 3.62 (s, 3H), 3.61 – 3.52 (m, 1H), 3.50 – 3.23 (m, 3H), 3.02 – 2.89 (m, 1H), 2.89 – 2.70 (m, 1H), 2.16 – 1.82 (m, 4H), 1.82 – 1.70 (m, 1H), 1.51 – 1.35 (m, 1H).

^{13}C NMR (75 MHz, CD_3OD) δ 171.75 (s), 137.48 (s), 128.48 (s), 128.31 (s), 126.59 (s), 57.82 (s), 51.30 (s), 50.25 (s), 45.72 (s), 33.94 (s), 25.39 (s), 21.87 (s).

threo methyl 3-phenyl-2-(piperidin-2-yl)propanoate hydrochloride (Compound IX *threo*)



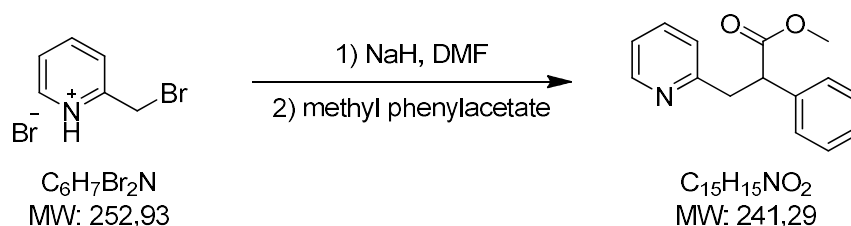
threo N-Boc methyl 3-phenyl-2-(piperidin-2-yl)propanoate (250 mg, 0.72 mmol) was dissolved in excess 3N HCl/EtOH and stirred at RT overnight. The solvent was evaporated under reduced pressure and the obtained residue was slurried in cold diethyl ether to give 200 mg (100%) of superior methyl 3-phenyl-2-(piperidin-2-yl)propanoate hydrochloride (Compound IX *threo*) as a white solid (mp: 161.90° C). Retention Time (HPLC) = 8.06'; A% (HPLC) = 94%.



^1H NMR (300 MHz, CD_3OD) δ 7.33 – 7.28 (m, 2H), 7.25 – 7.19 (m, 3H), 3.61 (s, 3H), 3.48 – 3.38 (m, 1H), 3.37 – 3.27 (m, 1H), 3.15 – 3.05 (m, 1H), 3.05 – 2.94 (m, 3H), 2.06 – 1.83 (m, 3H), 1.83 – 1.63 (m, 1H), 1.63 – 1.49 (m, 2H).

^{13}C NMR (75 MHz, CD_3OD) δ 172.53, 137.26, 128.46, 128.27, 126.64, 57.94, 51.28, 50.57, 45.76, 34.28, 26.88, 21.87, 21.80.

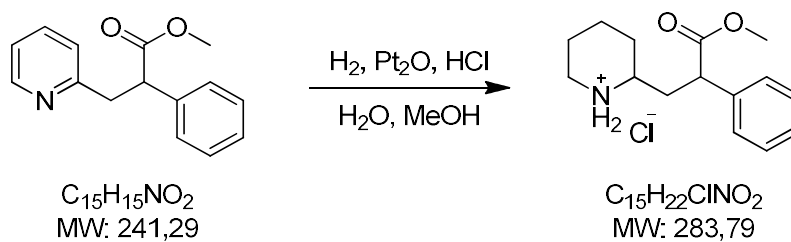
Methyl 2-phenyl-3-(pyridin-2-yl)propanoate



A solution of 2-(bromomethyl)pyridine hydrobromide (8.84 g, 35.0 mmol) in DMF (50 mL) and a solution of methyl phenylacetate (5.00 g, 33.3 mmol) in DMF (50 mL) were added dropwise to a suspension of NaH (1.64 g, 68.2 mmol) in DMF (30 mL) at 0° C. The mixture was stirred 4 hours at RT and the solvent was evaporated under reduced pressure. The obtained residue was taken up in ethyl acetate (75 mL) and washed with 10% NaCl (4x25 mL). The organic phase was dried over MgSO₄, evaporated under reduced pressure and the resulting crude was purified by flash chromatography on silica gel. Elution with cyclohexane/ethyl acetate 70/30 gave 5.40 g (67%) of methyl 2-phenyl-3-(pyridin-2-yl)propanoate as a light yellow oil.

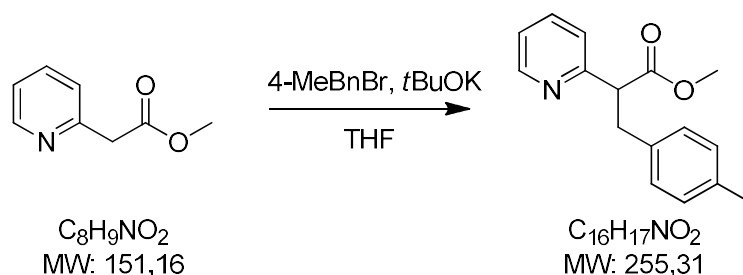
¹H NMR (300 MHz, CDCl₃) δ 8.55 – 8.51 (m, 1H), 7.51 (td, *J* = 7.7, 1.8 Hz, 1H), 7.36 – 7.22 (m, 5H), 7.11 – 7.07 (m, 1H), 7.05 (d, *J* = 7.8 Hz, 1H), 4.28 (dd, *J* = 9.2, 6.3 Hz, 1H), 3.62 (dd, *J* = 9.4 Hz, 1H), 3.61 (s, 3H), 3.16 (dd, *J* = 14.2, 6.3 Hz, 1H).

Methyl 2-phenyl-3-(piperidin-2-yl)propanoate (Compound XI *threo* + *erythro*)



Methyl 2-phenyl-3-(pyridin-2-yl)propanoate (5.40 g, 22.4 mmol) was dissolved in MeOH (100 mL) and Pt₂O (0.42 g) and conc. HCl (2.0 mL) were added. The mixture was vigorously stirred under H₂ (1.5 atm) at RT for 4 hours and filtered on a celite/Florisil pad. The solvents were evaporated under reduced pressure to yield 6.16 g (97%) of a mixture of *threo* and *erythro* methyl 2-phenyl-3-(piperidin-2-yl)propanoate as a white solid.

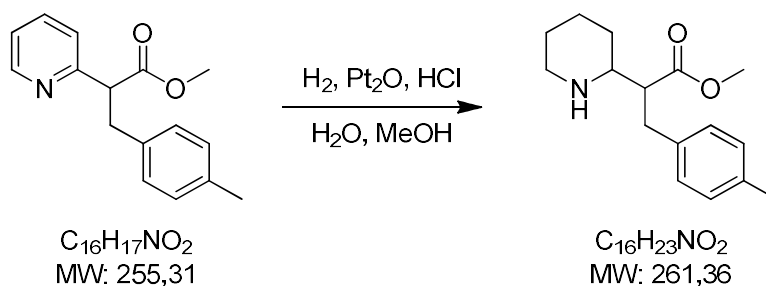
Methyl 2-(pyridin-2-yl)-3-(p-tolyl)propanoate



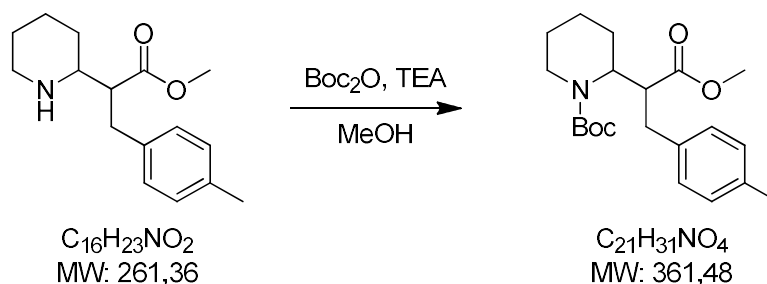
Potassium *tert*-butylate (1.56 g, 13.9 mmol) was added to a solution of methyl 2-(pyridin-2-yl)acetate (1.77 mL, 13.2 mmol) in anhydrous THF (80 mL) at 0° C under nitrogen atmosphere and the mixture was stirred at the same temperature for 30 minutes. 4-methylbenzyl bromide (1.78 mL, 13.2 mmol) was added and stirring was continued at RT overnight. The solvent was evaporated under reduced pressure, the residue was taken up in ethyl ether (50 mL) and washed with 10% NaCl (20 mL). The organic phase was dried over MgSO₄, evaporated under reduced pressure and the resulting crude was purified by flash chromatography on silica gel. Elution with cyclohexane/ethyl acetate 80/20 gave 0.56 g (18%) of methyl 2-(pyridin-2-yl)-3-(p-tolyl)propanoate as a yellow oil.

¹H NMR (300 MHz, CDCl₃) δ 8.58 (ddd, *J* = 4.8, 1.8, 0.9 Hz, 1H), 7.60 (dt, *J* = 7.7, 1.9 Hz, 1H), 7.24 – 7.17 (m, 1H), 7.17 – 7.13 (m, 1H), 7.05 – 6.98 (m, 4H), 4.12 – 4.05 (m, 1H), 3.41 (dd, *J* = 13.8, 8.0 Hz, 1H), 3.19 (dd, *J* = 13.8, 8.0 Hz, 1H), 2.28 (s, 3H).

Methyl 2-(piperidin-2-yl)-3-(p-tolyl)propanoate



Methyl 2-(pyridin-2-yl)-3-(p-tolyl)propanoate (0.53 g, 2.20 mmol) was dissolved in MeOH (70 mL) and Pt₂O (0.05 g) and conc. HCl (0.18 mL) were added. The mixture was vigorously stirred under H₂ (1.5 atm) at RT for 2 hours and filtered on a celite/Florisil pad. The solvents were evaporated under reduced pressure to give 0.66 g of crude green solid which was used in the next step without further purification.

N-Boc methyl 2-(piperidin-2-yl)-3-(*p*-tolyl)propanoate (*threo/erythro*)

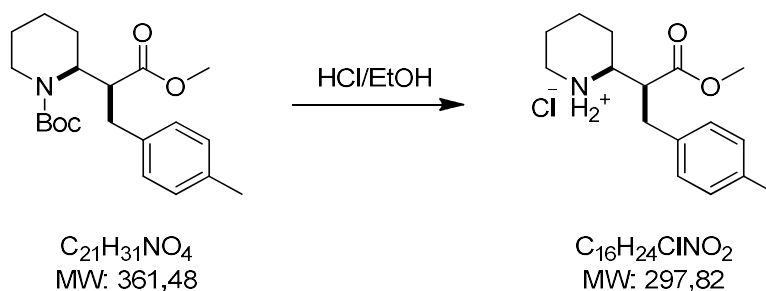
Crude methyl 2-(piperidin-2-yl)-3-(*p*-tolyl)propanoate (0.66 g, 2.20 mmol) and TEA (0.95 mL, 6.82 mmol) were dissolved in MeOH (15 mL) and a solution of Boc_2O (0.96 g, 4.40 mmol) in MeOH (10 mL) was added dropwise. The mixture was refluxed for 2 hours and the solvent was evaporated under reduced pressure. The obtained residue was taken up in ethyl acetate (20 mL) and washed with 10% NaCl (2x10 mL). The organic phase was dried over MgSO_4 , evaporated under reduced pressure and the resulting crude was purified by flash chromatography on silica gel. Elution with cyclohexane/ethyl acetate 90/10 gave 0.09 g (11% over 2 steps) of *threo* *N*-Boc methyl 2-(piperidin-2-yl)-3-(*p*-tolyl)propanoate and 0.09 g (11% over 2 steps) of *erythro* *N*-Boc methyl 2-(piperidin-2-yl)-3-(*p*-tolyl)propanoate as light yellow oils.

 ^1H NMR (300 MHz, CD_3OD)

threo: δ 7.06 (d, $J = 8.0$ Hz, 2H), 6.99 (d, $J = 8.1$ Hz, 2H), 4.58 – 4.39 (m, 1H), 4.16 – 3.90 (m, 1H), 3.50 (s, 3H), 3.27 – 3.18 (m, 1H), 2.88 – 2.68 (m, 2H), 2.61 (dd, $J = 13.5, 4.2$ Hz, 1H), 2.27 (s, 3H), 1.74 – 1.55 (m, 5H), 1.49 (s, 9H), 1.49 – 1.45 (m, 1H).

erythro: δ 7.10 – 6.96 (m, 4H), 4.51 – 4.40 (m, 1H), 3.99 – 3.88 (m, 1H), 3.45 (s, 3H), 3.28 – 3.20 (m, 1H), 3.06 – 2.91 (m, 1H), 2.85 – 2.73 (m, 2H), 2.27 (s, 3H), 2.01 – 1.92 (m, 1H), 1.73 – 1.54 (m, 3H), 1.52 – 1.34 (m, 2H), 1.43 (s, 9H).

threo methyl 2-(piperidin-2-yl)-3-(*p*-tolyl)propanoate hydrochloride (Compound X *threo*)

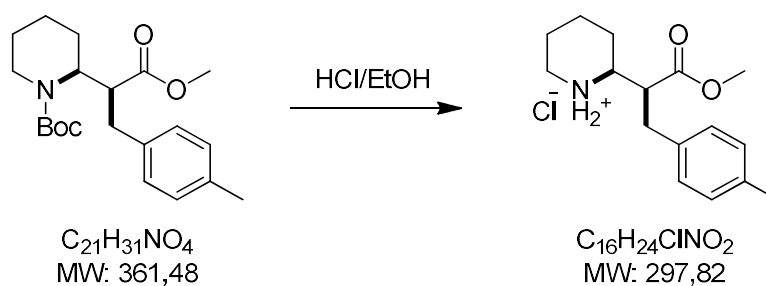


threo *N*-Boc methyl 2-(piperidin-2-yl)-3-(*p*-tolyl)propanoate (90 mg, 0.25 mmol) was dissolved in excess 3N HCl/EtOH and stirred at RT overnight. The solvent was evaporated under reduced pressure and the obtained residue was slurried in hot IPE to give 40 mg (54%) of *threo* methyl 3-phenyl-2-(piperidin-2-yl)propanoate hydrochloride (Compound X *threo*) as a light yellow solid (mp: 196.37° C).

1H NMR (300 MHz, CD_3OD) δ 7.11 (d, $J = 8.2$ Hz, 2H), 7.06 (d, $J = 8.3$ Hz, 2H), 3.61 (s, 3H), 3.00 – 2.85 (m, 2H), 2.29 (s, 3H), 2.01 – 1.78 (m, 3H), 1.76 – 1.33 (m, 5H).

^{13}C NMR (75 MHz, CD_3OD) δ 136.38, 134.24, 128.95, 128.31, 57.76, 51.31, 50.35, 45.74, 33.40, 25.38, 21.91, 19.64.

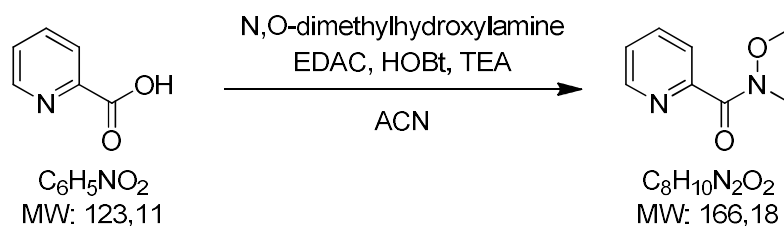
erythro methyl 2-(piperidin-2-yl)-3-(p-tolyl)propanoate hydrochloride (Compound X *erythro*)



erythro N-Boc methyl 2-(piperidin-2-yl)-3-(p-tolyl)propanoate (90 mg, 0.25 mmol) was dissolved in excess 3N HCl/EtOH and stirred at RT overnight. The solvent was evaporated under reduced pressure and the obtained residue was slurried in hot IPE to give 40 mg (54%) of *erythro* methyl 3-phenyl-2-(piperidin-2-yl)propanoate hydrochloride (Compound X *erythro*) as a light yellow solid (mp: 180.67° C).

¹H NMR (300 MHz, CD₃OD) δ 7.11 (d, *J* = 8.2 Hz, 2H), 7.05 (d, *J* = 8.2 Hz, 2H), 3.59 (s, 3H), 3.48 – 3.34 (m, 2H), 3.00 – 2.87 (m, 4H), 2.29 (s, 3H), 2.15 – 2.04 (m, 1H), 1.98 – 1.84 (m, 2H), 1.78 – 1.33 (m, 3H).

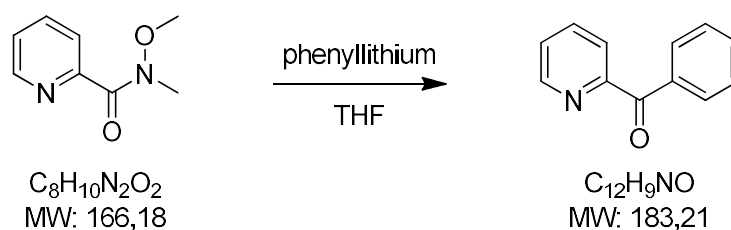
¹³C NMR (75 MHz, CD₃OD) δ 136.37, 134.06, 128.87, 128.32, 57.89, 51.26, 50.62, 45.75, 33.90, 26.96, 21.92, 21.81, 19.62.

N-methoxy-*N*-methylpicolinamide

TEA (5.94 mL, 42.6 mmol) was added dropwise to a suspension of picolinic acid (5.00 g, 40.6 mmol), *N,O*-dimethylhydroxylamine (4.16 g, 42.6 mmol), EDAC (9.34 g, 48.7 mmol) and HOBT (1.87 g, 12.2 mmol) in ACN (50 mL) under nitrogen atmosphere and the mixture was stirred at RT for 3 days. Saturated NaCl (60 mL) was added and ACN was evaporated under reduced pressure. The aqueous phase was extracted with ethyl acetate (3x20 mL), the collected organic phases were washed with 10% NaHCO₃ (20 mL), dried over MgSO₄ and evaporated under reduced pressure to yield 5.99 g (89%) of *N*-methoxy-*N*-methylpicolinamide as a yellow oil.

¹H NMR (CDCl₃) δ 8.61 (m, 1H), 7.79-7.76 (m, 1H), 7.70 – 7.59 (m, 1H), 7.39-7.32 (m, 1H), 3.74(s, 3H), 3.2 (s, 3H).

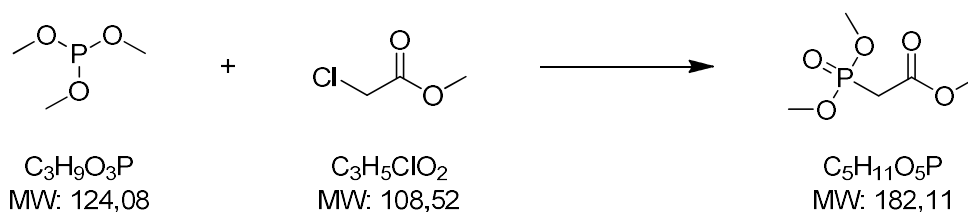
Phenyl(pyridin-2-yl)methanone



1.9M phenyllithium (4.90 mL, 9.41 mmol) was added to a solution of *N*-methoxy-*N*-methylpicolinamide (0.98 g, 5.88 mmol) in anhydrous THF (10 mL) at -20°C under nitrogen atmosphere and stirred for 2 hours. The reaction was quenched with the dropwise addition of 2N HCl/MeOH (5.88 mL, 11.8 mmol) at the same temperature. The solvent was evaporated under reduced pressure and the obtained residue was dissolved in ethyl acetate (60 mL). The organic phase was extracted with 10% HCl (3x20 mL) and the collected aqueous phases were basified with NaOH pellets and extracted with ethyl acetate (3x20 mL). The collected organic phases were dried over $MgSO_4$ and evaporated under reduced pressure to yield 0.91 g (84%) of phenyl(pyridin-2-yl)methanone as a yellow oil.

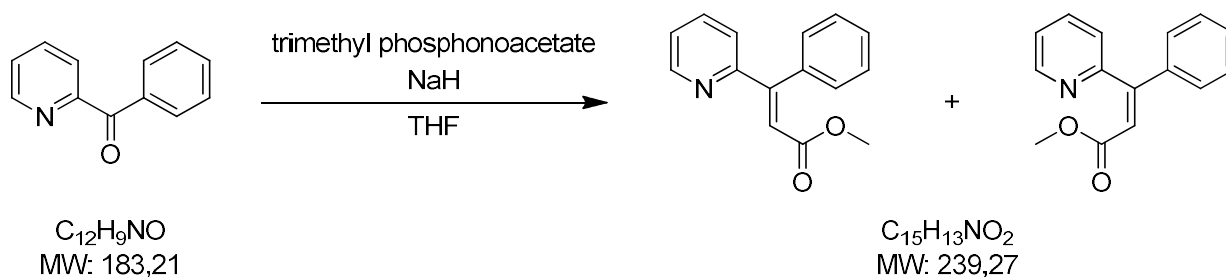
$^1\text{H NMR (CDCl}_3)$ δ 8.79 – 8.66 (m, 1H), 8.05 (ddd, $J = 6.9, 6.0, 1.1$ Hz, 3H), 7.95 – 7.85 (m, 1H), 7.66 – 7.55 (m, 1H), 7.53 – 7.44 (m, 3H).

Trimethyl phosphonoacetate



Trimethyl phosphite (4.75 mL, 40.3 mmol) and methyl chloroacetate (2.05 mL, 33.6 mmol) were stirred at 100° C for 3 days. The mixture was then diluted with ethyl acetate (60 mL) and washed with water (2x20 mL) and 10% NaCl (20 mL). The organic phase was dried over MgSO₄ and carefully evaporated under reduced pressure to yield 2.71 g (44%) of trimethyl phosphonoacetate as a light yellow oil.

¹H NMR (300 MHz, CDCl₃) δ 3.81 (d, *J* = 11.3 Hz, 6H), 3.75 (s, 3H), 3.02 (d, *J* = 0.9 Hz, 1H), 2.95 (d, *J* = 0.9 Hz, 1H).

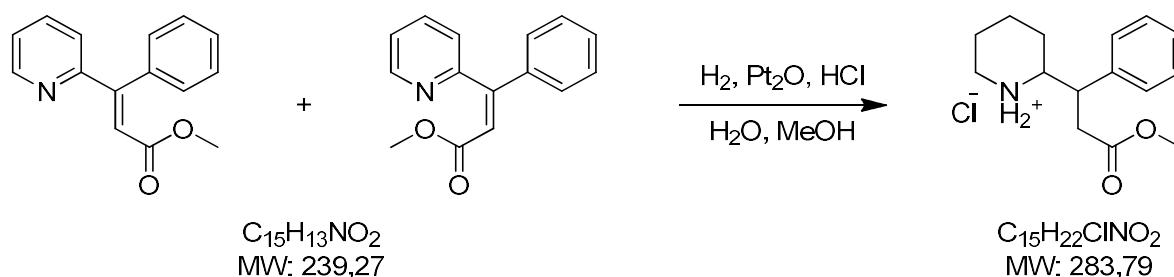
(E,Z)-methyl 3-phenyl-3-(pyridin-2-yl)acrylate

A solution of trimethyl phosphonoacetate (4.73 g, 25.9 mmol) in anhydrous THF (10 mL) was added dropwise to a suspension of NaH (0.62 g, 25.9 mmol) in anhydrous THF (10 mL) at 0° C under nitrogen atmosphere. After stirring for 1 hour, a solution phenyl(pyridin-2-yl)methanone (4.33 g, 23.6 mmol) in anhydrous THF (20 mL) was added and stirring was continued for 3 days. The reaction was quenched with the addition of 10% HCl (15 mL) and THF was evaporated under reduced pressure. The mixture was then diluted with 10% HCl (10 mL) and water (25 mL) and washed with ethyl ether (10 mL). The aqueous phase was basified with NaOH pellets and extracted with ethyl acetate (3x20 mL). The collected organic phases were dried over MgSO₄, evaporated under reduced pressure and the resulting crude was purified by flash chromatography on silica gel. Elution with toluene/ethyl acetate 95/5 gave 1.18 g (21%) of (*Z*)-methyl 3-phenyl-3-(pyridin-2-yl)acrylate and 1.00 g (18%) of (*E*)-methyl 3-phenyl-3-(pyridin-2-yl)acrylate as light yellow oils.

***E* isomer ¹H NMR (300 MHz, CDCl₃)** δ 8.68 – 8.65 (m, 1H), 7.58 (dt, *J* = 7.7, 1.9 Hz, 1H), 7.44 – 7.39 (m, 3H), 7.28 – 7.22 (m, 3H), 7.18 (s, 1H), 7.00 (dt, *J* = 8.0, 1.0 Hz, 1H), 3.61 (s, 3H).

***Z* isomer ¹H NMR (300 MHz, CDCl₃)** δ 8.69 (dd, *J* = 4.1, 1.1 Hz, 1H), 7.75 (td, *J* = 7.7, 1.1 Hz, 1H), 7.46 – 7.13 (m, 7H), 6.49 (s, 1H), 3.61 (s, 3H)

erythro methyl 3-phenyl-3-(piperidin-2-yl)propanoate hydrochloride (Compound XII *erythro*)

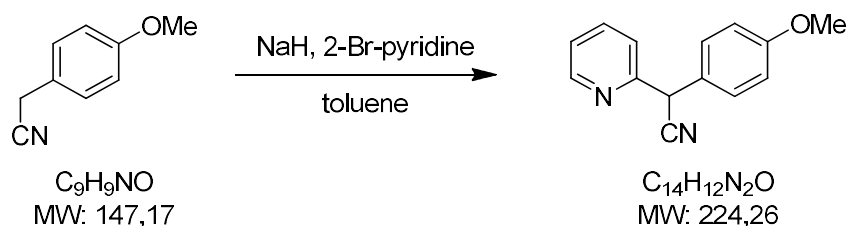


(*E,Z*)-methyl 3-phenyl-3-(pyridin-2-yl)acrylate (2.20 g, 9.20 mmol) was dissolved in MeOH (70 mL) and Pt₂O (0.11 g) and conc. HCl (0.90 mL) were added. The mixture was vigorously stirred under H₂ (1.5 atm) at RT for 4 hours and filtered on a celite/Florisil pad. The solvents were evaporated under reduced pressure and the obtained crude was crystallized from IPE to yield 2.57 g (98%) of *erythro* methyl 3-phenyl-3-(piperidin-2-yl)propanoate (Compound XII *erythro*) as a white solid (mp: 171.27° C).

Configuration established from the *N*-Boc derivative ¹H NMR:

¹H NMR (300 MHz, CD₃OD) δ 7.25 – 7.20 (m, 5H), 4.48 – 4.40 (m, 1H), 3.85 – 3.73 (m, 1H), 3.65 (ddd, *J* = 11.1, 10.2, 5.0 Hz, 1H), 3.47 (s, 3H), 2.92 – 2.81 (m, 1H), 2.76 (dd, *J* = 15.2, 4.9 Hz, 1H), 2.61 (dd, *J* = 15.2, 10.0 Hz, 1H), 1.95 – 1.81 (m, 1H), 1.81 – 1.71 (m, 1H), 1.72 – 1.57 (m, 3H), 1.47 – 1.28 (m, 1H), 1.21 (s, 9H).

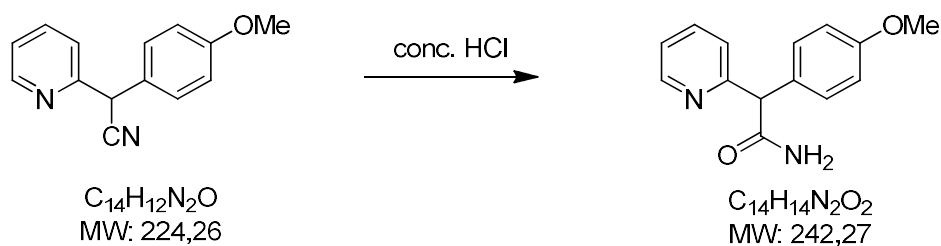
2-(4-methoxyphenyl)-2-(pyridin-2-yl)acetonitrile



4-methoxyphenylacetonitrile (4.60 mL, 34.0 mmol) and 2-bromopyridine (3.08 mL, 32.3 mmol) were added dropwise at 0° C to a suspension of NaH (1.55 g, 64.7 mmol) in toluene (50 mL) under nitrogen atmosphere. After stirring at 80° C overnight the reaction was quenched with the careful addition of water (20 mL). The organic phase was washed with 10% NaCl (2x20 mL), dried over Mg₂SO₄ and evaporated under reduced pressure. The obtained crude was crystallized from MeOH to yield 2.86 g (38%) of 2-(4-methoxyphenyl)-2-(pyridin-2-yl)acetonitrile as a solid (mp: 86-89° C).

¹H NMR (300 MHz, CDCl₃) 8.59 (d, *J* = 4.8 Hz, 1H), 7.69 (ddd, *J* = 7.8, 4.8, 1.8 Hz, 1H), 7.36 (d, *J* = 1.9 Hz, 1H), 7.38 – 7.33 (m, 1H), 7.33 (d, *J* = 1.9 Hz, 1H), 7.27 – 7.19 (m, 1H), 6.91 (d, *J* = 2.0 Hz, 1H), 6.88 (d, *J* = 2.0 Hz, 1H), 5.26 (s, 1H), 3.78 (s, 3H).

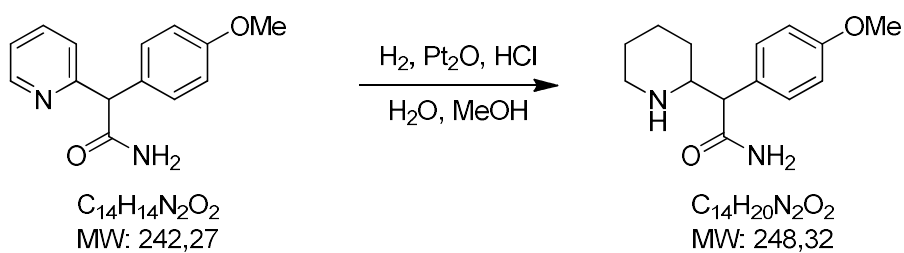
2-(4-methoxyphenyl)-2-(pyridin-2-yl)acetamide



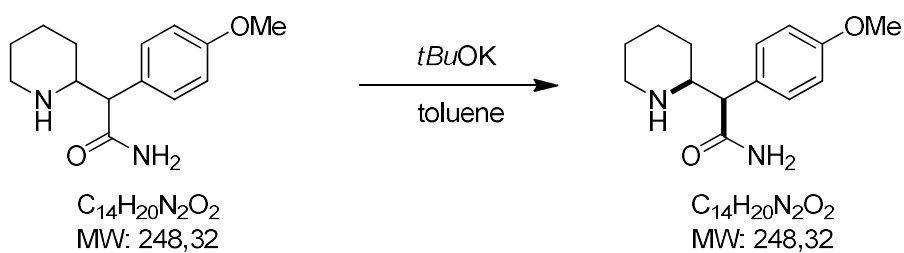
2-(4-methoxyphenyl)-2-(pyridin-2-yl)acetonitrile (1.00 g, 4.46 mmol) was dissolved in conc. HCl (10 mL) and stirred at RT for 2 hours. The mixture was poured into iced water (50 mL), basified to pH 10 with 10% NaOH and extracted with DCM (3x30 mL). The collected organic phases were dried over Mg_2SO_4 , evaporated under reduced pressure and the obtained crude was purified by flash chromatography on silica gel. Elution with DCM/MeOH 97:3 gave 0.52 g (48%) of 2-(4-methoxyphenyl)-2-(pyridin-2-yl)acetamide as a yellow oil.

^1H NMR (300 MHz, CDCl_3) 8.60 (ddd, $J = 4.8, 1.8, 0.9$ Hz, 1H), 7.66 (dt, $J = 7.7, 1.9$ Hz, 1H), 7.38 – 7.31 (m, 2H), 7.29 (t, $J = 0.9$ Hz, 1H), 7.20 (ddd, $J = 7.6, 4.9, 1.1$ Hz, 1H), 6.88 – 6.82 (m, 2H), 4.96 (s, 1H), 3.77 (s, 3H).

2-(4-methoxyphenyl)-2-(piperidin-2-yl)acetamide

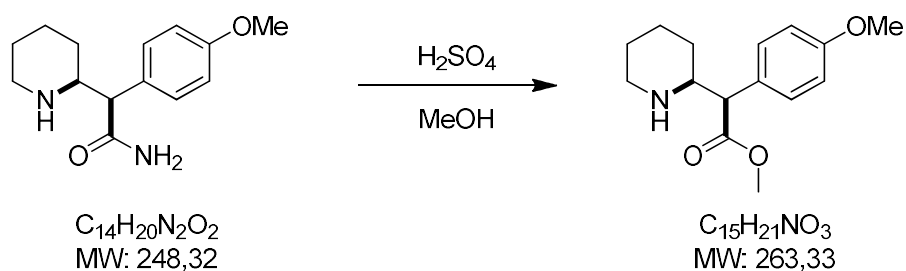


2-(4-methoxyphenyl)-2-(pyridin-2-yl)acetamide (640 mg, 2.64 mmol) was dissolved in MeOH (70 mL) and Pt₂O (64 mg) and conc. HCl (0.50 mL) were added. The mixture was vigorously stirred under H₂ (1.5 atm) at RT for 2.5 hours and filtered on a celite/Florasil pad. The solvents were evaporated under reduced pressure and the obtained residue was taken up in water (30 mL) and basified to pH=10 with 10% NaOH. The aqueous phase was extracted with ethyl acetate (3x10 mL); the collected organic phases were dried over Mg₂SO₄ and evaporated under reduced pressure to yield 380 mg (56%) of a mixture of *threo* and *erythro* 2-(4-methoxyphenyl)-2-(piperidin-2-yl)acetamide as a white waxy solid.

threo 2-(4-methoxyphenyl)-2-(piperidin-2-yl)acetamide

2-(4-methoxyphenyl)-2-(piperidin-2-yl)acetamide (*threo* + *erythro*) (0.38 g, 1.48 mmol) was dissolved in toluene (10 mL) and potassium *tert*-butylate (0.33 g, 2.96 mmol) was added under nitrogen atmosphere. After stirring at 70° C overnight, the mixture was brought to 0° C, diluted with ethyl acetate and washed with 10% NaCl. The organic phase was dried over Mg₂SO₄ and evaporated under reduced pressure to yield 0.38 g (100%) of *threo* 2-(4-methoxyphenyl)-2-(piperidin-2-yl)acetamide as a white waxy solid.

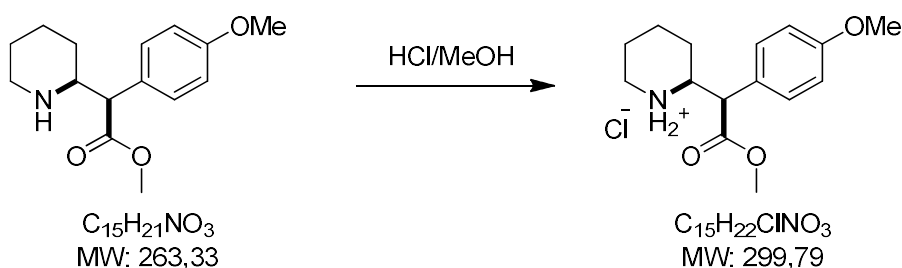
¹H NMR (300 MHz, CD₃OD) δ 7.26 – 7.21 (d, *J* = 8.8 Hz, 2H), 6.89 – 6.83 (d, *J* = 8.8 Hz, 2H), 3.76 (s, 3H), 3.27 (d, *J* = 10.1 Hz, 1H), 3.05 (dt, *J* = 10.5, 2.4 Hz, 1H), 3.03 – 2.98 (m, 1H), 2.66 (dt, *J* = 11.8, 2.9 Hz, 1H), 1.73 – 1.52 (m, 2H), 1.50 – 1.32 (m, 1H), 1.32 – 1.18 (m, 2H), 1.05 – 0.90 (m, 1H).

threo methyl 2-(4-methoxyphenyl)-2-(piperidin-2-yl)acetate

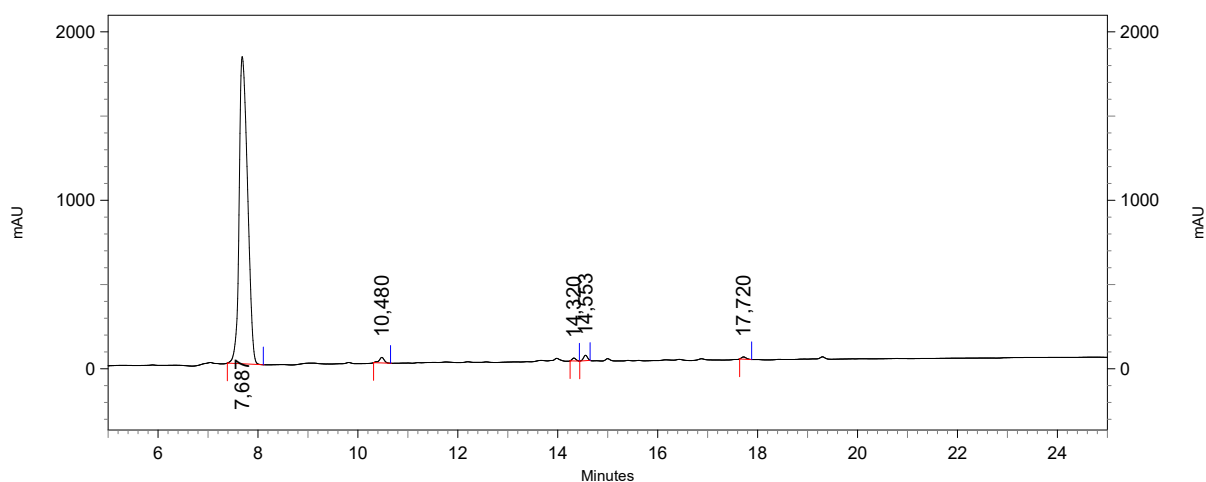
threo 2-(4-methoxyphenyl)-2-(piperidin-2-yl)acetamide (0.38 g, 1.48 mmol) was dissolved in MeOH (5 mL) and conc. H_2SO_4 (0.5 mL) was added. The mixture was stirred at 70° C overnight and diluted with water (20 mL) and ethyl acetate (20 mL). The aqueous phase was then basified to pH=10 with 10% NaOH and extracted with ethyl acetate (3x10 mL). The collected organic phases were dried over Mg_2SO_4 , evaporated under reduced pressure and the obtained crude was purified by flash chromatography on silica gel. Elution with DCM/MeOH 97:3 gave 0.20 g (49%) of *threo* methyl 2-(4-methoxyphenyl)-2-(piperidin-2-yl)acetate as a waxy solid.

1H NMR (300 MHz, CD_3OD) δ 7.18 (d, $J = 8.7$ Hz, 2H), 6.87 (d, $J = 8.7$ Hz, 2H), 3.77 (s, 3H), 3.64 (s, 3H), 3.40 (d, $J = 10.3$ Hz, 1H), 3.13 (dt, $J = 10.8, 2.5$ Hz, 1H), 3.04 – 3.00 (m, 1H), 2.66 (dt, $J = 12.0, 2.9$ Hz, 1H), 1.73 – 1.63 (m, 1H), 1.63 – 1.53 (m, 1H), 1.49 – 1.30 (m, 1H), 1.30 – 1.20 (m, 2H), 1.03 – 0.86 (m, 1H).

threo methyl 2-(4-methoxyphenyl)-2-(piperidin-2-yl)acetate hydrochloride (Compound VI *threo*)



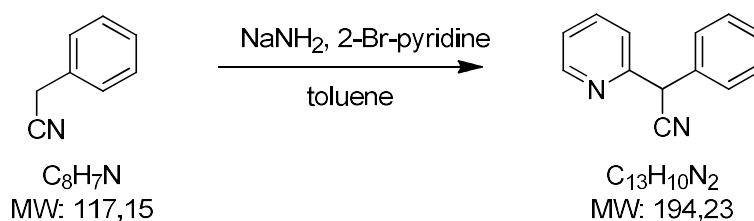
threo methyl 2-(4-methoxyphenyl)-2-(piperidin-2-yl)acetate (0.20 g, 0.76 mmol) was dissolved in MeOH (2.5 mL) and 3N HCl/MeOH (0.5 mL) was added. After stirring at RT for 5 hours, the solvent was evaporated under reduced pressure and the obtained crude was crystallized from IPE/IPA 1:2 to yield 0.11 g (48%) of *threo* methyl 2-(4-methoxyphenyl)-2-(piperidin-2-yl)acetate hydrochloride (Compound VI *threo*) as a white solid (mp: 192.88° C). Retention Time (HPLC) = 7.69'; A% (HPLC) = 97%.



^1H NMR (300 MHz, CD_3OD) δ 7.19 (d, J = 8.9 Hz, 2H), 6.94 (d, J = 8.9 Hz, 2H), 3.79 (s, 3H), 3.77 – 3.72 (m, 2H), 3.72 (s, 3H), 3.45 – 3.41 (m, 1H), 3.41 – 3.37 (m, 1H), 3.08 (dt, J = 12.7, 3.3 Hz, 1H), 1.94 – 1.75 (m, 2H), 1.75 – 1.39 (m, 3H), 1.38 – 1.22 (m, 1H).

^{13}C NMR (75 MHz, CD_3OD) δ 159.98, 129.18, 125.43, 114.32, 57.94, 54.38, 53.27, 51.88, 45.24, 26.41, 22.11, 21.41.

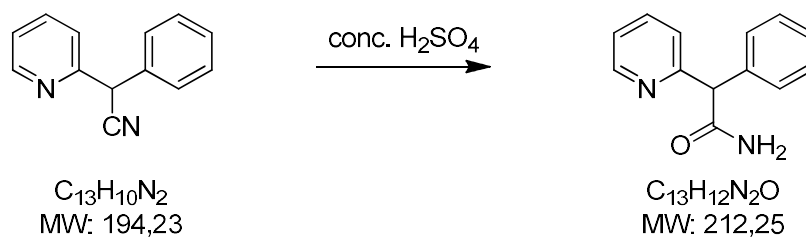
2-phenyl-2-(pyridin-2-yl)acetonitrile



Phenylacetonitrile (9.85 mL, 85.4 mmol) and 2-bromopyridine (7.75 mL, 81.3 mmol) were added dropwise at 0° C to a suspension of NaNH₂ (6.35 g, 162 mmol) in toluene (100 mL) under nitrogen atmosphere. After stirring at RT for 2.5 hours, the mixture was diluted with ethyl acetate (50 mL) and water (50 mL). The organic phase was washed with 10% NaCl (2x40 mL), dried over Mg₂SO₄ and evaporated under reduced pressure. The obtained crude was crystallized from MeOH to yield 8.43 g (53%) of 2-phenyl-2-(pyridin-2-yl)acetonitrile as a solid (mp: 83-86° C).

¹H NMR (300 MHz, DMSO-d₆) δ 8.61 – 8.56 (m, 1H), 7.83 (dt, *J* = 7.7, 1.6 Hz, 1H), 7.48 – 7.32 (m, 7H), 5.91 (s, 1H).

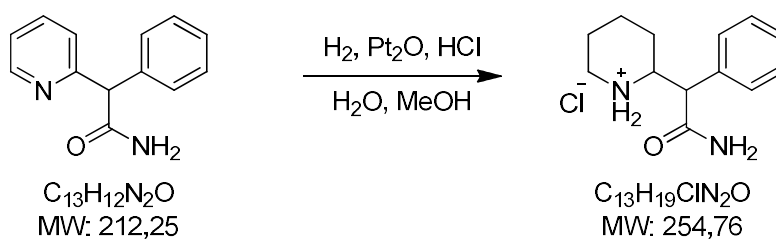
2-phenyl-2-(pyridin-2-yl)acetamide



2-phenyl-2-(pyridin-2-yl)acetonitrile (8.43 g, 43.4 mmol) was dissolved in conc. H_2SO_4 (20 mL) and stirred at RT overnight. Water (40 mL) was added carefully at 0°C and the mixture was basified to pH 12 with 10M NaOH. The precipitate was filtered and washed with water to afford 7.75 g (84%) of 2-phenyl-2-(pyridin-2-yl)acetamide as a light yellow solid (mp: $131\text{--}133^\circ\text{C}$)

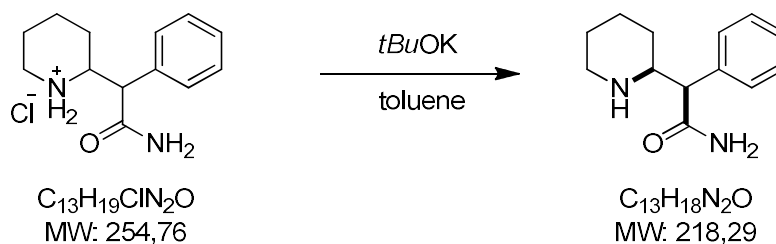
$^1\text{H NMR}$ (300 MHz, DMSO-d_6) δ 8.49 – 8.45 (m, 1H), 7.70 (dt, $J = 7.7, 1.9$ Hz, 2H), 7.37 – 7.18 (m, 6H), 7.11 (bs, 2H), 5.06 (s, 1H).

2-phenyl-2-(piperidin-2-yl)acetamide hydrochloride



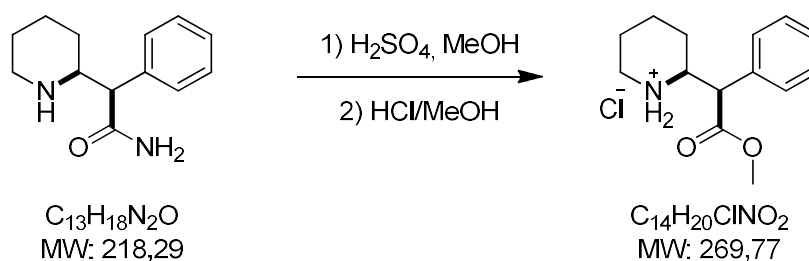
2-phenyl-2-(pyridin-2-yl)acetamide (3.94 g, 18.6 mmol) was dissolved in MeOH (75 mL) and Pt₂O (0.15 g) and conc. HCl (2.00 mL) were added. The mixture was vigorously stirred under H₂ (2 atm) at RT for 4.5 hours and filtered on a celite pad. The solvents were evaporated under reduced pressure to give 4.83 g of a mixture of *threo* and *erythro* 2-phenyl-2-(piperidin-2-yl)acetamide hydrochloride as a light brown solid that was used in the next step without further purification.

2-phenyl-2-(piperidin-2-yl)acetamide



2-phenyl-2-(piperidin-2-yl)acetamide hydrochloride (*threo* + *erythro*) (1.00 g, 3.92 mmol) was dissolved in toluene (30 mL) and potassium *tert*-butylate (1.03 g, 9.16 mmol) was added under nitrogen atmosphere. After stirring at 70° C for 6 hours, the mixture was brought to 0° C, water (2 mL) and 5N HCl (12 mL) were added and stirring was continued at RT overnight. The aqueous phase was basified with 30% NaOH and the precipitate was filtered and washed with water to afford 0.50 g (58%) of *threo* 2-phenyl-2-(piperidin-2-yl)acetamide as a white solid (mp: 173-175° C).

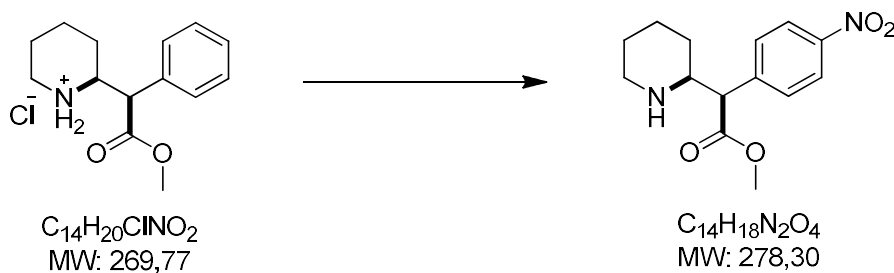
¹H NMR (300 MHz, CD₃OD) δ 7.44 – 7.18 (m, 5H), 3.39 – 3.23 (m, 1H), 3.18 – 2.96 (m, 2H), 2.66 (t, *J* = 10.8 Hz, 1H), 1.76 – 1.52 (m, 2H), 1.52 – 1.31 (m, 1H), 1.31 – 1.09 (m, 2H), 1.09 – 0.87 (m, 1H).

threo methylphenidate hydrochloride

threo 2-phenyl-2-(piperidin-2-yl)acetamide (0.50 g, 2.29 mmol) was dissolved in MeOH (5.5 mL) and conc. H₂SO₄ (0.65 mL) was added. The mixture was stirred at 65° C for 2 days and diluted with water (4 mL) and ethyl acetate (8 mL). The aqueous phase was then basified to pH=12 with 10% NaOH and extracted with ethyl acetate (3x10 mL). The collected organic phases were dried evaporated under reduced pressure and the obtained crude was taken up in 0.6 mL of conc. HCl and stirred at 0° C for 1 hour. The precipitate was filtered and washed with water to afford 0.15 g (25%) of *threo* methylphenidate hydrochloride as a solid (mp: 221-223° C).

¹H NMR (300 MHz, CD₃OD) δ 7.32 – 7.26 (m, 5H), 3.65 (s, 3H), 3.45 (d, *J* = 10.3 Hz, 1H), 3.13 (dt, *J* = 10.7, 2.6 Hz, 1H), 3.07 – 3.00 (m, 1H), 2.66 (dt, *J* = 12.0, 2.9 Hz, 1H), 1.73 – 1.63 (m, 1H), 1.63 – 1.54 (m, 1H), 1.48 – 1.35 (m, 1H), 1.25 – 1.21 (m, 1H), 1.21 – 1.16 (m, 2H), 1.03 – 0.87 (m, 1H).

threo 4-nitromethylphenidate (Compound VII *threo* freebase)



threo methylphenidate hydrochloride (0.27 g, 0.81 mmol) was dissolved in conc. H_2SO_4 (1.9 mL) and HNO_3 (1.9 mL) was added at $-10^\circ C$. The mixture was stirred at $-10^\circ C$ for 1 hours, poured into ice, neutralized with 10M NaOH and extracted with DCM (3x20 mL). The collected organic phases were dried over Mg_2SO_4 , evaporated under reduced pressure and the obtained crude was purified by flash chromatography on silica gel (DCM/MeOH 9:1) to give 0.04 g (13%) of *threo* 4-nitromethylphenidate (Compound VII *threo* freebase) as a colorless oil.

1H NMR (300 MHz, CD_3OD) δ 8.24 – 8.15 (m, 2H), 7.65 – 7.50 (m, 2H), 3.70 – 3.64 (m, 1H), 3.69 (s, 3H), 3.19 (ddd, $J = 10.6, 6.9, 2.9$ Hz, 1H), 3.11 – 2.99 (m, 1H), 2.66 (dt, $J = 11.9, 2.9$ Hz, 1H), 1.74 – 1.65 (m, 1H), 1.65 – 1.54 (m, 1H), 1.45 – 1.12 (m, 3H), 1.07 – 0.93 (m, 1H).

CHAPTER 2 – DESIGN, SYNTHESIS AND BINDING EVALUATION OF FLUORESCENT SMALL MOLECULE LIGAND-BASED PROBES FOR IMAGING THE NOREPINEPHRINE TRANSPORTER

Introduction

Live-cell fluorescence imaging microscopy is an extremely powerful tool in modern biology. It relies on the illumination of fluorescently labeled intracellular molecules with light of a defined wavelength, ideally close to the fluorophore excitation peak, and detection of the light emitted at a longer wavelength (Ettinger and Wittmann 2014). The direct visualization of sub-cellular dynamics in living cells enables the study of diverse processes such as protein location, associations, stability and turnover. The applications are not limited to proteins, with the possibility to visualize and quantify nucleic acids, small molecules, secondary metabolites, metals and ions and to provide insight into their localization, transport and metabolism. The careful selection of light wavelengths and intensity (in order to avoid photobleaching and/or phototoxicity), together with the use of specific fluorescent labels, confers minimal invasiveness and high selectivity to the approach. Advanced microscopy techniques and fluorescent labeling technologies have been extensively studied over the last two decades and are in constant evolution, opening up to exciting possibilities to address new biology problems and to shed a new light on previously unsolved questions.

In conventional light microscopy techniques, spatial resolution is limited by the diffraction of light. This diffraction limit is around 200-300 nm in the lateral and 500-700 nm in the axial directions (Thompson *et al.* 2002) and prevents the detailed observation of subcellular structures of comparable or smaller size. Super resolution microscopy (SRM) techniques are able to overcome the diffraction limit and allow for the observation of previously unresolved details of subcellular components (Huang *et al.* 2009), with greatly increased resolution in the 20-50 nm range. In traditional fluorescent microscopy, all the fluorophores are excited and emit quasi-simultaneously. For the ones residing in closer proximity to each other than the diffraction limit, emission beams are diffracted and detected together, making it impossible to discern between the contributions of single fluorophores. SRM techniques rely on the use of special fluorophores that can transition between an “on” (fluorescent) state and an “off” (dark) state. The right kinetics of the switching between light-emitting and dark states ensures that fluorophores closer than the diffraction limit are not detected at the same time and can be discerned from each

other, allowing for the obtainment of a full description of the spatial arrangement of molecules through the acquisition of repeated on-off cycles (Sahl *et al.* 2017).

In addition to general fluorophore properties such as solubility and membrane permeability, specific optimal characteristics are required for live-cell SRM applications (Wang *et al.* 2019). High brightness allows for the use of lower intensity lasers for excitation and limits phototoxicity. In addition, for some SRM techniques (collectively named Single-Molecule Localization Methods, or SMLM) high brightness is required for a more precise spatial localization of the emitting fluorophore. Photostability, defined as the ability of the fluorophore to give a consistent fluorescent signal over sustained and/or intense excitation without bleaching, is also crucial for some SRM techniques that require high power densities and, in general, for experiments demanding sustained or repeated stimulation and quantitative measurements. Suitable photoswitching kinetics and narrow emission wavelengths are also fundamental requirements of fluorophores suitable for SRM.

Protein Labeling Techniques for Fluorescent Live-Cell Imaging

This section will provide a brief overview of fluorescent protein labeling techniques, emphasizing their advantages and limitations in the application to live-cell super resolution imaging. The main approaches are:

1. **Fluorescent Fusion Proteins (FFP):** in this approach, the cloning of the target gene in frame with the sequence encoding a fluorescent protein (FP) generates a genetic construct that can be transferred into cells and expressed into a fluorescent chimeric variant of the target protein. Since the discovery of green fluorescent protein (GFP) in the *Aequorea* jellyfish (Shimomura *et al.* 1962), other naturally occurring FPs with different spectral properties have been characterized and some others have been obtained through protein engineering from previously existing ones, broadening the color palette and allowing for more diverse and complex experiment designs (Day and Davidson 2009, Kremers *et al.* 2011). Usually, FPs are relatively large in size (25 kDa, 220-240 aa) and their structure is characterized by 11 β -sheets domains arranged around a central α -helix. In GFP, the fluorophore is generated by the unique posttranslational modification of three residues on the α -helix (Ormö *et al.* 1996, Petersen *et al.* 2003, Loening *et al.* 2007). Since the fluorescent motif is embedded in the sequence of the protein labeling specificity is

very high and there is no need for additional labeling and/or other chemical procedures. In addition, the fixed 1:1 ratio between fluorescent label and target protein allows for precise quantitative measurements. On the other hand, the structural modification of the native protein can alter its localization, function, aggregation and expression levels. For the large majority of FFPs, brightness and photostability are not compatible with SRM, even though progress in direction has been made in recent years, also with the introduction of photoswitchable FPs (Nienhaus and Nienhaus 2014).

2. **In-situ Chemical Labeling:** in this approach target proteins are expressed as fusion proteins with an additional enzymatic “tag” that undergoes a specific bio-orthogonal reaction with a probe containing a synthetic organic fluorophore. The commercial availability of hundreds of organic fluorophores with tunable optical characteristics (**Figure 13**), including dyes suitable for SRM, provides great flexibility to the techniques. Notable technologies include SNAP-tag (Keppler *et al.* 2003), HaloTag (Los *et al.* 2008) and Clip-tag (Gautier *et al.* 2008). Tags are usually large in size (20-33 kDa) and can alter the native structure, function, localization and expression of the proteins of interest. Usually, the position of the tags is limited to the *N*- or *C*-terminus of the target proteins and this can interfere with their function. These issues can be addressed with the incorporation in proteins of more compact unnatural aminoacids featuring a biorthogonal handle that can react selectively with the probes through click-chemistry reactions. However, this approach is still technically challenging and is not routinely used method for live-cell imaging (Lang and Chin 2014).

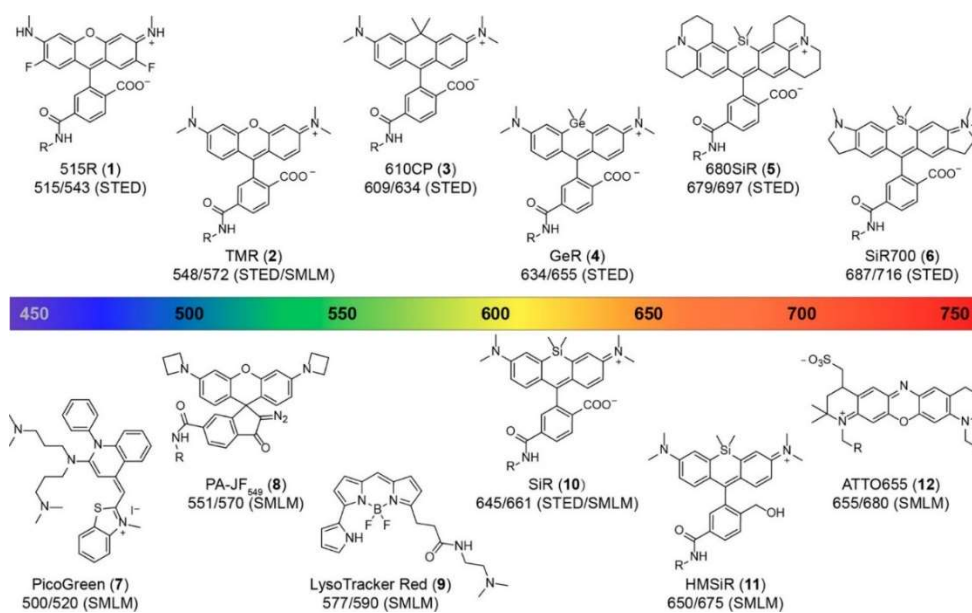


Figure 13: Small-molecule organic fluorophores and their distribution across the visible light spectrum (from Wang *et al.*, 2019)

3. **Fluorescent Antibodies (FABs):** immunofluorescence approaches are based on the use of antibodies labeled with a fluorophore. Different labeling strategies can be employed, from the generation of FP-antibodies fusion proteins to the labeling of the antibody with an organic fluorophore (**Figure 13**) through click chemistry. The latter approach opens up to the use of fluorophores compatible with SRM applications, but the large size (approx. 150 kDa) of the antibody conjugates historically limited their use in fixated, permeabilized cells. In general, immunofluorescence techniques can be divided into primary (direct) and secondary (indirect) techniques. In direct immunofluorescence, a single primary FAB is used, simplifying the experimental designs in spite of no amplification of fluorescence and reduced sensitivity. In indirect techniques, multiple secondary FABs can bind to a single primary antibody, providing enhanced selectivity, amplification of fluorescence and increased sensitivity (Wardyn and Jeyasekharan 2002). Several recent strategies have been developed to overcome size-related limitations of “traditional” methods, with the use of conjugates containing only a portion of the full-length antibody, either the antigen binding fragment (approx. 55 kDa), the single chain variable fragment (approx. 28 kDa) or the smaller recognition unit called nanobody (approx. 12 kDa) (Meyer *et al.* 2014, Specht *et al.* 2017). Relatively less invasive cell penetration methods such as microinjection and electroporation make this approaches suitable for live-cell imaging. General limitations

to the use of FABs include off-target binding, tendency to self-aggregation and the technically challenging nature of some experiment designs.

4. **Small Molecule Ligand-Based Probes:** this approach relies on the use of small molecule ligands with high affinity and selectivity for the target protein labeled with an organic synthetic fluorophore (**Figure 13**). The ease of use associated with the technique and the wide availability of fluorophores give great flexibility to the method. The low molecular weight of the probes (approx. 1 kDa) allows for non-invasive labeling of native proteins in living cells. In the context of SRM, limited size allows for more precise localization of the labeled proteins and becomes more and more crucial as resolution is pushed toward the molecular level (Wang *et al.* 2019). Limitations of the approach can derive from the unavailability of a suitable ligand and from non-optimal cell permeability.
5. **Other approaches:** fluorescent non-natural amino acids can be incorporated directly in proteins allowing for imaging in live cell. The smaller size of the modification can prevent some of the issues related to bulky FP fusions and the high specificity of fusion protein-based approaches is maintained (Specht *et al.* 2017). However, their use in SRM is still limited by low brightness. Quantum dots are nanometer size (2-10 nm) semiconductor crystals that can be covalently linked with a ligand (biomolecule or small molecule) in the design of fluorescent probes. They possess size-tunable light emission and excellent brightness and photostability. The main limitation to this approach is high potential cytotoxicity, due to the chemical composition of the crystals (usually heavy metals such as Cd, Pb, Hg) and to the generation of toxic oxygen species (Matea *et al.* 2017).

Fluorescent Small Molecule Ligand-Based Probes for Imaging Monoamine Transporters

Monoamine transporters (MATs) are a group of plasma membrane bound proteins that mediate the reuptake of monoamine neurotransmitters from the synaptic clefts into the presynaptic terminal. Three different MATs exist, named according to their preferential substrate: the serotonin transporter (SERT), the dopamine transporter (DAT) and the norepinephrine transporter (NET) (Grouleff *et al.* 2015). MATs are classified in the SLC6 (Solute Carrier 6) family of transporters, a group of active secondary cotransporters that use Na⁺ gradient across membranes to facilitate transport (Gu *et al.* 1994). Alterations in monoamine homeostasis are linked with disorders such as depression, anxiety disorders, schizophrenia, attention deficit

hyperactivity disorder, Parkinson's disease and obesity (Kristensen *et al.* 2011). In addition, MATs are the main targets of psychostimulant drugs of abuse (Rothman and Baumann 2003).

Small molecule ligand-based approaches possess additional specific advantages in the design of fluorescent probes for super resolution imaging of MATs. Specifically:

- Low molecular weight can represent a crucial advantage over other techniques in labeling proteins localized at presynaptic terminals, due to the limited size of the synaptic cleft (**Figure 14**).
- The absence of self-aggregation propensity provides valuable tools for studying protein dynamics processes such as hetero- and homo-oligomerization in native targets, overcoming some limitations of FABS-based methods (especially indirect methods).
- Extensive literature about MATs as “classic” pharmacological targets provides a wide variety of parent ligands to choose from, with excellent affinity and selectivity over off-target interactions and between different MATs.
- Membrane permeability issues are generally not a limitation in the labeling of membrane proteins. Anyhow, the use of membrane-permeable fluorophores (e.g. rhodamine derivatives) and the control of hydrophilicity of the probes could result in membrane-permeable probes.

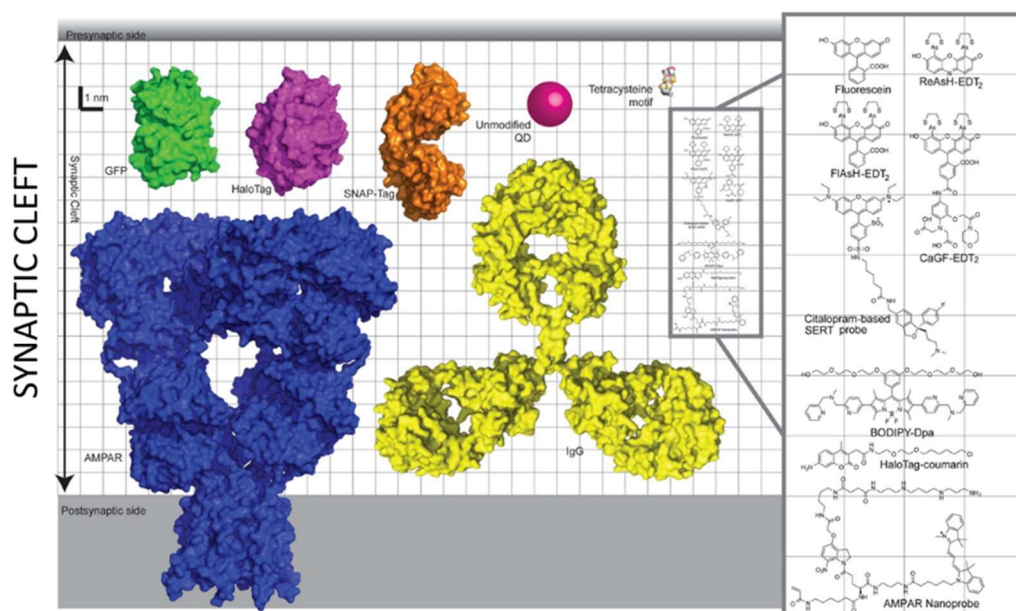
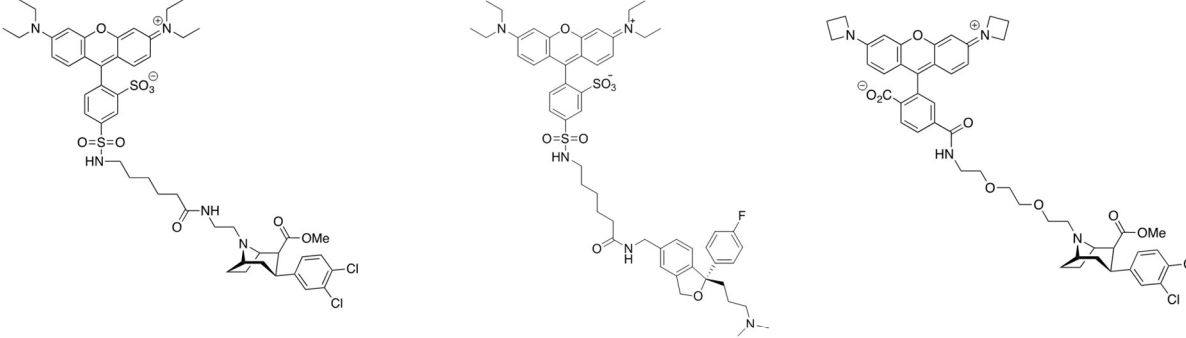


Figure 14: To scale representation of different protein labeling approaches in the synaptic space

Small molecule ligand-based approaches have been successfully used by Newman and coworkers for the design of fluorescent probes for imaging MATs, with different degrees of selectivity between DAT, SERT and NET (**Figure 15**). Significant examples from this expanding toolbox include JHC1-64 (Cha *et al.* 2005), a tropane-based probed with high affinity at all three MATs which has been employed to study DAT localization, trafficking and lysosomal degradation (Eriksen *et al.* 2009, Eriksen *et al.* 2010). VK2-83 (Kumar *et al.* 2014) is a based on a citalopram scaffold and shows very high affinity for SERT, with excellent selectivity over DAT and SERT. DG3-80 has been recently developed from a tropane scaffold combined with the JF-549 dye, a fluorophore suitable for SRM (Grimm *et al.* 2017), and shows very high affinity for all three MATs. Even though JHC1-64 has been successfully used for the imaging of NET (Vuorenpää *et al.* 2016), a NET-selective high affinity fluorescent probe would represent a valuable addition to the series and could provide useful insights into the target trafficking and function in living cells.



	JHC1-64		VK2-83		DG3-80	
	Binding Ki (nM)	Uptake Inhibition Ki (nM)	Uptake Inhibition Ki (nM)		Binding Ki (nM)	
DAT	18	62	DAT	IA	DAT	6
NET	-	194	NET	IA	NET	NT
SERT	16	392	SERT	34	SERT	43
	NT = Not Tested		IA = inactive at 10 μ M		NT = Not Tested	

Figure 15: Structures of monoamine fluorescent probes and their binding affinities at the three monoamine transporters

Aim of the Work

A first group of NET-selective fluorescent probes will be designed, synthesized and evaluated for their binding affinity and selectivity in radioligand binding assays. The most promising candidates will be employed in fluorescent microscopy experiments aimed at studying NET localization and trafficking in living cells.

Aim 1: Probe design

All the probes share a common design, based on a NET ligand connected to a fluorophore (Rhodamine Red) by an alkylamide linker chain. The choice of the parent ligand and of the insertion sites for the linker-dye moiety (tagging sites) are the main steps in the design process:

1. **Choice of the parent ligand:** multiple ligands with high affinity and selectivity for NET are reported in literature (McConathy *et al.* 2004, Zhou 2004, Eildal *et al.* 2008, Pontillo *et al.* 2008, Xu *et al.* 2008, Zeng *et al.* 2008). We decided to choose nisoxetine and talopram (**Figure 16**), based on affinity and selectivity values, known SAR and synthetic feasibility. All the compounds were synthesized as racemates.

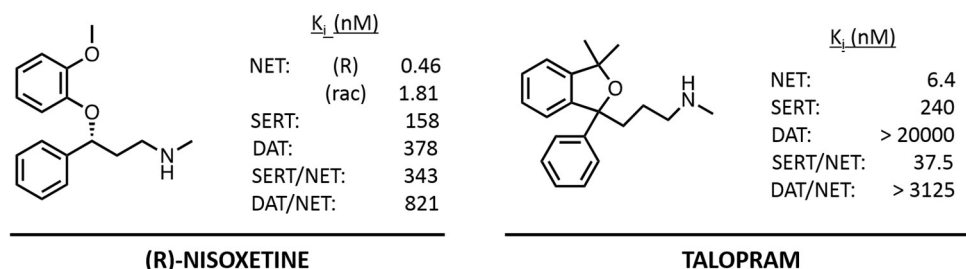


Figure 16: Structure and binding affinity and selectivity data of nisoxetine and talopram (from Zhou, 2004)

2. **Choice of the tagging sites:** the right point of insertion for the bulky sidechain is of crucial importance as the spatial arrangement of the whole probe will depend on it and an incorrect geometry can prevent the ligand to access the binding pocket, with considerable or total loss of affinity. In absence of a computational model that could support a more rational design, we decided to rely on the known SAR for the parent ligands. We planned to tag both parent ligands in two positions on opposite faces of the molecule,

alternatively, maintaining the structural determinant for NET affinity and selectivity. For both parent compounds, slight changes in ring substituents and amine basicity can drastically alter affinity and selectivity, with a complete shift towards SERT-selective binding (see fluoxetine and citalopram, **Figure 17**). In the design of the probes, the secondary amine of both nisoxetine and talopram was maintained, with the addition of an extra ethyleneamine handle for the insertions of the sidechain. For nisoxetine, we decided to tag Ring A, as the modification of Ring B could cause unexpected changes in selectivity in analogy with fluoxetine. For talopram, the comparison with citalopram was less informative and we decided to tag Ring B because part of the chemistry was already described in previous works (Eildal *et al.* 2008, Kumar *et al.* 2014). In both cases, the insertion point for the sidechain was provided by the addition of an extra methyleneamine handle on the selected phenyl rings of the parent ligands.

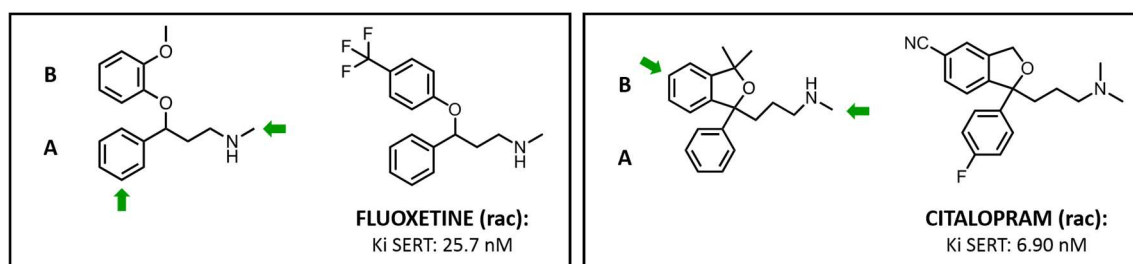


Figure 17: Tagging sites on nisoxetine and talopram and structures and binding affinities of their SERT-selective analogs fluoxetine and citalopram (Ki values calculated in previous experiments)

A first group of four probes (Compounds I-IV, reported in **Figure 18**) was defined.

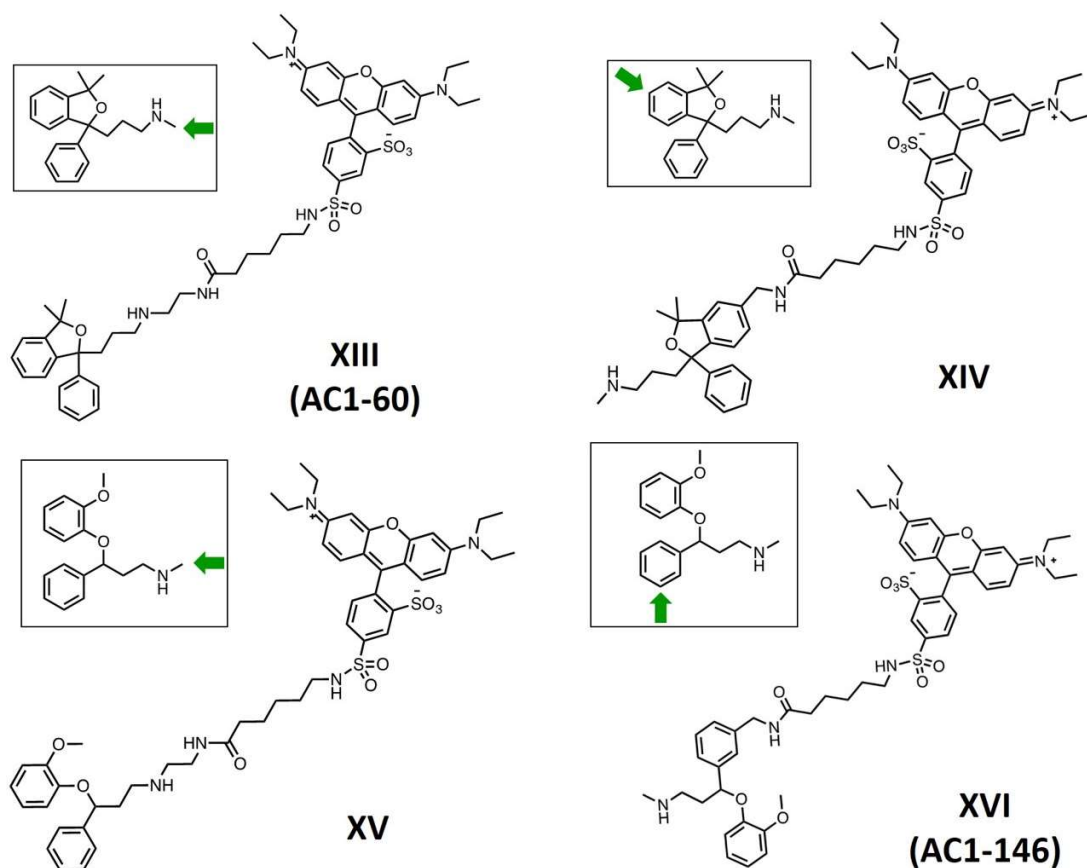


Figure 18: Structure of compounds I-IV

Aim 2: Radioligand binding evaluation

All the synthesized probes will be evaluated for their binding at the three monoamine transporters (NET, DAT, SERT) in order to assess their binding affinity and selectivity for NET.

Aim 3: Live-cell fluorescent microscopy

In particular, some aspects of NET dynamics will be studied:

- 1. Oligomerization:** the formation of protein oligomers is a common phenomenon and has been observed for other membrane transporters (Jess *et al.* 1996, Schmid *et al.* 2001, Kocabas *et al.* 2003, Anderluh *et al.* 2014). It has been speculated to participate in the regulation of membrane trafficking, function, regulation and turnover, even though its exact physiologic role is still unknown (Alguel *et al.* 2016). Oligomerization is supposed

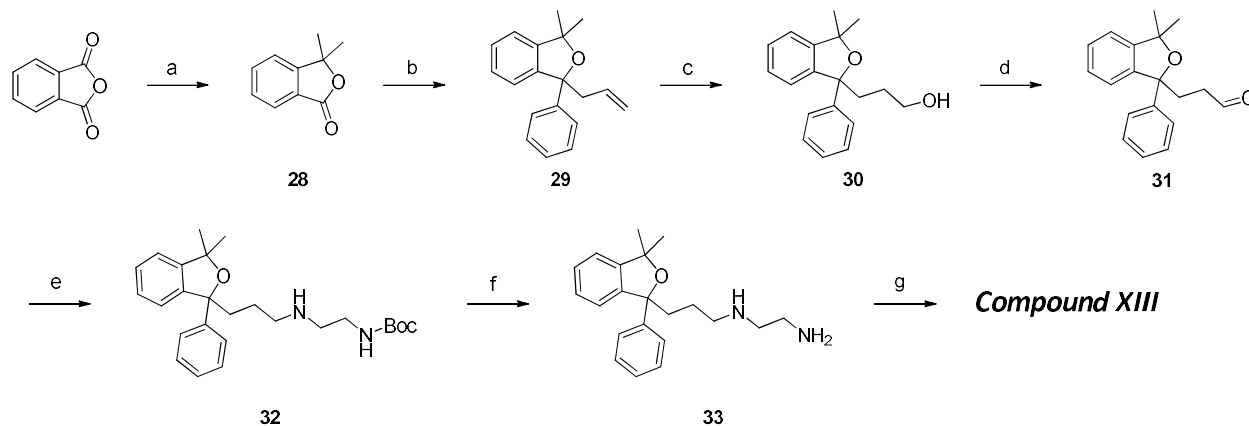
to be essential for DAT trafficking to the cell membrane (Torres *et al.* 2003) and to promote neurotransmitter efflux by the serotonin and GABA transporters (Seidel *et al.* 2005, Sitte and Freissmuth 2010). The existence of NET oligomers and their role in NET function and noradrenergic transmission are still to be elucidated.

2. **Distribution in neurons:** the exact distribution patterns of NET are still unknown and diffraction-limited microscopy experiments gave conflicting results (Savchenko *et al.* 2003, Vuorenpää *et al.* 2016). The application of the findings of the present work to the development of probes suitable for SRM and the super resolution imaging of NET could contribute to solve this ongoing controversy.
3. **Diffusion barriers in axons:** the deviation from free diffusion patterns of proteins and lipids along axons has been observed with a variety of techniques (Murase *et al.* 2004, Ruprecht *et al.* 2011, Di Rienzo *et al.* 2013, Andrade *et al.* 2015). Specific cytoskeletal structures have been implicated in this phenomenon and the selective imaging of NET could provide valuable insight into their localization and their influence on the transporter function.

Materials and Methods

Chemistry

Compound XIII

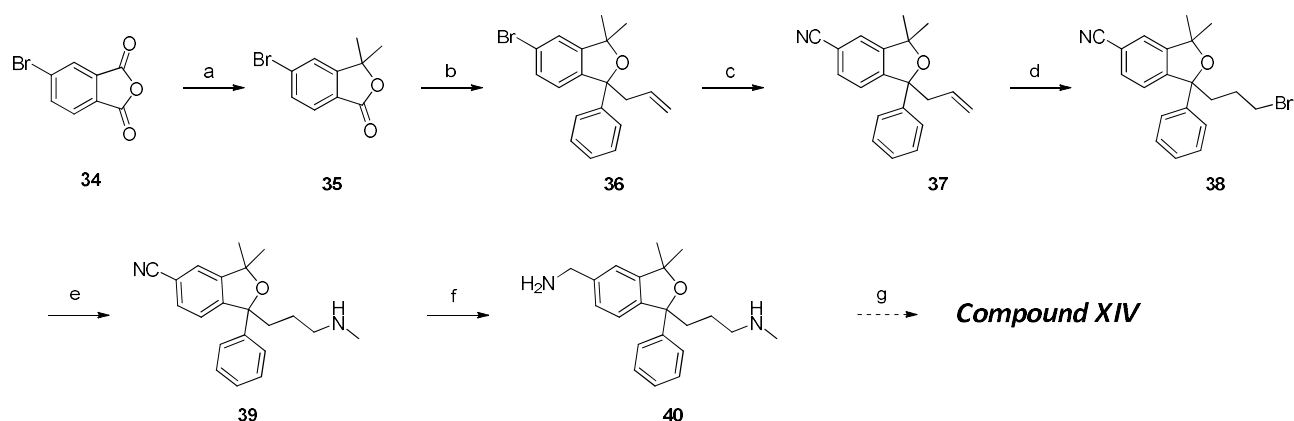


Scheme 7

Reagents and conditions: a) MeMgCl, THF, RT (quant.); b) 1) PhMgBr, THF, RT 2) allylmagnesium bromide, RT (quant.); c) 1) BH₃•THF, THF, RT 2) NaOH, H₂O₂ (51%); d) Dess-Martin Periodinane, DCM, RT (26%); e) 1) *N*-Boc dimethylamine, AcOH cat., DCE, RT 2) STAB, RT (14%); f) TFA, DCM, RT (40%); g) Rhodamine Red-X NHS ester, DIPEA, DMF, 40°C (83%).

Commercially available phthalic anhydride undergoes “double Grignard” reaction with MeMgCl to give dimethyl lactone **1**. A second “double Grignard” reaction with phenylmagnesium bromide and allylmagnesium bromide readily affords the talopram scaffold in quantitative yields. Hydroboration/oxidation to the terminal alcohol **3** and oxidation with Dess-Martin periodinane lead to aldehyde **4**, which reacts with *N*-Boc dimethylamine in reductive amination conditions. Deprotection gives diamine **6** and the primary amine reacts with good selectivity with Rhodamine Red-X NHS ester to yield **Compound XIII** (Scheme 7).

Compound XIV

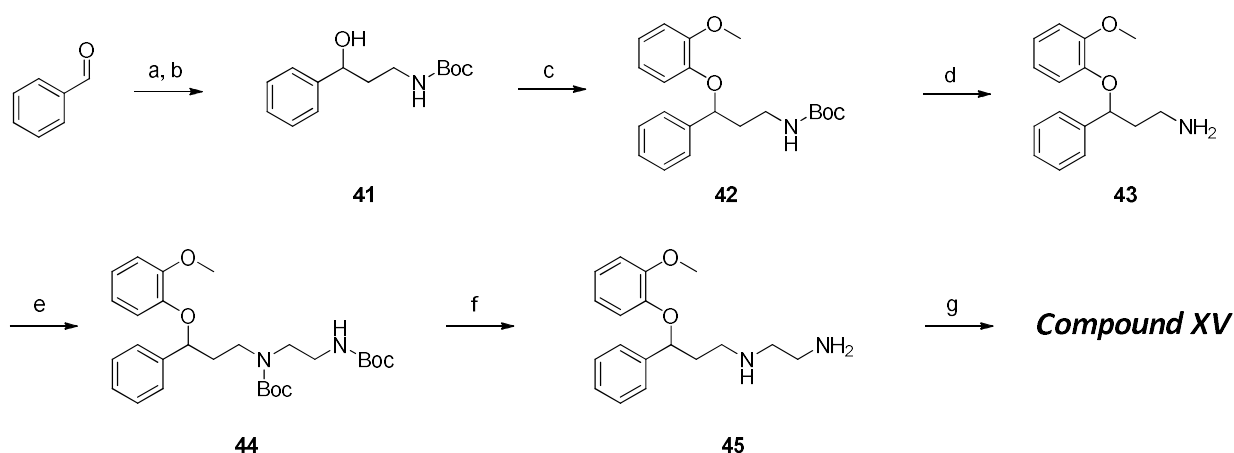


Scheme 8

Reagents and conditions: a) MeMgCl, THF, RT (quant.); b) 1) PhMgBr, THF, RT 2) allylmgBr, RT (quant.); c) Zn(CN)₂, Pd(PPh₃)₄, DMF, 80°C (58%); d) HBr/AcOH, hexane, 0°C (79%); e) methylamine in THF, DCM, RT (12%); f) LAH, THF, reflux (22%); g) Rhodamine Red-X NHS ester, DIPEA, DMF, 40°C.

In **Scheme 8**, two subsequent “double Grignard” reactions convert commercially available 4-bromophthalic anhydride in the 4-bromo talopram scaffold in quantitative yields, similarly to what described for Compound I. Cyanation of the aryl bromide affords aryl nitrile **4**. Radicalic hydrobromination selectively gives terminal bromide **5**, which is substituted with methylamine to yield 4-CN-talopram **6**. The generation of a primary amine through the reduction of the cyano group introduces a reactive handle for the reaction with Rhodamine Red-X NHS ester. To our disappointment, this last step did not work and **Compound XIV** was not obtained. Possible explanations include reduced reactivity of the starting materials and/or increased instability of the products in the reaction conditions employed. Based on these assumptions, future attempts for the obtainment of **Compound XIV** may rely on a more thorough screening of reaction conditions (mainly solvent and temperature) and/or on the use of different strategies for the insertion of the linker chain (e.g. cross-coupling reactions).

Compound XV

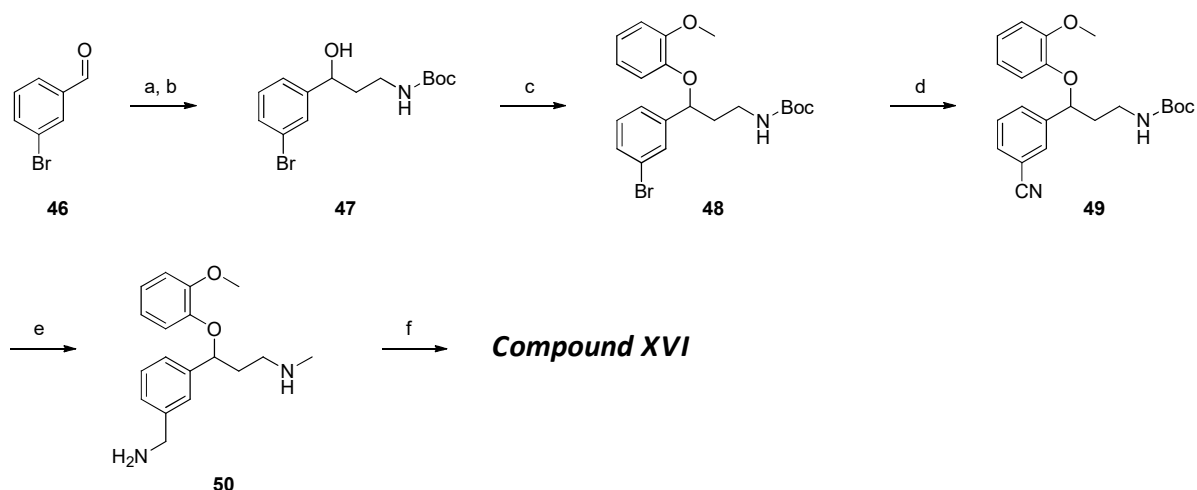


Scheme 9

Reagents and conditions: a) 1) CH_3CN , $n\text{-BuLi}$, THF, -78°C 2) LAH, RT; b) Boc_2O , TEA, DCM, RT (13%, 3 steps); c) guaiacol, TPP, DIAD, THF, -20°C to RT (53%); d) TFA, DCM, RT (48%); e) 1) $N\text{-Boc-2-aminoacetaldehyde}$, TEA, DCM, RT 2) STAB, Boc_2O , RT (17%); f) TFA, DCM; g) Rhodamine Red-X NHS ester, DIPEA, DMF, 40°C .

One-pot reaction of benzaldehyde with acetonitrile lithium salt and LAH reductions gives 3-amino-1-phenylpropan-1-ol, which is *N*-protected as a crude compound to yield **1**. Mitsunobu reaction with guaiacol affords (2-methoxy)phenoxy compound **2** which is readily deprotected to make the primary amine of **3** available for tandem reduction amination/Boc-protection step **e**. Treatment with TFA yields diamine **5**, which is reacted with Rhodamine Red-X NHS ester to give **Compound XV** (Scheme 9). Unfortunately, the final compound seems to be highly unstable in the workup or purification conditions (chromatography on silica gel) and its isolation was not possible.

Compound XVI



Scheme 10

Reagents and conditions: a) 1) CH_3CN , *n*-BuLi, THF, -78°C 2) LAH, RT (58%); b) Boc_2O , TEA, DCM, RT; c) guaiacol, TPP, DIAD, THF, -20°C to RT (47%); d) $\text{Zn}(\text{CN})_2$, $\text{Pd}(\text{PPh}_3)_4$, DMF, 80°C (54%); e) LAH, THF, reflux (21%); f) Rhodamine Red-X NHS ester, DIPEA, DMF, 40°C (87%).

Similarly to the previous scheme, commercially available 3-bromobenzaldehyde is converted into 3-amino-1-(3-bromophenyl)propan-1-ol by one-pot reaction with acetonitrile lithium salt and LAH reduction. Protection of the crude aminoalcohol yields **2**, which is treated with guaiacol in Mitsunobu conditions to afford (2-methoxy)phenoxy derivative **3**. Cyanation and subsequent reduction with LAH introduce the extra aminomethyl group for the reaction with Rhodamine Red-X NHS ester and formation of final **Compound XVI** (Scheme 10).

Radioligand Binding Assays

DAT Binding Assay. Frozen striatum membranes dissected from male Sprague–Dawley rat brains (supplied on ice by Bioreclamation, Hicksville, NY) were homogenized in 20 volumes (w/v) of ice cold modified sucrose phosphate buffer (0.32 M sucrose, 7.74 mM Na₂HPO₄, and 2.26 mM NaH₂PO₄, pH adjusted to 7.4) using a Brinkman Polytron (Setting 6 for 20 s) and centrifuged at 48,400 x g for 10 min at 4°C. The resulting pellet was resuspended in buffer, recentrifuged, and suspended in ice cold buffer again to a concentration of 20 mg/mL, original wet weight (OWW). Experiments were conducted in 96-well polypropylene plates containing 50 µL of various concentrations of the inhibitor, diluted using 30% DMSO vehicle, 300 µL of sucrose phosphate buffer, 50 µL of [³H]WIN 35,428 (Scheffel *et al.* 1989) (final concentration 1.5 nM; K_d = 28.2 nM; PerkinElmer Life Sciences, Waltham, MA), and 100 µL of tissue (2.0 mg/well OWW). All compound dilutions were tested in triplicate and the competition reactions started with the addition of tissue, and the plates were incubated for 120 min at 0–4°C. Nonspecific binding was determined using 10 µM indatraline.

SERT Binding Assay. Frozen stem membranes dissected from male Sprague–Dawley rat brains (supplied on ice by Bioreclamation, Hicksville, NY) were homogenized in 20 volumes (w/v) of 50 mM Tris buffer (120 mM NaCl and 5 mM KCl, adjusted to pH 7.4) at 25°C using a Brinkman Polytron (at setting 6 for 20 s) and centrifuged at 48,400 x g for 10 min at 4°C. The resulting pellet was resuspended in buffer, recentrifuged, and suspended in buffer again to a concentration of 20 mg/mL, OWW. Experiments were conducted in 96-well polypropylene plates containing 50 µL of various concentrations of the inhibitor, diluted using 30% DMSO vehicle, 300 µL of Tris buffer, 50 µL of [³H]citalopram (final concentration 1.5 nM; K_d = 6.91 nM; PerkinElmer Life Sciences, Waltham, MA), and 100 µL of tissue (2.0 mg/well OWW). All compound dilutions were tested in triplicate and the competition reactions started with the addition of tissue, and the plates were incubated for 60 min at room temperature. Nonspecific binding was determined using 10 µM fluoxetine.

NET Binding Assay. Frozen frontal cortex dissected from male Sprague–Dawley rat brains (supplied on ice from Bioreclamation, Hicksville, NY) were homogenized in 20 volumes (w/v) of 50 mM Tris buffer (300 mM NaCl and 5 mM KCl, adjusted to pH 7.4) at 25 °C using a Brinkman Polytron (at setting 6 for 20 s). The tissue was centrifuged at 48,400 x g for 10 min at 4 °C. The

resulting pellet was suspended in fresh buffer and centrifuged again. The final pellet was resuspended in cold binding buffer to a concentration of 80 mg/mL OWW. Experiments were conducted in glass assay tubes containing 50 μ L of various concentrations of the inhibitor, diluted using 30% DMSO vehicle, 300 μ L of Tris buffer. 50 μ L of [3 H]nisoxetine (final concentration 0.5 nM; $K_d = 1.81$ nM, Perkin-Elmer Life Sciences), and 100 μ L of tissue (8.0 mg/tube OWW). The reaction was started with the addition of the tissue, and the tubes were incubated for 180 min at 0–4 $^{\circ}$ C. Nonspecific binding was determined using 10 μ M desipramine.

For all binding assays, incubations were terminated by rapid filtration through Perkin Elmer Uni-Filter-96 GF/B (DAT and SERT) or Whatman GF/B filters (NET), presoaked in either 0.3% (SERT and NET) or 0.05% (DAT) polyethylenimine, using a Brandel 96-Well Plates Harvester Manifold or Brandel R48 filtering manifold (Brandel Instruments, Gaithersburg, MD). The filters were washed a total of 3 times with 3 mL (3×1 mL/well or 3×1 mL/tube) of ice cold binding buffer. For DAT and SERT binding experiment 65 μ L Perkin Elmer MicroScint 20 Scintillation Cocktail was added to each filter well. For NET binding experiment, the filters were transferred in 24-well scintillation plates and 600 μ L of CytoScint was added to each well. All the plates/filters were counted using a Perkin Elmer MicroBeta Microplate Counter. IC_{50} values for each compound were determined from inhibition curves and K_i values were calculated using the Cheng-Prusoff equation (Cheng and Prusoff 1973). When a complete inhibition could not be achieved at the highest tested concentrations, K_i values have been extrapolated by constraining the bottom of the dose-response curves (= 0% residual specific binding) in the non-linear regression analysis. These analyses were performed using GraphPad Prism version 8.00 for Macintosh (GraphPad Software, San Diego, CA). K_d values for the radioligands were determined via separate homologous competitive binding or radioligand binding saturation experiments. K_i values were determined from at least 3 independent experiments performed in triplicate and are reported as mean \pm SEM, and the results were rounded to the third significant figure.

Results and Discussion

At the moment, radioligand binding data are available only for compounds I (AC1-60) and IV (AC1-146) and are reported in **Table 1: Radioligand binding data for Compounds I and IV** **Table 1**.

	K_i (nM)		
	<u>NET</u>	<u>SERT</u>	<u>DAT</u>
XIII (AC1-60)	25697 ± 5843	53337 ± 18531	4866 ± 670
XVI (AC1-146)	43.97 ± 7.11	785 ± 90	1540 ± 177
TALOPRAM	2.88 ± 0.27	795 ± 24	14900 ± 1390

Table 1: Radioligand binding data for Compounds I and IV

In compound I, the labeling of talopram on the secondary amine resulted in complete loss of affinity at both NET and SERT and in a negligible increase in DAT affinity, suggesting that this design is not compatible with NET binding.

Since compound III shares a similar design and proved to be especially challenging to purify and characterize, its development has been suspended.

Interestingly, tagging nisooxetine on the phenyl ring side resulted in an interesting K_i value of 44 nM and in the conservation of most of the binding selectivity of the parent ligand. In line with previously developed probes, this affinity value was considered satisfactory and the evaluation of AC1-146 in live cell microscopy experiments is ongoing. This promising results corroborated our interest in the obtainment and evaluation of compound II, which shares a similar design.

Conclusion and Future Perspectives

In this work, a functional design for NET-selective high affinity fluorescent probes has been identified. Synthetic schemes for the obtainment of a first group of probes with overall satisfying yields and good reproducibility have been developed. The best candidate is now under evaluation in live-cell microscopy experiments.

Further structural modifications could be performed in order to evaluate their impact on the probes affinity, selectivity and physical properties. These modifications could be:

- Different tagging sites;
- Different linker chains with specific length and/or polarity;
- Different fluorophores: in a second phase of the project, the chemistry and the probe designs developed for the most promising ligands will be applied to the development of SRM probes with the use of suitable fluorophores.

Experimental

Starting materials and solvents were purchased from commercial suppliers and were used without further purification. Reaction conditions and yields were not optimized.

¹H-NMR spectra were performed at 400 MHz, using a Varian Mercury Plus 400 instrument; the chemical shifts are reported in ppm. Signal multiplicity is used according to the following abbreviations: s= singlet, d= doublet, dd= doublet of doublets, t = triplet, td= triplet of doublets, q = quadruplet, m = multiplet, sept= septuplet, and bs= broad singlet;

Melting points were measured with an OptiMelt melting point apparatus;

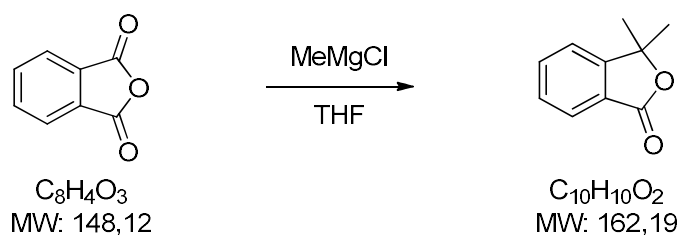
TLC were performed on standard analytical silica gel layers (Analtech Uniplate 250 μ m);

Chromatographic purifications were performed, in normal phase, using Teledyne ISCO instruments (CombiFlash Rf or CombiFlash EZ) over different RediSep Rf disposable chromatography cartridges.

High Resolution Mass Spectrometry spectra were acquired on a Orbitrap Velos (ThermoFisher) instrument coupled to an ESI source in positive ion mode.

Abbreviations used: DCE: dichloroethane; DCM: dichloromethane; DIAD: diisopropylazodicarboxylate; DIPEA: diisopropylethylamine; DMF: dimethylformamide; mp: melting point; MW: molecular weight; RT: room temperature; THF: tetrahydrofuran.

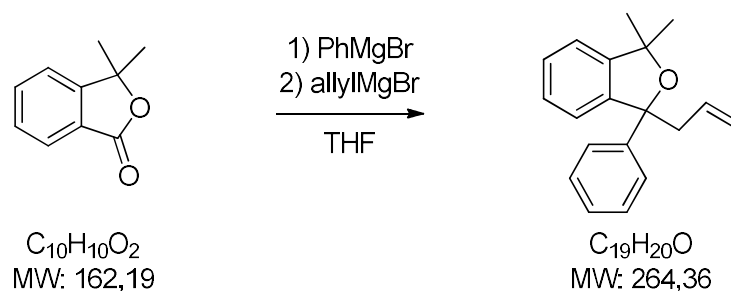
3,3-dimethyl-1,3-dihydroisobenzofuran-1-one



3.0 M methylmagnesium chloride (7.87 mL, 23.6 mmol) was added dropwise to a solution of phthalic anhydride (1.00 g, 6.75 mmol) in anhydrous THF (8 mL) at 0° C under argon atmosphere. After stirring at RT for 1.5 hours, the reaction was cooled down to 0° C and ethyl acetate (15 mL) and 2 N HCl (15 mL) were added dropwise. The aqueous phase was extracted with ethyl acetate (2x15 mL) and the collected organic phases were washed with brine (25 mL), dried over $MgSO_4$ and concentrated under reduced pressure to give 1.08 g (100%) of 3,3-dimethyl-1,3-dihydroisobenzofuran-1-one as a light yellow oil.

1H NMR (400 MHz, $CDCl_3$) δ 7.86 (d, $J = 7.2$ Hz, 1H), 7.66 (t, $J = 7.0$ Hz, 1H), 7.50 (t, $J = 7.0$ Hz, 1H), 7.39 (d, $J = 7.2$ Hz, 1H), 1.66 (s, 6H).

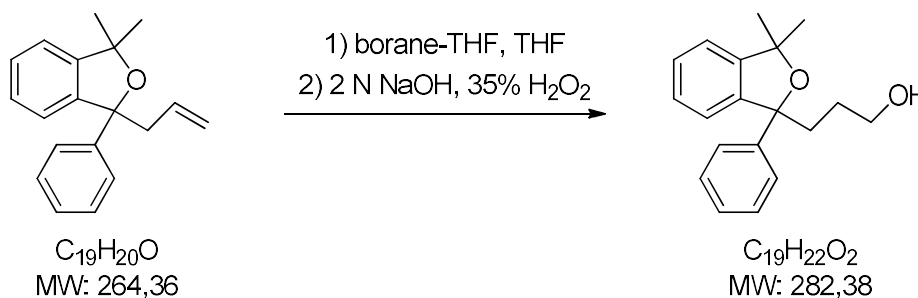
1-allyl-3,3-dimethyl-1-phenyl-1,3-dihydroisobenzofuran



3.0 M phenylmagnesium bromide (2.47 mL, 7.40 mmol) was added to a solution of 3,3-dimethyl-1,3-dihydroisobenzofuran-1-one (1.00 g, 6.16 mmol) in anhydrous THF (8 mL) at 0° C under argon atmosphere. After stirring at RT for 30 minutes, the reaction mixture was cooled down to 0° C and 1.0 M allylmagnesium bromide (12.32 mL, 12.32 mmol) was added. The mixture was left stirring overnight at RT and ethyl acetate (15 mL) and 2 N HCl (15 mL) were added dropwise at 0° C. The aqueous phase was extracted with ethyl acetate (2x15 mL) and the collected organic phases were washed with brine (25 mL) and concentrated under reduced pressure. The residue was dissolved in 1:1 EtOH/37% HCl (15 mL), concentrated under reduced pressure at 60° C for 30 minutes and then basified with 2 N NaOH (20 mL). The aqueous phase was extracted with ethyl acetate (3x15 mL) and the collected organic phases were dried over MgSO₄ and concentrated under reduced pressure to give 1.62 g (100%) of 1-allyl-3,3-dimethyl-1-phenyl-1,3-dihydroisobenzofuran as a brown oil.

¹H NMR (400 MHz, CDCl₃) δ 7.59 (d, *J* = 7.4 Hz, 2H), 7.40 – 7.17 (m, 6H), 7.09 (d, *J* = 4.8 Hz, 1H), 5.68 – 5.54 (m, 1H), 5.03 (d, *J* = 17.4 Hz, 1H), 4.97 (d, *J* = 10.2 Hz, 1H), 2.96 (dd, *J* = 14.5, 7.0 Hz, 1H), 2.82 (dd, *J* = 14.5, 7.0 Hz, 1H), 1.61 (s, 3H), 1.44 (s, 3H).

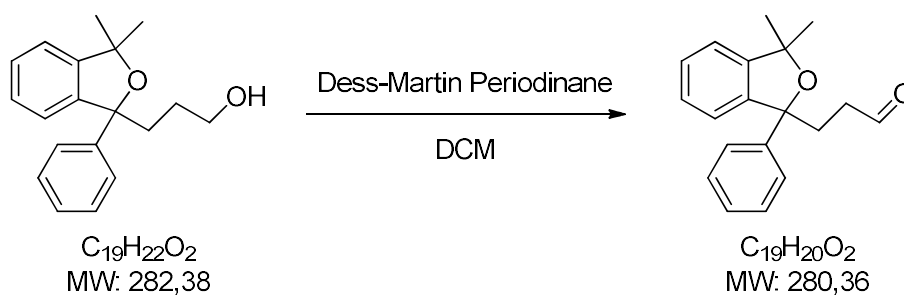
3-(3,3-dimethyl-1-phenyl-1,3-dihydroisobenzofuran-1-yl)propan-1-ol



1.0 M borane-THF (2.84 mL, 2.84 mmol) was added dropwise at 0° C to a solution of 1-allyl-3,3-dimethyl-1-phenyl-1,3-dihydroisobenzofuran (0.50 g, 1.89 mmol) in anhydrous THF (7.5 mL) under argon atmosphere. After stirring at RT for 3 hours, 2 N NaOH (4.5 mL) and 35% H₂O₂ were added dropwise at 0° C and the mixture was stirred at the same temperature for 2.5 hours. The reaction was quenched with the addition of brine (25 mL) and extracted with ethyl acetate (3x20 mL). The collected organic phases were dried over MgSO₄ and concentrated under reduced pressure. The resulting residue was purified by flash chromatography on silica gel. Elution with hexanes/ethyl acetate 100/0 to 60/40 gave 0.27 g (51%) of 3-(3,3-dimethyl-1-phenyl-1,3-dihydroisobenzofuran-1-yl)propan-1-ol as a colorless oil.

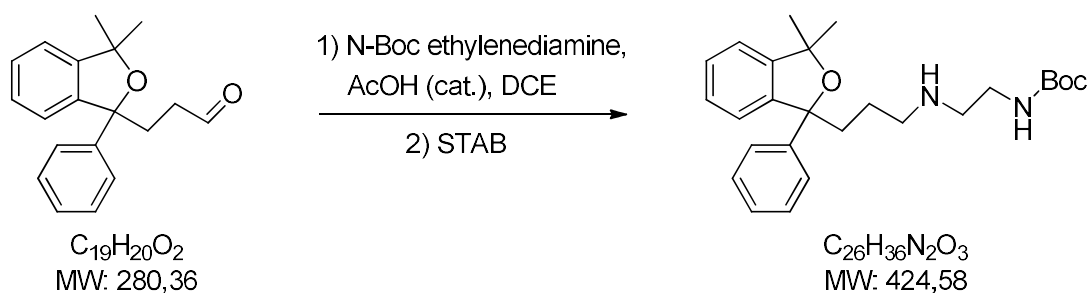
¹H NMR (400 MHz, CDCl₃) δ 7.59 (d, *J* = 7.8 Hz, 2H), 7.40 – 7.24 (m, 5H), 7.20 (t, *J* = 7.0 Hz, 1H), 7.09 (d, *J* = 5.7 Hz, 1H), 3.60 (t, *J* = 5.2 Hz, 2H), 2.41 – 2.30 (m, 1H), 2.19 (bs, 1H), 2.13 – 2.02 (m, 1H), 1.64 (s, 3H), 1.61 – 1.57 (m, 1H), 1.52 – 1.44 (m, 1H), 1.46 (s, 3H).

3-(3,3-dimethyl-1-phenyl-1,3-dihydroisobenzofuran-1-yl)propanal



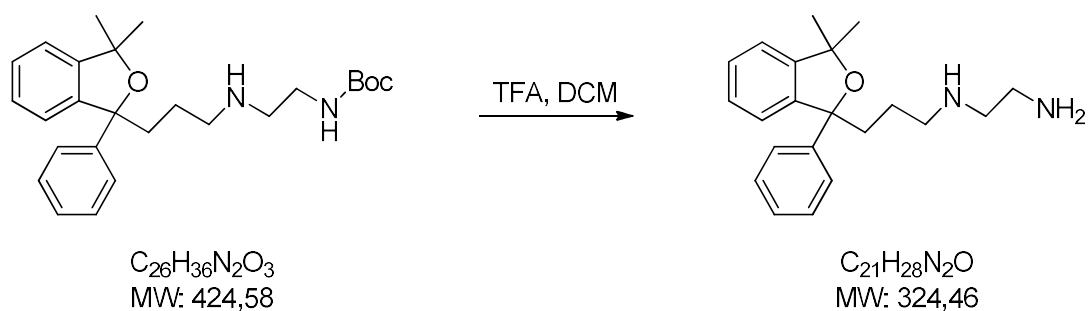
Dess-Martin periodinane (0.44 g, 1.05 mmol) was added portionwise at 0° C to a solution of 3-(3,3-dimethyl-1-phenyl-1,3-dihydroisobenzofuran-1-yl)propan-1-ol (0.27 g, 0.96 mmol) in DCM (10 mL) in an open flask. The reaction mixture was gradually brought to RT over the course of 1 hour, left stirring for 2 hours and then washed with saturated NaHCO₃ (3x10 mL). The organic phase was dried over MgSO₄ and concentrated under reduced pressure. The resulting crude was purified by flash chromatography on silica gel. Elution with hexanes/ethyl acetate 100/0 to 80/20 gave 0.07 g (26%) of 3-(3,3-dimethyl-1-phenyl-1,3-dihydroisobenzofuran-1-yl)propanal as a colorless oil.

¹H NMR (400 MHz, CDCl₃) δ 9.72 (s, 1H), 7.58 (d, *J* = 7.4 Hz, 2H), 7.40 – 7.27 (m, 5H), 7.21 (t, *J* = 7.1 Hz, 1H), 7.09 (d, *J* = 6.1 Hz, 1H), 2.59 – 2.49 (m, 1H), 2.42 – 2.26 (m, 3H), 1.59 (s, 3H), 1.41 (s, 3H).

N-(*N'*-Boc-aminoethyl)-*N*-desmethyltalopram

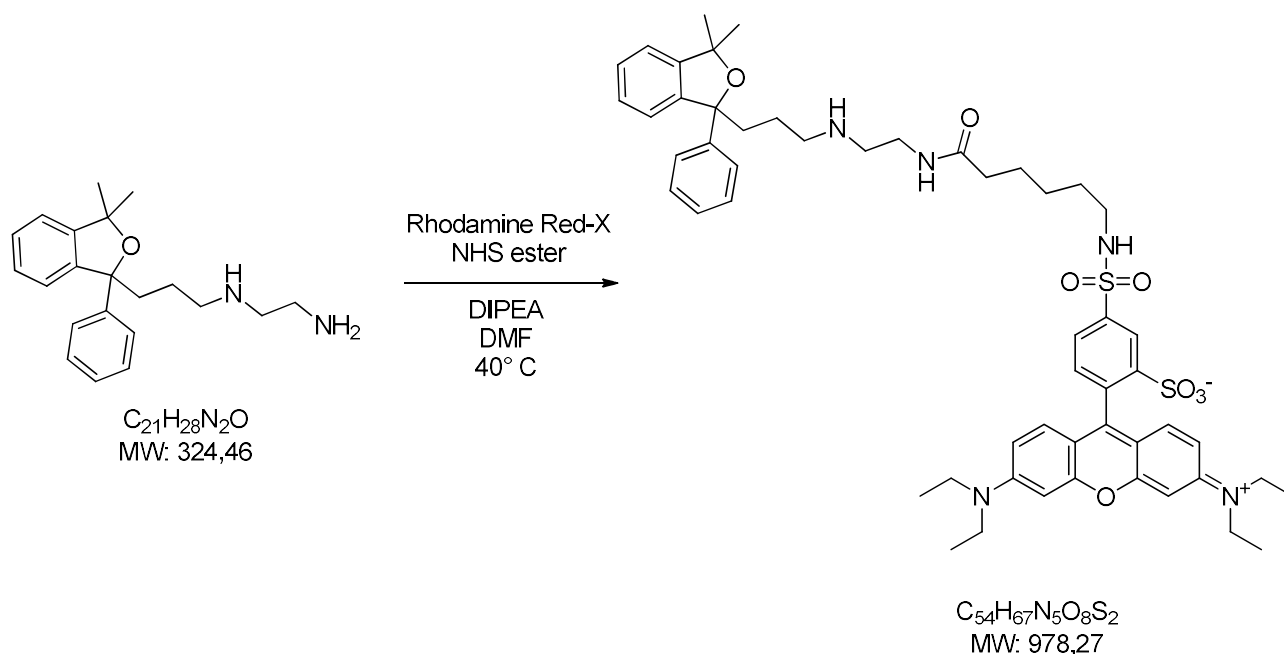
Acetic acid (2 drops, catalytic) was added to a solution of 3-(3,3-dimethyl-1-phenyl-1,3-dihydroisobenzofuran-1-yl)propanal (70 mg, 0.25 mmol) and *N*-Boc-ethylenediamine (42 mg, 0.26 mmol) in DCE (0.7 mL) under argon atmosphere. The reaction was stirred for 3 hours and sodium triacetoxyborohydride (159 mg, 0.75 mmol) was added. After stirring overnight, the mixture was washed with saturated Na_2CO_3 (1 mL) and brine (1 mL). The organic phase was dried over $MgSO_4$ and concentrated under reduced pressure. The resulting crude was purified by flash chromatography on silica gel. Elution with DCM/MeOH (with 10% 8N NH_4OH) 100/0 to 95/5 gave 15 mg (14%) of *N*-(*N'*-Boc-aminoethyl)-*N*-desmethyltalopram as a colorless oil.

1H NMR (400 MHz, $CDCl_3$) δ 7.57 (d, $J = 7.6$ Hz, 2H), 7.36 (d, $J = 6.3$ Hz, 1H), 7.33 – 7.24 (m, 4H), 7.19 (t, $J = 7.2$ Hz, 1H), 7.08 (d, $J = 5.8$ Hz, 1H), 4.87 (bs, 1H), 3.19 – 3.10 (m, 2H), 2.66 – 2.60 (m, 2H), 2.55 (t, $J = 6.7$ Hz, 2H), 2.19 (t, $J = 11.8$ Hz, 1H), 2.02 (t, $J = 11.8$ Hz, 1H), 1.61 (s, 3H), 1.52 – 1.39 (m, 1H), 1.42 (s, 12H), 1.39 – 1.28 (m, 1H).

N-(2-aminoethyl)-*N*-desmethyaltalopram

N-(*N'*-Boc-aminoethyl)-*N*-desmethyaltalopram (15 mg, 0.035 mmol) was dissolved in a 20% solution of trifluoroacetic acid in DCM (1 mL) and stirred at RT for 30 minutes. The solvent was evaporated, the obtained residue was dissolved in ethyl acetate and washed with aqueous 8N NH_4OH (1 mL). The organic phase was dried over MgSO_4 and concentrated under reduced pressure to give 4.4 mg (39%) of *N*-(2-aminoethyl)-*N*-desmethyaltalopram as a colorless oil.

^1H NMR (400 MHz, CDCl_3) δ 7.57 (d, $J = 7.7$ Hz, 2H), 7.35 (d, $J = 6.8$ Hz, 1H), 7.28 (dd, $J = 13.0, 5.6$ Hz, 4H), 7.19 (t, $J = 6.9$ Hz, 1H), 7.08 (d, $J = 6.0$ Hz, 1H), 2.76 – 2.71 (m, 2H), 2.61 – 2.54 (m, 4H), 2.20 (dt, $J = 13.8, 4.9$ Hz, 1H), 2.03 (dt, $J = 13.8, 4.9$ Hz, 1H), 1.61 (s, 3H), 1.56 – 1.45 (m, 1H), 1.42 (s, 3H), 1.33 (bs, 2H), 1.39 – 1.28 (m, 1H).

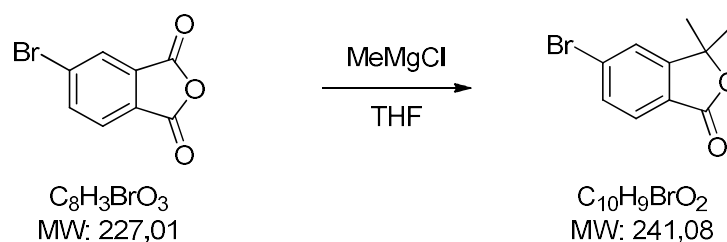
6-(Rhodamine Red-4-sulfonamido)hexanoyl-aminoethyl-*N*-desmethyltalopram (Compound XIII)

A solution of *N*-(2-aminoethyl)-*N*-desmethyltalopram (2.11 mg, 6 μ mol), Rhodamine Red-X NHS ester (5.00 mg, 6 μ mol) and DIPEA (1 μ L, 6 μ mol) in DMF (1 mL) was stirred at 40° C overnight. The solvent was evaporated under reduced pressure and the obtained crude was purified by flash chromatography on silica gel. Elution with DCM/MeOH (with 10% 8N NH_4OH) 100/0 to 85/15 gave 4.9 mg (83%) of 6-(Rhodamine Red-4-sulfonamido)hexanoyl-aminoethyl-*N*-desmethyltalopram (Compound XIII) as a dark purple oil.

1H NMR (400 MHz, $CDCl_3$) δ 8.81 – 8.78 (m, 1H), 8.03 (m, 1H), 7.70 (s, 1H), 7.55 (m, 1H), 7.37 (m, 1H), 7.23 (m, 10H), 7.04 (m, 1H), 6.87 (m, 1H), 6.67 (m, 1H), 5.28 (bs, 2H), 3.55 (m, 8H), 3.33 (m, 2H), 3.12 (m, 2H), 2.79 (m, 4H), 2.16 (m, 2H), 2.01 (m, 8H), 1.57 (s, 3H), 1.65 – 1.36 (m, 2H), 1.41 (s, 3H), 1.37 – 1.18 (m, 12H).

HRMS: m/z 978.44 ($M+1$), 697.23, 654.23.

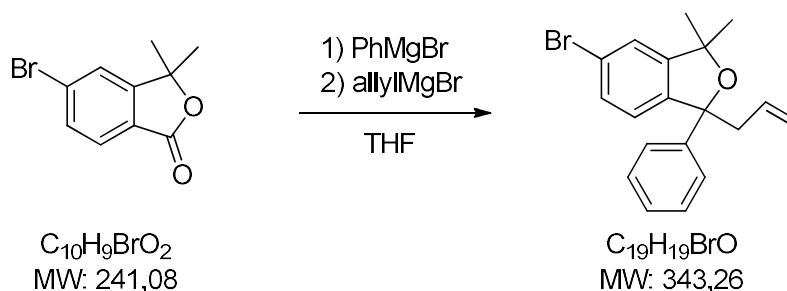
5-bromo-3,3-dimethyl-1,3-dihydroisobenzofuran-1-one



3.0 M methylmagnesium chloride (100 mL, 300 mmol) was added dropwise to a solution of 4-bromophthalic anhydride (20.0 g, 88.1 mmol) in anhydrous THF (160 mL) at -40°C under argon atmosphere. After stirring at RT for 1 hours, the reaction was cooled down to 0°C and ethyl acetate (200 mL) and 2 N HCl (100 mL) were added dropwise. The aqueous phase was extracted with ethyl acetate (2x100 mL) and the collected organic phases were washed with brine (200 mL), dried over MgSO_4 and concentrated under reduced pressure to give 24.4 g of crude oil. The crude was crystallized from EtOH (75 mL) to give 10.2 g (48%) of 5-bromo-3,3-dimethyl-1,3-dihydroisobenzofuran-1-one as white crystals (mp: $125.1\text{-}129.9^\circ\text{C}$).

$^1\text{H NMR}$ (400 MHz, CDCl_3) δ 7.65 (d, $J = 8.0$ Hz, 1H), 7.57 (d, $J = 8.0$ Hz, 1H), 7.50 (s, 1H), 1.59 (s, 6H).

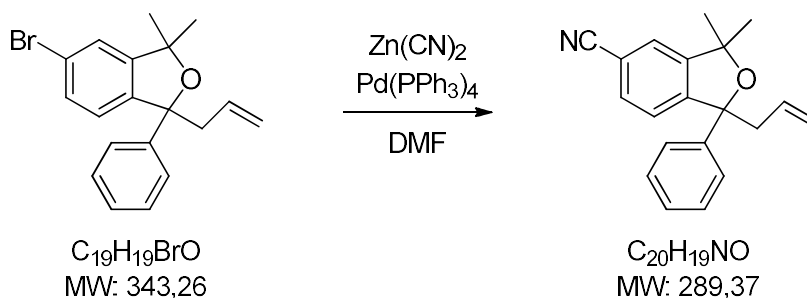
1-allyl-5-bromo-3,3-dimethyl-1-phenyl-1,3-dihydroisobenzofuran



3.0 M phenylmagnesiumbromide (1.67 mL, 5.01 mmol) was added to a solution of 5-bromo-3,3-dimethyl-1,3-dihydroisobenzofuran-1-one (1.00 g, 4.18 mmol) in anhydrous THF (8 mL) at 0° C under argon atmosphere. After stirring at RT for 30 minutes, the reaction mixture was cooled down to 0°C and 1.0 M allylmagnesium bromide (8.35 mL, 8.35 mmol) was added. The mixture was left stirring overnight at RT and ethyl acetate (15 mL) and 2 N HCl (15 mL) were added dropwise at 0° C. The aqueous phase was extracted with ethyl acetate (2x15 mL) and the collected organic phases were washed with brine (25 mL) and concentrated under reduced pressure. The residue was dissolved in 1:1 EtOH/37% HCl (15 mL), concentrated under reduced pressure at 60° C for 30 minutes and then basified with 2 N NaOH (20 mL). The aqueous phase was extracted with ethyl acetate (3x15 mL) and the collected organic phases were dried over MgSO₄ and concentrated under reduced pressure to give 1.37 g (96%) of 1-allyl-5-bromo-3,3-dimethyl-1-phenyl-1,3-dihydroisobenzofuran as a yellow oil.

¹H NMR (400 MHz, CDCl₃) δ 7.53 (d, *J* = 7.7 Hz, 2H), 7.42 (d, *J* = 7.8 Hz, 1H), 7.31 (t, *J* = 7.2 Hz, 2H), 7.28 – 7.16 (m, 2H), 7.22 (s, 1H), 5.66 – 5.53 (m, 1H), 5.02 (d, *J* = 18.3 Hz, 1H), 4.98 (d, *J* = 11.0 Hz, 1H), 2.93 (dd, *J* = 14.4, 6.7 Hz, 1H), 2.79 (dd, *J* = 14.4, 6.7 Hz, 1H), 1.59 (s, 3H), 1.41 (s, 3H).

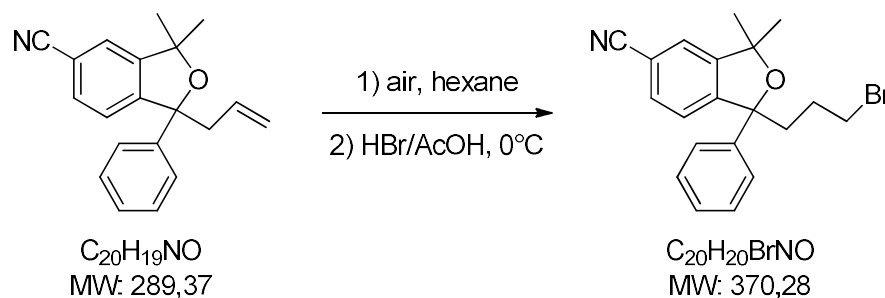
1-allyl-5-cyano-3,3-dimethyl-1-phenyl-1,3-dihydroisobenzofuran



Zinc cyanide (0.20 g, 1.70 mmol) was added to a solution of 1-allyl-5-bromo-3,3-dimethyl-1-phenyl-1,3-dihydroisobenzofuran (0.97 g, 2.83 mmol) in anhydrous DMF (20 mL). The mixture was degassed by bubbling argon for 5 minutes and $\text{Pd(PPh}_3)_4$ (0.13 g, 0.11 mmol) was added. The reaction was stirred at 80°C for 20 hours, constantly bubbling argon. The mixture was brought to RT and toluene (40 mL) was added. The organic phase was washed with 2N NH_4OH (2x25mL) and brine (25 mL), dried over MgSO_4 and concentrated under reduced pressure. The resulting crude was purified by flash chromatography on silica gel. Elution with hexanes/ethyl acetate 100/0 to 90/10 gave 0.48 g (48%) of 1-allyl-5-cyano-3,3-dimethyl-1-phenyl-1,3-dihydroisobenzofuran as a light yellow oil.

$^1\text{H NMR}$ (400 MHz, CDCl_3) δ 7.61 (d, $J = 7.8$ Hz, 1H), 7.52 (d, $J = 7.8$ Hz, 2H), 7.47 (d, $J = 7.9$ Hz, 1H), 7.38 (s, 1H), 7.33 (t, $J = 7.3$ Hz, 2H), 7.25 (d, $J = 6.4$ Hz, 1H), 5.66 – 5.50 (m, 1H), 5.03 (d, $J = 16.2$ Hz, 1H), 4.99 (d, $J = 9.5$ Hz, 1H), 2.96 (dd, $J = 14.5, 6.8$ Hz, 1H), 2.81 (dd, $J = 14.5, 6.8$ Hz, 1H), 1.62 (s, 3H), 1.44 (s, 3H).

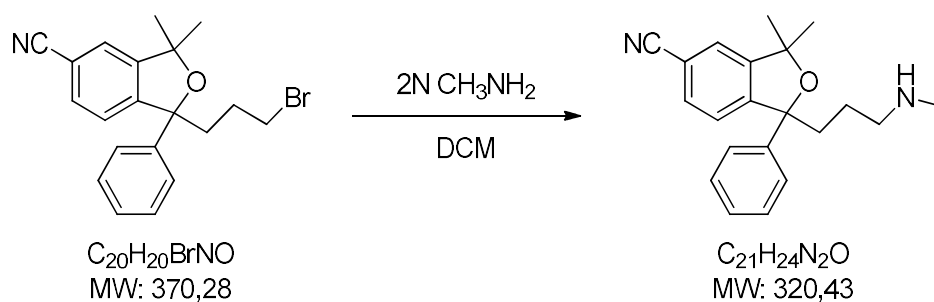
3-(5-cyano-3,3-dimethyl-1-phenyl-1,3-dihydroisobenzofuran-1-yl)-1-bromopropane



Air was bubbled through a solution of 1-allyl-5-cyano-3,3-dimethyl-1-phenyl-1,3-dihydroisobenzofuran (1.00 g, 3.46 mmol) in hexane (50 mL) for 30 minutes. 30% HBr in acetic acid (1.38 mL, 6.91) was added dropwise at 0° C and the reaction was stirred at the same temperature for 1 hour. Ethyl acetate (50 mL) and brine (50 mL) were added and the separated aqueous phase was extracted with 1:1 hexane/ethyl acetate (2x30 mL). The collected organic phases were dried over MgSO₄ and concentrated under reduced pressure. The resulting crude was purified by flash chromatography on silica gel. Elution with hexanes/ethyl acetate 100/0 to 80/20 gave 1.02 g (80%) of 3-(5-cyano-3,3-dimethyl-1-phenyl-1,3-dihydroisobenzofuran-1-yl)-1-bromopropane as a colorless oil.

¹H NMR (400 MHz, CDCl₃) δ 7.61 (dd, *J* = 7.9, 1.4 Hz, 1H), 7.54 – 7.50 (m, 2H), 7.47 (d, *J* = 7.9 Hz, 1H), 7.38 (d, *J* = 0.7 Hz, 1H), 7.33 (dd, *J* = 10.4, 4.8 Hz, 2H), 7.27 – 7.22 (m, 1H), 3.44 – 3.32 (m, 2H), 2.38 – 2.28 (m, 1H), 2.19 – 2.09 (m, 1H), 1.90 – 1.79 (m, 1H), 1.79 – 1.70 (m, 1H), 1.62 (s, 3H), 1.46 (d, *J* = 3.1 Hz, 3H).

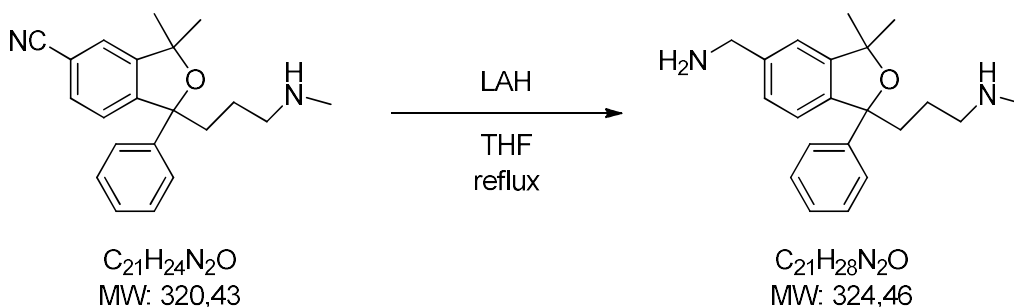
5-cyanotalopram



In a sealable flask, 2N methylamine in THF (14.9 mL, 29.8 mmol) was added to a solution of 3-(5-cyano-3,3-dimethyl-1-phenyl-1,3-dihydroisobenzofuran-1-yl)-1-bromopropane (1.47 g, 3.97 mmol) in DCM (15 mL). The flask was sealed and the reaction was stirred at RT for 24 hours. Solvents were evaporated under reduced pressure and the resulting crude was purified by flash chromatography on silica gel. Elution with DCM/MeOH (with 10% 8N NH_4OH) 100/0 to 90/10 gave 0.37 g (29%) of 5-cyanotalopram as a yellow oil.

^1H NMR (400 MHz, CDCl_3) δ 7.60 (dd, $J = 7.9, 1.4$ Hz, 1H), 7.52 (d, $J = 7.4$ Hz, 2H), 7.46 (d, $J = 7.9$ Hz, 1H), 7.37 (s, 1H), 7.31 (t, $J = 7.6$ Hz, 2H), 7.23 (d, $J = 7.4$ Hz, 1H), 2.54 (t, $J = 7.1$ Hz, 2H), 2.36 (s, 3H), 2.28 – 2.18 (m, 1H), 2.06 – 1.97 (m, 1H), 1.87 (bs, 1H), 1.62 (s, 3H), 1.54 – 1.43 (m, 1H), 1.45 (s, 3H), 1.40 – 1.28 (m, 1H).

5-aminomethyltalopram

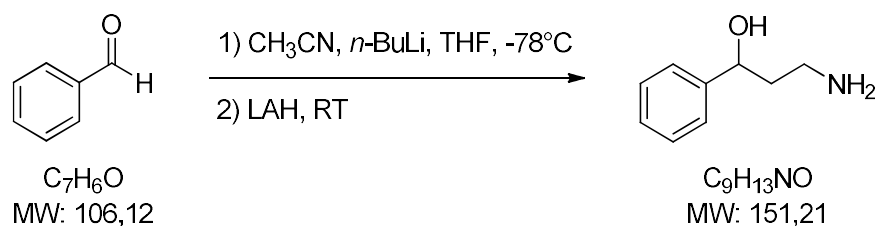


Lithium aluminum hydride (38 mg, 1.00 mmol) was suspended in anhydrous THF (5 mL) under argon atmosphere. A solution of 5-cyanotalopram (160 mg, 0.50 mmol) in anhydrous THF (2.5 mL) was added at 0°C and the mixture was stirred at reflux for 1 hour. The reaction was cooled down to 0°C and water (38 μl), 15% NaOH (38 μl) and water (114 μl) were added in sequence. The obtained mixture was stirred for 15 minutes at RT, MgSO_4 was added and stirring was continued for additional 15 minutes (Fieser workup). The solids were filtered, the solvents were evaporated under reduced pressure and the resulting crude was purified by flash chromatography on silica gel. Elution with DCM/MeOH (with 10% 8N NH_4OH) 100/0 to 80/20 gave 36 mg (22%) of 5-aminomethyltalopram as a colorless oil.

$^1\text{H NMR}$ (400 MHz, CDCl_3) δ 7.55 (d, $J = 7.4$ Hz, 2H), 7.34 (d, $J = 7.8$ Hz, 1H), 7.30 – 7.22 (m, 3H), 7.17 (t, $J = 7.3$ Hz, 1H), 7.04 (s, 1H), 3.87 (s, 2H), 3.56 (bs, 3H), 2.70 (t, $J = 7.4$ Hz, 2H), 2.39 (s, 3H), 2.27 – 2.17 (m, 1H), 2.09 – 1.99 (m, 1H), 1.69 – 1.58 (m, 1H), 1.59 (s, 3H), 1.54 – 1.43 (m, 1H), 1.40 (s, 3H).

The final reaction for this scheme and the obtainment of **Compound XIV** are still in progress.

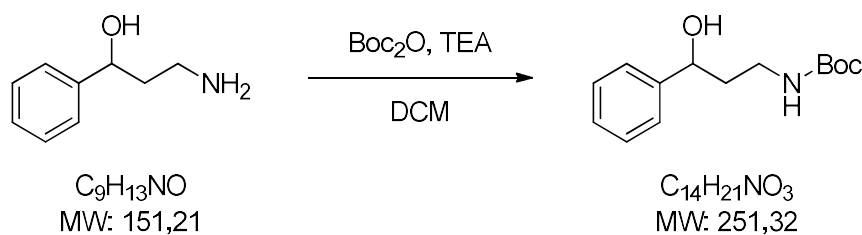
3-amino-1-phenylpropan-1-ol



2.5 M *n*-BuLi (9.42 mL, 23.6 mmol) was added to a solution of acetonitrile (1.47 mL, 28.3 mmol) in anhydrous THF (50 mL) at -78°C under argon atmosphere. The mixture was stirred 15 minutes and a solution of benzaldehyde (2.40 mL, 23.6 mmol) in anhydrous THF (15 mL) was added. The reaction was stirred for additional 5 hours at -78°C , after which it was brought to 0°C and lithium aluminum hydride (1.34 g, 35.3 mmol) was added. After stirring at RT overnight, sodium sulfate decahydrate was added and stirring was continued for 4 hours. Solids were filtered on celite and washed with DCM. Solvents were evaporated under reduced pressure to yield 1.42 g of 3-amino-1-phenylpropan-1-ol as a crude oil that was used in the next step without further purification.

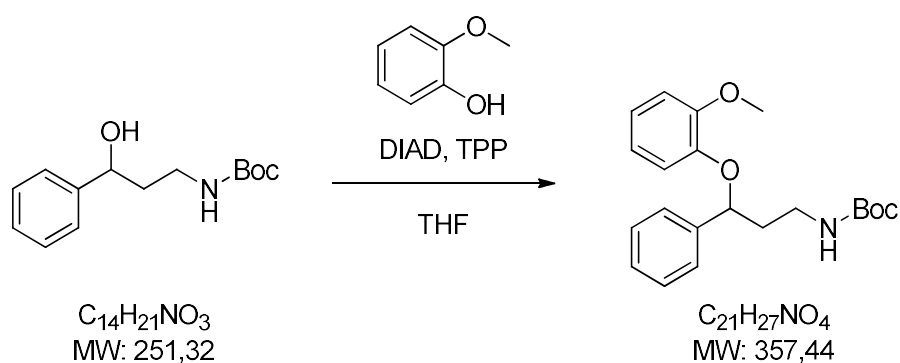
Purity of the crude was estimated at approx. 60% by NMR.

$^1\text{H NMR}$ (400 MHz, CDCl_3) δ 7.42 – 7.21 (m, 5H), 4.99 – 4.92 (m, 1H), 3.13 – 3.04 (m, 1H), 3.00 – 2.91 (m, 1H), 2.46 (bs, 3H), 1.92 – 1.82 (m, 1H), 1.82 – 1.70 (m, 1H).

N-Boc-3-amino-1-phenylpropan-1-ol

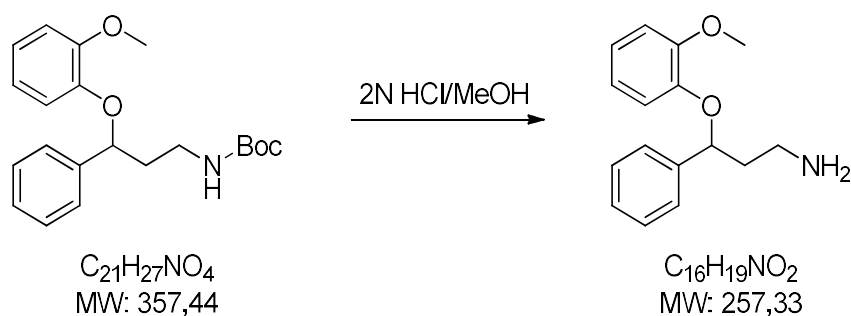
Crude 3-amino-1-phenylpropan-1-ol (60%, estimated 0.89 g), 5.88 mmol), Boc_2O (1.35 g, 6.18 mmol) and TEA (0.90 mL, 6.47 mmol) were dissolved in DCM (25 mL) and stirred at RT overnight. The mixture was washed with HCl 2N (15 mL), saturated NaHCO_3 (15 mL) and brine (15 mL), the separated organic phase was dried over MgSO_4 and concentrated under reduced pressure. The resulting crude was purified by flash chromatography on silica gel. Elution with hexanes/ethyl acetate 95/5 to 60/40 gave 0.80 g (13% over 2 steps) of *N*-Boc-3-amino-1-phenylpropan-1-ol as a colorless oil.

$^1\text{H NMR}$ (400 MHz, CDCl_3) δ 7.46 – 7.20 (m, 5H), 4.89 (bs, 1H), 4.78 – 4.72 (m, 1H), 3.48 (bs, 1H), 3.23 – 3.10 (m, 2H), 1.86 (dd, $J = 12.8, 6.0$ Hz, 1H), 1.45 (s, 9H).

N-Boc-*N*-desmethylnisoxetine

A solution of DIAD (0.62 mL, 3.18 mmol) in anhydrous THF (1.5 mL) was added dropwise to a solution of triphenylphosphine (1.25 g, 4.77 mmol) in anhydrous THF (8 mL) at -20°C under argon atmosphere. The mixture was stirred at the same temperature for 20 minutes and solutions of guaiacol (0.42 mL, 3.82 mmol) in anhydrous THF (2.5 mL) and *N*-Boc-3-amino-1-phenylpropan-1-ol 0.80 g, 3.18 mmol) in anhydrous THF (6 mL) were added in sequence. After stirring at RT over a weekend, the solvent was evaporated under reduced pressure and the resulting crude was purified by flash chromatography on silica gel. Elution with hexanes/ethyl acetate 100/0 to 70/30 gave 0.60 g (53%) of *N*-Boc-*N*-desmethylnisoxetine as a colorless oil.

$^1\text{H NMR}$ (400 MHz, CDCl_3) δ 7.37 – 7.24 (m, 5H), 6.91 – 6.86 (m, 2H), 6.72 – 6.65 (m, 1H), 6.56 (d, $J = 8.0$ Hz, 1H), 6.11 (bs, 1H), 5.17 – 5.11 (m, 1H), 3.94 (s, 3H), 3.60 – 3.48 (m, 1H), 3.32 – 3.22 (m, $J = 5.4$ Hz, 1H), 2.17 – 2.08 (m, 2H), 1.48 (s, 9H).

N-desmethylnisoxetine

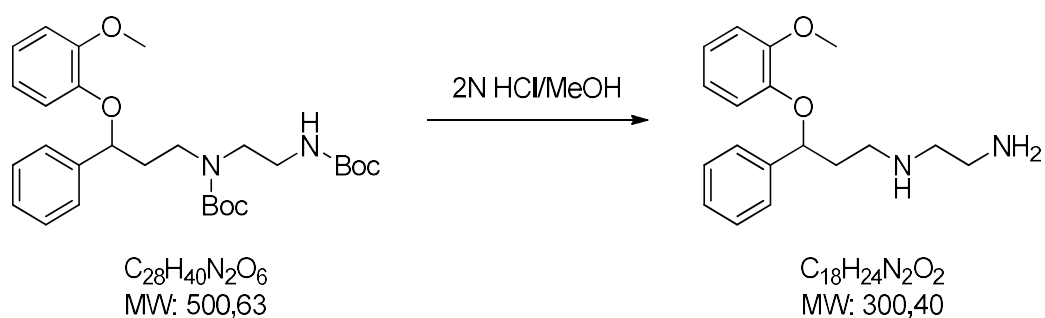
N-Boc-*N*-desmethylnisoxetine (0.60 g, 1.68 mmol) was dissolved in excess 2N HCl/MeOH and stirred at RT for 30 minutes. The solvent was evaporated under reduced pressure and the residue was dissolved in ethyl acetate (5 mL) and washed with 2N NaOH (5 mL). The aqueous phase was extracted with ethyl acetate (2x2.5 mL) and the collected organic phases were dried over MgSO₄, evaporated under reduced pressure to give 0.32 g (74%) of *N*-desmethylnisoxetine as a colorless oil.

¹H NMR (400 MHz, CDCl₃) δ 7.41 – 7.22 (m, 5H), 6.90 – 6.83 (m, 2H), 6.67 (t, *J* = 10.6 Hz, 2H), 5.24 – 5.18 (m, 1H), 3.89 (s, 3H), 3.02 – 2.93 (m, 2H), 2.30 – 2.19 (m, 1H), 2.16 (bs, 2H), 2.06 – 1.96 (m, 1H).

N-(*N'*-Boc-aminoethyl)-*N*-desmethylnisoxetine

N-Boc-2-aminoacetaldehyde (75 mg, 0.47 mmol) and TEA (0.16 mL, 1.17 mmol) were added to a solution of *N*-desmethylnisoxetine (120 mg, 0.47 mmol) in anhydrous DCM (10 mL). After stirring at RT for 1 hour, Boc_2O (120 mg, 0.56 mmol) and sodium triacetoxyborohydride (200 mg, 0.94 mmol) were added and the reaction was stirred for additional 3 hours. The mixture was washed with saturated NaHCO_3 (10 mL) and the aqueous phase was extracted with DCM (3x5 mL). The collected organic phases were dried over MgSO_4 , evaporated under reduced pressure and the resulting crude was purified by flash chromatography on silica gel. Elution with hexanes/ethyl acetate 100/0 to 60/40 gave 40 mg (17%) of *N*-(*N'*-Boc-aminoethyl)-*N*-desmethylnisoxetine as a colorless oil.

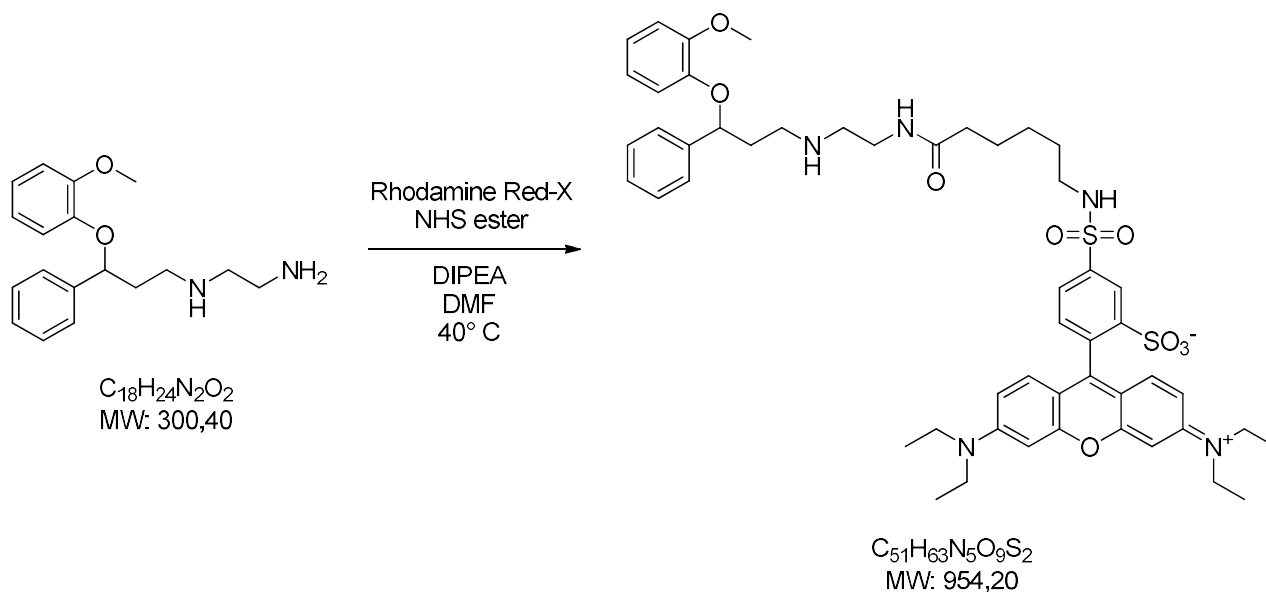
$^1\text{H NMR}$ (400 MHz, CDCl_3) δ 7.40 – 7.29 (m, 3H), 7.29 – 7.22 (m, 2H), 6.90 – 6.85 (m, 1H), 6.74 – 6.66 (m, 1H), 5.26 – 5.21 (m, 1H), 3.89 (s, 3H), 2.84 (t, $J = 6.1$ Hz, 2H), 2.80 (t, $J = 6.1$ Hz, 2H), 2.72 – 2.66 (m, 2H), 2.34 – 2.21 (m, 1H), 2.12 – 2.01 (m, 1H).

N-2-aminoethyl-*N*-desmethylisoxetine

N-(*N'*-Boc-aminoethyl)-*N*-desmethylisoxetine (40 mg, 0.08 mmol) was dissolved in excess 2N HCl/MeOH and stirred at RT for 30 minutes. 2N NH₄OH/MeOH was added dropwise until basic pH, the solvent was evaporated under reduced pressure and the residue was purified by flash chromatography on silica gel. Elution with DCM/MeOH (with 10% 8N NH₄OH) 100/0 to 80/20 gave 18 mg (75%) of *N*-2-aminoethyl-*N*-desmethylisoxetine as a colorless oil.

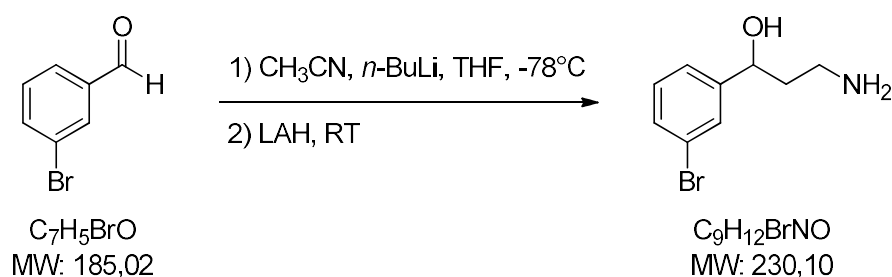
¹H NMR (400 MHz, CDCl₃) δ 7.40 – 7.28 (m, 3H), 7.28 – 7.21 (m, 2H), 6.90 – 6.82 (m, 2H), 6.74 – 6.64 (m, 2H), 5.27 – 5.20 (m, 1H), 3.89 (s, 3H), 2.86 (t, *J* = 6.3 Hz, 2H), 2.82 (t, *J* = 5.3 Hz, 2H), 2.70 (t, *J* = 5.3 Hz, 2H), 2.28 (m, 1H), 2.13 – 2.03 (m, 1H), 1.91 (bs, 3H).

N-[6-((Rhodamine Red-4-sulfonamido)hexanoyl)aminoethyl]-*N*-desmethylnisoxetine (Compound XV)



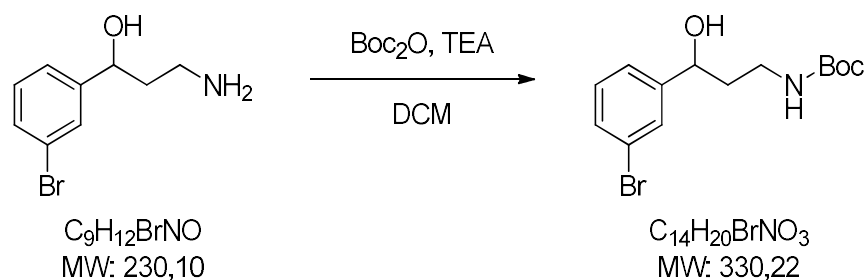
A solution of *N*-2-aminoethyl-*N*-desmethylnisoxetine (1.80 mg, 6 μ mol), Rhodamine Red-X NHS ester (5.00 mg, 6 μ mol) and DIPEA (1 μ L, 6 μ mol) in DMF (1 mL) was stirred at 40° C overnight. The solvent was evaporated under reduced pressure. NMR analysis of the crude confirmed the presence of *N*-[6-((Rhodamine Red-4-sulfonamido)hexanoyl)aminoethyl]-*N*-desmethylnisoxetine (Compound XV) but the product proved impossible to purify by chromatography due to suspect degradation on silica gel. (Elution with DCM/MeOH with 10% 8N NH_4OH 100/0 to 85/15)

3-amino-1-(3-bromophenyl)propan-1-ol



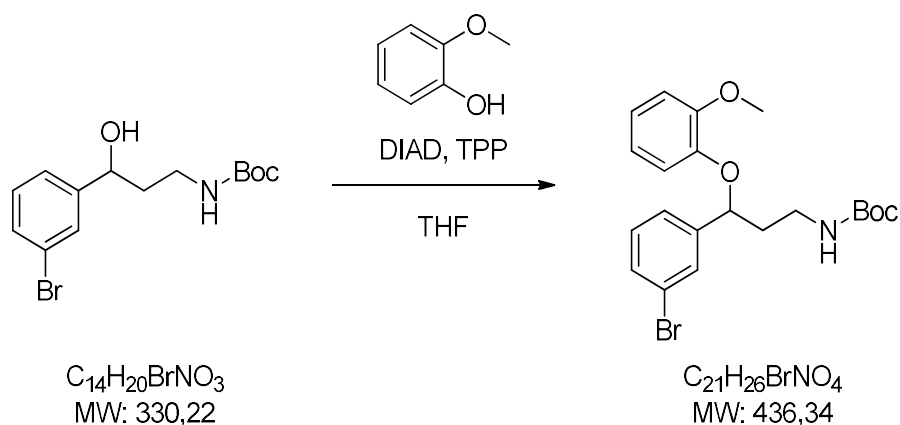
2.5 M *n*-BuLi (5.40 mL, 13.5 mmol) was added to a solution of acetonitrile (0.84 mL, 16.2 mmol) in anhydrous THF (65 mL) at -78°C under argon atmosphere. The mixture was stirred 15 minutes and a solution of 3-bromobenzaldehyde (1.57 mL, 13.5 mmol) in anhydrous THF (15 mL) was added. The reaction was stirred for additional 5 hours at -78°C after which it was brought to 0°C and lithium aluminum hydride (0.77 g, 20.3 mmol) was added. After stirring at 0°C for 1.5 hours, sodium sulfate decahydrate was added and stirring was continued for 45 minutes. Solids were filtered on celite and washed with DCM. Solvents were evaporated under reduced pressure to yield 2.17 g of 3-amino-1-(3-bromophenyl)propan-1-ol as a crude oil that was used in the next step without further purification.

Purity of the crude was estimated at approx. 85% by NMR.

N-Boc-3-amino-1-(3-bromophenyl)propan-1-ol

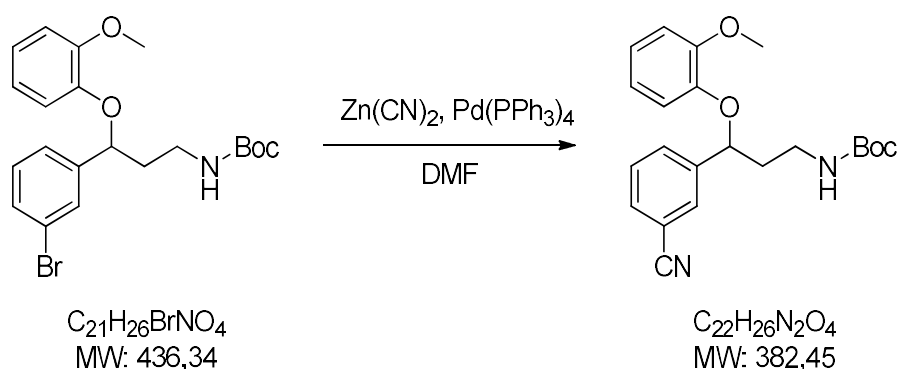
Crude 3-amino-1-phenylpropan-1-ol (85%, estimated 1.82 g, 7.91 mmol), Boc_2O (1.72 g, 7.91 mmol) and TEA (1.21 mL, 8.70 mmol) were dissolved in DCM (100 mL) and stirred at RT overnight. The mixture was washed with HCl 2N (40 mL), saturated NaHCO_3 (40 mL) and brine (40 mL), the separated organic phase was dried over MgSO_4 and concentrated under reduced pressure. The resulting crude was purified by flash chromatography on silica gel. Elution with hexanes/ethyl acetate 100/0 to 50/50 gave 0.79 g (17% over 2 steps) of *N*-Boc-3-amino-1-(3-bromophenyl)propan-1-ol as an orange oil.

$^1\text{H NMR}$ (400 MHz, CDCl_3) δ 7.53 (s, 1H), 7.42 – 7.33 (m, 1H), 7.31 – 7.25 (m, 1H), 7.20 (t, $J = 7.8$ Hz, 1H), 4.87 (bs, 1H), 4.74 – 4.68 (m, 1H), 3.58 (bs, 1H), 3.62 – 3.47 (m, 1H), 3.21 – 3.10 (m, 1H), 1.90 – 1.74 (m, 2H), 1.46 (s, 9H).

N-Boc-*m*-bromo-*N*-desmethylisoxetine

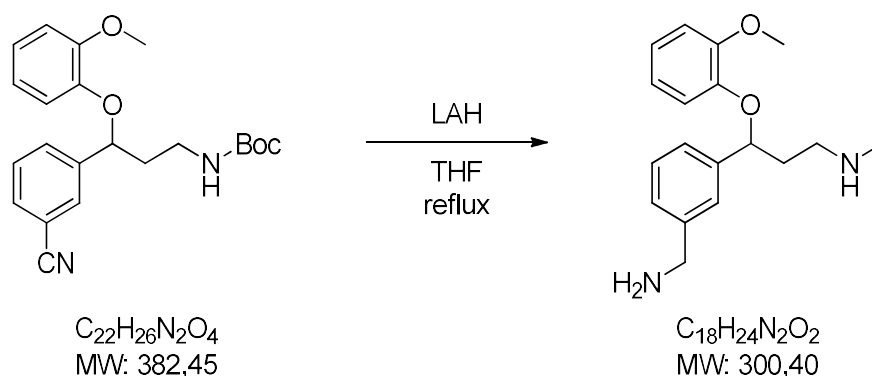
A solution of DIAD (0.10 mL, 0.51 mmol) in anhydrous THF (0.25 mL) was added dropwise to a solution of triphenylphosphine (0.20 g, 0.77 mmol) in anhydrous THF (1.25 mL) at -20°C under argon atmosphere. The mixture was stirred at the same temperature for 20 minutes and solutions of guaiacol (66 μL , 0.61 mmol) in anhydrous THF (0.50 mL) and *N*-Boc-3-amino-1-phenylpropan-1-ol 0.17 g, 0.51 mmol) in anhydrous THF (1.25 mL) were added in sequence. After stirring at RT for 3 hours, the solvent was evaporated under reduced pressure and the resulting crude was purified by flash chromatography on silica gel. Elution with hexanes/ethyl acetate 100/0 to 90/10 gave 0.11 g (49%) of *N*-Boc-*m*-bromo-*N*-desmethylisoxetine as a colorless oil.

$^1\text{H NMR}$ (400 MHz, CDCl_3) δ 7.52 (s, 1H), 7.40 (d, $J = 7.9$ Hz, 1H), 7.30 – 7.25 (m, 1H), 7.20 (t, $J = 7.6$ Hz, 1H), 6.93 – 6.88 (m, 2H), 6.75 – 6.68 (m, 1H), 6.56 (d, $J = 7.7$ Hz, 1H), 6.01 (bs, 1H), 5.09 (t, $J = 6.3$ Hz, 1H), 3.94 (s, 3H), 3.59 – 3.48 (m, 1H), 3.32 – 3.21 (m, 1H), 2.14 – 2.06 (m, 2H), 1.48 (s, 9H).

N-Boc-*m*-cyano-*N*-desmethylnisoxetine

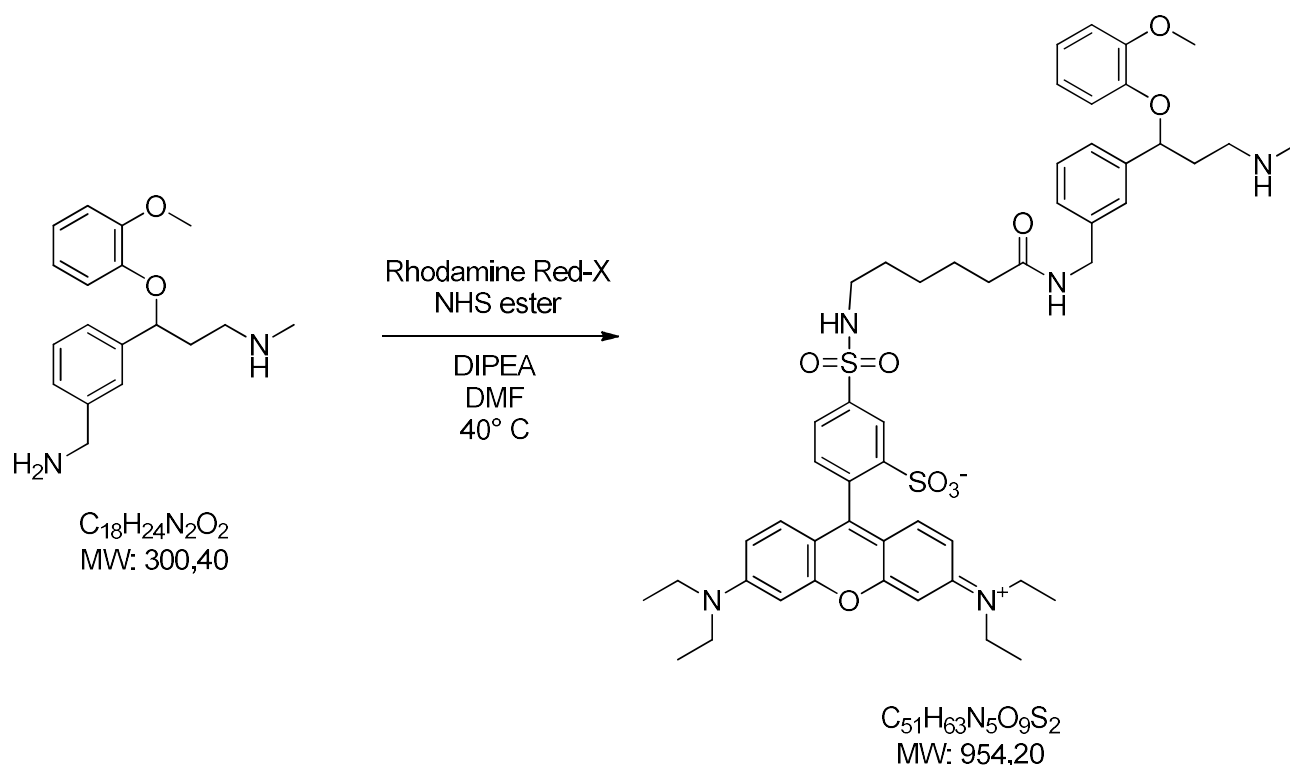
Zinc cyanide (39 mg, 0.34 mmol) was added to a solution of *N*-Boc-*m*-bromo-*N*-desmethylnisoxetine (250 mg, 0.57 mmol) in anhydrous DMF (5 mL). The mixture was degassed by bubbling argon for 5 minutes and Pd(PPh₃)₄ (53 mg, 0.06 mmol) was added. The reaction was stirred at 80°C for 24 hours, constantly bubbling argon. The mixture was brought to RT and toluene (20 mL) was added. The organic phase was washed with 2N NH₄OH (2x10mL) and brine (10 mL), dried over MgSO₄ and concentrated under reduced pressure. The resulting crude was purified by flash chromatography on silica gel. Elution with hexanes/ethyl acetate 100/0 to 60/40 gave 0.12 g (54%) of *N*-Boc-*m*-cyano-*N*-desmethylnisoxetine as a colorless oil.

¹H NMR (400 MHz, CDCl₃) δ 7.69 – 7.65 (m, 1H), 7.62 – 7.54 (m, 2H), 7.45 (t, *J* = 7.7 Hz, 1H), 6.95 – 6.89 (m, 2H), 6.75 – 6.67 (m, 1H), 6.51 (d, *J* = 7.7 Hz, 1H), 5.90 (bs, 1H), 5.18 (t, *J* = 6.0 Hz, 1H), 3.94 (s, 3H), 3.56 – 3.45 (m, 1H), 3.35 – 3.22 (m, 1H), 2.15 – 2.07 (m, 2H), 1.48 (s, 9H).

m-(aminomethyl)nisoxetine

Lithium aluminum hydride (47 mg, 1.25 mmol) was suspended in anhydrous THF (5 mL) under argon atmosphere. A solution of *tert*-butyl *N*-Boc-*m*-cyano-*N*-desmethylnisoxetine (120 mg, 1.25 mmol) in anhydrous THF (2.5 mL) was added at 0°C and the mixture was stirred at reflux for 4 hours. The reaction was cooled down to 0°C and quenched with saturated Na₂CO₃ (10 mL). The aqueous phase was extracted with ethyl acetate (3x5 mL) and the collected organic phases were dried over MgSO₄. The solvent was evaporated under reduced pressure and the resulting crude was purified by flash chromatography on silica gel. Elution with DCM/MeOH (with 10% 8N NH₄OH) 100/0 to 80/20 gave 20 mg (21%) of *m*-(aminomethyl)nisoxetine as a colorless oil.

¹H NMR (400 MHz, CDCl₃) δ 7.32 (s, 1H), 7.30 – 7.23 (m, 2H), 7.20 (d, *J* = 6.9 Hz, 1H), 6.90 – 6.84 (m, 2H), 6.74 – 6.65 (m, 2H), 5.23 – 5.16 (m, 1H), 3.89 (s, 3H), 3.85 (s, 2H), 2.86 – 2.76 (m, 2H), 2.46 (s, 3H), 2.32 – 2.20 (m, 1H), 2.12 – 1.98 (m, 1H).

m-[6-(Rhodamine Red-4-sulfonamido)hexanoyl]aminomethylnisoxetine (Compound XVI)

A solution of *m*-(aminomethyl)nisoxetine (1.95 mg, 6 μmol), Rhodamine Red-X NHS ester (5.00 mg, 6 μmol) and DIPEA (1 μL , 6 μmol) in DMF (1 mL) was stirred at 40° C overnight. The solvent was evaporated under reduced pressure and the obtained crude was purified by flash chromatography on silica gel. Elution with DCM/MeOH (with 10% 8N NH_4OH) 100/0 to 85/15 gave 4.98 mg (87%) of *m*-[6-(Rhodamine Red-4-sulfonamido)hexanoyl]aminomethylnisoxetine (Compound XVI) as a dark purple oil.

^1H NMR (400 MHz, CDCl_3) δ 8.87 – 8.78 (m, 1H), 8.06 (d, $J = 8.2$ Hz, 1H), 7.51 (s, 1H), 7.36 (s, 1H), 7.26 – 7.09 (m, 6H), 6.89 – 6.74 (m, 4H), 6.68 (s, 3H), 5.23 – 5.14 (m, 1H), 4.33 (dd, $J = 13.9, 4.8$ Hz, 1H), 4.29 (d, $J = 13.9, 3.7$ Hz, 1H), 3.88 (s, 3), 3.75 (bs, 1H), 3.67 – 3.45 (m, 8H), 3.20 – 3.11 (m, 2H), 2.90 – 2.80 (m, 2H), 2.48 (s, 3H), 2.45 – 2.32 (m, 1H), 2.27 – 2.15 (m, 3H), 1.85 (bs, 1H), 1.66 – 1.55 (m, 2H), 1.55 – 1.44 (m, 2H), 1.44 – 1.34 (m, 2H), 1.34 – 1.18 (m, 12H).

HRMS: m/z 787.31, 654.23, 626.23.

CHAPTER 3 – DESIGN AND SYNTHESIS OF FLUORESCENT PROBES BASED ON A METHYLPHENIDATE SCAFFOLD

Introduction

The results presented in Chapter 1, together with previous literature data, support the hypothesis that the modulation of α -syn/Syn-III interaction occurs through the binding of methylphenidate on Syn-III. However, this binding has never been verified and quantified with specific experiments. The employment of fluorescent probes based on a methylphenidate ligand in FRET experiments could provide valuable insight into binding dynamics and help us elucidate this crucial event in the modulation of α -syn/Syn-III interaction.

Aim of the Work

Fluorescent probes based on a methylphenidate scaffold were designed and synthesized. The general design is based on the ligand connected to a fluorophore by a linker chain. Multiple tagging sites are identifiable on the structure of the parent ligand, with the main ones being the methyl ester, the piperidine nitrogen and the phenyl ring. In absence of a computational model for the interaction of methylphenidate on Syn-III, we decided to exclude the piperidine nitrogen, based on the activity data on PK6 (see *Chapter 1 – Results and Discussion*). We then decided to focus on labeling the ester, given the increased synthetic feasibility of the approach over tagging at the phenyl ring level and the possibility to start from advanced intermediates.

In this first phase of the project, we designed and synthesized two probes with different structural features (**Figure 19**):

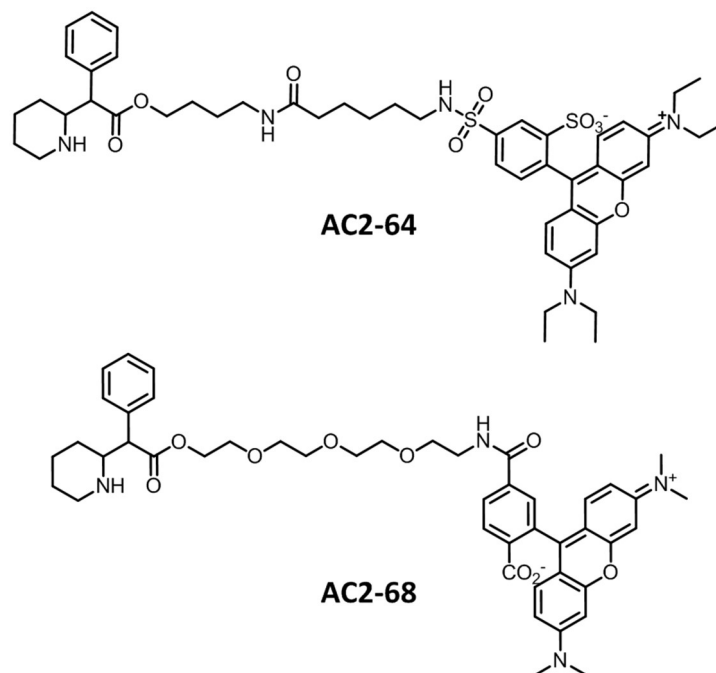
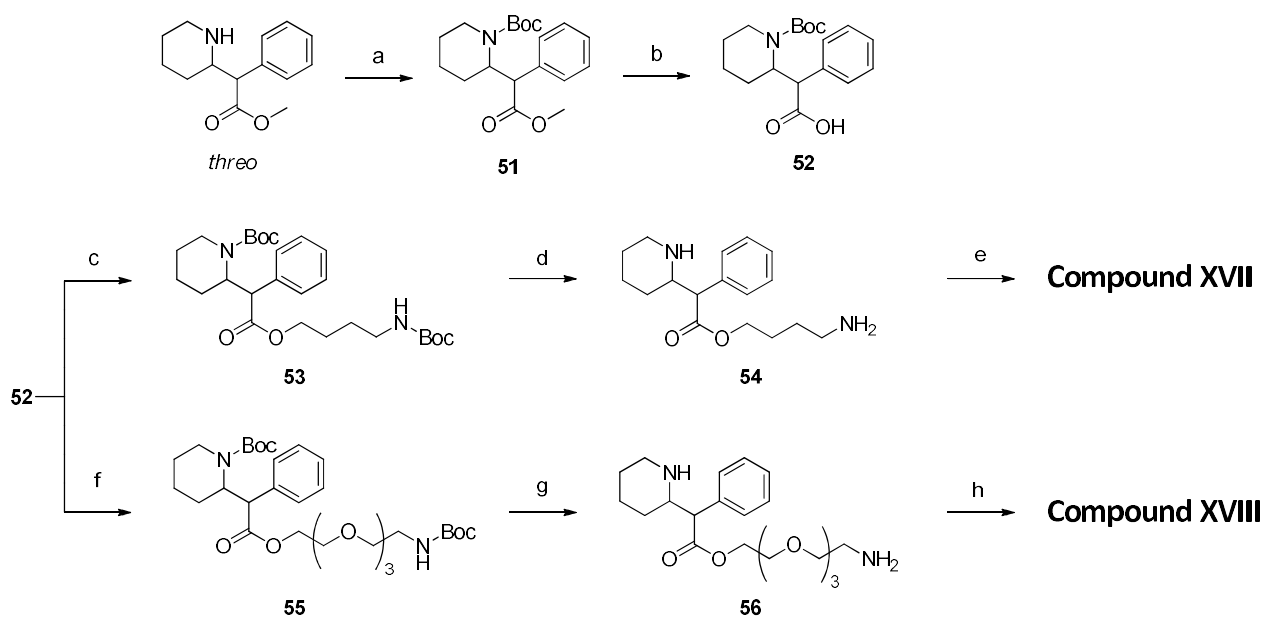


Figure 19: Structure of fluorescent methylphenidate probes Compound XVII and Compound XVIII

Compound XVII features an alkylamide linker chain and Rhodamine Red, while for Compound XVIII the linker chain is composed of amino-PEG4-alcohol, linked to tetramethylrhodamine (TAMRA) by an amide bond.

Chemistry

The synthesis of **Compound XVII** and **Compound XVIII** is reported in **Scheme 11**: (*d,l*)-*threo*-methylphenidate hydrochloride is *N*-protected with Boc and hydrolyzed in basic conditions to give *N*-Boc-(*d,l*)-*threo*-ritalinic acid **2**. Mitsunobu reaction with *N*-Boc-4-aminopropan-1-ol and subsequent deprotection lead to diamine **4**, whose primary amine reacts selectively with Rhodamine Red-X NHS ester to give **Compound XVII**. For the synthesis of **Compound XVIII**, the whole PEG linker chain is introduced *via* Mitsunobu reaction of **2** with *N*-Boc-amino-PEG4-alcohol. Deprotection of amines and amide coupling with 6-COOH-TAMRA give the final compound.



Scheme 11

Reagents and conditions: a) Boc_2O , NaHCO_3 , NaCl , H_2O , CHCl_3 , reflux (76%); b) NaOH , H_2O , EtOH ; c) *N*-Boc-4-aminopropan-1-ol, TPP, DIAD, THF, RT (85%); d) 2N HCl/MeOH (excess), RT (65%); e) Rhodamine Red-X NHS ester, DIPEA, DMF, 40°C (98%); f) *N*-Boc-amino-PEG4-alcohol, TPP, DIAD, THF, RT (49%); g) 2N HCl/MeOH (excess), RT (39%); h) 6-COOH-TAMRA, TSTU, DIPEA, RT (12%).

Future Work

The synthesized probes are now under evaluation in FRET experiments to measure FRET energy transfer between GFP-Syn-III and the probes fluorophores to obtain an indirect measurement of the binding of methylphenidate on Syn-III. Once proven and characterized, this would make a crucial contribution to our understanding of the interaction of methylphenidate and the analogs presented in Chapter 1 with their target protein and would support the proposed mechanism of action for the class.

If needed, structural modifications will be evaluated to insure the optimal interaction with the target and to enhance the selectivity and sensitivity of the approach. Specifically:

- Modifications of the linker chain length and/or polarity;
- Different tagging sites;
- Different fluorophores could be employed if the energy transfer is not optimal between the currently used FRET pairs.

In a second phase of the project, the rational design of a second generation of probes would be supported by a computational model for the interaction of methylphenidate and its analogs with Syn-III, obtained from the experimental work presented in Chapter 1 and from its future directions.

Experimental

Starting materials and solvents were purchased from commercial suppliers and were used without further purification. Reaction conditions and yields were not optimized.

¹H-NMR spectra were performed at 400 MHz, using a Varian Mercury Plus 400 instrument; the chemical shifts are reported in ppm. Signal multiplicity is used according to the following abbreviations: s= singlet, d= doublet, dd= doublet of doublets, t = triplet, td= triplet of doublets, q = quadruplet, m = multiplet, sept= septuplet, and bs= broad singlet;

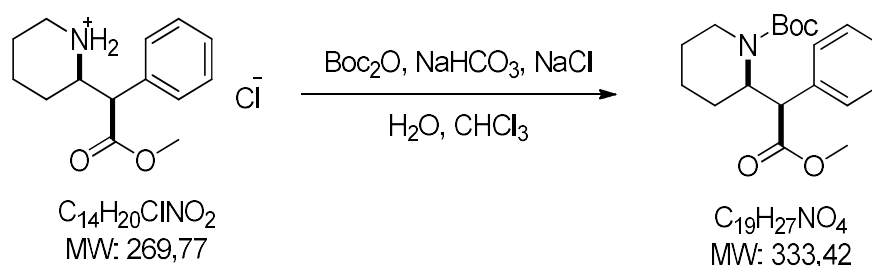
Melting points were measured with an OptiMelt melting point apparatus;

TLC were performed on standard analytical silica gel layers (Analtech Uniplat 250 μm);

Chromatographic purifications were performed, in normal phase, using Teledyne ISCO instruments (CombiFlash Rf or CombiFlash EZ) over different RediSep Rf disposable chromatography cartridges.

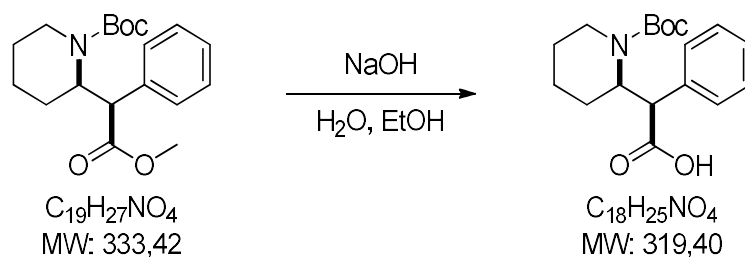
High Resolution Mass Spectrometry spectra were acquired on a Orbitrap Velos (ThermoFisher) instrument coupled to an ESI source in positive ion mode.

Abbreviations used: DCM: dichloromethane; DIAD: diisopropylazodicarboxylate; DIPEA: diisopropylethylamine; DMF: dimethylformamide; mp: melting point; MW: molecular weight; RT: room temperature; THF: tetrahydrofuran; TSTU: *N,N,N',N'*-Tetramethyl-*O*-(*N*-succinimidyl)uronium tetrafluoroborate.

N-Boc-*threo*-methylphenidate

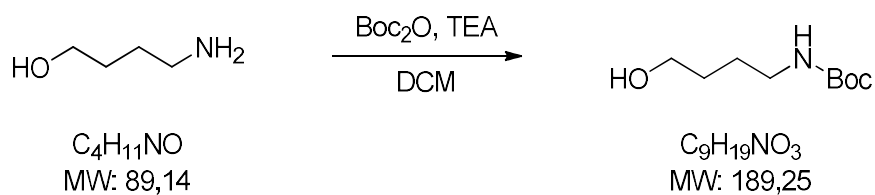
threo methylphenidate hydrochloride (1.00 g, 3.71 mmol), sodium bicarbonate (716 mg, 8.53 mmol), sodium chloride (867 mg, 14.8 mmol) and Boc_2O (809 mg, 3.71 mmol) were dissolved in a bifasic system made of water (5 mL) and chloroform (10 mL) and stirred at reflux for 2.5 hours. The organic phase was separated and washed with 1N HCl (1x5 mL) and evaporated under reduced pressure. The crude was dissolved in hot hexane (6 mL), stirred at 0° C for 1 hour and filtered to give 0.94 g (76%) of *N*-Boc *threo*-methylphenidate as a white solid (mp: 81.0-84.5).

$^1\text{H NMR}$ (400 MHz, CD_3OD) δ 7.50 – 7.41 (m, 2H), 7.38 – 7.26 (m, 3H), 4.94 – 4.82 (m, 1H), 4.26 (d, $J = 10.6$ Hz, 1H), 4.02 (t, $J = 13.4$ Hz, 1H), 3.60 (s, 3H), 3.18 – 2.98 (m, 1H), 1.74 – 1.59 (m, 2H), 1.51 (s, 9H), 1.41 – 1.28 (m, 2H), 1.26 – 1.16 (m, 2H).

N-Boc *threo*-ritalinic acid

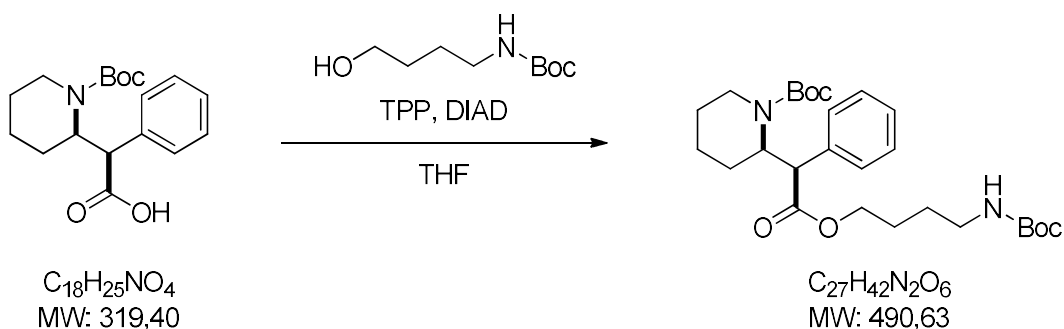
N-Boc *threo*-methylphenidate (330 mg, 1.0 mmol) and NaOH (48 mg, 1.2 mmol) were dissolved in a mixture of water (0.75 mL) and ethanol (0.75 mL) and refluxed for 2.5 hours. The solvents were evaporated under reduced pressure, the residue was taken up in 5% citric acid aqueous solution (1.28 g) and ethyl acetate (1 mL) and stirred at RT for 30 minutes. The aqueous phase was extracted with ethyl acetate (2x1 mL), the collected organic phases were dried over MgSO₄ and evaporated under reduced pressure to give 0.25 g (78%) of *N*-Boc *threo*-ritalinic acid as a white waxy solid.

¹H NMR (400 MHz, CD₃OD) δ 7.55 – 7.39 (m, 2H), 7.39 – 7.21 (m, 3H), 4.93 – 4.81 (m, 1H), 4.18 (d, *J* = 11.8 Hz, 1H), 4.10 – 3.92 (m, 1H), 3.19 – 3.01 (m, 1H), 1.72 – 1.59 (m, 2H), 1.50 (s, 9H), 1.42 – 1.30 (m, 2H), 1.29 – 1.08 (m, 2H).

N-Boc-4-aminobutanol

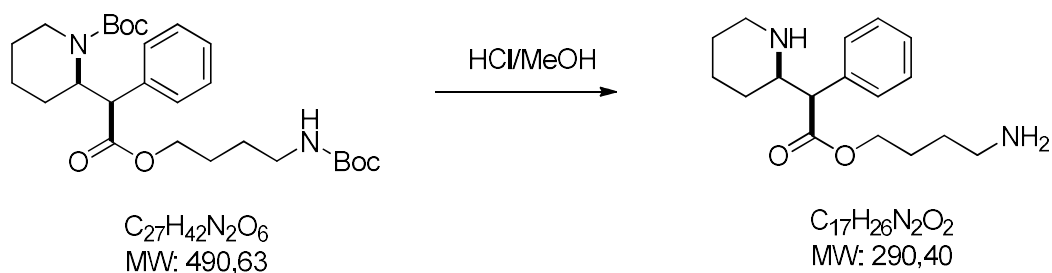
A solution of Boc_2O (3.67 g, 16.83 mmol) in DCM (15 mL) was added dropwise to a solution of 4-aminobutan-1-ol (1.5 g, 16.83 mmol) and TEA (2.81 mL, 20.20 mmol) in DCM (10 mL). The mixture was stirred at RT overnight. The solvent was evaporated under reduced pressure and rotary evaporation was continued for additional 20 minutes at 90° C. The resulting crude was purified by filtration on a silica plug, eluting at first with hexanes/ethyl acetate 60/40 and then with DCM/MeOH (with 10% 8N NH_4OH) 90/10, to give 1.21 g (38%) of *N*-Boc-4-aminobutanol as a colorless oil.

$^1\text{H NMR}$ (400 MHz, CDCl_3) δ 4.60 (bs, 1H), 3.67 (t, $J = 5.4$ Hz, 2H), 3.20 – 3.10 (m, 2H), 1.65 – 1.53 (m, 4H), 1.44 (s, 9H).

4-(*N*-Boc-amino)butyl-*N*-Boc-*threo*-phenidate

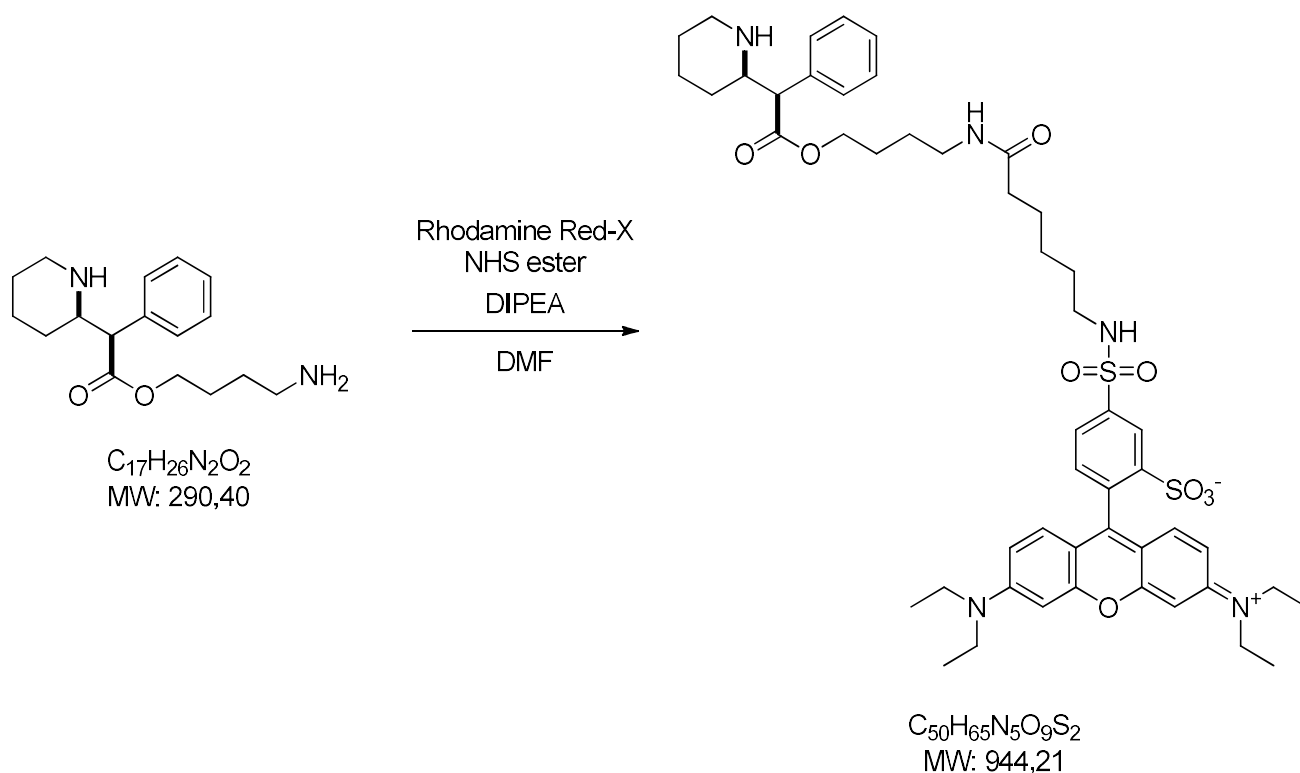
DIAD (92 μ L, 0.47 mmol) was added dropwise to a solution of *N*-Boc ritalinic acid (100 mg, 0.31 mmol), *N*-Boc-4-aminobutan-1-ol (89 mg, 0.47 mmol) and triphenylphosphine (123 mg, 0.47 mmol) in THF (5 mL) at 0° C under argon atmosphere. The mixture was kept in the dark and stirred at RT overnight. The solvent was evaporated under reduced pressure and the resulting crude was purified by flash chromatography on silica gel. Elution with hexanes/ethyl acetate 100/0 to 80/20 gave 130 mg (85%) of 4-(*N*-Boc-amino)butyl-*N*-Boc-*threo*-phenidate as a colorless oil.

1H NMR (400 MHz, $CDCl_3$) δ 7.44 (d, $J = 7.1$ Hz, 2H), 7.37 – 7.27 (m, 3H), 5.10 – 4.98 (m, 1H), 4.91 – 4.80 (m, 1H), 4.22 – 4.09 (m, 2H), 4.04 – 3.85 (m, 2H), 3.15 – 2.94 (m, 2H), 1.68 – 1.56 (m, 3H), 1.56 – 1.46 (m, 4H), 1.51 (s, 9H), 1.44 (s, 9H), 1.33 – 1.18 (m, 3H).

threo-4-aminobutylphenidate

4-(*N*-Boc-amino)butyl-*N*-Boc-*threo*-phenidate (0.13 g, 0.26 mmol) was dissolved in excess 2N HCl/MeOH and stirred at RT for 1 hour. 2.0M NH₃ in isopropanol was added dropwise until basic pH and the solvents were evaporated under reduced pressure and the obtained crude was purified by flash chromatography on silica gel. Elution with DCM/MeOH (with 10% 8N NH₄OH) 100/0 to 80/20 gave 49 mg (65%) of *threo*-4-aminobutylphenidate as a colorless oil.

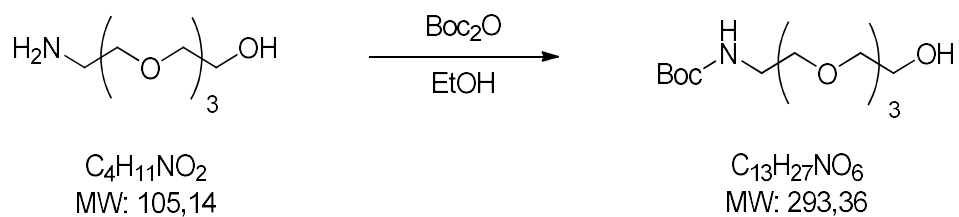
¹H NMR (400 MHz, CDCl₃) δ 7.34 – 7.23 (m, 5H), 4.13 – 4.02 (m, 2H), 3.43 (t, *J* = 5.0 Hz, 1H), 3.13 (dt, *J* = 10.5, 2.5 Hz, 1H), 3.09 – 3.03 (m, 1H), 2.70 (dt, *J* = 11.9, 2.8 Hz, 1H), 2.63 – 2.57 (m, 2H), 1.72 – 1.65 (m, 2H), 1.68 (bs, 3H), 1.62 – 1.53 (m, 2H), 1.45 – 1.31 (m, 3H), 1.31 – 1.16 (m, 2H), 1.02 – 0.88 (m, 1H).

4-*N*-[6-(Rhodamine Red-4-sulfonamido)hexanoyl]aminobutyl-*threo*-phenidate (Compound XVII)

A solution of *threo*-4-aminobutylphenidate (1.89 mg, 6 μ mol), Rhodamine Red-X NHS ester (5.00 mg, 6 μ mol) and DIPEA (1 μ L, 6 μ mol) in DMF (1 mL) was stirred at 50° C overnight. The solvent was evaporated under reduced pressure and the obtained crude was purified by flash chromatography on silica gel. Elution with DCM/MeOH (with 10% 8N NH_4OH) 100/0 to 85/15 gave 6.0 mg (98%) of 4-*N*-[6-(Rhodamine Red-4-sulfonamido)hexanoyl]aminobutyl-*threo*-phenidate (Compound XVII) as a dark purple oil.

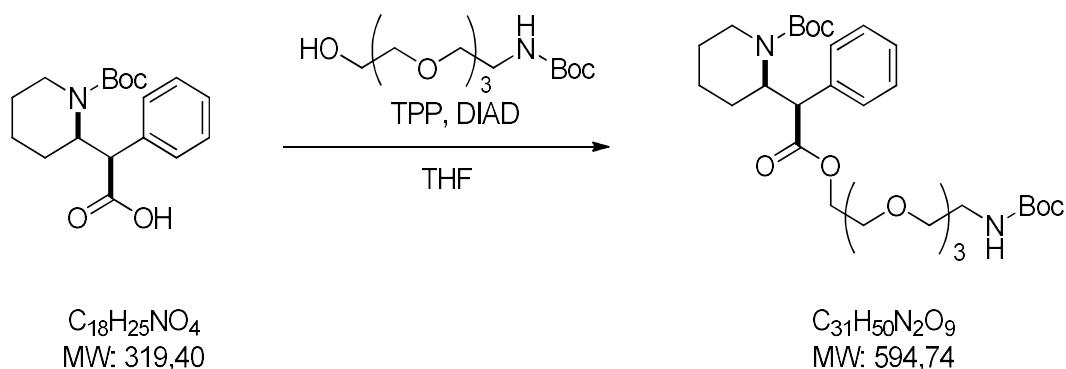
1H NMR (400 MHz, $CDCl_3$) δ 8.81 (d, J = 1.8 Hz, 1H), 8.02 (dd, J = 7.9, 1.9 Hz, 1H), 7.30 – 7.20 (m, 9H), 7.03 (t, J = 5.6 Hz, 1H), 6.86 – 6.79 (m, 1H), 6.67 (d, J = 2.3 Hz, 1H), 4.03 (dt, J = 11.9, 6.7 Hz, 1H), 3.92 (dt, J = 11.0, 6.6 Hz, 1H), 3.56 (q, J = 7.1 Hz, 8H), 3.43 (d, J = 10.1 Hz, 1H), 3.11 (t, J = 6.6 Hz, 2H), 3.11 – 3.02 (m, 2H), 2.98 (dd, J = 12.9, 6.6 Hz, 2H), 2.67 (dt, J = 11.7, 2.6 Hz, 1H), 2.06 (t, J = 7.5 Hz, 2H), 1.70 – 1.19 (m, 6H), 1.29 (t, J = 7.1 Hz, 12H).

HRMS: m/z 743.31, 654.22, 559.16.

N-Boc-amino-PEG4-alcohol

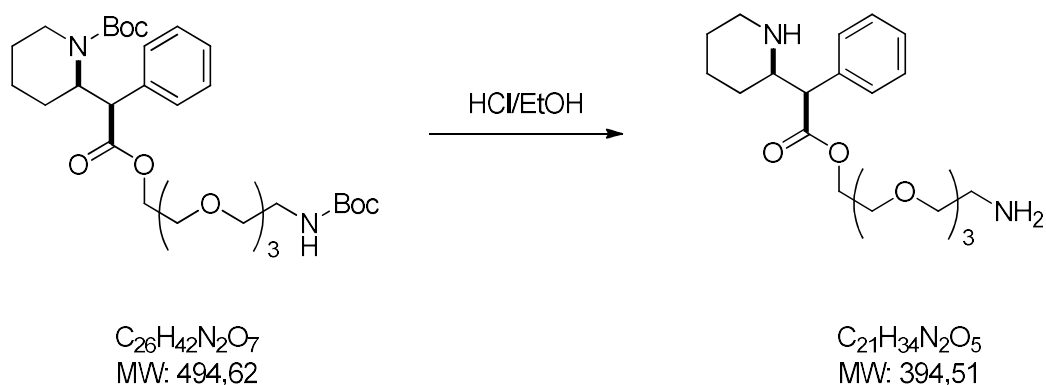
A solution of Boc_2O (1.24 g, 5.69 mmol) in EtOH (1 mL) was added dropwise to a solution of amino-PEG4-alcohol (1.00 g, 5.17 mmol) in EtOH (9 mL) under argon atmosphere. The mixture was stirred at RT for 4 hours. DCM (20 mL) was added and the organic phase was washed with 1N HCl (10 mL), saturated NaHCO_3 (10 mL) and brine (10 mL). The resulting crude was purified by filtration on a silica plug, eluting at first with hexanes/ethyl acetate 70/30 and then with DCM/MeOH (with 10% 8N NH_4OH) 90/10, to give 1.12 g (74%) of *N*-Boc-amino-PEG4-alcohol as a colorless oil.

^1H NMR (400 MHz, CDCl_3) δ 5.61 (bs, 1H), 3.77 – 3.68 (m, 4H), 3.68 – 3.59 (m, 8H), 3.55 – 3.51 (m, 2H), 3.36 – 3.27 (m, 2H), 3.01 (bs, 1H), 1.44 (s, 9H).

[*N*-Boc(amino-PEG4)yl] *N*-Boc-*threo*-phenidate

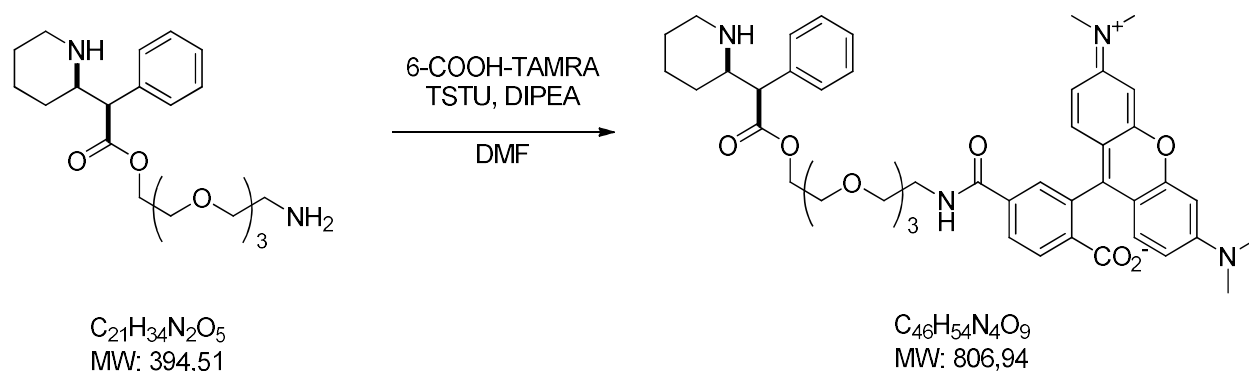
DIAD (0.30 mL, 1.55 mmol) was added dropwise to a solution of *N*-Boc ritalinic acid (0.33 g, 1.03 mmol), *N*-Boc-amino-PEG4-alcohol (0.45 g, 1.55 mmol) and triphenylphosphine (0.41 g, 1.55 mmol) in THF (15 mL) at 0° C under argon atmosphere. The mixture was kept in the dark and stirred at RT for 24 hours. The solvent was evaporated under reduced pressure and the resulting crude was purified by flash chromatography on silica gel. Elution with hexanes/ethyl acetate 100/0 to 60/40 gave 0.20 g (49%) of *N,N'*-diBoc-*threo*-ritalinic acid (amino-PEG4)ester as a colorless oil.

¹H NMR (400 MHz, CDCl₃) δ 7.50 – 7.40 (m, 2H), 7.37 – 7.27 (m, 3H), 5.09 – 4.79 (m, 1H), 4.30 – 4.05 (m, 4), 4.04 – 3.91 (m, 1H), 3.69 – 3.49 (m, 12H), 3.35 – 3.26 (m, 2H), 3.16 – 2.95 (m, 1H), 1.68 – 1.13 (m, 6H), 1.51 (s, 9H), 1.44 (s, 9H).

(amino-PEG4)yl-*threo*-phenidate

N,N'-diBoc *threo*-ritalinic acid(amino-PEG4)ester (0.20 g, 0.50 mmol) was dissolved in excess 2N HCl/MeOH and stirred at RT for 1 hour. 2.0M NH₃ in isopropanol was added dropwise until basic pH, the solvents were evaporated under reduced pressure and the obtained crude was purified by flash chromatography on silica gel. Elution with DCM/MeOH (with 10% 8N NH₄OH) 100/0 to 80/20 gave 0.08 g (39%) of (amino-PEG4)yl-*threo*-phenidate as a colorless oil.

¹H NMR (400 MHz, CDCl₃) δ 7.31 – 7.21 (m, 5H), 4.30 – 4.23 (m, 1H), 4.17 (dt, *J* = 11.9, 4.6 Hz, 1H), 3.63 – 3.56 (m, 6H), 3.56 – 3.43 (m, 7H), 3.11 (dt, *J* = 10.5, 2.5 Hz, 1H), 3.08 – 3.02 (m, 1H), 2.85 (t, *J* = 5.2 Hz, 2H), 2.67 (dt, *J* = 11.9, 2.8 Hz, 1H), 1.70 – 1.63 (m, 1H), 1.59 – 1.51 (m, 1H), 1.44 – 1.29 (m, 1H), 1.29 – 1.14 (m, 2H), 1.01 – 0.87 (m, 1H).

(Rhodamine Red-4-sulfonyl)amino(PEG4)yl-*threo*-phenidate (Compound XVIII)

A solution of (amino-PEG4)yl-*threo*-phenidate (4.73 mg, 12 μ mol), 6-COOH-TAMRA (5.00 mg, 12 μ mol) and DIPEA (2 EQ) (8.4 μ L, 24 μ mol) in DMF (2 mL) was stirred at RT overnight. The solvent was evaporated under reduced pressure and the obtained crude was purified by flash chromatography on silica gel. Elution with DCM/MeOH (with 10% 8N NH_4OH) 100/0 to 80/20 gave 1.2 mg (12%) of (Rhodamine Red-4-sulfonyl)amino(PEG4)yl-*threo*-phenidate (Compound XVIII) as a dark purple oil.

1H NMR (400 MHz, $CDCl_3$) δ 8.10 (s, 1H), 7.64 (s, 1H), 7.35 – 7.20 (m, 7H), 6.66 (d, J = 8.9 Hz, 2H), 6.50 (s, 1H), 6.42 (d, J = 8.5 Hz, 2H), 4.32- 4.26 (m, 1H), 4.07 – 3.99 (m, 1H), 3.71 – 3.31 (m, 14H), 3.00 (s, 6H), 3.00 (s, 6H), 2.89 – 2.79 (m, 1H), 1.94 – 1.28 (m, 6H).

HRMS: m/z 606.29, 588.24, 544.24, 472.15, 456.19, 418.15.

CONCLUSIONS

In this work, we designed and synthesized a class of methylphenidate analogs by systematically altering the structure of the parent drug. We evaluated modulatory activity of the analogs on the interaction between α -synuclein and Synapsin-III and their ability to prevent the formation of α -synuclein aggregates. The fluorescent probes chemistry developed in the synthesis of fluorescent ligands for the norepinephrine transporter has been applied to the development of fluorescent methylphenidate analogs, in order to elucidate the binding of methylphenidate on Synapsin-III and to clarify a crucial step in the mechanism of action of the proposed analogs. A combination of different concepts and approaches, ranging from classic SAR studies to the design of fluorescent ligands, together with the development of specific biological assays and computational methods, was employed to address novel medicinal chemistry challenges and to investigate the complex biology of protein-protein interactions and protein misfolding. The present work set the basis for a multidisciplinary project that will contribute, with the completion of the ongoing studies, to the validation of the interaction between α -synuclein and Synapsin-III as a novel target for the treatment of Parkinson's Disease and to the definition of new possibilities for its pharmacological modulation.

CONTRIBUTIONS TO THE RESEARCH

Unit 1: University of Milan – Department of Pharmaceutical Sciences (PI: Prof. Ermanno Valoti)

- Dr. Valentina Straniero: design of synthetic pathways and design of methylphenidate analogs (Chapter 1 and 3), synthetic medicinal chemistry mentoring
- Lorenzo Suigo, Erica Sorvillo, Marina Condomitti, Federica Spotti

Unit 2: University of Brescia – Department of Molecular and Translational Medicine (PI: Prof. Arianna Bellucci)

- Dr. Francesca Longhena and Dr. Federica Bono: design and execution of FRET, FLIM-FRET, immunocytochemistry and MTT assay experiments (Chapter 1)

Unit 3: University of Parma – Department of Food and Drug (PI: Prof. Gabriele Costantino)

- Dr. Agostino Bruno: preliminary computational studies on methylphenidate binding on Syn-III (Chapter 1)

Unit 4: NIH – National Institute on Drug Abuse – Intramural Research Program (PI: Dr. Amy Newman)

- Dr. Daryl Guthrie: design of fluorescent probes and synthetic pathways (Chapter 2 and 3), synthetic chemistry mentoring
- Dr. Therese Ku: design and execution of radioligand binding experiments (Chapter 2), radioligand binding pharmacology mentoring

PRODUCTS OF THE RESEARCH

Publications Related to the Thesis

- Faustini G., Longhena F., Bruno A., Bono F., Grigoletto J., La Via L. Barbon A., **Casiraghi A.**, Straniero V., Valoti E., Costantino G., Benfenati F., Missale C., Pizzi M., Spillantini M. G., Bellucci A.

Alpha-synuclein/synapsin III pathological interplay boosts the motor response to methylphenidate

Submitted

Other Publications

- Straniero V.; Sebastián-Pérez V.; Hrast M.; Zanotto C.; **Casiraghi A.**; Suigo L.; Zdovc I.; Radaelli A.; De Giuli Morghen C.; Valoti E.

Benzodioxane-benzamides as antibacterial agents: Computational and SAR studies to evaluate the influence of the 7-substitution in FtsZ interaction

ChemMedChem, Published Online, doi: 10.1002/cmdc.201900537

- **Casiraghi A.**, Valoti E., Suigo L., Artasensi A., Sorvillo E., Straniero V.
How Reaction Conditions May Influence the Regioselectivity in the Synthesis of 2,3-Dihydro-1,4- benzoxathiine Derivatives
Journal of Organic Chemistry, 2018, 83(21), 13217-13227
- Straniero V., Valoti E., **Casiraghi A.**, Fumagalli L.
How Do Reaction Conditions Affect the Enantiopure Synthesis of 2-substituted-1,4-benzodioxane Derivatives?
Chirality, 2018, 30(7), 943-950
- Straniero V., Zanotto C., Straniero L., **Casiraghi A.**, Duga S., Radaelli A., De Giuli Morghen C., Valoti E.
2,6-Difluorobenzamide Inhibitors of Bacterial Cell Division Protein FtsZ: Design, Synthesis and Structure-Activity Relationships
ChemMedChem, 2017, 12(16), 1303-1318

Grants

- Personalized Internal Supplemental Application - Michael J. Fox Foundation for Parkinson's Research
Preclinical screening of compounds modulating α -synuclein/Synapsin-III pathological interplay for the treatment of Parkinson's Disease
Submitted
Role on Project: Consultant

Posters and Oral Communications

- Straniero V., Sebastián-Pérez V., Hrast M., Zanotto C., **Casiraghi A.**, Suigo L., Zdovc I., Radaelli A., Valoti E.
How to productively interact with FtsZ to block bacterial replication: a computational and SAR investigation for developing potent antimicrobials
MYCS 2019, Rimini (RN), November 25-27, 2019 (oral communication).
- Suigo L., Straniero V., **Casiraghi A.**, Valoti E.
Study of isosteric 1,4-benzodioxanes oxygen atoms in benzamides FtsZ inhibitors
MYCS 2019, Rimini (RN), November 25-27, 2019.
- **Casiraghi A.**, Longhena F., Suigo L., Bono F., Bruno A., Straniero V., Bellucci A., Valoti E.
Design and synthesis of methylphenidate analogs as modulators of the α -synuclein/synapsin-III interaction
CeMM Workshop "Future Leaders in Molecular Medicine" – Vienna, Austria, October 29-31 2019 (oral communication).

- Straniero V., Sebastián-Pérez V., Hrast M., Zanotto C., **Casiraghi A.**, Suigo L., Zdovc I., Radaelli A., Valoti E.
Inhibition of Ftsz to Block Bacterial Replication: Development of Potent Antimicrobials
XXVI National Meeting in Medicinal Chemistry - Milano, Italy - July 16-19 2019.
- **Casiraghi A.**, Guthrie D., Ku T., Valoti E., Newman A. H.
Small Molecule Ligand-Based Fluorescent Probes for Imaging the Norepinephrine Transporter
XXVI National Meeting in Medicinal Chemistry - Milano, Italy - July 16-19 2019.
- **Casiraghi A.**, Guthrie D., Ku T., Valoti E., Newman A. H.
Design and Synthesis of Fluorescent Ligands for Imaging the Norepinephrine Transporter
Gordon Research Conference Bioorganic Chemistry – Translational Chemical Biology, Andover (NH), USA, June 9-14 2019.
- **Casiraghi A.**, Guthrie D., Ku T., Valoti E., Newman A. H.
Design and Synthesis of Fluorescent Ligands for Imaging the Norepinephrine Transporter
NIDA/IRP Poster Session, Baltimore (MD), USA, May 29, 2019.
- **Casiraghi A.**, Guthrie D., Ku T., Valoti E., Newman A. H.
Design and Synthesis of Fluorescent Ligands for Imaging the Norepinephrine Transporter
MTMDB Branch Meeting, Baltimore (MD), May 17 2019 (oral communication).
- **Casiraghi A.**, Guthrie D., Ku T., Valoti E., Newman A. H.
Design and Synthesis of Fluorescent Ligands for Imaging the Norepinephrine Transporter
12th Annual Frontiers in Chemistry and Biology Interface Symposium, Bethesda (MD), USA, May 3, 2019.
- **Casiraghi A.**, Guthrie D., Ku T., Valoti E., Newman A. H.
Design and Synthesis of Fluorescent Nanoprobes for Imaging the Norepinephrine Transporter
11th Annual Behavior, Biology and Chemistry Conference, San Antonio (TX), USA, March 2-3, 2019.
- Straniero V, **Casiraghi A.**, Valoti E.
How to fight antimicrobial resistance: design and synthesis of FTSZ inhibitors as novel potent gram-positive antibiotics
XXV EFMC-ISMC, Ljubljana, Slovenia, September 2-6, 2018.
- **Casiraghi A.**, Straniero V., Bellucci A., Bruno A., Longhena F., Bono F., Costantino G., Valoti E.
Novel modulators of α -Synuclein/Synapsin-III interaction as potential antiparkinsonian agents
MedChemSicily 2018, Palermo (PA), Italy, July 17-20, 2018 (oral communication).

- **Casiraghi A.**, Straniero V., Valoti E.
Synthesis and Structure-Activity Relationship of Novel Inhibitors of the Prokaryotic Divisome Protein FtsZ
VII European Workshop on Drug Synthesis, Pontignano (SI), Italy, May 20-24, 2018.
- Straniero V., **Casiraghi A.**, Valoti E.
Battle against antimicrobial resistance: FtsZ inhibitors as novel potent Gram-positive antibiotics
SCI Congress 2017, Paestum (SA), Italy, September 11-14, 2017.
- Straniero V., **Casiraghi A.**, Valoti E.
Novel inhibitors of FtsZ as antimicrobial agents: synthesis and structure activity relationship
ISOS 2017 – Gargnano (BS), Italy, June 18-23, 2017.

ACKNOWLEDGEMENTS

I would like to express my deepest gratitude to all the people that took part in various ways to the work presented in this Thesis:

To my advisor Prof. Valoti for the opportunity to be trained as a master's and PhD student in his laboratory and for his guidance through all the steps of this long and greatly interesting journey.

To Dr. Amy Newman for welcoming me in her research group and for having been a great tutor during my period at NIDA. It has been an amazing experience during which I had the chance to learn a lot and broaden my perspective on medicinal chemistry and research in general.

To Dr. Valentina Straniero for mentoring and teaching me in the lab over these years. I really appreciate your experience and skills and your uncompromisingly high standards for work and research quality. I hope we will have the opportunity to collaborate again in the future.

To Prof. Arianna Bellucci for the opportunity to collaborate in a very interesting research project and for her invaluable help with the neurobiology section of this work.

To Dr. Francesca Longhena, for her work on the biological evaluation of the compounds and for being a great scientist to collaborate with.

To Dr. Agostino Bruno for his computational work on methylphenidate binding on Syn-III.

To Dr. Daryl Guthrie for being my mentor at NIDA and for introducing me to the wonders of fluorescent probes chemistry.

To Dr. Theresa Ku for her patient mentoring and her help with radioligand binding assays.

To Lorenzo Suigo for the time shared in the lab and for the help with the chemistry, and to students Erica, Marina and Federica for their participation in the projects.

BIBLIOGRAPHY

- Alegre-Abarrategui, J., K. R. Brimblecombe, R. F. Roberts, E. Velentza-Almpani, B. S. Tilley, N. Bengoa-Vergniory and C. Proukakis (2019). "Selective vulnerability in α -synucleinopathies." Acta neuropathologica.
- Alguel, Y., A. D. Cameron, G. Diallinas and B. Byrne (2016). "Transporter oligomerization: form and function." Biochemical Society transactions **44**(6): 1737–1744.
- Alim, M. A., M. S. Hossain, K. Arima, K. Takeda, Y. Izumiyama, M. Nakamura, H. Kaji, T. Shinoda, S. Hisanaga and K. Ueda (2002). "Tubulin seeds alpha-synuclein fibril formation." The Journal of biological chemistry **277**(3): 2112–2117.
- Alvarez-Castelao, B. and J. G. Castaño (2011). "Synphilin-1 inhibits alpha-synuclein degradation by the proteasome." Cellular and molecular life sciences : CMLS **68**(15): 2643–2654.
- Anderluh, A., E. Klotzsch, A. W. A. F. Reismann, M. Brameshuber, O. Kudlacek, A. H. Newman, H. H. Sitte and G. J. Schütz (2014). "Single molecule analysis reveals coexistence of stable serotonin transporter monomers and oligomers in the live cell plasma membrane." The Journal of biological chemistry **289**(7): 4387–4394.
- Anderson, J. P., D. E. Walker, J. M. Goldstein, R. d. Laat, K. Banducci, R. J. Caccavello, R. Barbour, J. Huang, K. Kling, M. Lee, L. Diep, P. S. Keim, X. Shen, T. Chataway, M. G. Schlossmacher, P. Seubert, D. Schenk, S. Sinha, W. P. Gai and T. J. Chilcote (2006). "Phosphorylation of Ser-129 is the dominant pathological modification of alpha-synuclein in familial and sporadic Lewy body disease." The Journal of biological chemistry **281**(40): 29739–29752.
- Andrade, D. M., M. P. Clausen, J. Keller, V. Mueller, C. Wu, J. E. Bear, S. W. Hell, B. C. Lagerholm and C. Eggeling (2015). "Cortical actin networks induce spatio-temporal confinement of phospholipids in the plasma membrane--a minimally invasive investigation by STED-FCS." Scientific reports **5**: 11454.
- Athauda, D., K. Maclagan, S. S. Skene, M. Bajwa-Joseph, D. Letchford, K. Chowdhury, S. Hibbert, N. Budnik, L. Zampedri, J. Dickson, Y. Li, I. Aviles-Olmos, T. T. Warner, P. Limousin, A. J. Lees, N. H. Greig, S. Tebbs and T. Foltynie (2017). "Exenatide once weekly versus placebo in Parkinson's disease: a randomised, double-blind, placebo-controlled trial." The Lancet **390**(10103): 1664–1675.
- Augustine, G. J., M. P. Charlton and S. J. Smith (1985). "Calcium entry and transmitter release at voltage-clamped nerve terminals of squid." The Journal of physiology **367**: 163–181.
- Axten, J. M., L. Krim, H. F. Kung and J. D. Winkler (1998). "A Stereoselective Synthesis of dl-threo-Methylphenidate: Preparation and Biological Evaluation of Novel Analogues." The Journal of Organic Chemistry **63**(26): 9628-9629.
- Bähler, M., F. Benfenati, F. Valtorta, A. J. Czernik and P. Greengard (1989). "Characterization of synapsin I fragments produced by cysteine-specific cleavage: a study of their interactions with F-actin." The Journal of cell biology **108**(5): 1841–1849.
- Bähler, M. and P. Greengard (1987). "Synapsin I bundles F-actin in a phosphorylation-dependent manner." Nature **326**(6114): 704–707.
- Baldelli, P., A. Fassio, F. Valtorta and F. Benfenati (2007). "Lack of synapsin I reduces the readily releasable pool of synaptic vesicles at central inhibitory synapses." The Journal of neuroscience : the official journal of the Society for Neuroscience **27**(49): 13520–13531.
- Bartels, T., J. G. Choi and D. J. Selkoe (2011). " α -Synuclein occurs physiologically as a helically folded tetramer that resists aggregation." Nature **477**(7362): 107–110.
- Bartus, R. T., T. L. Baumann, J. Siffert, C. D. Herzog, R. Alterman, N. Boulis, D. A. Turner, M. Stacy, A. E. Lang, A. M. Lozano and C. W. Olanow (2013). "Safety/feasibility of targeting the substantia nigra with AAV2-neurturin in Parkinson patients." Neurology **80**(18): 1698–1701.
- Beach, T. G., C. H. Adler, L. I. Sue, L. Vedders, L. Lue, C. L. White Iii, H. Akiyama, J. N. Caviness, H. A. Shill, M. N. Sabbagh and D. G. Walker (2010). "Multi-organ distribution of phosphorylated alpha-synuclein histopathology in subjects with Lewy body disorders." Acta neuropathologica **119**(6): 689–702.

- Bellucci, A., A. Antonini, M. Pizzi and P. Spano (2017). "The End Is the Beginning: Parkinson's Disease in the Light of Brain Imaging." Frontiers in aging neuroscience **9**: 330.
- Bellucci, A., G. Collo, I. Sarnico, L. Battistin, C. Missale and P. Spano (2008). "Alpha-synuclein aggregation and cell death triggered by energy deprivation and dopamine overload are counteracted by D2/D3 receptor activation." Journal of neurochemistry **106**(2): 560–577.
- Bellucci, A., N. B. Mercuri, A. Venneri, G. Faustini, F. Longhena, M. Pizzi, C. Missale and P. Spano (2016). "Review: Parkinson's disease: from synaptic loss to connectome dysfunction." Neuropathology and applied neurobiology **42**(1): 77–94.
- Bellucci, A., L. Navarria, E. Falarti, M. Zaltieri, F. Bono, G. Collo, M. G. Spillantini, M. Grazia, C. Missale and P. Spano (2011). "Redistribution of DAT/ α -synuclein complexes visualized by "in situ" proximity ligation assay in transgenic mice modelling early Parkinson's disease." PloS one **6**(12): e27959.
- Benfenati, F., M. Böhler, R. Jahn and P. Greengard (1989). "Interactions of synapsin I with small synaptic vesicles: distinct sites in synapsin I bind to vesicle phospholipids and vesicle proteins." The Journal of cell biology **108**(5): 1863–1872.
- Benfenati, F., F. Valtorta, M. C. Rossi, F. Onofri, T. Sihra and P. Greengard (1993). "Interactions of synapsin I with phospholipids: possible role in synaptic vesicle clustering and in the maintenance of bilayer structures." The Journal of cell biology **123**(6 Pt 2): 1845–1855.
- Béraud, D., H. A. Hathaway, J. Trecki, S. Chasovskikh, D. A. Johnson, J. A. Johnson, H. J. Federoff, M. Shimoji, T. R. Mhyre and K. A. Maguire-Zeiss (2013). "Microglial Activation and Antioxidant Responses Induced by the Parkinson's Disease Protein α -Synuclein." Journal of Neuroimmune Pharmacology **8**(1): 94–117.
- Berg, D., J. Godau, C. Trenkwalder, K. Eggert, I. Csoti, A. Storch, H. Huber, M. Morelli-Canelo, M. Stamelou, V. Ries, M. Wolz, C. Schneider, T. Di Paolo, F. Gasparini, S. Hariry, M. Vandemeulebroecke, W. Abi-Saab, K. Cooke, D. Johns and B. Gomez-Mancilla (2011). "AFQ056 treatment of levodopa-induced dyskinesias: results of 2 randomized controlled trials." Movement disorders : official journal of the Movement Disorder Society **26**(7): 1243–1250.
- Beuming, T., J. Kniazeff, M. L. Bergmann, L. Shi, L. Gracia, K. Raniszewska, A. H. Newman, J. A. Javitch, H. Weinstein, U. Gether and C. J. Loland (2008). "The binding sites for cocaine and dopamine in the dopamine transporter overlap." Nature neuroscience **11**(7): 780–789.
- Bhatt, M. A., A. Messer and J. H. Kordower (2013). "Can intrabodies serve as neuroprotective therapies for Parkinson's disease? Beginning thoughts." Journal of Parkinson's disease **3**(4): 581–591.
- Blandini, F., G. Nappi, C. Tassorelli and E. Martignoni (2000). "Functional changes of the basal ganglia circuitry in Parkinson's disease." Progress in neurobiology **62**(1): 63–88.
- Blits, B. and H. Petry (2016). "Perspective on the Road toward Gene Therapy for Parkinson's Disease." Frontiers in neuroanatomy **10**: 128.
- Bodner, C. R., A. S. Maltsev, C. M. Dobson and A. Bax (2010). "Differential phospholipid binding of alpha-synuclein variants implicated in Parkinson's disease revealed by solution NMR spectroscopy." Biochemistry **49**(5): 862–871.
- Bollmann, J. H., B. Sakmann and J. G. Borst (2000). "Calcium sensitivity of glutamate release in a calyx-type terminal." Science (New York, N.Y.) **289**(5481): 953–957.
- Bonanomi, D., A. Menegon, A. Miccio, G. Ferrari, A. Corradi, H.-T. Kao, F. Benfenati and F. Valtorta (2005). "Phosphorylation of synapsin I by cAMP-dependent protein kinase controls synaptic vesicle dynamics in developing neurons." The Journal of neuroscience : the official journal of the Society for Neuroscience **25**(32): 7299–7308.
- Braak, H., K. Del Tredici, U. Rüb, R. A. I. d. Vos, E. N. H. Jansen Steur and E. Braak (2003). "Staging of brain pathology related to sporadic Parkinson's disease." Neurobiology of aging **24**(2): 197–211.
- Braak, H., R. A. I. d. Vos, J. Bohl and K. Del Tredici (2006). "Gastric alpha-synuclein immunoreactive inclusions in Meissner's and Auerbach's plexuses in cases staged for Parkinson's disease-related brain pathology." Neuroscience letters **396**(1): 67–72.
- Brundin, P., K. D. Dave and J. H. Kordower (2017). "Therapeutic approaches to target alpha-synuclein pathology." Experimental neurology **298**(Pt B): 225–235.

- Burré, J., M. Sharma, T. Tsetsenis, V. Buchman, M. R. Etherton and T. C. Südhof (2010). "Alpha-synuclein promotes SNARE-complex assembly in vivo and in vitro." Science (New York, N.Y.) **329**(5999): 1663–1667.
- Caccia, C., R. Maj, M. Calabresi, S. Maestroni, L. Faravelli, L. Curatolo, P. Salvati and R. G. Fariello (2006). "Safinamide: from molecular targets to a new anti-Parkinson drug." Neurology **67**(7 Suppl 2): S18-23.
- Carnwath, T., R. Mohammed and D. Tsiang (2018). "The direct and indirect effects of α -synuclein on microtubule stability in the pathogenesis of Parkinson's disease." Neuropsychiatric disease and treatment **14**: 1685–1695.
- Cha, J. H., M.-F. Zou, E. M. Adkins, S. G. F. Rasmussen, C. J. Loland, B. Schoenenberger, U. Gether and A. H. Newman (2005). "Rhodamine-labeled 2beta-carbomethoxy-3beta-(3,4-dichlorophenyl)tropane analogues as high-affinity fluorescent probes for the dopamine transporter." Journal of medicinal chemistry **48**(24): 7513–7516.
- Chadchankar, H., J. Ihalainen, H. Tanila and L. Yavich (2012). "Methylphenidate modifies overflow and presynaptic compartmentalization of dopamine via an α -synuclein-dependent mechanism." The Journal of pharmacology and experimental therapeutics **341**(2): 484–492.
- Chandra, S., F. Fornai, H.-B. Kwon, U. Yazdani, D. Atasoy, X. Liu, R. E. Hammer, G. Battaglia, D. C. German, P. E. Castillo and T. C. Südhof (2004). "Double-knockout mice for alpha- and beta-synucleins: effect on synaptic functions." Proceedings of the National Academy of Sciences of the United States of America **101**(41): 14966–14971.
- Chandra, S., G. Gallardo, R. Fernández-Chacón, O. M. Schlüter and T. C. Südhof (2005). "Alpha-synuclein cooperates with CSPalpha in preventing neurodegeneration." Cell **123**(3): 383–396.
- Chartier-Harlin, M.-C., J. Kachergus, C. Roumier, V. Mouroux, X. Douay, S. Lincoln, C. Levecque, L. Larvor, J. Andrieux, M. Hulihan, N. Waucquier, L. Defebvre, P. Amouyel, M. Farrer and A. Destée (2004). " α -synuclein locus duplication as a cause of familial Parkinson's disease." The Lancet **364**(9440): 1167–1169.
- Charvin, D., T. Di Paolo, E. Bezard, L. Gregoire, A. Takano, G. Duvey, E. Pioli, C. Halldin, R. Medori and F. Conquet (2018). "An mGlu4-Positive Allosteric Modulator Alleviates Parkinsonism in Primates." Movement disorders : official journal of the Movement Disorder Society **33**(10): 1619–1631.
- Chatterjee, D., M. Bhatt, D. Butler, E. d. Genst, C. M. Dobson, A. Messer and J. H. Kordower (2018). "Proteasome-targeted nanobodies alleviate pathology and functional decline in an α -synuclein-based Parkinson's disease model." npj Parkinson's Disease **4**(1): 25.
- Chaudhuri, K. R. and A. H. V. Schapira (2009). "Non-motor symptoms of Parkinson's disease: dopaminergic pathophysiology and treatment." The Lancet Neurology **8**(5): 464–474.
- Cheetham, J. J., S. Hilfiker, F. Benfenati, T. Weber, P. Greengard and A. J. Czernik (2001). "Identification of synapsin I peptides that insert into lipid membranes." The Biochemical journal **354**(Pt 1): 57–66.
- Cheetham, J. J., J. Murray, M. Ruhkalova, L. Cuccia, R. McAloney, K. U. Ingold and L. J. Johnston (2003). "Interaction of synapsin I with membranes." Biochemical and biophysical research communications **309**(4): 823–829.
- Chen, Y.-H., B. K. Harvey, A. F. Hoffman, Y. Wang, Y.-H. Chiang and C. R. Lupica (2008). "MPTP-induced deficits in striatal synaptic plasticity are prevented by glial cell line-derived neurotrophic factor expressed via an adeno-associated viral vector." FASEB journal : official publication of the Federation of American Societies for Experimental Biology **22**(1): 261–275.
- Chen, Y. A. and R. H. Scheller (2001). "SNARE-mediated membrane fusion." Nature Reviews Molecular Cell Biology **2**(2): 98–106.
- Cheng, H.-C., C. M. Ulane and R. E. Burke (2010). "Clinical progression in Parkinson disease and the neurobiology of axons." Annals of neurology **67**(6): 715–725.
- Cheng, Y.-C. and W. H. Prusoff (1973). "Relationship between the inhibition constant (KI) and the concentration of inhibitor which causes 50 per cent inhibition (I50) of an enzymatic reaction." Biochemical Pharmacology **22**(23): 3099–3108.

- Chi, P., P. Greengard and T. A. Ryan (2003). "Synaptic Vesicle Mobilization Is Regulated by Distinct Synapsin I Phosphorylation Pathways at Different Frequencies." Neuron **38**(1): 69–78.
- Chin, L. S., L. Li, A. Ferreira, K. S. Kosik and P. Greengard (1995). "Impairment of axonal development and of synaptogenesis in hippocampal neurons of synapsin I-deficient mice." Proceedings of the National Academy of Sciences of the United States of America **92**(20): 9230–9234.
- Choi, B.-K., M.-G. Choi, J.-Y. Kim, Y. Yang, Y. Lai, D.-H. Kweon, N. K. Lee and Y.-K. Shin (2013). "Large α -synuclein oligomers inhibit neuronal SNARE-mediated vesicle docking." Proceedings of the National Academy of Sciences of the United States of America **110**(10): 4087–4092.
- Christine, C. W., P. A. Starr, P. S. Larson, J. L. Eberling, W. J. Jagust, R. A. Hawkins, H. F. VanBrocklin, J. F. Wright, K. S. Bankiewicz and M. J. Aminoff (2009). "Safety and tolerability of putaminal AADC gene therapy for Parkinson disease." Neurology **73**(20): 1662–1669.
- Cingolani, L. A. and Y. Goda (2008). "Actin in action: the interplay between the actin cytoskeleton and synaptic efficacy." Nature reviews. Neuroscience **9**(5): 344–356.
- Clayton, D. F. and J. M. George (1998). "The synucleins: a family of proteins involved in synaptic function, plasticity, neurodegeneration and disease." Trends in Neurosciences **21**(6): 249–254.
- Cole, J. C., B. R. Villa and R. S. Wilkinson (2000). "Disruption of actin impedes transmitter release in snake motor terminals." The Journal of physiology **525 Pt 3**: 579–586.
- Connolly, B. S. and A. E. Lang (2014). "Pharmacological treatment of Parkinson disease: a review." JAMA **311**(16): 1670–1683.
- Conway, K. A., J. C. Rochet, R. M. Bieganski and P. T. Lansbury (2001). "Kinetic stabilization of the alpha-synuclein protofibril by a dopamine-alpha-synuclein adduct." Science (New York, N.Y.) **294**(5545): 1346–1349.
- Cremades, N., S. I. A. Cohen, E. Deas, A. Y. Abramov, A. Y. Chen, A. Orte, M. Sandal, R. W. Clarke, P. Dunne, F. A. Aprile, C. W. Bertocini, N. W. Wood, T. P. J. Knowles, C. M. Dobson and D. Klenerman (2012). "Direct observation of the interconversion of normal and toxic forms of α -synuclein." Cell **149**(5): 1048–1059.
- Crowther, R. A., R. Jakes, M. G. Spillantini and M. Goedert (1998). "Synthetic filaments assembled from C-terminally truncated α -synuclein." FEBS Letters **436**(3): 309–312.
- Danzer, K. M., D. Haasen, A. R. Karow, S. Moussaud, M. Habeck, A. Giese, H. Kretschmar, B. Hengerer and M. Kostka (2007). "Different species of alpha-synuclein oligomers induce calcium influx and seeding." The Journal of neuroscience : the official journal of the Society for Neuroscience **27**(34): 9220–9232.
- Danzer, K. M., L. R. Kranich, W. P. Ruf, O. Cagsal-Getkin, A. R. Winslow, L. Zhu, C. R. Vanderburg and P. J. McLean (2012). "Exosomal cell-to-cell transmission of alpha synuclein oligomers." Molecular neurodegeneration **7**: 42.
- Davidson, W. S., A. Jonas, D. F. Clayton and J. M. George (1998). "Stabilization of alpha-synuclein secondary structure upon binding to synthetic membranes." The Journal of biological chemistry **273**(16): 9443–9449.
- Davies, H. M. L., D. W. Hopper, T. Hansen, Q. Liu and S. R. Childers (2004). "Synthesis of methylphenidate analogues and their binding affinities at dopamine and serotonin transport sites." Bioorganic & medicinal chemistry letters **14**(7): 1799–1802.
- Day, R. N. and M. W. Davidson (2009). "The fluorescent protein palette: tools for cellular imaging." Chemical Society reviews **38**(10): 2887–2921.
- Del Tredici, K., C. H. Hawkes, E. Ghebremedhin and H. Braak (2010). "Lewy pathology in the submandibular gland of individuals with incidental Lewy body disease and sporadic Parkinson's disease." Acta neuropathologica **119**(6): 703–713.
- Del Tredici, K., U. Rüb, R. A. I. d. Vos, J. R. E. Bohl and H. Braak (2002). "Where does parkinson disease pathology begin in the brain?" Journal of neuropathology and experimental neurology **61**(5): 413–426.
- Dent, E. W. and K. Kalil (2001). "Axon Branching Requires Interactions between Dynamic Microtubules and Actin Filaments." The Journal of Neuroscience **21**(24): 9757–9769.

- Desplats, P., H.-J. Lee, E.-J. Bae, C. Patrick, E. Rockenstein, L. Crews, B. Spencer, E. Masliah and S.-J. Lee (2009). "Inclusion formation and neuronal cell death through neuron-to-neuron transmission of alpha-synuclein." Proceedings of the National Academy of Sciences of the United States of America **106**(31): 13010–13015.
- Deutsch, H., X. Ye, Q. Shi, Z. Liu and M. M. Schweri (2001). "Synthesis and pharmacology of site specific cocaine abuse treatment agents: a new synthetic methodology for methylphenidate analogs based on the Blaise reaction." European Journal of Medicinal Chemistry **36**(4): 303–311.
- Deutsch, H. M., Q. Shi, E. Gruszecka-Kowalik and M. M. Schweri (1996). "Synthesis and Pharmacology of Potential Cocaine Antagonists. 2. Structure–Activity Relationship Studies of Aromatic Ring-Substituted Methylphenidate Analogs." Journal of Medicinal Chemistry **39**(6): 1201-1209.
- Dev, K., K. Hofele, S. Barbieri, B. V. L. and H. van der Putten (2003). "Part II: α -synuclein and its molecular pathophysiological role in neurodegenerative disease." Neuropharmacology **45**(1): 14–44.
- Devos, D., C. Moreau, J. C. Devedjian, J. Kluza, M. Petrault, C. Laloux, A. Jonneaux, G. Ryckewaert, G. Garçon, N. Rouaix, A. Duhamel, P. Jissendi, K. Dujardin, F. Auger, L. Ravasi, L. Hopes, G. Grolez, W. Firdaus, B. Sablonnière, I. Strubi-Vuillaume, N. Zahr, A. Destée, J.-C. Corvol, D. Pörtl, M. Leist, C. Rose, L. Defebvre, P. Marchetti, Z. I. Cabantchik and R. Bordet (2014). "Targeting chelatable iron as a therapeutic modality in Parkinson's disease." Antioxidants & redox signaling **21**(2): 195–210.
- Di Maio, R., E. K. Hoffman, E. M. Rocha, M. T. Keeney, L. H. Sanders, B. R. d. Miranda, A. Zharikov, A. van Laar, A. F. Stepan, T. A. Lanz, J. K. Kofler, E. A. Burton, D. R. Alessi, T. G. Hastings and J. T. Greenamyre (2018). "LRRK2 activation in idiopathic Parkinson's disease." Science translational medicine **10**(451).
- Di Rienzo, C., E. Gratton, F. Beltram and F. Cardarelli (2013). "Fast spatiotemporal correlation spectroscopy to determine protein lateral diffusion laws in live cell membranes." Proceedings of the National Academy of Sciences of the United States of America **110**(30): 12307–12312.
- Dorsey, E. R., A. Elbaz, E. Nichols, F. Abd-Allah, A. Abdelalim, J. C. Adsuar, M. G. Ansha, C. Brayne, J.-Y. J. Choi, D. Collado-Mateo, N. Dahodwala, H. P. Do, D. Edessa, M. Endres, S.-M. Fereshtehnejad, K. J. Foreman, F. G. Gankpe, R. Gupta, G. J. Hankey, S. I. Hay, M. I. Hegazy, D. T. Hibstu, A. Kasaeian, Y. Khader, I. Khalil, Y.-H. Khang, Y. J. Kim, Y. Kokubo, G. Logroscino, J. Massano, N. Mohamed Ibrahim, M. A. Mohammed, A. Mohammadi, M. Moradi-Lakeh, M. Naghavi, B. T. Nguyen, Y. L. Nirayo, F. A. Ogbo, M. O. Owolabi, D. M. Pereira, M. J. Postma, M. Qorbani, M. A. Rahman, K. T. Roba, H. Safari, S. Safiri, M. Satpathy, M. Sawhney, A. Shafieesabet, M. S. Shiferaw, M. Smith, C. E. I. Szoeki, R. Tabarés-Seisdedos, N. T. Truong, K. N. Ukwaja, N. Venketasubramanian, S. Villafaina, K. g. weldegwergs, R. Westerman, T. Wijeratne, A. S. Winkler, B. T. Xuan, N. Yonemoto, V. L. Feigin, T. Vos and C. J. L. Murray (2018). "Global, regional, and national burden of Parkinson's disease, 1990–2016: a systematic analysis for the Global Burden of Disease Study 2016." The Lancet Neurology **17**(11): 939–953.
- Dresbach, T., B. Qualmann, M. M. Kessels, C. C. Garner and E. D. Gundelfinger (2001). "The presynaptic cytomatrix of brain synapses." Cellular and molecular life sciences : CMLS **58**(1): 94–116.
- Du, H.-N., L. Tang, X.-Y. Luo, H.-T. Li, J. Hu, J.-W. Zhou and H.-Y. Hu (2003). "A peptide motif consisting of glycine, alanine, and valine is required for the fibrillization and cytotoxicity of human alpha-synuclein." Biochemistry **42**(29): 8870–8878.
- Eberling, J. L., A. P. Kells, P. Pivrotto, J. Beyer, J. Bringas, H. J. Federoff, J. Forsayeth and K. S. Bankiewicz (2009). "Functional effects of AAV2-GDNF on the dopaminergic nigrostriatal pathway in parkinsonian rhesus monkeys." Human gene therapy **20**(5): 511–518.
- Eildal, J. N. N., J. Andersen, A. S. Kristensen, A. M. Jørgensen, B. Bang-Andersen, M. Jørgensen and K. Strømgaard (2008). "From the selective serotonin transporter inhibitor citalopram to the selective norepinephrine transporter inhibitor talopram: synthesis and structure-activity relationship studies." Journal of medicinal chemistry **51**(10): 3045–3048.
- el-Agnaf, O. M. A. and G. B. Irvine (2002). "Aggregation and neurotoxicity of alpha-synuclein and related peptides." Biochemical Society transactions **30**(4): 559–565.
- Eliezer, D., E. Kutluay, R. Bussell and G. Browne (2001). "Conformational properties of alpha-synuclein in its free and lipid-associated states." Journal of molecular biology **307**(4): 1061–1073.

- Engelender, S. and O. Isacson (2017). "The Threshold Theory for Parkinson's Disease." Trends in neurosciences **40**(1): 4–14.
- Eriksen, J., W. E. Bjørn-Yoshimoto, T. N. Jørgensen, A. H. Newman and U. Gether (2010). "Postendocytic sorting of constitutively internalized dopamine transporter in cell lines and dopaminergic neurons." The Journal of biological chemistry **285**(35): 27289–27301.
- Eriksen, J., S. G. F. Rasmussen, T. N. Rasmussen, C. B. Vaegter, J. H. Cha, M.-F. Zou, A. H. Newman and U. Gether (2009). "Visualization of dopamine transporter trafficking in live neurons by use of fluorescent cocaine analogs." The Journal of neuroscience : the official journal of the Society for Neuroscience **29**(21): 6794–6808.
- Ettinger, A. and T. Wittmann (2014). "Fluorescence live cell imaging." Methods in cell biology **123**: 77–94.
- Fahn, S., D. Oakes, I. Shoulson, K. Kieburts, A. Rudolph, A. Lang, C. W. Olanow, C. Tanner and K. Marek (2004). "Levodopa and the progression of Parkinson's disease." The New England journal of medicine **351**(24): 2498–2508.
- Faustini, G., F. Bono, A. Valerio, M. Pizzi, P. Spano and A. Bellucci (2017). "Mitochondria and α -Synuclein: Friends or Foes in the Pathogenesis of Parkinson's Disease?" Genes **8**(12).
- Faustini, G., F. Longhena, A. Bruno, F. Bono, J. Grigoletto, L. La Via, A. Barbon, A. Casiraghi, V. Straniero, E. Valoti, G. Costantino, F. Benfenati, C. Missale, M. Pizzi, M. G. Spillantini and A. Bellucci (2019). "Alpha-synuclein/synapsin III pathological interplay boosts the motor response to methylphenidate."
- Faustini, G., F. Longhena, T. Varanita, L. Bubacco, M. Pizzi, C. Missale, F. Benfenati, A. Björklund, P. Spano and A. Bellucci (2018). "Synapsin III deficiency hampers α -synuclein aggregation, striatal synaptic damage and nigral cell loss in an AAV-based mouse model of Parkinson's disease." Acta neuropathologica **136**(4): 621–639.
- Feng, J., P. Chi, T. A. Blanpied, Y. Xu, A. M. Magarinos, A. Ferreira, R. H. Takahashi, H.-T. Kao, B. S. McEwen, T. A. Ryan, G. J. Augustine and P. Greengard (2002). "Regulation of Neurotransmitter Release by Synapsin III." The Journal of Neuroscience **22**(11): 4372–4380.
- Ferreira, A., L. S. Chin, L. Li, L. M. Lanier, K. S. Kosik and P. Greengard (1998). "Distinct roles of synapsin I and synapsin II during neuronal development." Molecular medicine (Cambridge, Mass.) **4**(1): 22–28.
- Ferreira, A., H.-T. Kao, J. Feng, M. Rapoport and P. Greengard (2000). "Synapsin III: Developmental Expression, Subcellular Localization, and Role in Axon Formation." The Journal of Neuroscience **20**(10): 3736–3744.
- Ferreira, A., K. S. Kosik, P. Greengard and H. Q. Han (1994). "Aberrant neurites and synaptic vesicle protein deficiency in synapsin II-depleted neurons." Science (New York, N.Y.) **264**(5161): 977–979.
- Follett, K. A., F. M. Weaver, M. Stern, K. Hur, C. L. Harris, P. Luo, W. J. Marks, J. Rothlind, O. Sagher, C. Moy, R. Pahwa, K. Burchiel, P. Hogarth, E. C. Lai, J. E. Duda, K. Holloway, A. Samii, S. Horn, J. M. Bronstein, G. Stoner, P. A. Starr, R. Simpson, G. Baltuch, A. d. Salles, G. D. Huang and D. J. Reda (2010). "Pallidal versus subthalamic deep-brain stimulation for Parkinson's disease." The New England journal of medicine **362**(22): 2077–2091.
- Font, B. and E. Aubert-Foucher (1989). "Detection by chemical cross-linking of bovine brain synapsin I self-association." The Biochemical journal **264**(3): 893–899.
- Forno, L. S. (1996). "Neuropathology of Parkinson's disease." Journal of neuropathology and experimental neurology **55**(3): 259–272.
- Fox, S. H., R. Katzenschlager, S.-Y. Lim, B. Ravina, K. Seppi, M. Coelho, W. Poewe, O. Rascol, C. G. Goetz and C. Sampaio (2011). "The Movement Disorder Society Evidence-Based Medicine Review Update: Treatments for the motor symptoms of Parkinson's disease." Movement disorders : official journal of the Movement Disorder Society **26 Suppl 3**: S2-41.
- Froimowitz, M., Y. Gu, L. A. Dakin, C. J. Kelley, D. Parrish and J. R. Deschamps (2005). "Vinyllogous amide analogs of methylphenidate." Bioorganic & medicinal chemistry letters **15**(12): 3044–3047.

- Froimowitz, M., Y. Gu, L. A. Dakin, P. M. Nagafuji, C. J. Kelley, D. Parrish, J. R. Deschamps and A. Janowsky (2007). "Slow-onset, long-duration, alkyl analogues of methylphenidate with enhanced selectivity for the dopamine transporter." Journal of medicinal chemistry **50**(2): 219–232.
- Fujiwara, H., M. Hasegawa, N. Dohmae, A. Kawashima, E. Masliah, M. S. Goldberg, J. Shen, K. Takio and T. Iwatsubo (2002). "alpha-Synuclein is phosphorylated in synucleinopathy lesions." Nature cell biology **4**(2): 160–164.
- Fujiwara, H., M. Hasegawa, N. Dohmae, A. Kawashima, E. Masliah, M. S. Goldberg, J. Shen, K. Takio and T. Iwatsubo (2002). "α-Synuclein is phosphorylated in synucleinopathy lesions." Nature Cell Biology **4**(2): 160–164.
- Gao, H.-M., P. T. Kotzbauer, K. Uryu, S. Leight, J. Q. Trojanowski and V. M.-Y. Lee (2008). "Neuroinflammation and oxidation/nitration of alpha-synuclein linked to dopaminergic neurodegeneration." The Journal of neuroscience : the official journal of the Society for Neuroscience **28**(30): 7687–7698.
- Garcia-Reitböck, P., O. Anichtchik, A. Bellucci, M. Iovino, C. Ballini, E. Fineberg, B. Ghetti, L. Della Corte, P. Spano, G. K. Tofaris, M. Goedert and M. G. Spillantini (2010). "SNARE protein redistribution and synaptic failure in a transgenic mouse model of Parkinson's disease." Brain : a journal of neurology **133**(Pt 7): 2032–2044.
- Gatley, S. J., D. Pan, R. Chen, G. Chaturvedi and Y.-S. Ding (1996). "Affinities of methylphenidate derivatives for dopamine, norepinephrine and serotonin transporters." Life Sciences **58**(12): PL231-PL239.
- Gaugler, M. N., O. Genc, W. Bobela, S. Mohanna, M. T. Ardah, O. M. El-Agnaf, M. Cantoni, J.-C. Bensadoun, R. Schneggenburger, G. W. Knott, P. Aebischer and B. L. Schneider (2012). "Nigrostriatal overabundance of α-synuclein leads to decreased vesicle density and deficits in dopamine release that correlate with reduced motor activity." Acta neuropathologica **123**(5): 653–669.
- Gautier, A., A. Juillerat, C. Heinis, I. R. Corrêa, M. Kindermann, F. Beaufils and K. Johnsson (2008). "An engineered protein tag for multiprotein labeling in living cells." Chemistry & biology **15**(2): 128–136.
- George, S. and P. Brundin (2015). "Immunotherapy in Parkinson's Disease: Micromanaging Alpha-Synuclein Aggregation." Journal of Parkinson's disease **5**(3): 413–424.
- Giasson, B. I., J. E. Duda, I. V. J. Murray, Q. Chen, J. M. Souza, H. I. Hurtig, H. Ischiropoulos, J. Q. Trojanowski and V. M. Y. Lee (2000). "Oxidative Damage Linked to Neurodegeneration by Selective α-Synuclein Nitration in Synucleinopathy Lesions." Science **290**(5493): 985.
- Giasson, B. I., I. V. Murray, J. Q. Trojanowski and V. M. Lee (2001). "A hydrophobic stretch of 12 amino acid residues in the middle of alpha-synuclein is essential for filament assembly." The Journal of biological chemistry **276**(4): 2380–2386.
- Gibbons, C. H., J. Garcia, N. Wang, L. C. Shih and R. Freeman (2016). "The diagnostic discrimination of cutaneous α-synuclein deposition in Parkinson disease." Neurology **87**(5): 505–512.
- Gitler, A. D., B. J. Bevis, J. Shorter, K. E. Strathearn, S. Hamamichi, L. J. Su, K. A. Caldwell, G. A. Caldwell, J.-C. Rochet, J. M. McCaffery, C. Barlowe and S. Lindquist (2008). "The Parkinson's disease protein alpha-synuclein disrupts cellular Rab homeostasis." Proceedings of the National Academy of Sciences of the United States of America **105**(1): 145–150.
- Gitler, D., Q. Cheng, P. Greengard and G. J. Augustine (2008). "Synapsin IIa controls the reserve pool of glutamatergic synaptic vesicles." The Journal of neuroscience : the official journal of the Society for Neuroscience **28**(43): 10835–10843.
- Gitler, D., Y. Takagishi, J. Feng, Y. Ren, R. M. Rodriguiz, W. C. Wetsel, P. Greengard and G. J. Augustine (2004). "Different presynaptic roles of synapsins at excitatory and inhibitory synapses." The Journal of neuroscience : the official journal of the Society for Neuroscience **24**(50): 11368–11380.
- Gitler, D., Y. Xu, H.-T. Kao, D. Lin, S. Lim, J. Feng, P. Greengard and G. J. Augustine (2004). "Molecular determinants of synapsin targeting to presynaptic terminals." The Journal of neuroscience : the official journal of the Society for Neuroscience **24**(14): 3711–3720.
- Goedert, M., R. Jakes and M. G. Spillantini (2017). "The Synucleinopathies: Twenty Years On." Journal of Parkinson's disease **7**(s1): S51-S69.

- Goldman, S. M. (2014). "Environmental toxins and Parkinson's disease." Annual review of pharmacology and toxicology **54**: 141–164.
- Gould, N., D. E. Mor, R. Lightfoot, K. Malkus, B. Giasson and H. Ischiropoulos (2014). "Evidence of native α -synuclein conformers in the human brain." The Journal of biological chemistry **289**(11): 7929–7934.
- Greengard, P., F. Valtorta, A. J. Czernik and F. Benfenati (1993). "Synaptic vesicle phosphoproteins and regulation of synaptic function." Science (New York, N.Y.) **259**(5096): 780–785.
- Grégoire, L., N. Morin, B. Ouattara, F. Gasparini, G. Bilbe, D. Johns, I. Vranesic, S. Sahasranaman, B. Gomez-Mancilla and T. Di Paolo (2011). "The acute antiparkinsonian and antidyskinetic effect of AFQ056, a novel metabotropic glutamate receptor type 5 antagonist, in L-Dopa-treated parkinsonian monkeys." Parkinsonism & related disorders **17**(4): 270–276.
- Grimm, J. B., A. K. Muthusamy, Y. Liang, T. A. Brown, W. C. Lemon, R. Patel, R. Lu, J. J. Macklin, P. J. Keller, N. Ji and L. D. Lavis (2017). "A general method to fine-tune fluorophores for live-cell and in vivo imaging." Nature methods **14**(10): 987–994.
- Grouleff, J., L. K. Ladefoged, H. Koldsø and B. Schiøtt (2015). "Monoamine transporters: insights from molecular dynamics simulations." Frontiers in pharmacology **6**: 235.
- Gu, H., S. C. Wall and G. Rudnick (1994). "Stable expression of biogenic amine transporters reveals differences in inhibitor sensitivity, kinetics, and ion dependence." The Journal of biological chemistry **269**(10): 7124–7130.
- Gurry, T., O. Ullman, C. K. Fisher, I. Perovic, T. Pochapsky and C. M. Stultz (2013). "The dynamic structure of α -synuclein multimers." Journal of the American Chemical Society **135**(10): 3865–3872.
- Hansen, C., E. Angot, A.-L. Bergström, J. A. Steiner, L. Pieri, G. Paul, T. F. Outeiro, R. Melki, P. Kallunki, K. Fog, J.-Y. Li and P. Brundin (2011). " α -Synuclein propagates from mouse brain to grafted dopaminergic neurons and seeds aggregation in cultured human cells." The Journal of Clinical Investigation **121**(2): 715–725.
- Herrera, F. E., A. Chesi, K. E. Paleologou, A. Schmid, A. Munoz, M. Vendruscolo, S. Gustincich, H. A. Lashuel and P. Carloni (2008). "Inhibition of alpha-synuclein fibrillization by dopamine is mediated by interactions with five C-terminal residues and with E83 in the NAC region." PloS one **3**(10): e3394.
- Hilfiker, S., V. A. Pieribone, A. J. Czernik, H. T. Kao, G. J. Augustine and P. Greengard (1999). "Synapsins as regulators of neurotransmitter release." Philosophical transactions of the Royal Society of London. Series B, Biological sciences **354**(1381): 269–279.
- Hirokawa, N., K. Sobue, K. Kanda, A. Harada and H. Yorifuji (1989). "The cytoskeletal architecture of the presynaptic terminal and molecular structure of synapsin 1." The Journal of cell biology **108**(1): 111–126.
- Holmes, B. B., S. L. DeVos, N. Kfoury, M. Li, R. Jacks, K. Yanamandra, M. O. Ouidja, F. M. Brodsky, J. Marasa, D. P. Bagchi, P. T. Kotzbauer, T. M. Miller, D. Papy-Garcia and M. I. Diamond (2013). "Heparan sulfate proteoglycans mediate internalization and propagation of specific proteopathic seeds." Proceedings of the National Academy of Sciences of the United States of America **110**(33): E3138–3147.
- Hosaka, M., R. E. Hammer and T. C. Südhof (1999). "A Phospho-Switch Controls the Dynamic Association of Synapsins with Synaptic Vesicles." Neuron **24**(2): 377–387.
- Hosaka, M. and T. C. Südhof (1998). "Synapsin III, a novel synapsin with an unusual regulation by Ca²⁺." The Journal of biological chemistry **273**(22): 13371–13374.
- Hosaka, M. and T. C. Südhof (1999). "Homo- and heterodimerization of synapsins." The Journal of biological chemistry **274**(24): 16747–16753.
- Huang, B., M. Bates and X. Zhuang (2009). "Super-resolution fluorescence microscopy." Annual review of biochemistry **78**: 993–1016.
- Illes-Toth, E., M. R. Ramos, R. Cappai, C. Dalton and D. P. Smith (2015). "Distinct higher-order α -synuclein oligomers induce intracellular aggregation." The Biochemical journal **468**(3): 485–493.

- Iwanaga, K., K. Wakabayashi, M. Yoshimoto, I. Tomita, H. Satoh, H. Takashima, A. Satoh, M. Seto, M. Tsujihata and H. Takahashi (1999). "Lewy body-type degeneration in cardiac plexus in Parkinson's and incidental Lewy body diseases." Neurology **52**(6): 1269–1271.
- Jahn, R., T. Lang and T. C. Südhof (2003). "Membrane Fusion." Cell **112**(4): 519–533.
- Jankovic, J., I. Goodman, B. Safirstein, T. K. Marmon, D. B. Schenk, M. Koller, W. Zago, D. K. Ness, S. G. Griffith, M. Grundman, J. Soto, S. Ostrowitzki, F. G. Boess, M. Martin-Facklam, J. F. Quinn, S. H. Isaacson, O. Omidvar, A. Ellenbogen and G. G. Kinney (2018). "Safety and Tolerability of Multiple Ascending Doses of PRX002/RG7935, an Anti- α -Synuclein Monoclonal Antibody, in Patients With Parkinson Disease: A Randomized Clinical Trial." JAMA neurology **75**(10): 1206–1214.
- Jensen, P. H., J. Y. Li, A. Dahlström and C. G. Dotti (1999). "Axonal transport of synucleins is mediated by all rate components." The European journal of neuroscience **11**(10): 3369–3376.
- Jensen, P. H., M. S. Nielsen, R. Jakes, C. G. Dotti and M. Goedert (1998). "Binding of alpha-synuclein to brain vesicles is abolished by familial Parkinson's disease mutation." The Journal of biological chemistry **273**(41): 26292–26294.
- Jess, U., H. Betz and P. Schloss (1996). "The membrane-bound rat serotonin transporter, SERT1, is an oligomeric protein." FEBS Letters **394**(1): 44–46.
- Jovanovic, J. N., F. Benfenati, Y. L. Siow, T. S. Sihra, J. S. Sanghera, S. L. Pelech, P. Greengard and A. J. Czernik (1996). "Neurotrophins stimulate phosphorylation of synapsin I by MAP kinase and regulate synapsin I-actin interactions." Proceedings of the National Academy of Sciences of the United States of America **93**(8): 3679–3683.
- Kahle, P. J., M. Neumann, L. Ozmen, V. Müller, H. Jacobsen, A. Schindzielorz, M. Okochi, U. Leimer, H. van der Putten, A. Probst, E. Kremmer, H. A. Kretzschmar and C. Haass (2000). "Subcellular Localization of Wild-Type and Parkinson's Disease-Associated Mutant α -Synuclein in Human and Transgenic Mouse Brain." The Journal of Neuroscience **20**(17): 6365–6373.
- Kao, H.-T., P. Li, H. M. Chao, S. Janoschka, K. Pham, J. Feng, B. S. McEwen, P. Greengard, V. A. Pieribone and B. Porton (2008). "Early involvement of synapsin III in neural progenitor cell development in the adult hippocampus." The Journal of comparative neurology **507**(6): 1860–1870.
- Kao, H. T., B. Porton, A. J. Czernik, J. Feng, G. Yiu, M. Häring, F. Benfenati and P. Greengard (1998). "A third member of the synapsin gene family." Proceedings of the National Academy of Sciences of the United States of America **95**(8): 4667–4672.
- Kaur, D., F. Yantiri, S. Rajagopalan, J. Kumar, J. Q. Mo, R. Boonplueang, V. Viswanath, R. Jacobs, L. Yang, M. F. Beal, D. DiMonte, I. Volitaskis, L. Ellerby, R. A. Cherny, A. I. Bush and J. K. Andersen (2003). "Genetic or Pharmacological Iron Chelation Prevents MPTP-Induced Neurotoxicity In Vivo." Neuron **37**(6): 899–909.
- Kells, A. P., J. Eberling, X. Su, P. Pivrotto, J. Bringas, P. Hadaczek, W. C. Narrow, W. J. Bowers, H. J. Federoff, J. Forsayeth and K. S. Bankiewicz (2010). "Regeneration of the MPTP-lesioned dopaminergic system after convection-enhanced delivery of AAV2-GDNF." The Journal of neuroscience : the official journal of the Society for Neuroscience **30**(28): 9567–9577.
- Keppler, A., S. Gendreau, T. Gronemeyer, H. Pick, H. Vogel and K. Johnsson (2003). "A general method for the covalent labeling of fusion proteins with small molecules in vivo." Nature biotechnology **21**(1): 86–89.
- Kile, B. M., T. S. Guillot, B. J. Venton, W. C. Wetsel, G. J. Augustine and R. M. Wightman (2010). "Synapsins differentially control dopamine and serotonin release." The Journal of neuroscience : the official journal of the Society for Neuroscience **30**(29): 9762–9770.
- Kocabas, A. M., G. Rudnick and F. Kilic (2003). "Functional consequences of homo- but not hetero-oligomerization between transporters for the biogenic amine neurotransmitters." Journal of neurochemistry **85**(6): 1513–1520.
- Kondo, T. and Y. Mizuno (2015). "A long-term study of istradefylline safety and efficacy in patients with Parkinson disease." Clinical neuropharmacology **38**(2): 41–46.

- Kordower, J. H., Y. Chu, R. A. Hauser, T. B. Freeman and C. W. Olanow (2008). "Lewy body-like pathology in long-term embryonic nigral transplants in Parkinson's disease." Nature Medicine **14**: 504 EP -.
- Kordower, J. H., H. B. Dodiya, A. M. Kordower, B. Terpstra, K. Paumier, L. Madhavan, C. Sortwell, K. Steece-Collier and T. J. Collier (2011). "Transfer of host-derived α synuclein to grafted dopaminergic neurons in rat." Neurobiology of disease **43**(3): 552–557.
- Kordower, J. H., C. D. Herzog, B. Dass, R. A. E. Bakay, J. Stansell, M. Gasmi and R. T. Bartus (2006). "Delivery of neurturin by AAV2 (CERE-120)-mediated gene transfer provides structural and functional neuroprotection and neurorestoration in MPTP-treated monkeys." Annals of neurology **60**(6): 706–715.
- Kremers, G.-J., S. G. Gilbert, P. J. Cranfill, M. W. Davidson and D. W. Piston (2011). "Fluorescent proteins at a glance." Journal of Cell Science **124**(15): 2676.
- Krishnan, R., H. Tsubery, M. Y. Proschitsky, E. Asp, M. Lulu, S. Gilead, M. Gartner, J. P. Waltho, P. J. Davis, A. M. Hounslow, D. A. Kirschner, H. Inouye, D. G. Myszyka, J. Wright, B. Solomon and R. A. Fisher (2014). "A bacteriophage capsid protein provides a general amyloid interaction motif (GAIM) that binds and remodels misfolded protein assemblies." Journal of molecular biology **426**(13): 2500–2519.
- Kristensen, A. S., J. Andersen, T. N. Jørgensen, L. Sørensen, J. Eriksen, C. J. Loland, K. Strømgaard and U. Gether (2011). "SLC6 neurotransmitter transporters: structure, function, and regulation." Pharmacological reviews **63**(3): 585–640.
- Kumar, V., T. Rahbek-Clemmensen, C. B. Billesbølle, T. N. Jørgensen, U. Gether and A. H. Newman (2014). "Novel and high affinity fluorescent ligands for the serotonin transporter based on (s)-citalopram." ACS medicinal chemistry letters **5**(6): 696–699.
- Kurowska, Z., E. Englund, H. Widner, O. Lindvall, J.-Y. Li and P. Brundin (2011). "Signs of degeneration in 12-22-year old grafts of mesencephalic dopamine neurons in patients with Parkinson's disease." Journal of Parkinson's disease **1**(1): 83–92.
- Lai, Y., S. Kim, J. Varkey, X. Lou, J.-K. Song, J. Diao, R. Langen and Y.-K. Shin (2014). "Nonaggregated α -synuclein influences SNARE-dependent vesicle docking via membrane binding." Biochemistry **53**(24): 3889–3896.
- Lang, K. and J. W. Chin (2014). "Cellular incorporation of unnatural amino acids and bioorthogonal labeling of proteins." Chemical reviews **114**(9): 4764–4806.
- Lashuel, H. A., C. R. Overk, A. Oueslati and E. Masliah (2013). "The many faces of α -synuclein: from structure and toxicity to therapeutic target." Nature reviews. Neuroscience **14**(1): 38–48.
- Lee, S.-J., P. Desplats, H.-J. Lee, B. Spencer and E. Masliah (2012). "Cell-to-cell transmission of α -synuclein aggregates." Methods in molecular biology (Clifton, N.J.) **849**: 347–359.
- Lei, Z., Y. Jiang, T. Li, J. Zhu and S. Zeng (2011). "Signaling of glial cell line-derived neurotrophic factor and its receptor GFR α 1 induce Nurr1 and Pitx3 to promote survival of grafted midbrain-derived neural stem cells in a rat model of Parkinson disease." Journal of neuropathology and experimental neurology **70**(9): 736–747.
- LeWitt, P. A., A. R. Rezai, M. A. Leehey, S. G. Ojemann, A. W. Flaherty, E. N. Eskandar, S. K. Kostyk, K. Thomas, A. Sarkar, M. S. Siddiqui, S. B. Tatter, J. M. Schwalb, K. L. Poston, J. M. Henderson, R. M. Kurlan, I. H. Richard, L. van Meter, C. V. Sapan, M. J. Doring, M. G. Kaplitt and A. Feigin (2011). "AAV2-GAD gene therapy for advanced Parkinson's disease: a double-blind, sham-surgery controlled, randomised trial." The Lancet Neurology **10**(4): 309–319.
- Li, J.-Y., E. Englund, J. L. Holton, D. Soulet, P. Hagell, A. J. Lees, T. Lashley, N. P. Quinn, S. Rehncrona, A. Björklund, H. Widner, T. Revesz, O. Lindvall and P. Brundin (2008). "Lewy bodies in grafted neurons in subjects with Parkinson's disease suggest host-to-graft disease propagation." Nature Medicine **14**(5): 501–503.
- Li, L., L. S. Chin, O. Shupliakov, L. Brodin, T. S. Sihra, O. Hvalby, V. Jensen, D. Zheng, J. O. McNamara and P. Greengard (1995). "Impairment of synaptic vesicle clustering and of synaptic transmission, and increased seizure propensity, in synapsin I-deficient mice." Proceedings of the National Academy of Sciences of the United States of America **92**(20): 9235–9239.

- Li, W., E. Englund, H. Widner, B. Mattsson, D. van Westen, J. Lätt, S. Rehncrona, P. Brundin, A. Björklund, O. Lindvall and J.-Y. Li (2016). "Extensive graft-derived dopaminergic innervation is maintained 24 years after transplantation in the degenerating parkinsonian brain." Proceedings of the National Academy of Sciences of the United States of America **113**(23): 6544–6549.
- Li, W., N. West, E. Colla, O. Pletnikova, J. C. Troncoso, L. Marsh, T. M. Dawson, P. Jäkälä, T. Hartmann, D. L. Price and M. K. Lee (2005). "Aggregation promoting C-terminal truncation of alpha-synuclein is a normal cellular process and is enhanced by the familial Parkinson's disease-linked mutations." Proceedings of the National Academy of Sciences of the United States of America **102**(6): 2162–2167.
- Lieberman, A., A. Goodgold, S. Jonas and M. Leibowitz (1975). "Comparison of dopa decarboxylase inhibitor (carbidopa) combined with levodopa and levodopa alone in Parkinson's disease." Neurology **25**(10): 911–916.
- Lin, L. F., D. H. Doherty, J. D. Lile, S. Bektesh and F. Collins (1993). "GDNF: a glial cell line-derived neurotrophic factor for midbrain dopaminergic neurons." Science (New York, N.Y.) **260**(5111): 1130–1132.
- Lipski, J., R. Nistico, N. Berretta, E. Guatteo, G. Bernardi and N. B. Mercuri (2011). "L-DOPA: a scapegoat for accelerated neurodegeneration in Parkinson's disease?" Progress in neurobiology **94**(4): 389–407.
- Loening, A. M., T. D. Fenn and S. S. Gambhir (2007). "Crystal structures of the luciferase and green fluorescent protein from *Renilla reniformis*." Journal of molecular biology **374**(4): 1017–1028.
- Longhena, F., G. Faustini, M. G. Spillantini and A. Bellucci (2019). "Living in Promiscuity: The Multiple Partners of Alpha-Synuclein at the Synapse in Physiology and Pathology." International journal of molecular sciences **20**(1).
- Longhena, F., G. Faustini, T. Varanita, M. Zaltieri, V. Porrini, I. Tessari, P. L. Poliani, C. Missale, B. Borroni, A. Padovani, L. Bubacco, M. Pizzi, P. Spano and A. Bellucci (2018). "Synapsin III is a key component of α -synuclein fibrils in Lewy bodies of PD brains." Brain pathology (Zurich, Switzerland) **28**(6): 875–888.
- Los, G. V., L. P. Encell, M. G. McDougall, D. D. Hartzell, N. Karassina, C. Zimprich, M. G. Wood, R. Learish, R. F. Ohana, M. Urh, D. Simpson, J. Mendez, K. Zimmerman, P. Otto, G. Vidugiris, J. Zhu, A. Darzins, D. H. Klaubert, R. F. Bulleit and K. V. Wood (2008). "HaloTag: a novel protein labeling technology for cell imaging and protein analysis." ACS chemical biology **3**(6): 373–382.
- Lozano, A. M., N. Lipsman, H. Bergman, P. Brown, S. Chabardes, J. W. Chang, K. Matthews, C. C. McIntyre, T. E. Schlaepfer, M. Schulder, Y. Temel, J. Volkmann and J. K. Krauss (2019). "Deep brain stimulation: current challenges and future directions." Nature reviews. Neurology **15**(3): 148–160.
- Ma, S. Y., M. Røyttä, J. O. Rinne, Y. Collan and U. K. Rinne (1997). "Correlation between neuromorphometry in the substantia nigra and clinical features in Parkinson's disease using disector counts." Journal of the neurological sciences **151**(1): 83–87.
- Malek, N., D. Swallow, K. A. Grosset, O. Anichtchik, M. Spillantini and D. G. Grosset (2014). "Alpha-synuclein in peripheral tissues and body fluids as a biomarker for Parkinson's disease - a systematic review." Acta neurologica Scandinavica **130**(2): 59–72.
- Mao, X., M. T. Ou, S. S. Karuppagounder, T.-I. Kam, X. Yin, Y. Xiong, P. Ge, G. E. Umanah, S. Brahmachari, J.-H. Shin, H. C. Kang, J. Zhang, J. Xu, R. Chen, H. Park, S. A. Andrabi, S. U. Kang, R. A. Gonçalves, Y. Liang, S. Zhang, C. Qi, S. Lam, J. A. Keiler, J. Tyson, D. Kim, N. Panicker, S. P. Yun, C. J. Workman, D. A. A. Vignali, V. L. Dawson, H. S. Ko and T. M. Dawson (2016). "Pathological α -synuclein transmission initiated by binding lymphocyte-activation gene 3." Science (New York, N.Y.) **353**(6307).
- Margolesky, J. and C. Singer (2018). "Extended-release oral capsule of carbidopa-levodopa in Parkinson disease." Therapeutic advances in neurological disorders **11**: 1756285617737728.
- Marks, W. J., R. T. Bartus, J. Siffert, C. S. Davis, A. Lozano, N. Boulis, J. Vitek, M. Stacy, D. Turner, L. Verhagen, R. Bakay, R. Watts, B. Guthrie, J. Jankovic, R. Simpson, M. Tagliati, R. Alterman, M. Stern, G. Baltuch, P. A. Starr, P. S. Larson, J. L. Ostrem, J. Nutt, K. Kieburtz, J. H. Kordower and C. W. Olanow (2010). "Gene delivery of AAV2-neurturin for Parkinson's disease: a double-blind, randomised, controlled trial." The Lancet Neurology **9**(12): 1164–1172.

- Marks, W. J., J. L. Ostrem, L. Verhagen, P. A. Starr, P. S. Larson, R. A. E. Bakay, R. Taylor, D. A. Cahn-Weiner, A. J. Stoessl, C. W. Olanow and R. T. Bartus (2008). "Safety and tolerability of intraputamin delivery of CERE-120 (adeno-associated virus serotype 2–neurturin) to patients with idiopathic Parkinson's disease: an open-label, phase I trial." The Lancet Neurology **7**(5): 400–408.
- Maroteaux, L., J. T. Campanelli and R. H. Scheller (1988). "Synuclein: a neuron-specific protein localized to the nucleus and presynaptic nerve terminal." The Journal of Neuroscience **8**(8): 2804–2815.
- Matea, C. T., T. Mocan, F. Tabaran, T. Pop, O. Mosteanu, C. Puia, C. Iancu and L. Mocan (2017). "Quantum dots in imaging, drug delivery and sensor applications." International journal of nanomedicine **12**: 5421–5431.
- McConathy, J., M. J. Owens, C. D. Kilts, E. J. Malveaux, V. M. Camp, J. R. Votaw, C. B. Nemeroff and M. M. Goodman (2004). "Synthesis and biological evaluation of 11Ctalo Pram and 11Ctalsupram: candidate PET ligands for the norepinephrine transporter." Nuclear medicine and biology **31**(6): 705–718.
- McCormack, A. L., S. K. Mak, J. M. Henderson, D. Bumcrot, M. J. Farrer and D. A. Di Monte (2010). "Alpha-synuclein suppression by targeted small interfering RNA in the primate substantia nigra." PLoS one **5**(8): e12122.
- McMahan, H. T., M. Missler, C. Li and T. C. Südhof (1995). "Complexins: Cytosolic proteins that regulate SNAP receptor function." Cell **83**(1): 111–119.
- Meade, R. M., D. P. Fairlie and J. M. Mason (2019). "Alpha-synuclein structure and Parkinson's disease - lessons and emerging principles." Molecular Neurodegeneration **14**(1): 29.
- Menegon, A., D. Bonanomi, C. Albertinazzi, F. Lotti, G. Ferrari, H.-T. Kao, F. Benfenati, P. Baldelli and F. Valtorta (2006). "Protein kinase A-mediated synapsin I phosphorylation is a central modulator of Ca²⁺-dependent synaptic activity." The Journal of neuroscience : the official journal of the Society for Neuroscience **26**(45): 11670–11681.
- Merola, A., A. Romagnolo, L. Rizzi, M. G. Rizzone, M. Zibetti, M. Lanotte, G. Mandybur, A. P. Duker, A. J. Espay and L. Lopiano (2017). "Impulse control behaviors and subthalamic deep brain stimulation in Parkinson disease." Journal of neurology **264**(1): 40–48.
- Meuvius, J., M. Gerard, L. Desender, V. Baekelandt and Y. Engelborghs (2010). "The conformation and the aggregation kinetics of α -synuclein depend on the proline residues in its C-terminal region." Biochemistry **49**(43): 9345–9352.
- Meyer, T. d., S. Muyldermans and A. Depicker (2014). "Nanobody-based products as research and diagnostic tools." Trends in biotechnology **32**(5): 263–270.
- Misra, M., Q. Shi, X. Ye, E. Gruszecka-Kowalik, W. Bu, Z. Liu, M. M. Schweri, H. M. Deutsch and C. A. Venanzi (2010). "Quantitative structure-activity relationship studies of threo-methylphenidate analogs." Bioorganic & medicinal chemistry **18**(20): 7221–7238.
- Mittal, S., K. Bjørnevik, D. S. Im, A. Flierl, X. Dong, J. J. Locascio, K. M. Abo, E. Long, M. Jin, B. Xu, Y. K. Xiang, J.-C. Rochet, A. Engeland, P. Rizzu, P. Heutink, T. Bartels, D. J. Selkoe, B. J. Caldarone, M. A. Glicksman, V. Khurana, B. Schüle, D. S. Park, T. Riise and C. R. Scherzer (2017). " β 2-Adrenoreceptor is a regulator of the α -synuclein gene driving risk of Parkinson's disease." Science (New York, N.Y.) **357**(6354): 891–898.
- Monaldi, I., M. Vassalli, A. Bachi, S. Giovedì, E. Millo, F. Valtorta, R. Raiteri, F. Benfenati and A. Fassio (2010). "The highly conserved synapsin domain E mediates synapsin dimerization and phospholipid vesicle clustering." The Biochemical journal **426**(1): 55–64.
- Moors, T. E., J. J. M. Hoozemans, A. Ingrassia, T. Beccari, L. Parnetti, M.-C. Chartier-Harlin and W. D. J. van de Berg (2017). "Therapeutic potential of autophagy-enhancing agents in Parkinson's disease." Molecular Neurodegeneration **12**(1): 11.
- Moors, T. E., C. A. Maat, D. Niedieker, D. Mona, D. Petersen, E. Timmermans-Huisman, J. Kole, S. F. El-Mashtoly, L. Spycher, W. Zago, R. Barbour, O. Mundigl, K. Kaluza, S. Huber, M. N. Hug, T. Kremer, M. Ritter, S. Dziadek, J. J. G. Geurts, K. Gerwert, M. Britschgi and W. D. J. van de Berg (2019).

"Subcellular orchestration of alpha-synuclein variants in Parkinson's disease brains revealed by 3D multicolor STED microscopy." [BioRxiv](#).

- Mor, D. E., S. E. Ugras, M. J. Daniels and H. Ischiropoulos (2016). "Dynamic structural flexibility of α -synuclein." [Neurobiology of disease](#) **88**: 66–74.
- Müller, T. (2015). "Catechol-O-methyltransferase inhibitors in Parkinson's disease." [Drugs](#) **75**(2): 157–174.
- Muramatsu, S.-i., K.-i. Fujimoto, S. Kato, H. Mizukami, S. Asari, K. Ikeguchi, T. Kawakami, M. Urabe, A. Kume, T. Sato, E. Watanabe, K. Ozawa and I. Nakano (2010). "A phase I study of aromatic L-amino acid decarboxylase gene therapy for Parkinson's disease." [Molecular therapy : the journal of the American Society of Gene Therapy](#) **18**(9): 1731–1735.
- Murase, K., T. Fujiwara, Y. Umemura, K. Suzuki, R. Iino, H. Yamashita, M. Saito, H. Murakoshi, K. Ritchie and A. Kusumi (2004). "Ultrafine membrane compartments for molecular diffusion as revealed by single molecule techniques." [Biophysical journal](#) **86**(6): 4075–4093.
- Murthy, V. N. and C. F. Stevens (1999). "Reversal of synaptic vesicle docking at central synapses." [Nature Neuroscience](#) **2**(6): 503–507.
- Nam, M.-K., J.-H. Han, J.-Y. Jang, S.-E. Yun, G.-Y. Kim, S. Kang and H. Rhim (2015). "A novel link between the conformations, exposure of specific epitopes, and subcellular localization of α -synuclein." [Biochimica et biophysica acta](#) **1850**(12): 2497–2505.
- Nienhaus, K. and G. U. Nienhaus (2014). "Fluorescent proteins for live-cell imaging with super-resolution." [Chemical Society reviews](#) **43**(4): 1088–1106.
- Novick, P. and M. Zerial (1997). "The diversity of Rab proteins in vesicle transport." [Current Opinion in Cell Biology](#) **9**(4): 496–504.
- Olanow, C. W. and F. Stocchi (2018). "Levodopa: A new look at an old friend." [Movement disorders : official journal of the Movement Disorder Society](#) **33**(6): 859–866.
- Orimo, S., T. Uchihara, A. Nakamura, F. Mori, A. Kakita, K. Wakabayashi and H. Takahashi (2008). "Axonal alpha-synuclein aggregates herald centripetal degeneration of cardiac sympathetic nerve in Parkinson's disease." [Brain : a journal of neurology](#) **131**(Pt 3): 642–650.
- Ormö, M., A. B. Cubitt, K. Kallio, L. A. Gross, R. Y. Tsien and S. J. Remington (1996). "Crystal structure of the *Aequorea victoria* green fluorescent protein." [Science \(New York, N.Y.\)](#) **273**(5280): 1392–1395.
- Outeiro, T. F., J. Klucken, K. Bercury, J. Tetzlaff, P. Putcha, L. M. A. Oliveira, A. Quintas, P. J. McLean and B. T. Hyman (2009). "Dopamine-induced conformational changes in alpha-synuclein." [PloS one](#) **4**(9): e6906.
- Paleologou, K. E., A. W. Schmid, C. C. Rospigliosi, H.-Y. Kim, G. R. Lamberto, R. A. Fredenburg, P. T. Lansbury, C. O. Fernandez, D. Eliezer, M. Zweckstetter and H. A. Lashuel (2008). "Phosphorylation at Ser-129 but not the phosphomimics S129E/D inhibits the fibrillation of alpha-synuclein." [The Journal of biological chemistry](#) **283**(24): 16895–16905.
- Palfi, S., J. M. Gurruchaga, G. S. Ralph, H. Lepetit, S. Lavis, P. C. Buttery, C. Watts, J. Miskin, M. Kelleher, S. Deeley, H. Iwamuro, J. P. Lefaucheur, C. Thiriez, G. Fenelon, C. Lucas, P. Brugières, I. Gabriel, K. Abhay, X. Drouot, N. Tani, A. Kas, B. Ghaleh, P. Le Corvoisier, P. Dolphin, D. P. Breen, S. Mason, N. V. Guzman, N. D. Mazarakis, P. A. Radcliffe, R. Harrop, S. M. Kingsman, O. Rascol, S. Naylor, R. A. Barker, P. Hantraye, P. Remy, P. Cesaro and K. A. Mitrophanous (2014). "Long-term safety and tolerability of ProSavin, a lentiviral vector-based gene therapy for Parkinson's disease: a dose escalation, open-label, phase 1/2 trial." [The Lancet](#) **383**(9923): 1138–1146.
- Pankratz, N. and T. Foroud (2004). "Genetics of Parkinson disease." [NeuroRx : the journal of the American Society for Experimental NeuroTherapeutics](#) **1**(2): 235–242.
- Paolone, G., A. Brugnoli, L. Arcuri, D. Mercatelli and M. Morari (2015). "Etopazine prevents levodopa-induced dyskinesias by reducing striatal glutamate and direct pathway activity." [Movement disorders : official journal of the Movement Disorder Society](#) **30**(13): 1728–1738.
- Peelaerts, W. and V. Baekelandt (2016). " α -synuclein folds: the cards are on the table." [Nature structural & molecular biology](#) **23**(5): 359–360.

- Perutz, M. F., B. J. Pope, D. Owen, E. E. Wanker and E. Scherzinger (2002). "Aggregation of proteins with expanded glutamine and alanine repeats of the glutamine-rich and asparagine-rich domains of Sup35 and of the amyloid beta-peptide of amyloid plaques." Proceedings of the National Academy of Sciences of the United States of America **99**(8): 5596–5600.
- Petersen, J., P. G. Wilmann, T. Beddoe, A. J. Oakley, R. J. Devenish, M. Prescott and J. Rossjohn (2003). "The 2.0-Å crystal structure of eqFP611, a far red fluorescent protein from the sea anemone *Entacmaea quadricolor*." The Journal of biological chemistry **278**(45): 44626–44631.
- Phan, J.-A., K. Stokholm, J. Zareba-Paslawska, S. Jakobsen, K. Vang, A. Gjedde, A. M. Landau and M. Romero-Ramos (2017). "Early synaptic dysfunction induced by α -synuclein in a rat model of Parkinson's disease." Scientific reports **7**(1): 6363.
- Pivato, M., G. d. Franceschi, L. Tosatto, E. Frare, D. Kumar, D. Aioanei, M. Brucale, I. Tessari, M. Bisaglia, B. Samori, P. P. d. Laureto and L. Bubacco (2012). "Covalent α -synuclein dimers: chemico-physical and aggregation properties." PLoS one **7**(12): e50027.
- Pontillo, J., D. Wu, B. Ching, S. Hudson, M. J. Genicot, Y. Gao, T. Ewing, B. A. Fleck, K. Gogas, A. Aparicio, H. Wang, J. Wen and W. S. Wade (2008). "Synthesis and structure-activity relationships of selective norepinephrine reuptake inhibitors (sNRI) with improved pharmaceutical characteristics." Bioorganic & medicinal chemistry letters **18**(23): 6151–6155.
- Porton, B., A. Ferreira, L. E. DeLisi and H. T. Kao (2004). "A rare polymorphism affects a mitogen-activated protein kinase site in synapsin III: possible relationship to schizophrenia." Biological psychiatry **55**(2): 118–125.
- Porton, B., H.-T. Kao and P. Greengard (1999). "Cloning of cDNAs Encoding Human Synapsins Ha and IIb." DNA Sequence **10**(1): 49–54.
- Porton, B., H. T. Kao and P. Greengard (1999). "Characterization of transcripts from the synapsin III gene locus." Journal of neurochemistry **73**(6): 2266–2271.
- Porton, B., R. M. Rodriguiz, L. E. Phillips, J. W. Gilbert, J. Feng, P. Greengard, H.-T. Kao and W. C. Wetsel (2010). "Mice lacking synapsin III show abnormalities in explicit memory and conditioned fear." Genes, brain, and behavior **9**(3): 257–268.
- Porton, B. and W. C. Wetsel (2007). "Reduction of synapsin III in the prefrontal cortex of individuals with schizophrenia." Schizophrenia research **94**(1-3): 366–370.
- Postuma, R. B., D. Berg, M. Stern, W. Poewe, C. W. Olanow, W. Oertel, J. Obeso, K. Marek, I. Litvan, A. E. Lang, G. Halliday, C. G. Goetz, T. Gasser, B. Dubois, P. Chan, B. R. Bloem, C. H. Adler and G. Deuschl (2015). "MDS clinical diagnostic criteria for Parkinson's disease." Movement disorders : official journal of the Movement Disorder Society **30**(12): 1591–1601.
- Prasad, K., T. G. Beach, J. Hedreen and E. K. Richfield (2012). "Critical role of truncated α -synuclein and aggregates in Parkinson's disease and incidental Lewy body disease." Brain pathology (Zurich, Switzerland) **22**(6): 811–825.
- Price, D. L., M. A. Koike, A. Khan, W. Wrasidlo, E. Rockenstein, E. Masliah and D. Bonhaus (2018). "The small molecule α -synuclein misfolding inhibitor, NPT200-11, produces multiple benefits in an animal model of Parkinson's disease." Scientific reports **8**(1): 16165.
- Rao, J. N., C. C. Jao, B. G. Hegde, R. Langen and T. S. Ulmer (2010). "A combinatorial NMR and EPR approach for evaluating the structural ensemble of partially folded proteins." Journal of the American Chemical Society **132**(25): 8657–8668.
- Rascol, O., D. J. Brooks, A. D. Korczyn, P. P. d. Deyn, C. E. Clarke and A. E. Lang (2000). "A five-year study of the incidence of dyskinesia in patients with early Parkinson's disease who were treated with ropinirole or levodopa." The New England journal of medicine **342**(20): 1484–1491.
- Rekas, A., K. J. Ahn, J. Kim and J. A. Carver (2012). "The chaperone activity of α -synuclein: Utilizing deletion mutants to map its interaction with target proteins." Proteins **80**(5): 1316–1325.
- Reynolds, A. D., D. K. Stone, R. L. Mosley and H. E. Gendelman (2009). "Nitrated α -synuclein-induced alterations in microglial immunity are regulated by CD4+ T cell subsets." Journal of immunology (Baltimore, Md. : 1950) **182**(7): 4137–4149.

- Riboldi, G. M. and A. B. Di Fonzo (2019). "GBA, Gaucher Disease, and Parkinson's Disease: From Genetic to Clinic to New Therapeutic Approaches." Cells **8**(4).
- Richards, D. A., C. Guatimosim, S. O. Rizzoli and W. J. Betz (2003). "Synaptic Vesicle Pools at the Frog Neuromuscular Junction." Neuron **39**(3): 529–541.
- Rieker, C., K. K. Dev, K. Lehnhoff, S. Barbieri, I. Ksiazek, S. Kauffmann, S. Danner, H. Schell, C. Boden, M. A. Ruegg, P. J. Kahle, H. van der Putten and D. R. Shimshek (2011). "Neuropathology in mice expressing mouse alpha-synuclein." PloS one **6**(9): e24834.
- Rizzoli, S. O. and W. J. Betz (2005). "Synaptic vesicle pools." Nature reviews. Neuroscience **6**(1): 57–69.
- Roos, J. and R. B. Kelly (1999). "The endocytic machinery in nerve terminals surrounds sites of exocytosis." Current Biology **9**(23): 1411–1414.
- Rosahl, T. W., D. Spillane, M. Missler, J. Herz, D. K. Selig, J. R. Wolff, R. E. Hammer, R. C. Malenka and T. C. Südhof (1995). "Essential functions of synapsins I and II in synaptic vesicle regulation." Nature **375**(6531): 488–493.
- Rosenmund, C. and C. F. Stevens (1996). "Definition of the Readily Releasable Pool of Vesicles at Hippocampal Synapses." Neuron **16**(6): 1197–1207.
- Rossi, A., K. Berger, H. Chen, D. Leslie, R. B. Mailman and X. Huang (2018). "Projection of the prevalence of Parkinson's disease in the coming decades: Revisited." Movement disorders : official journal of the Movement Disorder Society **33**(1): 156–159.
- Rothman, R. B. and M. H. Baumann (2003). "Monoamine transporters and psychostimulant drugs." European journal of pharmacology **479**(1-3): 23–40.
- Ruprecht, V., S. Wieser, D. Marguet and G. J. Schütz (2011). "Spot variation fluorescence correlation spectroscopy allows for superresolution chronoscopy of confinement times in membranes." Biophysical journal **100**(11): 2839–2845.
- Ryan, T. A., L. Li, L. S. Chin, P. Greengard and S. J. Smith (1996). "Synaptic vesicle recycling in synapsin I knock-out mice." The Journal of cell biology **134**(5): 1219–1227.
- Sahl, S. J., S. W. Hell and S. Jakobs (2017). "Fluorescence nanoscopy in cell biology." Nature reviews. Molecular cell biology **18**(11): 685–701.
- Salveson, P. J., R. K. Spencer and J. S. Nowick (2016). "X-ray Crystallographic Structure of Oligomers Formed by a Toxic β -Hairpin Derived from α -Synuclein: Trimers and Higher-Order Oligomers." Journal of the American Chemical Society **138**(13): 4458–4467.
- San Sebastian, W., A. P. Kells, J. Bringas, L. Samaranch, P. Hadaczek, A. Ciesielska, M. Macayan, P. J. Pivrotto, J. Forsayeth, S. Osborne, J. F. Wright, F. Green, G. Heller and K. S. Bankiewicz (2014). "Safety and Tolerability of MRI-Guided Infusion of AAV2-hAADC into the Mid-Brain of Non-Human Primates." Molecular therapy. Methods & clinical development **3**.
- Sankaranarayanan, S., P. P. Atluri and T. A. Ryan (2003). "Actin has a molecular scaffolding, not propulsive, role in presynaptic function." Nature Neuroscience **6**(2): 127–135.
- Sardi, S. P., S. H. Cheng and L. S. Shihabuddin (2015). "Gaucher-related synucleinopathies: the examination of sporadic neurodegeneration from a rare (disease) angle." Progress in neurobiology **125**: 47–62.
- Savchenko, V., U. Sung and R. D. Blakely (2003). "Cell surface trafficking of the antidepressant-sensitive norepinephrine transporter revealed with an ectodomain antibody." Molecular and Cellular Neuroscience **24**(4): 1131–1150.
- Scheffel, U., J. W. Boja and M. J. Kuhar (1989). "Cocaine receptors - In vivo labeling with H-3 (-)cocaine, H-3 Win-35,065-2, and H-3 Win-35,428." Synapse **4**(4): 390-392.
- Schell, H., T. Hasegawa, M. Neumann and P. J. Kahle (2009). "Nuclear and neuritic distribution of serine-129 phosphorylated alpha-synuclein in transgenic mice." Neuroscience **160**(4): 796–804.
- Schenk, D. B., M. Koller, D. K. Ness, S. G. Griffith, M. Grundman, W. Zago, J. Soto, G. Atiee, S. Ostrowitzki and G. G. Kinney (2017). "First-in-human assessment of PRX002, an anti- α -synuclein monoclonal antibody, in healthy volunteers." Movement disorders : official journal of the Movement Disorder Society **32**(2): 211–218.

- Schikorski, T. and C. F. Stevens (2001). "Morphological correlates of functionally defined synaptic vesicle populations." Nature Neuroscience **4**(4): 391–395.
- Schimmöller, F., I. Simon and S. R. Pfeffer (1998). "Rab GTPases, directors of vesicle docking." The Journal of biological chemistry **273**(35): 22161–22164.
- Schmid, J. A., P. Scholze, O. Kudlacek, M. Freissmuth, E. A. Singer and H. H. Sitte (2001). "Oligomerization of the human serotonin transporter and of the rat GABA transporter 1 visualized by fluorescence resonance energy transfer microscopy in living cells." The Journal of biological chemistry **276**(6): 3805–3810.
- Schuepbach, W. M. M., J. Rau, K. Knudsen, J. Volkman, P. Krack, L. Timmermann, T. D. Hälbig, H. Hesekamp, S. M. Navarro, N. Meier, D. Falk, M. Mehdorn, S. Paschen, M. Maarouf, M. T. Barbe, G. R. Fink, A. Kupsch, D. Gruber, G.-H. Schneider, E. Seigneuret, A. Kistner, P. Chaynes, F. Ory-Magne, C. Brefel Courbon, J. Vesper, A. Schnitzler, L. Wojtecki, J.-L. Houeto, B. Bataille, D. Maltête, P. Damier, S. Raoul, F. Sixel-Doering, D. Hellwig, A. Gharabaghi, R. Krüger, M. O. Pinsker, F. Amtage, J.-M. Régis, T. Witjas, S. Thobois, P. Mertens, M. Kloss, A. Hartmann, W. H. Oertel, B. Post, H. Speelman, Y. Agid, C. Schade-Brittinger and G. Deuschl (2013). "Neurostimulation for Parkinson's disease with early motor complications." The New England journal of medicine **368**(7): 610–622.
- Schweri, M. M., H. M. Deutsch, A. T. Massey and S. G. Holtzman (2002). "Biochemical and behavioral characterization of novel methylphenidate analogs." The Journal of pharmacology and experimental therapeutics **301**(2): 527–535.
- Seidel, S., E. A. Singer, H. Just, H. Farhan, P. Scholze, O. Kudlacek, M. Holy, K. Koppatz, P. Krivanek, M. Freissmuth and H. H. Sitte (2005). "Amphetamines Take Two to Tango: an Oligomer-Based Counter-Transport Model of Neurotransmitter Transport Explores the Amphetamine Action." Molecular Pharmacology **67**(1): 140–151.
- Sevcsik, E., A. J. Trexler, J. M. Dunn and E. Rhoades (2011). "Allostery in a disordered protein: oxidative modifications to α -synuclein act distally to regulate membrane binding." Journal of the American Chemical Society **133**(18): 7152–7158.
- Shahmoradian, S. H., A. J. Lewis, C. Genoud, J. Hench, T. E. Moors, P. P. Navarro, D. Castaño-Díez, G. Schweighauser, A. Graff-Meyer, K. N. Goldie, R. Sütterlin, E. Huisman, A. Ingrassia, Y. d. Gier, A. J. M. Rozemuller, J. Wang, A. d. Paepe, J. Erny, A. Staempfli, J. Hoernschemeyer, F. Großerüschkamp, D. Niedieker, S. F. El-Mashtoly, M. Quadri, W. F. J. van IJcken, V. Bonifati, K. Gerwert, B. Bohrmann, S. Frank, M. Britschgi, H. Stahlberg, W. D. J. van de Berg and M. E. Lauer (2019). "Lewy pathology in Parkinson's disease consists of crowded organelles and lipid membranes." Nature neuroscience **22**(7): 1099–1109.
- Shannon, K. M., A. Keshavarzian, E. Mutlu, H. B. Dodiya, D. Daian, J. A. Jaglin and J. H. Kordower (2012). "Alpha-synuclein in colonic submucosa in early untreated Parkinson's disease." Movement disorders : official journal of the Movement Disorder Society **27**(6): 709–715.
- Sharon, R., M. S. Goldberg, I. Bar-Josef, R. A. Betensky, J. Shen and D. J. Selkoe (2001). "alpha-Synuclein occurs in lipid-rich high molecular weight complexes, binds fatty acids, and shows homology to the fatty acid-binding proteins." Proceedings of the National Academy of Sciences of the United States of America **98**(16): 9110–9115.
- Shi, M.-M., C.-H. Shi and Y.-M. Xu (2017). "Rab GTPases: The Key Players in the Molecular Pathway of Parkinson's Disease." Frontiers in cellular neuroscience **11**: 81-81.
- Shimomura, O., F. H. Johnson and Y. Saiga (1962). "Extraction, Purification and Properties of Aequorin, a Bioluminescent Protein from the Luminous Hydromedusan, Aequorea." Journal of Cellular and Comparative Physiology **59**(3): 223–239.
- Shupliakov, O., O. Bloom, J. S. Gustafsson, O. Kjaerulff, P. Low, N. Tomilin, V. A. Pieribone, P. Greengard and L. Brodin (2002). "Impaired recycling of synaptic vesicles after acute perturbation of the presynaptic actin cytoskeleton." Proceedings of the National Academy of Sciences of the United States of America **99**(22): 14476–14481.

- Sitte, H. H. and M. Freissmuth (2010). "The reverse operation of Na(+)/Cl(-)-coupled neurotransmitter transporters--why amphetamines take two to tango." Journal of neurochemistry **112**(2): 340–355.
- Smith, W. W., R. L. Margolis, X. Li, J. C. Troncoso, M. K. Lee, V. L. Dawson, T. M. Dawson, T. Iwatsubo and C. A. Ross (2005). "Alpha-synuclein phosphorylation enhances eosinophilic cytoplasmic inclusion formation in SH-SY5Y cells." The Journal of neuroscience : the official journal of the Society for Neuroscience **25**(23): 5544–5552.
- Söllner, T., S. W. Whiteheart, M. Brunner, H. Erdjument-Bromage, S. Geromanos, P. Tempst and J. E. Rothman (1993). "SNAP receptors implicated in vesicle targeting and fusion." Nature **362**(6418): 318–324.
- Song, S.-H. and G. J. Augustine (2015). "Synapsin Isoforms and Synaptic Vesicle Trafficking." Molecules and cells **38**(11): 936–940.
- Sonntag, K.-C., B. Song, N. Lee, J. H. Jung, Y. Cha, P. Leblanc, C. Neff, S. W. Kong, B. S. Carter, J. Schweitzer and K.-S. Kim (2018). "Pluripotent stem cell-based therapy for Parkinson's disease: Current status and future prospects." Progress in neurobiology **168**: 1–20.
- Souza, J. M., B. I. Giasson, Q. Chen, V. M. Lee and H. Ischiropoulos (2000). "Dityrosine cross-linking promotes formation of stable alpha -synuclein polymers. Implication of nitrative and oxidative stress in the pathogenesis of neurodegenerative synucleinopathies." The Journal of biological chemistry **275**(24): 18344–18349.
- Specht, E. A., E. Braselmann and A. E. Palmer (2017). "A Critical and Comparative Review of Fluorescent Tools for Live-Cell Imaging." Annual review of physiology **79**: 93–117.
- Spillantini, M. G., R. A. Crowther, R. Jakes, M. Hasegawa and M. Goedert (1998). "alpha-Synuclein in filamentous inclusions of Lewy bodies from Parkinson's disease and dementia with lewy bodies." Proceedings of the National Academy of Sciences of the United States of America **95**(11): 6469–6473.
- Spillantini, M. G. and M. Goedert (2000). "The alpha-synucleinopathies: Parkinson's disease, dementia with Lewy bodies, and multiple system atrophy." Annals of the New York Academy of Sciences **920**: 16–27.
- Stefani, G., F. Onofri, F. Valtorta, P. Vaccaro, P. Greengard and F. Benfenati (1997). "Kinetic analysis of the phosphorylation-dependent interactions of synapsin I with rat brain synaptic vesicles." The Journal of physiology **504 (Pt 3)**: 501–515.
- Sudhof, T. C. (2004). "The synaptic vesicle cycle." Annual review of neuroscience **27**: 509–547.
- Südhof, T. C., A. J. Czernik, H. T. Kao, K. Takei, P. A. Johnston, A. Horiuchi, S. D. Kanazir, M. A. Wagner, M. S. Perin and P. d. Camilli (1989). "Synapsins: mosaics of shared and individual domains in a family of synaptic vesicle phosphoproteins." Science (New York, N.Y.) **245**(4925): 1474–1480.
- Sugeno, N., A. Takeda, T. Hasegawa, M. Kobayashi, A. Kikuchi, F. Mori, K. Wakabayashi and Y. Itoyama (2008). "Serine 129 phosphorylation of alpha-synuclein induces unfolded protein response-mediated cell death." The Journal of biological chemistry **283**(34): 23179–23188.
- Surmeier, D. J., J. A. Obeso and G. M. Halliday (2017). "Selective neuronal vulnerability in Parkinson disease." Nature Reviews Neuroscience **18**: 101 EP -.
- Thai, D. L., M. T. Sapko, C. T. Reiter, D. E. Bierer and J. M. Perel (1998). "Asymmetric synthesis and pharmacology of methylphenidate and its para-substituted derivatives." Journal of medicinal chemistry **41**(4): 591–601.
- Thayanidhi, N., J. R. Helm, D. C. Nycz, M. Bentley, Y. Liang and J. C. Hay (2010). "Alpha-synuclein delays endoplasmic reticulum (ER)-to-Golgi transport in mammalian cells by antagonizing ER/Golgi SNAREs." Molecular biology of the cell **21**(11): 1850–1863.
- Theillet, F.-X., A. Binolfi, B. Bekei, A. Martorana, H. M. Rose, M. Stuiver, S. Verzini, D. Lorenz, M. van Rossum, D. Goldfarb and P. Selenko (2016). "Structural disorder of monomeric α -synuclein persists in mammalian cells." Nature **530**: 45 EP -.
- Thomas, C. E., A. Ehrhardt and M. A. Kay (2003). "Progress and problems with the use of viral vectors for gene therapy." Nature reviews. Genetics **4**(5): 346–358.

- Thompson, R. E., D. R. Larson and W. W. Webb (2002). "Precise Nanometer Localization Analysis for Individual Fluorescent Probes." Biophysical journal **82**(5): 2775–2783.
- Titova, N., C. Padmakumar, S. J. G. Lewis and K. R. Chaudhuri (2017). "Parkinson's: a syndrome rather than a disease?" Journal of neural transmission (Vienna, Austria : 1996) **124**(8): 907–914.
- Tofaris, G. K., H. T. Kim, R. Houriez, J.-W. Jung, K. P. Kim and A. L. Goldberg (2011). "Ubiquitin ligase Nedd4 promotes alpha-synuclein degradation by the endosomal-lysosomal pathway." Proceedings of the National Academy of Sciences of the United States of America **108**(41): 17004–17009.
- Torres, G. E., A. Carneiro, K. Seamans, C. Fiorentini, A. Sweeney, W.-D. Yao and M. G. Caron (2003). "Oligomerization and trafficking of the human dopamine transporter. Mutational analysis identifies critical domains important for the functional expression of the transporter." The Journal of biological chemistry **278**(4): 2731–2739.
- Trexler, A. J. and E. Rhoades (2012). "N-Terminal acetylation is critical for forming α -helical oligomer of α -synuclein." Protein science : a publication of the Protein Society **21**(5): 601–605.
- Tsigelny, I. F., Y. Sharikov, W. Wrasidlo, T. Gonzalez, P. A. Desplats, L. Crews, B. Spencer and E. Masliah (2012). "Role of α -synuclein penetration into the membrane in the mechanisms of oligomer pore formation." The FEBS journal **279**(6): 1000–1013.
- Turnbull, A. P., C. Phillips, A. C. W. Pike, J. M. Elkins, C. Gileadi, E. Salah, F. H. Niesen, N. Burgess, O. Gileadi, F. Gorrec, C. Umeano, F. v. Delft, J. Weigelt, A. Edwards, C. H. Arrowsmith, M. Sundstrom and D. Doyle (2007). The crystal structure of human synapsin III (SYN3) in complex with AMPNP.
- Uéda, K., H. Fukushima, E. Masliah, Y. Xia, A. Iwai, M. Yoshimoto, D. A. Otero, J. Kondo, Y. Ihara and T. Saitoh (1993). "Molecular cloning of cDNA encoding an unrecognized component of amyloid in Alzheimer disease." Proceedings of the National Academy of Sciences of the United States of America **90**(23): 11282–11286.
- Uhl, G. R. and Z. Lin (2003). "The top 20 dopamine transporter mutants: structure-function relationships and cocaine actions." European journal of pharmacology **479**(1-3): 71–82.
- Ulrih, N. P., C. H. Barry and A. L. Fink (2008). "Impact of Tyr to Ala mutations on alpha-synuclein fibrillation and structural properties." Biochimica et biophysica acta **1782**(10): 581–585.
- US-NIH. (2012). "AAV2-GDNF for Advanced Parkinson s Disease." from <https://clinicaltrials.gov/ct2/show/NCT01621581?term=gdnf&rank=1>.
- Vamvaca, K., M. J. Volles and P. T. Lansbury (2009). "The first N-terminal amino acids of alpha-synuclein are essential for alpha-helical structure formation in vitro and membrane binding in yeast." Journal of molecular biology **389**(2): 413–424.
- Varkey, J., J. M. Isas, N. Mizuno, M. B. Jensen, V. K. Bhatia, C. C. Jao, J. Petrlova, J. C. Voss, D. G. Stamou, A. C. Steven and R. Langen (2010). "Membrane curvature induction and tubulation are common features of synucleins and apolipoproteins." The Journal of biological chemistry **285**(42): 32486–32493.
- Vaughan, R. A., D. S. Sakrikar, M. L. Parnas, S. Adkins, J. D. Foster, R. A. Duval, J. R. Lever, S. S. Kulkarni and A. Hauck-Newman (2007). "Localization of cocaine analog 125IRTI 82 irreversible binding to transmembrane domain 6 of the dopamine transporter." The Journal of biological chemistry **282**(12): 8915–8925.
- Venton, B. J., A. T. Seipel, P. E. M. Phillips, W. C. Wetsel, D. Gitler, P. Greengard, G. J. Augustine and R. M. Wightman (2006). "Cocaine increases dopamine release by mobilization of a synapsin-dependent reserve pool." The Journal of neuroscience : the official journal of the Society for Neuroscience **26**(12): 3206–3209.
- Vijayakumar, D. and J. Jankovic (2016). "Drug-Induced Dyskinesia, Part 1: Treatment of Levodopa-Induced Dyskinesia." Drugs **76**(7): 759–777.
- Volpicelli-Daley, L. A. (2017). "Effects of α -synuclein on axonal transport." Neurobiology of disease **105**: 321–327.
- Volz, T. J., S. J. Farnsworth, G. R. Hanson and A. E. Fleckenstein (2008). "Methylphenidate-induced alterations in synaptic vesicle trafficking and activity." Annals of the New York Academy of Sciences **1139**: 285–290.

- Volz, T. J. and J. O. Schenk (2005). "A comprehensive atlas of the topography of functional groups of the dopamine transporter." Synapse (New York, N.Y.) **58**(2): 72–94.
- Vuorenpää, A., T. N. Jørgensen, A. H. Newman, K. L. Madsen, M. Scheinin and U. Gether (2016). "Differential Internalization Rates and Postendocytic Sorting of the Norepinephrine and Dopamine Transporters Are Controlled by Structural Elements in the N Termini." The Journal of biological chemistry **291**(11): 5634–5651.
- Wagle Shukla, A., P. Zeilman, H. Fernandez, J. A. Bajwa and R. Mehanna (2017). "DBS Programming: An Evolving Approach for Patients with Parkinson's Disease." Parkinson's disease **2017**: 8492619.
- Wakamatsu, M., A. Ishii, Y. Ukai, J. Sakagami, S. Iwata, M. Ono, K. Matsumoto, A. Nakamura, N. Tada, K. Kobayashi, T. Iwatsubo and M. Yoshimoto (2007). "Accumulation of phosphorylated alpha-synuclein in dopaminergic neurons of transgenic mice that express human alpha-synuclein." Journal of Neuroscience Research **85**(8): 1819–1825.
- Wang, L., U. Das, D. A. Scott, Y. Tang, P. J. McLean and S. Roy (2014). "α-synuclein multimers cluster synaptic vesicles and attenuate recycling." Current biology : CB **24**(19): 2319–2326.
- Wang, L., M. S. Frei, A. Salim and K. Johnsson (2019). "Small-Molecule Fluorescent Probes for Live-Cell Super-Resolution Microscopy." Journal of the American Chemical Society **141**(7): 2770–2781.
- Wardyn, J. D. and A. D. Jeyasekharan (2002). Immunofluorescence. Encyclopedia of life sciences. J. W. Ltd and Sons. London; New York; Vols. 21-32; Chichester, West Sussex, U.K., Nature Pub. Group Wiley. **347**: 1–9.
- Warren Olanow, C., R. T. Bartus, T. L. Baumann, S. Factor, N. Boulis, M. Stacy, D. A. Turner, W. Marks, P. Larson, P. A. Starr, J. Jankovic, R. Simpson, R. Watts, B. Guthrie, K. Poston, J. M. Henderson, M. Stern, G. Baltuch, C. G. Goetz, C. Herzog, J. H. Kordower, R. Alterman, A. M. Lozano and A. E. Lang (2015). "Gene delivery of neurturin to putamen and substantia nigra in Parkinson disease: A double-blind, randomized, controlled trial." Annals of neurology **78**(2): 248–257.
- Waxman, E. A., J. R. Mazzulli and B. I. Giasson (2009). "Characterization of hydrophobic residue requirements for alpha-synuclein fibrillization." Biochemistry **48**(40): 9427–9436.
- Wayment, H. K., H. Deutsch, M. M. Schweri and J. O. Schenk (1999). "Effects of methylphenidate analogues on phenethylamine substrates for the striatal dopamine transporter: potential as amphetamine antagonists?" Journal of neurochemistry **72**(3): 1266–1274.
- Wislet-Gendebien, S., C. D'Souza, T. Kawarai, P. St George-Hyslop, D. Westaway, P. Fraser and A. Tandon (2006). "Cytosolic proteins regulate alpha-synuclein dissociation from presynaptic membranes." The Journal of biological chemistry **281**(43): 32148–32155.
- Xilouri, M., O. R. Brekk and L. Stefanis (2013). "α-Synuclein and protein degradation systems: a reciprocal relationship." Molecular neurobiology **47**(2): 537–551.
- Xing, L.-X., C.-W. Shen, Y.-Y. Sun, L. Huang, Y.-Y. Zheng and J.-Q. Li (2017). "An Improved and Efficient Process for the Production of Highly Pure Dexamethylphenidate Hydrochloride." Journal of Heterocyclic Chemistry **54**(2): 1298–1303.
- Xu, W., D. L. Gray, S. A. Glase and N. S. Barta (2008). "Design and synthesis of reboxetine analogs morpholine derivatives as selective norepinephrine reuptake inhibitors." Bioorganic & medicinal chemistry letters **18**(20): 5550–5553.
- Yang, M.-L., L. Hasadsri, W. S. Woods and J. M. George (2010). "Dynamic transport and localization of alpha-synuclein in primary hippocampal neurons." Molecular Neurodegeneration **5**(1): 9.
- Zaltieri, M., J. Grigoletto, F. Longhena, L. Navarria, G. Favero, S. Castrezzati, M. A. Colivicchi, L. Della Corte, R. Rezzani, M. Pizzi, F. Benfenati, M. G. Spillantini, C. Missale, P. Spano and A. Bellucci (2015). "α-synuclein and synapsin III cooperatively regulate synaptic function in dopamine neurons." Journal of cell science **128**(13): 2231–2243.
- Zeng, F., N. Jarkas, J. S. Stehouwer, R. J. Voll, M. J. Owens, C. D. Kilts, C. B. Nemeroff and M. M. Goodman (2008). "Synthesis, in vitro characterization, and radiolabeling of reboxetine analogs as potential PET radioligands for imaging the norepinephrine transporter." Bioorganic & medicinal chemistry **16**(2): 783–793.

- Zeng, X.-S., W.-S. Geng, J.-J. Jia, L. Chen and P.-P. Zhang (2018). "Cellular and Molecular Basis of Neurodegeneration in Parkinson Disease." Frontiers in aging neuroscience **10**: 109.
- Zharikov, A. D., J. R. Cannon, V. Tapias, Q. Bai, M. P. Horowitz, V. Shah, A. El Ayadi, T. G. Hastings, J. T. Greenamyre and E. A. Burton (2015). "shRNA targeting α -synuclein prevents neurodegeneration in a Parkinson's disease model." The Journal of clinical investigation **125**(7): 2721–2735.
- Zhou, J. (2004). "Norepinephrine transporter inhibitors and their therapeutic potential." Drugs of the future **29**(12): 1235–1244.
- Zhou, R. M., Y. X. Huang, X. L. Li, C. Chen, Q. Shi, G. R. Wang, C. Tian, Z. Y. Wang, Y. Y. Jing, C. Gao and X. P. Dong (2010). "Molecular interaction of α -synuclein with tubulin influences on the polymerization of microtubule in vitro and structure of microtubule in cells." Molecular biology reports **37**(7): 3183–3192.
- Zhu, M., J. Li and A. L. Fink (2003). "The association of alpha-synuclein with membranes affects bilayer structure, stability, and fibril formation." The Journal of biological chemistry **278**(41): 40186–40197.